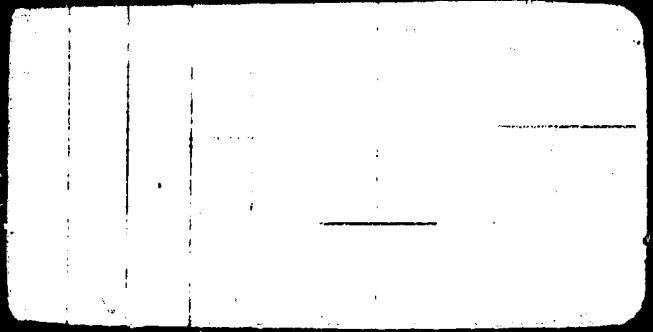

(NASA-CR-135348) STUDY OF THE EFFECTS OF GASEOUS ENVIRONMENTS ON SULFIDATION ATTACK OF SUPERALLOYS Final Report (United Technologies Research Center) 166 p
HC A08/MF A01 CSCL 11F G3/26

N78-21268
Unclas
14130

NASA CR-135348

UNITED TECHNOLOGIES RESEARCH CENTER

East Hartford, Connecticut 06108

R77-912613-5

Study of the Effects of Gaseous Environments on Sulfidation Attack of Superalloys

Work Performed for
NASA-Lewis Research Center
Contract No. NAS3-20039

Final Report

REPORTED BY John G. Smeggil
John G. Smeggil

Norman S. Bornstein

APPROVED BY M. A. DeCrescente
M. A. DeCrescente

DATE November 1977

NO. OF PAGES _____ COPY NO. _____

1 Report No	2 Government Accession No	3 Recipient's Catalog No
NASA CR-135348		

4 Title and Subtitle	5 Report Date
STUDY OF THE EFFECTS OF GASEOUS ENVIRONMENTS ON SULFIDATION ATTACK OF SUPERALLOYS	November 1977
	6 Performing Organization Code
7 Author(s)	8 Performing Organization Report No
J. G. Smeggil and N. S. Bornstein	R77-912613-5
	10 Work Unit No
9 Performing Organization Name and Address	
United Technologies Research Center East Hartford, Connecticut 06108	11 Contract or Grant No. NAS3-20039
	13. Type of Report and Period Covered
12 Sponsoring Agency Name and Address	Contractor Report
National Aeronautics and Space Administration Washington, DC 20546	14 Sponsoring Agency Code

15 Supplementary Notes

NASA-Lewis Research Center, Materials and Structures Division, Cleveland, Ohio 44135. Final Report. Project Manager, Carl A. Stearns.

16 Abstract

Studies have been conducted to examine the effect of the gaseous corrodents NaCl, HCl, and NaOH on the high temperature oxidation and Na_2SO_4-induced corrosion behavior of the alumina former NiAl, the chromia former Ni-25 wt.% Cr, elemental Cr, and the superalloy B-1900. Experiments were conducted at 900° and 1050°C in air in the presence and absence of the gaseous corrodents. Effects involving both reaction rates and microstructural changes in oxide morphology were observed due to the presence of these corrodents at levels anticipated to be present in operating industrial and marine gas turbines. The effect of gaseous NaCl, HCl, and possibly NaOH on NiAl in simple oxidation was to remove aluminum from below the protective alumina layer and to simultaneously weaken the adherence of the protective alumina oxide scale to the substrate. The aluminum removed from below the oxide scale was redeposited on its surface as α-Al_2O_3 whiskers. With respect to the chromia formers, gaseous NaCl and HCl promoted breakaway oxidation kinetics and changes in the microstructures of the oxide scales. The scale on Ni-25Cr contained significant amounts of $NiCr_2O_4$ along with Cr_2O_3; for Cr, the scale was more extensively convoluted with NaCl(g) than with air alone.

With respect to sulfidation-corrosion, NaCl vapors were found to mitigate the corrosive effect of Na_2SO_4 on NiAl at 1050°C. Conversely, the NaCl(g) attack of chromium in oxidation was found to be retarded by Na_2SO_4(c) deposits. It was also determined that the NaCl inherently present within deposited Na_2SO_4 at impurity levels, i.e., low ppm values, was sufficient to interact with alumina scales.

In simple oxidation, the effect of NaCl(g) on B-1900 was found to be similar to that observed for NiAl. Frequently, regions extensively depleted of gamma prime (Ni_3Al) precipitates were observed in the substrate. Additionally, substrate microstructures analogous to those found in the Na_2SO_4-induced hot corrosion of this alloy--except for the obvious absence of sulfide precipitates--were produced.

17 Key Words (Suggested by Author(s))	18 Distribution Statement
Corrosion, oxidation, sodium chloride, sodium sulfate, chromium, aluminum oxide, superalloys, thermogravimetry, corrosion growth morphology	Unclassified - unlimited STAR Category 26

19 Security Classif (of this report)	20 Security Classif (of this page)	21 No of Pages	22 Price*
Unclassified	Unclassified		

* For sale by the National Technical Information Service Springfield Virginia 22161

NASA-C-168 (Rev 10-75)

Study of the Effects of Gaseous Environments on Sulfidation Attack of Superalloys

TABLE OF CONTENTS

TABLE OF CONTENTS (Cont'd)

TABLE OF CONTENTS (Cont'd)

ABSTRACT

Studies have been conducted to examine the effect of the gaseous corrodents NaCl, HCl and NaOH on the high temperature oxidation and Na_2SO_4-induced corrosion behavior of the alumina former NiAl, the chromia former Ni-25 wt.% Cr, and elemental Cr, and lastly the superalloy B-1900. Experiments were conducted at 900° and 1050°C in air in the presence and absence of the gaseous corrodents. Effects involving both reaction rates and microstructural changes in oxide morphology were observed due to the presence of these corrodents at levels anticipated to be present in operating industrial and marine gas turbines. The effect of gaseous NaCl, HCl and possibly NaOH on NiAl in simple oxidation was to remove aluminum from below the protective alumina layer and to simultaneously weaken the adherence of the protective alumina oxide scale to the substrate. The aluminum removed from below the oxide scale was redeposited on its surface as α-Al_2O_3 whiskers. With respect to the chromia formers, gaseous NaCl and HCl promoted breakaway oxidation kinetics and heterogeneous scale development.

With respect to sulfidation-corrosion, NaCl vapors were found to mitigate the corrosive effect of Na_2SO_4 on NiAl at 1050°C. Conversely the NaCl(g) attack of chromium in oxidation was found to be retarded by Na_2SO_4(c) deposits. It was also determined that the NaCl inherently present within deposited Na_2SO_4 at impurity levels, i.e., low ppm values, was sufficient to interact with alumina scales. Moreover, at these levels NaCl was found not to be preferentially lost from condensed Na_2SO_4.

In simple oxidation the effect of NaCl(g) on B-1900 was found to be similar to that observed for NiAl, i.e., α-Al_2O_3 crystals were deposited on the surface of the protective oxide. Frequently regions extensively depleted of gamma prime (Ni_3Al) precipitates were observed in the substrate. Additionally, substrate microstructures analogous to those found in the Na_2SO_4-induced hot corrosion of this alloy - except for the obvious absence of sulfide precipitates - were produced.

Study of the Effects of Gaseous Environments on Sulfidation Attack of Superalloys

I. INTRODUCTION

The families of alloys developed for use in the gas turbine engine are among the strongest and most oxidation resistant structural materials designed for use at elevated temperatures. The desire for more efficient engines required higher and higher gas turbine temperatures which in turn spurred the development of the family of alloys currently known as the nickel- and cobalt-base superalloys. These alloys are, with respect to their melting points, among the strongest alloys known.

The alloys developed for use in gas turbines, upon exposure to air at elevated temperatures, form oxide scales enriched in chromium and/or aluminum. However, simple oxidation is not the only corrosion problem encountered in gas turbine engines. Salt crystals present in the intake air and impurities present in the fuels can combine within the gas turbine combustor to form minute quantities of corrosive salts which can deposit onto turbine components. These fused alkali salts increase the rate of metal wastage orders of magnitude. Although protective coatings have been developed to extend the life of turbine components, in the presence of these alkali salts, the coatings all too soon are defeated and the substrates corroded.

The attack of gas turbine components by fused salts is commonly referred to as hot corrosion. The attack associated with the presence of fused sulfates is commonly referred to as sulfidation attack. The term "sulfidation attack" is based upon the observation that sulfur-rich precipitates are metallographically observed in the microstructures of corroded components.

The sulfidation phenomenon has been intensively studied for more than a decade, and it is realized that a solution to the sulfidation problem requires a basic understanding of the corrosion mechanism(s) so that appropriate corrective action can be taken. It is important to also realize that, based upon current knowledge, the sulfidation problem currently encountered will be a major problem for machines using coal-derived synthetic fuel oils and gases because corrodents are formed from naturally occurring impurities in the coal. Furthermore, these impurities are not readily removed by current processing techniques. Corrosive compounds that are likely to be found in the hot section of turbines operating in marine and industrial environments include Na_2SO_4, NaCl as well as NaOH and HCl.

Condensed NaCl, either alone or in mixtures containing Na_2SO_4, has been known for many years to be highly corrosive with respect to structural alloys. Similarly, high activities of NaOH and HCl are very aggressive species for metallic materials. However the effect of NaCl, HCl, NaOH vapors and similar vapor species identified within the gaseous turbine environment is not known. Accordingly, little effort has been expended until relatively recently to determine if any interaction exists between low activity gaseous corrodents and metallic substrates and to adequately characterize such interactions.

The critical step in the corrosion phenomenon, sulfidation attack, is the destruction of the normally protective oxide layer which separates the fused salt from the substrate. In laboratory tests it has been shown that one means by which the normally protective layer is rendered ineffectual is by dissolution of the oxide as a result of interaction between the scale and oxide ions present in the melt. Other means by which the normally protective scale can be compromised are (a) local reducing conditions, (b) mechanical erosion, (c) mechanical faults accompanying oxide growth, (d) thermal stresses, (e) superimposed operating stresses and (f) mechanical disruption resulting from chemical reactions.

An understanding of the mechanisms by which the normally protective scales are rendered ineffectual is a prerequisite for the attenuation of and/or prevention of sulfidation corrosion. The mechanism which relates to scale breakdown as a result of chemical reactions with various chemical species, e.g., NaCl, HCl, NaOH, present in the gas phase has received little attention and is little understood even though it is potentially as important as any other mechanism. Hence, the thrust of this work is directed toward understanding the mechanism(s) by which the protection normally afforded by alumina and chromia scales is compromised as a result of chemical reactions involving reactants present in the gas phase.

This work was supported by the NASA-Lewis Research Center under Contract No. NAS3-20039; Mr. Carl Stearns, NASA Project Manager.

II. BACKGROUND

A. Oxidation

The strength of the nickel-base superalloys is due primarily to the presence of the gamma prime (γ') phase whose nominal composition is Ni_3Al. But in reality Ni_3Al is alloyed principally with titanium and also contains various percentages of cobalt, chromium and the refractory metals present in the superalloy. On the other hand, cobalt-based alloys are primarily strengthened by solid solution elements and precipitated secondary phases, usually carbides. Major solid solution strengtheners in the cobalt system are chromium and tungsten. Frequently, the description of oxide phases forming on such superalloy substrates at elevated temperatures is overly simplified. Thusly, the nickel- and cobalt-based superalloys are labeled "alumina-" and "chromia-formers", respectively. However in actuality a panorama of different oxide phases can form on both the nickel- and cobalt-based alloys. The exact oxide scales formed will depend on a number of factors, e.g., alloy composition, the composition of the oxidizing atmosphere, the time at temperature in this atmosphere, etc. (Ref. 1).

There are many factors which can affect the adhesion of oxides to alloy substrates of which mechanical faults accompanying oxide growth, mechanical erosion and superimposed operating stresses are just a few. It has been shown that, in the presence of trace quantities of rare-earth additions, the adherence of alumina scales is markedly improved. The presence of inert oxides such as thoria markedly improves the oxidation behavior of certain nickel and nickel-chromium alloys.

B. Hot Corrosion

1. History

Sulfidation is defined as the accelerated rate of oxidation of materials which occurs when an alkali salt is present in the condensed state. The composition of salt is a variable but the major constituent is usually an alkali sulfate. The attack is characterized by the presence of a loose, nonprotective oxide scale separated from a substrate matrix by an alloy affected zone containing sulfur-rich precipitates.

One of the first sulfidation mechanisms was proposed by Simons, Browning and Liebhafsky (Ref. 2). According to these authors a reducing agent, R, reacted with the sodium sulfate to release sulfur,

$$Na_2SO_4 + 3R \rightarrow Na_2O + 3RO + S \quad (1)$$

and the metal or component of the alloy M reacted with the sulfur,

$$M + S \rightarrow MS. \quad (2)$$

The "destruction reactions" which subsequently occur are

$$Na_2SO_4 + 3MS \rightarrow 4S + 3MO + Na_2O \quad (3)$$

$$4M + 4S \rightarrow 4MS. \quad (4)$$

and finally enhanced oxidation occurs via

$$2M + 2MS \rightarrow 2M \cdot MS \quad (5)$$

$$2M \cdot MS + O_2 \rightarrow 2MO + 2MS. \quad (6)$$

With respect to the "triggering" reaction, Eq. (1), any localized reducing condition will suffice. Dean (Ref. 3) indicated that in gas turbine engines carbon particles could be the reducing agent, i.e.,

$$2Na_2SO_4 + 6C + 3O_2 \rightarrow 2Na_2O + 6CO_2 + 2S. \quad (7)$$

Gambino (Ref. 4) studied the oxidation behavior of Na_2SO_4-coated nickel-base alloys and proposed that the Na_2SO_4 reacts with the nickel to form nickel sulfide,

$$Na_2SO_4 + 9/2Ni \rightarrow Na_2O + 3NiO + 1/2Ni_3S_2. \quad (8)$$

Oxygen penetrates the molten salt layer and reacts with the sulfide,

$$9/2O_2 + Ni_3S_2 \rightarrow 3NiO + 2SO_3. \quad (9)$$

The SO_3 formed reacts with the Na_2O to regenerate the sodium sulfate

$$Na_2O + SO_3 \rightarrow Na_2SO_4. \quad (10)$$

Seybolt and Beltran (Ref. 5) studied the oxidation of nickel and cobalt in Na_2SO_4 and modified the theory of Simons et al., such that the reducing agent and the alloy substrate are one and the same. It was later proposed by Seybolt (Ref. 6) that the accelerated rates of oxidation of commercial superalloys were due to a loss of oxidation inhibition by chromium-depletion through formation of chromium-rich sulfide precipitates.

The effect of sulfur on the oxidation of a number of binary and complex nickel- and cobalt-base alloys has been studied by many investigators (Refs. 7, 8, 9, and 10). In general, the oxidation resistance of simple or complex M_xS_y phases is markedly inferior to that of the parent substrate although, as shown by Seybolt, the rate of oxidation of "CrS" is comparable to that of chromium. The formation of a liquid sulfide layer would adversely affect the oxidation properties of an alloy as would the generation of SO_2 at a scale-substrate interface. The observation that, once sulfur has entered into an alloy, its removal is difficult has been made by Bergman (Ref. 11) as well as by Spengler and Viswanathan (Ref. 12). But in order for sulfur to enter the alloy at any appreciable rate the normally protective oxide scale which separates the fused salt from the substrate must be rendered ineffectual.

DeCrescente and Bornstein (Ref. 13) presented thermodynamic arguments and experimentally demonstrated that in order for sulfidation attack to occur, a fused salt must be present in the condensed state. Thusly, condensed Na_2SO_4 caused accelerated oxidation of a nickel-base superalloy while gaseous mixtures of Na_2SO_4 and air are relatively harmless.

In a series of publications, Bornstein et al. proposed (Refs. 14, 15, 16 and 17) that the accelerated rate of oxidation associated with sulfidation attack is not related to the preferential oxidation of either sulfur-rich phases or the alloy affected zone but rather is due to the inability of the alloy to form a protective oxide scale due to the presence of oxide ions in the Na_2SO_4 melt. Goebel and Pettit (Ref. 18) confirmed that the products of the reaction between the normally protective oxide scale and oxide ions is nonprotective.

Brown, Bornstein and DeCrescente (Ref. 19) devised and constructed a reversible galvanic cell with which they were able to demonstrate the effect of various oxides on the oxide ion content of sodium sulfate. They used Na_2SO_4 as the electrolyte and demonstrated that the cell was reversible to oxide ions and oxygen. They then demonstrated that oxides such as Cr_2O_3 react with and reduce the oxide ion content of sodium sulfate.

The relative ability of various oxides to reduce the oxide ion content of Na_2SO_4 can also be calculated if the available thermodynamic data are available. This technique uses the calculated equilibrium SO_3 partial pressure over a mixture of the salt and oxide in question as a measure of the ability of the oxide to reduce the oxide ion content of Na_2SO_4.

2. Deposition Mechanisms

During the combustion of a fuel oil, the oil droplets decompose in stages. The lighter hydrocarbons distill and burn leaving heavier hydrocarbons which crack to form viscous tar-like material and subsequently carbon, which upon complete combustion oxidizes to carbon dioxide (Ref. 20). Fuel-soluble metallic impurities present in the fuel are not very volatile and tend to concentrate in the unburnt portion of the fuel. Thus, the concentration of the unwanted corrosive forming impurities in the transient combustion product, the fuel char, can be several orders of magnitude greater than the initial concentration of the impurity in the starting fuel. The carbonaceous tars which can accumulate within areas in the combustors can further carbonize to hard particles which strike the leading edge and concave surfaces of the first stage nozzle guide vanes. If the temperature is such that the particles are highly viscous fluids or plastic solids, they could adhere to turbine components forming corrosive deposits.

Alkali metal compounds can also enter into a gas turbine engine as particulate matter with the intake air. Under these conditions, such turbines will continually ingest NaCl as a contaminant of both the atmosphere and the fuel (Refs. 21, 22). Several ppm of NaCl may be ingested into naval turbines operating in foul weather (Refs. 21, 22).

Bessen and Fryxell have shown turbines to be effective separators of the chloride and sulfate components of sea salt (Ref. 23). They reported constant levels of Na_2SO_4, 0.1 mg/cm^2, present on all stages of the compressor of an LM-2500 engine which had been operated for over 7000 hours. NaCl, on the other hand, was found to vary from 0.1 mg/cm^2 at the first stage of compressor to 0.02 mg/cm^2 at the seventh stage. After this stage and through the sixteenth stage, no meaningful chloride levels were detected, i.e., less than 0.01 mg/cm^2. Furthermore their surveys of the high pressure turbine components from several engines failed to reveal the presence of any condensed chlorides. Then, as shown by Bessen and Fryxell (Ref. 23), the sodium chloride component of sea salt is not preferentially removed from ingested sea salt crystals and selectively deposited as a condensed phase on turbine hardware surfaces ahead of combustor sections. Therefore, hot section atmospheres in gas turbines will continually contain low partial pressures of chloride-bearing species.

Another mode of atmospheric NaCl ingestion into hot turbine sections involves the random breaking off of condensed salts from compressor sections (Ref. 21). Again, depending upon compressor location, the particle will have a composition ranging from dried sea salt to virtually NaCl-void sea salt. Furthermore, depending on the size and the chemical composition of such particles, they may not totally vaporize in the combustion chamber and so can

impact on the high pressure blades and vanes (Ref. 22). When particles originate from the latter stages of the compressor, they will have the same composition as the salt deposits found on high pressure turbine hardware. On the other hand, particulate matter from the first stages of the compressor involves NaCl-containing material but the description of the role of the NaCl in such particles is difficult. The high vapor pressure of NaCl, e.g., 0.35 torr at 800°C, would be expected to lead to its rapid removal from condensed particles (Ref. 24), thus accounting for the virtual absence of chlorides in deposits found on hardware surfaces, i.e., 0.01 mg/cm^2 (Ref. 23).

Once NaCl has entered the combustion chamber of a gas turbine via either the gas phase or condensed onto particulate matter shed by the compressor, the role of NaCl has been controversial. Specifically, questions have arisen in the past as to whether sufficient time (5-10 millisec) exists in gas turbine combustion chambers for the conversion of NaCl to Na_2SO_4:

$$NaCl(c,g) + H_2O(g) \rightarrow NaOH(c,g) + HCl(g)^* \qquad (11)$$

$$2NaOH(c,g) + SO_2(g) + 1/2\ O_2(g) \rightarrow Na_2SO_4(c,g) + H_2O(g) \qquad (12)$$

However, although the detailed mechanism for the conversion of NaCl(g) to $Na_2SO_4(c,g)$ has not been worked out, Stearns et al. have demonstrated that $Na_2SO_4(g)$ can be formed in NaCl-sulfur-doped methane-oxygen flames in residence times of less than 1 millisecond (Ref. 25). Large amounts of unreacted NaCl(g) were also observed in the oxygen-rich flames (Ref. 25). Expanding on this work, results of burner rig studies recently reported by Kohl et al. (Ref. 26) have shown that significant amounts of NaCl can be converted by Na_2SO_4 in less than 2.2 milliseconds. Earlier, Hanby had conducted a series of experiments to determine if the kinetics of the Na_2SO_4 reaction is sufficiently rapid under gas burner conditions to contribute to the hot corrosion process in high pressure turbine sections (Ref. 27). He concluded that (1) the 8 millisec required to form Na_2SO_4 was too slow to be a significant contribution to the hot corrosion process and (2) at 1500°K the equilibrium composition of sodium salts in combustion products contains 8.5 percent Na_2SO_4 and, since sea salt already contains 10 percent Na_2SO_4, the gases at elevated temperatures are already saturated with Na_2SO_4. However, Stearns et al. (Ref. 25) have concluded that $Na_2SO_4(g)$ is not expected to form under the conditions employed by Hanby. Moreover, the extent to which Na_2SO_4 is produced in a gas turbine by these reactions, cf. Eqs. (11) and (12), could be influenced by hardware geometry, i.e. combustor design (Ref. 28).

*In this report the bracketed c implies the phase is present in the condensed state, either solid or liquid. The bracketed g similarly refers to the gaseous state.

Accordingly, depending on the extent to which ingested NaCl is involved in the conversion of sulfur to Na_2SO_4, when the partial pressure of Na_2SO_4 in turbine hot sections is sufficiently large, Na_2SO_4 will condense onto turbine hardware surfaces. DeCrescente et al. (Ref. 13) have published a dew point curve of Na_2SO_4 as a function of NaCl concentration and vapor pressure data then available (Refs. 29, 30). Similar sets of curves have been published by Bessen and Fryxell (Ref. 23), Tschinkel (Ref. 31) and Kohl et al. (Ref. 32).

However, irrespective of whether ingested NaCl is totally or partially converted to Na_2SO_4 in gas turbines, in the absence of an unidentified chloride sink (Ref. 23), gas turbine hot sections will be exposed to atmospheres containing low partial pressures of chloride-bearing species, e.g. NaCl, HCl, etc. Moreover, as pointed out by Stearns et al. (Ref. 25) and by Kohl et al. (Ref. 32), gaseous NaCl is expected to be a major sodium-bearing vapor species in turbine hot sections based on thermodynamic calculations.

3. Mechanisms of Scale Breakdown

It is apparent that in order for sulfidation or accelerated attack to occur, the integrity of the normally protective oxide scale which separates the corrosive salt from the metallic substrate must be compromised. This can be accomplished by a number of methods, some of which are: (a) chemical dissolution, (b) local reducing conditions, (c) mechanical erosion, (d) mechanical faults within the scale as well as the effect of thermal stresses and superimposed operating stresses and (e) mechanical disruption resulting from chemical reactions.

The role of stress in predicting oxidation behavior was first studied by Pilling and Bedworth (Ref. 33) who proposed that oxidation resistance should be related to the volume ratio of oxide and metal; i.e.,

$$R = Wd/Dw \qquad (13)$$

where W = formula weight of oxide
w = atomic weight of metal
D = specific density of oxide
d = specific density of metal
R = the ratio of the volume of oxide formed from a unit volume of metal.

Ideally for a stress-free oxide the value of R should be unity. Values of R much greater than unity tend to introduce large compressive stresses and for values less than unity the stresses are tensile. The Pilling-Bedworth ratio is at best a poor method for predicting oxidation behavior since it does not take into account the differences in coefficient of thermal expansion, melting point, adherence, plasticity and diffusion rates. However, the work of Pilling and Bedworth clearly demonstrated the importance of stress in oxidation.

The effect of stress as it relates to oxidation and corrosion has been studied by Hancock and his associates, e.g., Ref. 34. It has been shown that the rate of isothermal oxidation is dependent upon the mechanical properties of a growing scale; and most recently it was shown by Ward, Hockenhull and Hancock (Ref. 34) that, under fatigue conditions, stress-accelerated oxidation occurs when the peak cyclic tensile strain exceeds the fracture strain of the surface oxide. Current studies at Cranfield are directed at studying the relationships between accelerated oxidation and stresses either imposed by differences in coefficients of thermal expansion or superimposed as a result of component operation, as well as stresses due to mechanical faults present in the growing scale. In these studies a vibrational technique is used which measures the natural flexural resonance frequency of a freely suspended rod during high temperature exposure. It has been shown that this technique as well as the standard thermogravimetric technique can be used to verify changes that occur during oxidation as a result of cracking or spallation of the oxide scale.

The general environment within the gas turbine engine is highly oxidizing; however it is possible, under certain engine conditions, to produce unburnt hydrocarbons and deposit elemental carbon onto turbine components. The total inlet air-to-fuel ratio of advanced gas turbines is on the order of about 50-60 to 1 by weight. However a large fraction of this compressor air is used for cooling. The atmosphere within combustor-first stage turbine sections can be described by air-to-fuel ratios of about 20-30 to 1 by weight. It is known that the current fuels burn efficiently at a ratio of about 16 to 1. During start-up or shut-down it is possible, as a result of local perturbations, to produce fuel-rich mixtures which result in the formation of unburnt hydrocarbons and elemental carbon in combustion and first stage turbine sections.

Bornstein (Ref. 35), in a recent study of the deposits that form on industrial gas turbines, found that more than 6000 mg of insoluble matter can adhere to a first stage vane. The vanes in question were removed from an industrial gas turbine engine after approximately 500 hrs of service. Of the total quantity of insoluble matter, approximately 0.045 percent or 2.7 mg was analyzed as carbonaceous material.

Elemental carbon, a strong reducing agent, can possibly directly affect protective scale breakdown. McKee and Romeo (Ref. 36) have shown that the dwell time for the existence of carbon on a metal substrate under oxidizing conditions is directly related to the type of carbon that forms. The fine sooty carbon that appears as lamp black or carbon black is more readily oxidized than the crystalline graphitic types.

Carbon is frequently present within alloys in the form of carbides for strengthening purposes. This is particularly true in the case of cobalt-based alloys. The role of carbides with respect to Na_2SO_4 attack has been studied by both Romeo and McKee (Ref. 37) and El-Dahshan et al. (Ref. 38) and the latter concluded that carbides within the structures do not markedly influence the hot corrosion properties of the alloy when considering only Na_2SO_4 attack. However, when condensed chlorides are present, the carbide network is severely attacked.

The normally protective scale that separates the metallic substrate from the hostile gas turbine environment can also be compromised as a result of chemical dissolution resulting from condensed salt effects. This mechanism is also referred to as the oxide ion theory of sulfidation. The salt can be deposited via an equilibrium process (i.e., condensation) or a nonequilibrium process (i.e., impaction). In either case a prerequisite is the presence of a condensed salt. Initially the salt is separated from the substrate by the normally protective oxide scale. If reactions are to occur between the substrate and the salt, the normally protective oxide scale must be rendered ineffectual.

According to the oxide ion theory of corrosion, the fused salt can be thought of as an ionized melt consisting of sodium ions and sulfate ions. The concentration of oxide ions is established by the equilibria:

$$SO_4^{=}(e) \rightleftarrows SO_3(g) + O^{=}(c) \qquad (14)$$

$$SO_4^{=}(c) \rightleftarrows SO_2(g) + 1/2\ O_2(g) + O^{=}(c). \qquad (15)$$

The loss of the oxides of sulfur corresponds to an increase in the oxide ion content of the melt. In a similar manner the diffusion of sulfur through the scale results in an increase in oxide ion concentration.

Oxide ions present in the melt react with the normally protective oxide scale. A product of the reaction for alumina-rich scale is aluminate, i.e.,

$$Al_2O_3(c) + O^{=}(c) \rightarrow 2AlO_2^{-}(c), \qquad (16)$$

which has been experimentally identified as $NaAlO_2$ by x-ray diffraction techniques (Ref. 15).

Once the scale has been compromised the fused salt can contact the substrate. The substrate is a reducing agent with respect to the salt. At the salt-substrate interface, the oxygen potential will decrease rapidly due to the formation of oxide nuclei and concurrently the sulfur potential will increase.

The precipitation of sulfides reduces the sulfur potential. As a result of the decrease in the oxygen and sulfur potentials, the oxide ion content of the melt then rises rapidly, i.e.,

$$SO_4^{=}(c) \rightarrow \frac{3}{2} O_2(g) + 1/2\ S_2(g) + O^{=}(c). \qquad (17)$$

The relatively high oxide ion content prevents reformation of a protective oxide scale which would tend to form as oxygen diffuses through the salt to the substrate-salt interface.

During the corrosion process in which sulfur had entered into the substrate, microstructural changes in the alloy will occur. A study of the microstructural changes that occur as a function of the rate of oxidation of a nickel-base superalloy has been performed (Ref. 16). The results of this work indicate that, whereas the most rapid rates of oxidation occur shortly after the fused salt reacts with the substrate, the microstructural changes associated with sulfidation attack are related to the subsequent oxidation and movement of sulfur into the alloy.

In the past empirical relationships have been formulated in which the propensity of an alloy to undergo sulfidation attack is related to an "equivalent" chromium content. The effect of various alloying elements was rated as negative (detrimental), positive (beneficial) or neutral (Ref. 39). Based upon the oxide ion theory, the effect of the various elements is dependent upon the nature and composition of the oxide scale that forms on the surface of the alloy.

The relative ability of various oxides to reduce the oxide ion content of Na_2SO_4 can also be calculated if the available thermodynamic data are available. This technique uses the calculated equilibrium SO_3 partial pressure over a mixture of the salt and oxide in question as a measure of the ability of the oxide to reduce the oxide ion content of Na_2SO_4.

According to this theory, the role of the refractory metals in sulfidation attack involves the ability of their oxides to react with and decrease the oxide ion content of sodium sulfate. Morrow et al. (Ref. 40) studied the effect of molybdenum on the sulfidation behavior of a series of Ni-Cr-Al alloys. They found that in general, as the molybdenum content of the alloy increased, the propensity toward sulfidation decreased. Similar results have been reported for transition metal-refractory metal binary alloys coated with Na_2SO_4 (Ref. 16). Gambino (Ref. 41) noted that the rate of oxidation of a sodium sulfate-coated Ni-Cr-Mo alloy oxidized at an accelerated rate but the same alloy free of salt underwent catastropic oxidation.

Goebel et al. (Ref. 42), studying the effect of Na_2SO_4 on various Ni-Cr-Al alloys with and without molybdenum, concluded that the alloys free of molybdenum underwent "accelerated oxidation" but those which contained molybdenum underwent "catastrophic oxidation". Based upon the results of their study they proposed that the introduction of oxides such as molybdenum can lower the oxide content of the Na_2SO_4 melt to a sufficiently low level such that the oxide scale dissolves by an acidic reaction:

$$Al_2O_3(c) \rightarrow 2Al^{+3}(c) + 3O^{=}(c). \qquad (18)$$

This theory provides an alternate mechanism to the basic attack for protective oxide scale removal. Accordingly, the ability of the refractory metals to impart sulfidation resistance can be interpreted via this model to depend upon the relative concentration (activity) of the oxide ion at the fused melt-alloy interface (Ref. 16). In simple oxidation the quantity of liquid refractory metal oxide which forms on the surface is either insufficient to dissolve appreciable quantities of the normally protective scale and/or is volatilized. Under a blanket of Na_2SO_4, volatilization is reduced. Initial oxide scale dissolution in the vicinity of the refractory metal oxide occurs by direct reaction with the oxide scale.

Of particular note here is that gaseous corrodents such as NaCl, if they have any effect on Na_2SO_4-induced hot corrosion processes, are not accounted for in these models.

Intensive work by many investigators has shown that condensed NaCl or NaCl-Na_2SO_4 mixtures are very corrosive (Refs. 28, 43-59). Most importantly, Hancock, using a vibrational technique, reported that gaseous NaCl adversely effects protective oxide adherence on various high temperature superalloys (Ref. 46). But Hancock supplied no quantitative experimental information concerning either the levels of NaCl(g) in the atmosphere required to effect this result or how this effect manifests itself microstructurally.

Furthermore, oxidation studies involving superalloys have normally shown complex scale formation, e.g. Ref. 1. Fryburg, Kohl and Stearns (Ref. 61) have examined the oxide scales found on a number of alloys some of which approximate the alloy compositions examined by Hancock (Ref. 46), and they report that heterogeneous oxide scales are formed. Thus the condition under which NaCl(g) adversely affects various protective scales is not well characterized.

Accordingly, the work reported here is concerned with the effect of gaseous NaCl, HCl and NaOH as they affect the oxidation and Na_2SO_4-induced hot corrosion behavior of NiAl, an alumina former, and Ni-25 wt % Cr, a chromia former. Specifically, the interactions between the gaseous species NaCl, HCl and NaOH

alone and in the presence of the condensed phases Na_2SO_4, carbon and Cr_2O_3 were studied. The program was divided into three tasks. The goals of each of the tasks are an understanding of (1) the effect of gaseous NaCl, NaOH and HCl on the alumina and chromia scales formed on Ni-25 wt % Cr and NiAl substrates, (2) the effect of gaseous NaCl, NaOH and HCl on the sulfidation behavior of Na_2SO_4-coated substrates, and (3) the combined effect of gaseous NaCl, NaOH and HCl on the sulfidation behavior of Na_2SO_4-coated substrates in the presence of a strong reducing agent, carbon, and a known sulfidation inhibitor, Cr_2O_3.

Questions arose in the course of this study as to whether certain effects involving the Ni-25 wt % Cr alloy resulted from alloy effects (i.e., the nickel component of the alloy) or were intrinsically the result of the behavior of chromia itself. A limited number of experiments with elemental chromium clarified those uncertainties. Additionally, in order to determine if the effects of NaCl(g) on the oxidation behavior of the chemically simple alumina former NiAl could also occur in the case of more complex superalloys, a few experiments were conducted with the complex superalloy B-1900.

III. EXPERIMENTAL APPROACH

A. Materials

The alloys studied were Ni-25 (wt %) Cr and the intermetallic NiAl. Ingots of these two alloys were prepared by RF melting the desired nominal compositions in an argon atmosphere and pouring the melt into an alumina mold. The ingots were then appropriately heat treated in a hydrogen atmosphere: two days at 1100°C for the Ni-25 Cr, and two days at 1350°C for the NiAl. Subsequently, sections of these annealed ingots were submitted for chemical analysis and the Ni-25 Cr was found to contain 24.55 ± 0.05 wt % Cr. The NiAl was found to contain 31.06 ± 0.09 wt % Al.

The elemental chromium used was of 4N+ purity and was supplied by Mr. C. A. Stearns, NASA-Lewis Research Center. Energy dispersive x-ray (EDAX) analysis of this material indicated trace levels of Ca present in the chromium. This calcium likely derived from the refining process used to prepare and purify the elemental chromium.

For all experiments sample specimens approximately 2.5 cm x 1.0 cm x 0.2 cm were prepared and ground to 600 grit SiC. A Pt wire was then spot welded on one end for sample support. The samples, prior to insertion into the experimental apparatus, were washed and degreased, the final rinse given with absolute ethanol.

The air used in the experiments was taken from the laboratory service strip. The water content of this air was brought to a constant level by passage over anhydrous calcium sulfate (Drierite). The gas flow rate for all the experiments was 300 sce/min and the flow velocity was 0.18 cm/sec.

The HCl gas was purchased commercially as primary standard HCl-N_2 gas mixtures. Three blends were obtained so that, when they were each mixed with air at ratios of 1 to 9, they yielded slightly nitrogen-rich air atmospheres with 10, 128 and 1260 ppm (by wt) HCl.

The NaCl and Na_2SO_4 used in this program were an ultrapure grade obtained from Alfa-Ventron Products. The NaOH used was ACS electrolytic grade pellets obtained from Fisher Scientific Co. The nominal chloride lot analysis for the NaOH pellets was 0.002 percent. In view of the interest here in gaseous corrodents at low levels the concentrations of the individual halide constituents of the NaOH and Na_2SO_4 were separately determined. These results are presented in Table I.

TABLE I

INTRINSIC HALIDE CONTAMINATION OF STARTING MATERIALS

Compound	Halide Composition*			
	NaF	NaCl	NaBr	NaI
NaOH	2.2	3.3	6.7	0.78
Na_2SO_4	4.4	2.3	4.2	0.08
$(NH_4)_2CrO_4$	6.6	7.3	4.5	0.19

*Expressed in terms of ppm by weight as the sodium salt.

The estimated accuracies of these analyzed values is ±20% of the value reported.

Hot corrosion experiments were conducted with sodium sulfate-coated specimens. The deposits were effected from aerosol sprays of aqueous solutions of Na_2SO_4 onto preheated substrates. The amount of sodium sulfate deposited was determined by weighing the sample before and after the coating application and was normally about 1 mg/cm^2. Occasionally heavier deposits were examined. Cr_2O_3 deposits were prepared by thermal decomposition of ammonium chromate obtained from Alfa-Ventron. The conversion of $(NH_4)_2CrO_4$ to Cr_2O_3 occurred at the beginning of an oxidation test as the sample heated up after insertion into the furnace at the desired temperature. The halogen analyses for the $(NH_4)_2CrO_4$ is listed in Table 1. The ammonium chromate-sodium sulfate deposits were effected from the aerosol spraying of a single aqueous solution. The relative concentrations of the ammonium chromate and sodium sulfate in the aqueous solution used was such that the deposit had a relative composition of two parts $(NH_4)_2CrO_4$ to one part Na_2SO_4 by weight. This was the only composition of the sodium sulfate-ammonium chromate mixture used here. The carbon coatings applied here were prepared by spraying the samples with Aerodag G obtained from the Acheson Colloids Co., Port Huron, Michigan. This product is composed of micron-sized pyrolytic graphite suspended in isopropyl alcohol and is packaged in an aerosol spray dispenser. When both carbon and Na_2SO_4 deposits were examined, the carbon was applied first to the desired level, and then the Na_2SO_4 coating was applied as described earlier. The amount of the deposit, i.e., Na_2SO_4, $(NH_4)_2CrO_4$-Na_2SO_4, carbon and Na_2SO_4-carbon, used in each experiment are appropriately listed in each figure. In the case of ammonium chromate-sodium sulfate mixtures, only the total amount of the deposit is listed.

B. Experimental Procedures

All oxidation experiments were conducted using an Ainsworth type RV-AU-1 balance which is readable to 0.01 mg and reproducible to ± 0.03 mg. The specimens were introduced into a quartz tube (2.5 in. OD) which was within a heated furnace. The temperature inside the three zone Marshall furnace was maintained ± 5°C by a Leeds and Northrup proportional controller series 60.

The NaCl vapors were generated from condensed NaCl in a platinum crucible fixtured to a movable pedestal in the oxidation tube. The temperature of the crucible was measured by a thermocouple fixtured into a quartz tube and lying immediately adjacent to the NaCl-containing platinum crucible.

The data of Ewing and Stern (Ref. 24) was used to calculate NaCl vapor pressures and gas phase compositions. Thus the temperatures of the NaCl-containing Pt crucible and the "anticipated" nominal gas phase compositions used here were 802°C - 1000 ppm, 710°C - 100 ppm, 630° - 10 ppm and 566°C - 1 ppm. However, recognizing that equilibrium may not have been established between NaCl in the condensed and vapor states, the actual NaCl partial pressure was determined from the difference in weights of platinum crucible before and after each experiment. From these calculations, it was found that the empirical vapor pressures were lower than those expected by a factor of about 10 at the three higher temperatures used here, i.e., 802°C, 630°C and 710°C. However, good agreement was observed at the lowest temperature, 566°C. Accordingly, the empirical (as opposed to theoretical) gas phase compositions for atmospheres involving NaCl vapor are herein cited. The weight change data for samples exposed to NaCl vapors at concentrations above 10 ppm were corrected for condensation of NaCl onto the Pt suspension wire. No correction was made for samples oxidized in atmospheres with NaCl vapors at concentrations of less than 10 ppm, nor were corrections made to samples exposed to NaOH or HCl vapors.

The NaOH vapors were similarly generated except that a silver crucible was used instead of the platinum crucible. At 800°C the useful lifetime of the crucible was limited by the differential solubility of silver in NaOH with the silver transporting from the hotter to the colder walls of the crucible. Typically at the end of 24 hours, the silver walls are frequently perforated near the surface of the molten NaOH. No such problems were encountered at the lower temperatures. Additionally, with the NaOH experiments, a tube filled with NaOH was inserted into the air line before the Drierite to remove CO_2 from the inlet air.

The thermodynamic data used to calculate vapor pressures for gaseous NaOH and $(NaOH)_2$ were the JANAF tables (Ref. 61). On the basis of this data, the

following vapor pressures and equilibrium gas phase compositions were calculated:

T(K)	P_{NaOH} (torr)	$P_{(NaOH)_2}$ (torr)	Vapor Pressure P* (torr)	Conc. (effective Conc.) NaOH** in ppm (by wt.)
700	9.07×10^{-7}	1.10×10^{-7}	1.02×10^{-6}	0.0024
800	7.19×10^{-5}	4.24×10^{-6}	7.61×10^{-5}	0.16
900	2.04×10^{-3}	9.16×10^{-5}	2.13×10^{-3}	4.36
1000	2.85×10^{-2}	9.86×10^{-4}	2.95×10^{-2}	58.9
1100	2.39×10^{-1}	6.50×10^{-3}	2.46×10^{-1}	481.

*$P = P_{NaOH} + P_{(NaOH)_2}$

**Effective conc. NaOH = conc. NaOH + 2 x conc. $(NaOH)_2$.

Thus, the temperatures and "nominal" anticipated concentrations used in this study are 727°C - 58.9 ppm, 627°C - 4.36 ppm, and 527°C - 0.16 ppm. No weight change data for the NaOH was recorded. This is due to experimental difficulties involved in precisely weighing condensed NaOH in an air atmosphere containing trace amounts of H_2O and CO_2. On the basis of our previous NaCl experience, the actual NaOH partial pressures are expected to be low by approximately an order of magnitude. Also, some of the NaOH vapors will be lost by interaction with the quartz tube walls. Accordingly, the actual NaOH partial pressures are likely considerably lower than theoretical values.

It should be emphasized that the oxidizing specimens were exposed to temperatures much higher than were seen by the NaCl-or NaOH-containing crucibles. Thus there was no chance that the vaporizing NaCl or NaOH had transported from the cooler crucibles to condense onto the hotter oxidizing specimens.

Subsequent to oxidation, selected samples were examined by optical metallography, x-ray diffraction, scanning electron microscopy (SEM) and transmission electron microscopy techniques. Chemical analyses were frequently performed in the course of scanning electron microscopy studies by energy dispersive x-ray analysis techniques (EDAX).

IV. EXPERIMENTAL RESULTS AND DISCUSSION

The results discussed in this section are divided into three catagories:

A. NiAl: An Alumina Former
B. Ni-25 wt% Cr and Chromium: Chromia Formers
C. B-1900: A Superalloy

A. NiAl: An Alumina Former

1. Gaseous Studies

a. Oxidation in Air Alone

i. Thermogravimetric results

NiAl is a classical alumina former. The rate of weight gain for NiAl oxidized in pure air at 900 and 1050°C is shown in Figs. 1 and 2, respectively, in excellent agreement with the literature (Ref. 62).

ii. Metallographic results

During 1050°C oxidation, an adherent dense Al_2O_3 layer is formed, Fig. 3. Occasionally an area of the NiAl substrate can be seen where the Al_2O_3 layer spalled on cooling to room temperature, Fig. 4. Such rupturing did not occur isothermally since the substrate would have attempted to reform a protective oxide scale and no indication of any such healing oxide scale was observed. Oxidized samples of NiAl when examined by x-ray diffraction techniques indicated only the β-NiAl substrate because the Al_2O_3 scale was so thin.

The sample oxidized in air at 900°C exhibited a microstructure that appears identical to that exhibited by the sample oxidized at 1050°C, Fig. 5.

b. Oxidation in Air with NaCl(g)

i. Thermogravimetric results

The thermogravimetric data for samples oxidized at 900 and 1050°C in atmospheres containing approximately 1-140 ppm NaCl is also shown in Figs. 1 and 2, respectively. No significant differences in the thermogravimetric data occur between samples exposed to pure air and those exposed to NaCl-containing air atmospheres. However, this does not mean that NaCl vapors are innocuous. The effect of NaCl vapor on the weight gain data is further discussed in the following section.

ii. Metallographic results

In the presence of NaCl vapors, marked differences are seen in the morphologies of the Al_2O_3 scales formed on NiAl. At 1050°C the whiskers, formed on the surface of samples of NiAl exposed to 10 and 130 ppm NaCl, were shown by transmission electron microscopy techniques to be α-Al_2O_3, Figs. 6 and 7. No dramatic differences are seen in the whiskers grown with two different NaCl vapor concentrations (10 and 130 ppm) except that the higher NaCl level produces whiskers which are more blade-like while the lower level results in more needle-like Al_2O_3 crystals. EDAX techniques indicated only the presence of alumina in these fibers. Even though they were extensively sought for, neither sodium nor chlorine (above background levels) were detected in the whiskers growing on the surface, in the NiAl substrate or at the gas-oxide interface of the dense Al_2O_3 layer. The Al_2O_3 whiskers grew from the dense Al_2O_3 layer which, in turn, formed on the NiAl substrate, Fig. 8.

The surface of a sample oxidized for 24 hours at 900°C in the presence of 16 ppm NaCl is shown in Fig. 9. The dense oxide layer has extensively spalled upon cooling. The spallation did not occur at temperature since there is no evidence of oxide reformation in any of the spalled areas. Furthermore, this type of spallation was not observed in the samples exposed in the absence of gaseous NaCl. At higher NaCl vapor concentrations, numerous small Al_2O_3 crystals had grown on the dense Al_2O_3 scale, producing a plush carpet-like appearance, Fig. 10.

In an attempt to determine if very low levels of NaCl had a similar effect on the oxidizing substrate, an NiAl sample was oxidized at 900°C in an atmosphere containing 0.61 ppm NaCl. The general surface of the oxidized sample appears as if, at temperature, the oxide scale was in the continual process of locally forming, breaking and then reforming, Fig. 11. At a higher magnification a large amount of surface heterogeneity in the growing oxide scale is apparent, Fig. 12, as well as cracks in the growing oxide scale. In localized regions of the oxide surface, Al_2O_3 whiskers predominate, Fig. 13. While the density of whiskers is much smaller than were observed on the surface of the sample exposed at 900°C to 16 ppm, the whiskers seen here are comparatively larger. In other areas, the compact Al_2O_3 oxide scale has spalled and was at various stages of reforming and healing when the experiment was terminated, Figs. 14-16. The black appearing regions in Fig. 17 represent areas where the oxide scale has broken and fallen back to the compact oxide-surface showing the side of the oxide scale which was initially attached to the substrate metal, Fig. 18. By comparison, Fig. 19 shows that Al_2O_3 whiskers are growing from the inverted base (or original surface) of a similar spalled Al_2O_3 oxide layer. The sample shown in Fig. 18, however, had been oxidized at 1050°C in air containing 128 ppm HCl, not NaCl, cf. section IV, A, 1, c. The EDAX technique applied to the sample oxidized in an HCl - air atmosphere indicated no chlorine in the fibrous Al_2O_3 growths either on the original surface or on the upturned sections. Furthermore, no chlorine was detected at the surface of the exposed substrate.

The microstructure of the sample exposed to 0.01 ppm NaCl is of particular interest. Fine Al_2O_3 fibers have formed on the blackened surfaces, Fig. 19. This effect suggests that the compact oxide spalled at temperature and that spallation occurred long enough before the experiment was terminated to allow for the Al_2O_3 fibrous growth to occur there. Furthermore, examination of the base of the overturned oxide in regions where Al_2O_3 fibrous growths were not present indicated a substantial level of both sodium and chlorine at levels commensurate with what was obtained from the examination of an NaCl standard, Fig. 20. This is the only kind of region where Na and/or Cl has been detected in NiAl samples oxidized in NaCl(g) bearing atmospheres. The detection of Na and Cl on this type of surface was not limited to this isolated area of the spalled surface. This analysis was typical of numerous separate overturned oxide surfaces. However, the appearance of Na and Cl only on this kind of surface is difficult to understand. Questions arise such as: 1) why it was observed there and not on the original surface of the oxidizing sample and 2) how it could have survived any period of time at that site without vaporizing since at 900°C the partial pressure of NaCl is approximately 3.5×10^{-5} torr (Ref. 24)? Thus it seems possible that this sodium and chlorine are incorporated, at reduced activities, (but not necessarily as NaCl) into the dense Al_2O_3 layer.

It has been shown that, by decreasing the NaCl(g) level (10 to 0.01 ppm) in the oxidizing atmosphere at 900°C, a trend is noted. This trend relates to both Al_2O_3 whisker morphology and the nature of isothermal scale spallation. By increasing the NaCl concentration, the number of Al_2O_3 fibers is increased while their individual size is decreased. Similarly, isothermal scale spallation is decreased by increasing the NaCl(g) level in this range.

Experiments were conducted to determine if the aluminum in the Al_2O_3 whiskers reported here derived either from a rearrangement of the surface Al_2O_3 at the gas-oxide surface or from aluminum at the metal-oxide interface. Both impure (a Coor's alumina crucible of ordinary commercial quality) and high purity dense (99.5 percent from Western Gold and Platinum Co.) alumina were exposed to both pure air and to air containing NaCl vapors. The concentration of NaCl was in the range of 100-200 ppm, at a temperature of 1050°C for 24 hours. Subsequently both samples were examined by scanning electron microscopy techniques. In all cases, whiskers were not observed, Fig. 21. This indicates that the aluminum source for forming the Al_2O_3 does not lie at the surface of the oxidizing NiAl coupons. The Al_2O_3 whiskers are not forming simply in response to a drive to lower the free energy of the surface Al_2O_3 layer.

The inability to grow Al_2O_3 whiskers on Al_2O_3 substrates under the "mild" experimental conditions used here is in full agreement with literature reports describing the preparation of such whiskers where substantially higher temperatures (~1300°C) and more vigorous atmospheres are required (Ref. 25).

Occasionally, a citation in the literature briefly mentions observing a few Al_2O_3 whiskers which formed on oxide scales in the course of an oxidation study.

e.g., Kuenzly and Douglass (Ref. 64). However, because such whisker growth is not concommitantly associated with a large difference in the thermogravimetric weight change data, their presence has been largely ignored.

In the results reported herein, the representative oxide scale formed on the NiAl sample oxidized at 900°C in air has been previously described, Fig. 5. However, an isolated area of that sample indicated a very localized growth of Al_2O_3 whiskers about an imperfection in the dense oxide scale, Fig. 22. The general dense oxide scale surface exhibited an EDAX pattern indicating a very high aluminum level as expected, with only trace amounts of nickel. The latter results perhaps from the electron beam sampling below the oxide into the substrate metal. However, the central particle in Fig. 22 exhibited a high nickel concentration. Since NaCl at trace levels i.e., low ppm values, is expected to be found virtually everywhere and on the basis of both the composition of the central oxide particle and the regular disposition of the Al_2O_3 fibers around it, it may be suggested that an aluminum-rich vapor species formed below the surface of the compact oxide layer, Fig. 22. A certain amount of this chemical species then exited the dense Al_2O_3 oxide layer at the imperfection site. Once in the ambient atmosphere, this moiety then experienced unfavorable thermodynamic conditions and decomposed to yield Al_2O_3 in the form of the whiskers seen in Fig. 22.

The fact that such whiskers have not been observed more frequently likely results from two factors. In the first place, equipment used for oxidation experiments is frequently kept very clean. This itself would tend to minimize the concentration of NaCl vapors which would cause such effects. In the second place, oxidation studies generally emphasize optical metallography as the tool to examine oxide-substrate interface. Although optical metallographic techniques can be used to see whiskers under favorable circumstances, it is not the optimum instrument for examining features such as the Al_2O_3 blades discussed here.

c. Oxidation in Air with HCl(g)

i. Thermogravimetric results

The effect of HCl gas, in the concentrations examined, on the 900 and 1050°C oxidation of NiAl from the viewpoint of affecting the thermogravimetric behavior is not apparent, Figs. 23 and 24.

ii. Metallographic studies

The surface oxide layer of the NiAl sample oxidized at 900°C in the presence of 1260 ppm HCl shows evidence for locally continually forming, breaking and reforming of the oxide scale, Fig. 25. The surface of the oxide scale is replete with short

stubby Al_2O_3 fibers, Fig. 26. By increasing the temperature to 1050°C, and by decreasing the level of HCl in the atmosphere to 128 ppm, long thin Al_2O_3 fibers were obtained, Fig. 27. The trend in which a higher concentration of HCl in the atmosphere results in more but smaller whiskers mirrors the behavior observed for NaCl(g).

The sample of NiAl oxidized at 1050°C in air containing 10 ppm HCl, Fig. 28, shows significantly fewer whiskers than were seen on the surfaces of samples similarly oxidized in atmospheres containing higher levels of HCl gas. Additionally, the whiskers found here exhibit a large range of sizes. Most are a few tenths of a micron in length while a few have lengths of greater than 10 microns. The latter size is more nearly like that observed after exposure to higher levels of HCl in the oxidizing atmosphere.

To further confirm that the aluminum for the transport process is derived from below the metal oxide interface, a sample of NiAl was oxidized at 1050°C for 64 hours in air in a pristine apparatus in order to develop a thick protective oxide scale. Then without removing the sample from the furnace, HCl(g) was added to the atmosphere at a level of 128 ppm and oxidation was continued an additional 25 hours. Examination of the sample by SEM techniques showed, Fig. 29, far fewer whiskers than were observed in the case of the sample oxidized at the same temperature and HCl(g) concentration. This is the anticipated result if the formation of these whiskers is controlled by diffusion through a protective alumina scale.

d. Oxidation in Air with NaOH(g)

i. Thermogravimetric results

The thermogravimetric data for NiAl exposed to NaOH vapors at 58.9, 4.4 and 0.16 levels are shown in Fig. 30.

ii. Metallographic results

Examination of the NiAl sample exposed to nominally 58.9 ppm NaOH at 1050°C for 24 hours via SEM techniques indicates a surface for the most part similar to that seen on simple oxidation, cf. Figs. 3 and 5. However, there are some important differences. Shown in Fig. 31, large areas of the scale had spalled apparently on cooling since the underlying exposed metal substrate exhibited no indication of additional oxidation. The sample oxidized at 1050°C in the absence of NaOH(g) exhibited no such tendency to spallation upon cooling. However, not infrequently, regions of the surface were encountered where crystals of Al_2O_3 were observed, Fig. 32. No Na was detected by EDAX techniques anywhere on the surface. It was expected that a condensed sodium aluminate phase might have formed on the surface as a result of the interaction of NaOH with the Al_2O_3 surface.

In view of the fact that impurity levels, i.e. ppm values, of chloride were present in the condensed NaOH, it cannot be unequivocally concluded that the Al_2O_3 blades observed here resulted from the NaOH. Also the morphology of the Al_2O_3 crystallites found here is different from that seen in oxidation involving the NaCl(g). The reason for this difference in morphology is not currently understood.

The large degree of spallation present, cf. Fig. 31, is likely the result of the NaOH(g) present. Spallation of the precise nature found here was not observed in the case of NaCl and HCl vapors in the oxidizing atmosphere.

e. General Discussion of the Effects of NaCl(g), HCl(g) and NaOH(g) on the Oxidation Behavior of NiAl

The results of these experiments show that gaseous products interact with oxidizing NiAl. A product of this interaction is Al_2O_3 whiskers which form on the dense Al_2O_3 layer. These whiskers are not observed unless the environment contains gaseous NaCl or HCl and possibly NaOH.

A number of mechanisms involving fiber growth are possible. Potential growth mechanisms can involve compact oxide growth stresses or chemical vapor transport processes. Chemical vapor transport processes might result from reactions involving either Al_2O_3(c) alone or Al_2O_3(c) with a gas phase corrodent, i.e., HCl, NaOH or NaCl(g). In turn, NaCl(g) could react with Al_2O_3 either directly as NaCl or indirectly as its hydrolysis products, NaOH and HCl. These possibilities will be discussed further.

Kuenaly and Douglass (Ref. 64) have suggested that Al_2O_3 whiskers, observed in oxidation experiments involving Ni_3Al specimens, grew by a cation diffusion mechanism resulting from growth stresses in the compact oxide scale. If this is the case in the work discussed here, then it might be expected that, if oxide scale growth stresses and cation, i.e., Al^{+3}, diffusion through Al_2O_3 were the dominant factors in Al_2O_3 whisker growth, Al_2O_3 whisker growth should have occurred independently of the presence or absence of NaCl(g) in the oxidizing atmosphere. Furthermore, differences in NaCl(g) concentrations should have no effect on whisker morphology. However, differences --though subtle -- in Al_2O_3 whisker morphology are seen for samples oxidized at the same temperature and different levels of NaCl(g) in the oxidizing atmosphere. Thus, this mechanism does not explain the effects reported here. Similar comments can be made for experiments involving HCl and NaOH.

With respect to the possible chemical vapor transport processes, a conceptual reaction for the Al_2O_3 fiber growth might involve the disproportionation-vaporization of Al_2O_3(c):

$$Al_2O_3(c) \rightarrow AlO(g) + AlO_2(g). \qquad (10)$$

However, the blank experiments involving dense Al_2O_3 failed to show any whisker growth. This result is readily anticipated since at 1300°K the calculated K_p for the above reaction is approximately 10^{-43} (Ref. 61). Therefore, a disproportionation-vaporization mechanism is again not applicable.

Another chemical transport process could involve the reaction of HCl(g) with Al_2O_3. The HCl vapors for such reactions could be intentionally present in the oxidizing atmosphere or derive from the hydrolysis of NaCl, i.e.,

$$NaCl(g) + H_2O(g) \rightarrow NaOH(g) + HCl(g). \qquad (20)$$

The HCl(g) present would then diffuse through the dense Al_2O_3 scale formed on the oxidizing NiAl sample. At the metal-oxide layer interface the HCl could react either with the Al_2O_3 scale itself or with the aluminum in the substrate. Examples of the former equilibria are:

$$Al_2O_3(c) + 2HCl(g) = 2AlOCl(g) + H_2O(g), \text{ and} \qquad (21)$$

$$Al_2O_3(c) + 6HCl(g) = 2AlCl_3(g) + 3H_2O(g). \qquad (22)$$

The free energy values for these reactions at 1300°K are positive and quite large, i.e., 142 and 77 kcal for reaction 21 and 22, respectively (Ref. 61). Similarly, the reaction involving the substrate can be represented by

$$Al(\text{in NiAl}) + nHCl(g) = AlCl_n(g) + \frac{n}{2} H_2(g), \; n = 1, 2, 3. \qquad (23)$$

The free energies for these reactions at 1300°K are -13, -27, and -50 kcal for the formation of the monochloride, dichloride and trichloride, respectively, (Ref. 61).

Thus, if the dense Al_2O_3 oxide layer can keep the oxygen potential sufficiently low at the metal-oxide interface and if the HCl and aluminum halides and oxyhalides can diffuse through the dense Al_2O_3 scale, then Al_2O_3 whiskers could form from the appropriate disproportionation reactions. Such a mechanism would not allow for easy "short circuit" diffusion of aluminum halide gaseous species through cracks in the protective Al_2O_3 scale because, if HCl and the appropriate aluminum vapor species can diffuse through such cracks, so could oxygen. Such oxygen would then interact with the transporting aluminum vapor species forming Al_2O_3 which would be expected to plug up such easy diffusion paths. The localized Al_2O_3 crystals observed in the blank specimen oxidized at 900°C are not readily explained by such a model unless local inhomogeneities, e.g., differences in chemical composition of the substrate, excluding oxide cracks were responsible. Grain boundary diffusion would not be precluded by such a model as long as the diffusivity of the oxygen was much less than that for the responsible halogen and aluminum-halogen vapor species.

A mechanism such as this would suggest extensive and virtually continuous dense oxide scale rupture, spallation and reformation at constant temperature. As more and more material was removed from the scale-metal interface, the oxide scale would become locally nonadherent. Cracks then would locally develop in the scale because of heterogeneous dense scale growth kinetics. Gross oxidation of the substrate immediately below the locally spalled area would then proceed rapidly as a protective scale tried to reform. This type of behavior was observed in NiAl oxidized at 900°C in an atmosphere containing 0.61 ppm NaCl(g).

The transport of aluminum to form Al_2O_3 blades has been described in terms of a cycle involving aluminum chloride or aluminum-oxychloride vapor species derived from HCl vapors. Stearns et al. (Ref. 65) and Fryburg et al. (Ref. 66) have observed the gaseous species $(NaCl)_{1,2,3}$ CrO_3, $(NaOH)_{1,2}$ CrO_3, $(NaCl)_{1,2}(MoO_3)_3$ and $(NaOH)\cdot MoO_3$. These vapor species may be viewed as volatile complexes of NaCl (or its hydrolysis product NaOH) and a metal oxide. If similar but as yet unidentified species exist in case of alumina, the overall interpretation of the transport effect suggested above in the case of HCl remains the same while the specifics, e.g., the vapor species responsible for transport, will obviously differ.

On the basis of the surface structures seen for NiAl samples exposed to slowly moving oxidizing atmospheres containing NaCl and HCl vapors, the thermogravimetric data for such samples should not yield net weight losses. The aluminum removed from the alloy by such vapor processes is partially redeposited on the outer surface of the oxide layer. However, in a rapidly moving gas stream, the fine Al_2O_3 whiskers would not be expected to form on the substrate surface. Rather the chemical species responsible for their growth would be swept down the turbulent gas stream. Accordingly, examination of turbine hardware would only fortuitously be expected to show the presence of such Al_2O_3 fibers.

Furthermore, from empirical observations of the factors leading to Al_2O_3 whisker formation, the higher the temperature the more effective will be the diffusivity of pertinent vapor species through the dense Al_2O_3 oxide layer and so aluminum will be increasingly more rapidly removed from below the dense Al_2O_3 scale. Again, NaCl and HCl for such processes need not be reformed in the chemical cycle. In the 1 ppm NaCl-air composition range, the NaCl(g) should be lost to and gained from the atmosphere of a marine or industrial gas turbine, in the absence of an unidentified chloride sink, at approximately equal rates (Ref. 21). Although these experiments dealt strictly with NiAl, similar NaCl(g), HCl(g) and possibly NaOH(g) effects are expected with other coating and alloy compositions which are also Al_2O_3 formers.

This description has primarily considered the effects of NaCl(g) on the oxidation behavior of NiAl and inferred that HCl(g) and possibly NaOH(g) behave similarly. However, differences may exist. For example with 1260 ppm HCl in the atmosphere at 1050°C isothermal buckling and cracking of the Al_2O_3 scale was evidenced. It is not known if NaCl(g) at these concentrations and temperatures would behave similarly.

The description here of aluminum transport effects has been both speculative and qualitative because of our present lack of knowledge of specific factors controlling this effect. The precise nature (composition and properties) and the diffusion mechanism(s) responsible for transport through an otherwise dense alumina scale are unknown. Thusly, later in this report, when reference is made to an aluminum-containing vapor species responsible for alumina whisker growth, the notation "Al-NaCl" will be used to empirically describe this moiety. Furthermore, this notation is not meant to imply that only one chemically distinct aluminum-bearing vapor species is responsible for all the aluminum transport effects observed here.

2. Condensed Studies

a. Loss of NaCl from Pure Na_2SO_4

The amount of sodium chloride observed in the nominally ultrapure grade Na_2SO_4 is greater than that needed in simple oxidation to yield both α-Al_2O_3 whisker growth and isothermal Al_2O_3 scale spallation, cf. Table 1. Accordingly, the anticipated rate of loss of NaCl from pure condensed Na_2SO_4 was examined as a function of time at 900°C. Samples of the pure Na_2SO_4 were placed into a box furnace held at 900°C for periods of 2, 6, 24 and 48 hours. The samples were subsequently analyzed in duplicate and the data presented in Fig. 33. These results show that, contrary to expectations, the level of sodium chloride in the Na_2SO_4 melts rose over a period of 24 hours to a level of about 20 ppm. This increase in chloride content cannot be attributed to the preferential vaporization of Na_2SO_4 and concomitant enrichment of the residue in NaCl. At 900°C Na_2SO_4 and NaCl exhibit partial pressures of 2.5×10^{-5} and 2.5 torr, respectively, (Refs. 67 and 24). Therefore the NaCl responsible for the chloride increase in the melt must have come from the furnace atmosphere. The furnace used for this work was an ordinary laboratory box furnace which has been frequently used in the past for Na_2SO_4 corrosion studies and no special precautions were taken to assure that NaCl was not present.

Thus, these results indicate that NaCl at low ppm levels is not easily lost by preferential vaporization from molten Na_2SO_4. It can be suggested that Na_2SO_4 deposits in actual corrosion environments contain at least this concentration of NaCl. Wolters determined the NaCl-Na_2SO_4 phase diagram and found it to be a simple eutectic with no significant solid solution of NaCl in the Na_2SO_4 (Ref. 68). Flood has remeasured the Na_2SO_4 branch of the liquidus and has shown that these salts form a practically ideal solution (Ref. 69). Thus it is reasonable to expect that NaCl present at impurity levels (low ppm values) in Na_2SO_4 deposits thermodynamically behaves as it does in the gas phase at similar concentrations.

b. Na_2SO_4 in Air

i. Thermogravimetric results

The thermogravimetric data for Na_2SO_4-coated samples of NiAl oxidized at 900 and 1050°C are shown in Figs. 34 and 35, respectively.

ii. Metallographic results

The microstructure of the Na_2SO_4-coated NiAl exposed at 900°C has been described in the literature and is shown in Fig. 36 (Ref. 42). The precipitated phases at the base of the oxide scale (in the Ni_3Al layer) are rich in aluminum and sulfur and are presumably Al_2S_3, Fig. 37. Occasionally, however, the larger of these particles extend into the Al-depleted NiAl region, Fig. 38. Of significance, however, is the observation that the portions which extend furthest into the aluminum-depleted β (or NiAl) area are enriched in oxygen, not sulfur, Fig. 39. In traversing these particles from the β substrate to the oxide-atmosphere interface, the composition of such particles converts from oxides, to sulfides, to a mixture of sulfides and oxides and finally to only oxides. This result is not anticipated from results reported in the literature which only report the presence of sulfur-rich particles, presumably Al_2S_3, in this region of the oxidized sample (Ref. 42). Furthermore, such oxygen-rich areas are not found in particles totally retained in the γ' zone near the NiAl interface.

It can be argued that this morphology is anticipated if the protective alumina scale ruptured and suddenly exposed the aluminum-depleted substrate to a high oxygen potential, i.e., the sulfate melt. The rapid depletion of oxygen by oxide formation would then result in a sudden increase in sulfur potential leading to aluminum sulfide formation behind the oxide front (Refs. 13-17).

c. Na_2SO_4 in Air With NaCl(g)

i. Thermogravimetric results

The thermogravimetric data for samples coated with Na_2SO_4 and oxidized in air with various amounts of NaCl(g) present at 900 and 1050°C is shown in Figs. 34 and 35, respectively. At 900°C there is apparently no significant difference observed in the oxidation behavior of Na_2SO_4-coated NiAl for NaCl(g) concentrations ranging from 1 to 144 ppm. However, examination of the surface of the Na_2SO_4-coated NiAl sample exposed to 144 ppm NaCl(g) at 900°C shows profuse deposits of α-Al_2O_3 whiskers, Fig. 41. Similar whiskers were observed on samples oxidized in NaCl vapor-containing atmospheres. One possible explanation for such whisker growth involved stresses in a growing protective alumina oxide scale. However, as shown in Fig. 41, the Al_2O_3 whiskers observed here have clearly not developed on a highly

stressed oxide substrate. A potential mechanism for the growth of such crystals here is most likely the same chemical vapor transport processes involved in the oxidation of NiAl in atmospheres containing NaCl, HCl and possibly NaOH. In light of the possibly enhanced vaporization of $Na_2SO_4(c)$ effected by NaCl vapor alone (Ref. 55), a spot test was used to confirm the presence of $Na_2SO_4(c)$ on the surface of the sample. The results of the spot test were positive. Therefore, these whiskers did not grow on the surface of the NiAl sample after all the Na_2SO_4 had been removed from the oxidizing surface. Since NaCl(g) has been shown to cause whisker growth, the source of the whisker promotor is the small quantity always present in the alkali salt at contaminant levels.

At 1050°C, Fig. 35, the addition of NaCl(g) to the atmosphere apparently mitigates the corrosion effects from condensed Na_2SO_4 over the time span examined here, i.e., 24 hours. The greater the NaCl(g) partial pressure at 1050°C the longer is the incubation period before accelerated oxidation effects occur. The sample of Na_2SO_4-coated NiAl oxidized at 1050°C for twenty-four hours in an atmosphere containing 199 ppm NaCl has been largely unaffected by the molten Na_2SO_4 deposit, Fig. 40.

The experimental results show that NaCl present in the air or in solution in Na_2SO_4 can result with and transport aluminum from the scale-substrate interface to the outer surface. At 900°C, the role of NaCl is most likely restricted to scale rupture and the development of an aluminum depletion zone in the substrate. The local absence of a protective Al_2O_3 layer and the presence of an extended aluminum-depletion layer have been shown to be sufficient to yield accelerated rates of attack of presulfidized NiAl oxidized at 1000°C in oxygen, cf., Fig. 12 in Ref. 70. This situation is exactly analogous to that reported here once the protective Al_2O_3 layer is ruptured. This interpretation is not in contradiction with results in the literature in which presulfidized B-1900, Waspalloy and U-700 were found to oxidize at rates comparable to that of the sulfur-free alloy even though the presulfidation treatment yielded substrate microstructures with sulfide precipitates in depletion zones similar to those found after exposure of the base materials to Na_2SO_4-induced corrosion (Ref. 71). Although microprobe results are not presented, the sulfides formed were most likely those of Cr and refractory metal compounds. However, the aluminum content of the affected zone remained constant. As far as the chemical components comprising gamma and gamma prime, the aluminum level may have been slightly increased because of the loss of the elements which are more prone toward sulfide formation. Thus, the oxidation of those presulfidized samples is expected to yield oxidation behavior similar to that seen by the sulfur-free specimens unless the oxidation behavior of the sulfide particles was critical to the propagation phase of the corrosion process. The affected zone formed in the work presented herein and also by Goebel and Pettit (Ref. 70) involves depletion effects for the element needed at a critical concentration to effect protective scale foundation, i.e., aluminum.

The effect of NaCl vapor on the 1050°C Na_2SO_4-induced hot corrosion of NiAl was to mitigate the effects of the condensed Na_2SO_4. This may occur via the following reaction

$$Al\left[\begin{array}{l}\text{from the substrate or from}\\ \text{the scale at the scale}\\ \text{substrate interface}\end{array}\right] + NaCl(g) \rightarrow \text{"Al-NaCl"}(g). \qquad (24)$$

It has already been proposed that the "Al-NaCl" species, forming at the metal-oxide interface, is stable under low partial pressures of oxygen. Upon diffusing through the Al_2O_3 scale, this species encounters a higher oxygen partial pressure in the ambient atmosphere in which it is thermodynamically unstable. The result is the decomposition of this species to yield Al_2O_3 whiskers as has been discussed earlier. Similarly, the "Al-NaCl" species also experiences an increased oxygen activity if a film of Na_2SO_4 is present. The effect of Na_2SO_4 can be described in terms of the following equilibrium:

$$Na_2SO_4(c) = Na_2O(c) + SO_2(g) + 1/2\ O_2(g). \qquad (25)$$

The "Al-NaCl" species will remove oxygen from $Na_2SO_4(c)$ or the phases in equilibrium with it (cf. Eq. 25) to yield a form of alumina "Al_2O_3" and release NaCl(g) to regenerate the cycle. If this "Al_2O_3" is available in sufficient amounts to react with the sodium oxide yielding $NaAlO_2$, the protective scale breakdown process will be delayed as will the sulfidation-initiation process. It is suggested, based on the results presented here, that the "Al-NaCl" flux is large enough at 1050°C but not at 900°C for the NaCl(g) levels examined here to supply the necessary amount of aluminum (as "Al_2O_3") to delay the protective scale breakdown process. Furthermore, the transport of "Al-NaCl" across the protective scale may be sufficiently rapid so that the production of Al_2O_3 is high compared with its removal by interaction with Na_2SO_4 and the phases in equilibrium with it, particularly sodium oxide. Under such circumstances, alumina whiskers are anticipated to be found on the oxide surface. This situation will be particularly possible in atmospheres with high NaCl(g) levels, cf. Fig. 41.

It is tempting to describe the beneficial behavior of NaCl(g) toward the Na_2SO_4-induced hot corrosion of NiAl at 1050°C by the term "inhibitor." However, as is obvious from the discussion, NaCl(g) does not function as an inhibitor in the usual sense of the word. Cr_2O_3, an example of such an inhibitor, reacts directly with the Na_2SO_4 deposits. The metallic substrate does not interact with the Cr_2O_3. On the other hand, the beneficial effect of NaCl(g) is only obtained by direct interaction with the substrate. The mode of this interaction results in the direct

sacrificial loss of aluminum from the substrate. This work suggests the use of an aluminum compound as an inhibitor (in the usual sense of the word) injected into the combustion chambers may or may not be effective. The success, however, will depend on whether, in the gas or condensed state, suitable reducing conditions exist under which an "Al-NaCl" moiety can preferentially be formed with the aluminum contributed by the inhibitor.

d. Na_2SO_4 in Air with HCl(g)

i. Thermogravimetric results

The thermogravimetric data for the effect of HCl(g) on the Na_2SO_4-induced oxidation of NiAl is presented in Figs. 43 and 44.

ii. Metallographic results

The microstructure of the sample corroded at 1050°C with 128 ppm HCl shows oxide-filled pores connected to the surface. Some of these pores also appear empty and are connected to the oxide-filled pores; finally there are some empty pores which appear isolated and exhibit smooth and shiny internal surface, Fig. 45. These latter exhibit certain similarities to Kirkendall voids. If material was present in these voids, it was removed during metallographic polishing procedures. In the region of the substrate near the oxide filled pores, an apparent phase change to γ' is often observed. Also a martensitic-like structure is observed, Fig. 46. This latter feature is frequently noted in the depleted β-NiAl phase near oxide particles in Na_2SO_4-coated NiAl samples oxidized at 1050°C but is not seen in similar samples oxidized at 900°C.

e. Carbon in Air

i. Thermogravimetric results

The thermogravimetric data for the sample coated with 0.13 mg/cm^2 of carbon and oxidized at 1050°C is presented in Fig. 47. No observable difference is seen between this sample and the samples simply oxidized in air.

f. Carbon in Air with NaOH(g)

i. Thermogravimetric results

The thermogravimetric data for the carbon-coated samples oxidized at 1050°C in air with NaOH(g) present indicates no large effect of the NaOH species at the NaOH(g) levels examined, Fig. 48.

g. Carbon in Air with HCl(g) or NaCl(g)

i. Thermogravimetric results

Carbon-coated NiAl samples exposed to HCl(g) at 1050°C show initial rates of attack that are proportional to the amounts of HCl present in the oxidizing atmosphere, Fig. 49. The steady state oxidation rates are independent of HCl(g) concentration. Samples oxidized in NaCl(g)-bearing atmospheres at 900 and 1050°C do not reflect any effect of the carbon deposit, Fig. 50.

h. Na_2SO_4 with Carbon in Air

i. Thermogravimetric results

The NiAl samples coated with Na_2SO_4 and carbon and then oxidized at 900°C gives evidence of linear oxidation kinetics, after a brief incubation period, at a rate lower than that found in the absence of the carbon deposits, Fig. 51 and 34. The sample oxidized at 1050°C exhibits thermogravimetric behavior similar to that exhibited by the NiAl sample coated only with Na_2SO_4 and similarly oxidized, Fig. 52, cf. Fig. 35.

i. Na_2SO_4 and Carbon in Air with NaCl(g)

i. Thermogravimetric results

The thermogravimetric data is presented in Figs. 53 and 54 for samples oxidized at 900 and 1050°C, respectively. Here at 1050°C the apparent mitigating effect of NaCl in hot corrosion is again apparent, cf. Fig. 35. However, at 900°C the effect of chloride and carbon on Na_2SO_4-induced accelerated oxidation of NiAl suggests that no obvious relationship exists between the NaCl(g) concentration added to the atmosphere and the rates of attack.

j. Na_2SO_4 and Carbon in Air with HCl(g)

The samples oxidized at 900°C in atmospheres containing 128 and 1260 ppm HCl(g) give evidence of HCl(g) possibly functioning as a corrosion mitigator in the 24 hour period shown, Fig. 55. With 1260 ppm HCl(g) in the oxidizing atmosphere at 1050°C, the HCl(g) does not appear to be functioning as a corrosion inhibitor, Fig. 55. Moreover, in the case of the sample oxidized at 1050°C in an atmosphere of 128 ppm HCl, after about 45 hours, the corrosion rate increases rapidly, Fig. 56. It may be that at 900°C after a sufficiently long period of time accelerated attack will also occur. The nature of this behavior is not currently understood.

k. Na_2SO_4 and Carbon in Air with NaOH(g)

i. Thermogravimetric results

The thermogravimetric data for the samples oxidized at 900 and 1050°C for 24 hours in an atmosphere containing 58.9 ppm NaOH(g) is shown in Fig. 57. This behavior is possibly similar to the effects observed for NaCl(g) and NiAl coated with Na_2SO_4 alone.

l. Na_2SO_4 with Cr_2O_3 in Air

i. Thermogravimetric results

The thermogravimetric data for the samples oxidized at 900°C indicates a slight weight gain lasting for about two hours followed by a low rate of weight loss, Fig. 58. At 1050°C immediate weight loss effects were noted, Fig. 58. This weight loss likely derives from the loss of SO_3 (SO_2/O_2) and Na_2CrO_4 formed from the reaction involving Cr_2O_3 and Na_2SO_4.

B. Ni-25wt.% Cr and Chromium: Chromia Formers

1. Gaseous Studies

a. Oxidation in Air (dry)

i. Thermogravimetric results

The thermogravimetric data for Ni-25 wt% Cr oxidized in dry air at 900 and 1050°C is shown in Figs. 59 and 60, respectively. These data are in qualitative agreement with results published in the literature for similar alloy compositions oxidized in this temperature range (Refs. 72-74).

ii. Metallographic results

X-ray diffraction results of samples oxidized in air at 900 and 1050°C indicated only the presence of Cr_2O_3 in addition to the nickel substrate. Metallographic examination of samples oxidized 900 and 1050°C failed to show anything unusual. Microprobe examination of the surface of the sample oxidized at 900°C for 24 hours indicated a Cr depletion zone immediately adjacent to the oxide layer. This depletion zone had a width of 2.5μ and a chromium content of 19.2 wt% compared with the base alloy value of 25.1 wt%.

The samples oxidized at 900 and 1050°C showed dense compact oxide scales attached to the substrate metal. A variation of grain sizes and geometric crystalline shapes were seen on the surface of the oxidized sample, Figs. 61 and 62. EDAX scans of the oxide scale indicated the presence of only chromium with trace levels of nickel.

b. Oxidation in Air (wet)

i. Thermogravimetric results

The thermogravimetric data for samples oxidized in air bubbled through water at 25°C is shown in Fig. 63. At 1050°C it made little difference if the air was wet or dry, Fig. 63 cf. Fig. 60. The reason for the apparent differences noted at 900°C is not known, Fig. 63. In either case with or without water in the atmosphere, smooth kinetics are observed. The surface oxide structure of the samples oxidized at 900 and 1050°C appear very similar.

c. Oxidation in Air (dry and wet) with NaCl(g)

i. Thermogravimetric results

Statistical differences in the scaling rates of Ni-25 Cr oxidized in NaCl-bearing atmospheres were observed as compared with the scaling rates in simple oxidation, Figs. 64 and 65 . In the absence of NaCl vapors the oxidation behavior of the specimens was well behaved. However, at 900°C in the presence of NaCl vapors, "S"-shaped curves indicative of breakaway oxidation kinetics were frequently observed when the samples were exposed to NaCl vapors in the approximate range from 1 to 16 ppm. The Ni-25Cr samples exposed to about 100-200 ppm NaCl may have exhibited an "S"-shaped curve, however, the effect could have occurred too near the origin to be detected by the present experimental apparatus. At the lower levels of NaCl in the 0.1 ppm range no "S"-shaped curves were noted within the alloted experimental time. The presence of the "S"-shaped curves has not been observed each and every time NaCl(g) or HCl(g) are present, but this phenomena was not observed unless HCl(g) or NaCl(g) was present in the oxidizing atmosphere. Furthermore, the "breaks" when they occur only happen once. The effect suggests the nature of the scale changed dramatically at the time of the sudden break in the curve. Breakaway oxidation kinetics are not associated here with H_2O vapor unless NaCl(g) is also present in the oxidizing atmosphere, Fig. 66. These results are not in agreement with the work of Lowell and Deadmore relating the rupturing of protective Cr_2O_3 scales forming on a complex alloy with the presence of water vapor in the oxidizing atmosphere. (Ref. 75).

ii. Metallographic results

X-ray diffraction examination of oxide scales formed on Ni-25Cr after oxidation in air with NaCl vapors present at 900 and 1050°C indicated the presence of $NiCr_2O_4$ (spinel) in addition to Cr_2O_3 and the nickel substrate. The spinel was not detected in scales of samples oxidized in air alone.

After 24 hours at 900°C in air with 2.9 ppm NaCl, the surface of the sample appeurs covered with small oxide hills that have apparently formed and reformed numerous times, Fig. 67. The surface of this oxide scale exhibits grains which

for the most part are very poorly shaped. The total oxide layer appears porous. The small hills are frequently broken with their bases covered with small non-geometric grains like those seen on the surface, Fig. 68a. These grains according to the EDAX are Cr-enriched. Occasionally, however, a hill has its surface broken, and on the bottom are large geometrically shaped crystals, Fig. 68b. These oxide grains contain more Ni than occurs in the surface grains. It may be that the few hills which show this feature were not broken at temperature. On the other hand those with many fine nongeometric particles at their base ruptured during the oxidation experiment. Such features can be easily seen using optical metallography, Fig. 69. Microprobe examination of the sample oxidized at 900°C in air containing 150 ppm NaCl(g) for 24 hours indicated a substantial Cr-depletion zone, ~20μ, Fig. 70. An average Cr composition in the middle of this zone was 15.8 wt percent Cr. The protective oxide which formed adjacent to the substrate was Cr-enriched (58.3 w/o) but still contained about 5.1 w/o nickel. The oxide adjacent to the Cr-rich oxide scale was enriched in nickel (64.2 w/o percent) and contained 7.8 w/o percent Cr. The effect of the NaCl(g) in the oxidizing atmosphere has been to substantially decrease the levels of Cr near the metal-oxide surface and to effect a substantial Cr-depletion zone in the substrate compared to that found for the Ni-25 Cr alloy after oxidation in air alone.

The effect of NaCl vapors in the oxidizing atmosphere on the scales forming on the Ni-25Cr is more apparent in samples oxidized at 1050°C. The surface of the sample oxidized at 1050°C, in the absence of NaCl vapor, showed a highly convoluted Cr-rich oxide layer lying above the base metal alloy, Fig. 62. Only trace amounts of Ni were found in this outer oxide layer. As the NaCl(g) level is increased, the oxide scale becomes progressively more heterogeneous. At 3.50 ppm NaCl(g) in the oxidizing atmosphere, numerous breaks are observed in an inner compact oxide layer. The oxide forming in these breaks has the same approximate chromium and nickel levels as the base metal alloy, Figs. 71 and 72. As the concentration of NaCl is increased to 13.3 ppm NaCl, the oxide layer becomes increasingly more heterogeneous with crystals of pure Cr_2O_3 as well as eruptions of Ni-enriched Cr oxide (perhaps the $NiCr_2O_4$) spinel quite evident, Figs. 73 and 74. As the NaCl(g) concentration is increased even further to 128 ppm, the outer oxide surface consists of both large-grained oxide particles (rich in both Cr and Ni) and fine-grained oxide particles containing virtually only Cr, Fig. 75. Below these oxide particles, an apparently dense Cr_2O_3 oxide layer is found, Fig. 76.

The combined effect of water vapor and NaCl(g) on the oxide structure of the sample oxidized at 1050°C for 24 hours results in a more uniform and dense oxide scale than is found in the absence of the water vapor even with NaCl(g) present, Fig. 77.

It should also be pointed out that deposits collected in experiments involving the Ni-25Cr and elemental Cr indicate that Cr had been transported from the oxidizing samples and had collected on the cooler walls of the apparatus.

Unfortunately, the experimental apparatus used here is not appropriate for determining the nature of the chromium-bearing vapor species responsible for these deposits. In the past, chromium-chlorine containing species such as $CrCl_2$, $CrCl_3$ and CrO_2Cl_2 have been frequently proposed as the responsible moieties (Ref. 21, 45, 51 and 53). Recently Stearns et al. (Ref. 65) and Fryburg et al. (Ref. 66) have reported the results of mass spectrometric studies involving the oxidation of chromium and superalloys in oxygen atmospheres containing H_2O and NaCl vapors. They conducted exhaustive searches for the vapor molecules CrO_2Cl_2, $CrCl_2$, $CrCl_3$ and Na_2CrO_4. Their efforts in finding evidence for the presence of these species were unrewarded. The chromium vapor species which they did find were principally $(NaCl)_x\ CrO_3$, x = 1, 2 and 3 and $(NaOH)_x\ CrO_3$, x = 1, 2. Minor amounts of the species $Na_2Cr_2O_7$ and $CrO_2(OH)_2$ were also identified.

Experiments were also conducted in conjunction with Mr. C. A. Stearns, NASA-Lewis Research Center, to determine the effect of gas flow velocity on the rate of chromium removal from the oxidizing sample. Samples were oxidized in flowing oxygen at two different flow velocities, namely 0.18 cm/sec and 1.7 cm/sec. The samples were oxidized at 1050°C in an atmosphere containing 25 ppm NaCl(g). In the case of samples oxidized in oxygen at 0.17 cm/sec, the Cr collection rate was 35 µg/hr. Subsequent examination of the surfaces indicated that the higher flow velocity had elicited smaller but more numerous breaks in the oxide scale, Fig. 78. The lower flow rate on the other hand had caused fewer but comparatively larger breaks in the oxide scale, Fig. 79. Thus this brief experiment has shown that, at least in an atmosphere of oxygen containing small amounts of NaCl vapor, both the rate of chromium removal from the oxidizing surface and the oxide structure formed on that surface is a function of the flow velocity of the oxidizing gas.

d. Oxidation of Elemental Cr in Air (dry) with NaCl(g)

Because of their technological importance as corrosion resistant materials, much effort over the years has been expended investigating the chromia formers, (Refs. 72-99). Included in this work have been numerous studies involving alloys in the Ni-Cr system near the Ni-25 wt % Cr composition. The results of this work indicate that the scaling behavior of the Ni-25 Cr composition is quite complex. Some of the observations made in this study concerning the effect of NaCl(g) at very low levels on the scaling behavior of Ni-25 Cr have been attributed by others to the intrinsic scaling behavior of the alloy itself. Thus in order to clarify this matter a few experiments were conducted with pure chromium to see if NaCl(g) exhibited similar effects. The use of elemental Cr would avoid difficulties in the interpretation of oxidation data resulting from alloying effects.

i. Thermogravimetric results

The thermogravimetric results for the pure chromium samples oxidized at 900 and 1050°C are shown in Figs. 80 and 81, respectively. Except for the sample exposed at 1050°C to 111 ppm NaCl, the two sets of thermogravimetric data show little difference and agree with literature results for samples oxidized in air alone (Ref. 98). On the basis of the thermogravimetric data alone (except for the highest level of NaCl(g) examined at 1050°C), NaCl(g) has little or no effect on the oxidation process. The thermogravimetric data for the sample oxidized at 1050°C in an atmosphere with 111 ppm NaCl actually shows the continual formation of microcracks which have become integrated into an apparently smooth curve on the relatively insensitive scale used to represent the data in Fig. 81.

ii. Metallographic results

The surfaces of samples exposed at 900 to air and air containing 0.78 and 49 ppm NaCl vapor are shown in Figs. 82, 83, and 84, respectively. No significant differences exist between samples exposed to two levels of NaCl(g). Figs. 83 and 84. But a large difference exists between the samples exposed to air alone, Fig. 82, and those exposed to NaCl vapors, Figs. 83 and 84.

Similarly on the basis of the thermogravimetric data alone little difference is expected between the chromium samples exposed to NaCl vapors at 1050°C, Fig. 81. A possible exception to this might be the sample exposed to 111 ppm NaCl. The oxide scale formed on the sample exposed to air alone, Fig. 85, is strikingly different from that developed on the sample exposed to even 0.23 ppm NaCl, Fig. 86. Increasing the NaCl(g) concentration to the range of 2.2 - 14.4 ppm in atmospheres in which chromium is oxidizing at 1050° results in additional oxide morphology features not seen in the sample oxidized in pure air, Figs. 87 and 88, respectively. Finally, the scale of the sample oxidized in an air atmosphere containing 111 ppm NaCl shows a scale which was continually forming, rupturing and reforming, etc., Fig. 89. This scale is just the type of scale that would be predicted from the thermogravimetric data, cf. Fig. 81. Moreover, this type of scale has been reported for chromium oxidized at much higher temperatures (1200°C) in the absence of NaCl vapors (Ref. 98). However, concerning the sample oxidized at 1200°C (Ref. 98), the surface treatment involved electropolishing in a perchloric acid-acetic acid solution. The anodic oxide film which formed was not removed by subsequent etching. A chromium specimen subsequently etched to remove the anodic film caused by the electropolishing step and then similarly oxidized at 1200°C did not yield either breakaway oxidation kinetics or a ballooned microstructure (Ref. 98).

In all of the samples of chromium oxidized here in a NaCl(g) environment, neither Na nor Cl has been detected by EDAX techniques on the surface of the

scale, in the scale or on the undersurface of scale, or on the surface of the underlying metal. In effect, if it were not known beforehand that these scales had been formed in atmospheres containing varying amounts of gaseous NaCl, it would have been difficult to explain the variety of effects observed on the basis of oxidation in air alone.

Thin chromia platelets have been reported to form at the gas-scale interface of chromium oxidized in dry oxygen at 500°C for 120 hours (Ref. 76). However in the results reported here, cf. Fig. 88c, the chromia needles have grown at the substrate-scale interface, not at the scale-gas interface.

With respect to the "ballooned" oxide microstructure for elemental Cr shown in Fig. 89, it is informative to examine the work of Caplan, Harvey and Cohen (Ref. 98). In their work dealing with the oxidation of elemental chromium, they report largely parabolic oxidation kinetics for an entire range of surface treatments. These treatments range from simply abraded surfaces to various electropolishing and etching treatments. The preferred electrolytic polishing solution is a perchloric acid-acetic acid solution although other solutions were investigated. In each case in which the final treatment involved electropolishing with either a perchloric acid-acetic acid solution or perchloric acid alone and no subsequent etching to remove the anodic film formed, breakaway oxidation kinetics were invariably subsequently observed. Similar effects were reported for Fe-25 Cr (Ref. 98) and Fe-26 Cr-0.5 Si (Ref. 97). Furthermore, these investigators examined the effect of water vapor on the oxidation of chromium and found that it was not responsible for the breakaway oxidation kinetics and the ballooned oxide microstructure. Those results are in agreement with results of experiments reported here.

Giggins and Pettit studied the oxidation behavior of Ni-Cr alloys (including the Ni-20 Cr composition) at 800-1200°C and electropolished samples in a sulfuric acid-latic acid-methyl alcohol solution but did not report subsequent etching of their samples to remove the anodic film (Ref. 73). The significance of their results is that they did not, except for two cases (one involving Ni-15 Cr at 900°C and the second involving Ni-30 Cr at 1200°C), report any breakaway oxidation effects. Also Lowell (Ref. 74) and Davis, Graham, and Kvernes (Ref. 93), using mechanically abraded specimens, did not observe breaks in their thermogravimetric data. Similarly, Michels, in a study largely dealing with the effects of dispersoids on the oxidation behavior of Ni-20 Cr, did not report breaks in the thermogravimetric data relating to Ni-20 Cr (Ref. 95). These results are in agreement with the results presented here in that the blank samples prepared by mechanical abrasion did not evoke breakaway kinetics without NaCl(g) present, with or without water vapor added to the oxidizing atmosphere.

Wood and Hodgkiess (Ref. 72) studied the Ni-Cr alloys and in their work they used a quartz-spring balance which would make it easy to miss the occurrence

of the early scale breakage affect. However they did observe such an effect involving a Ni-27 Cr sample oxidized at 1000°C. In their study the samples were prepared by a variety of techniques and they attributed many of the effects in oxidation to differences in surface preparation. Interestingly enough the electrolytic etch used by Wood and Hodgkiess is the same one which yielded breaks in the TGA curves for Caplan, Harvey and Cohen (Ref. 97). Wood and Hodgkiess reported that not all electropolished specimens were given a subsequent cathodic etch. Some of the samples were thusly examined in the electrolytically polished condition. However no mention is made specifying which treatment each sample received. Wood and Hodgkiess suggested that a "Cr_2O_3" subscale plays a keying role which retains a protective oxide scale adjacent to the metal substrate. Failure then presumably occurs by a mechanism of lifting and cracking accounting for the break in the thermogravimetric data. However, by such a mechanism scale lifting and cracking will occur randomly and more than a single break might be expected to be observed in a thermogravimetric curve for an experiment continued for any reasonable length of time.

On the basis of the work presented herein, an alternative explanation may be suggested. During the electropolishing procedure some residual chloride from the etching solution is trapped within the anodic film which is not completely removed during the subsequent etching step.

Thus the samples of chromium anodically polished but not etched produced microstructures similar to those exhibited by mechanically abraded samples oxidized in an NaCl-bearing atmosphere. Chromium samples either anodically polished in chlorine-containing solutions and subsequently etched to remove the anodic oxide film or anodically polished in nonchloride-containing solutions do not contain intrinsic chloride sources. For the Fe-Cr alloys examined by Caplan and Cohen (Ref. 96), the samples shown to have been electropolished in a perchloric acid-acetic acid solution and not subsequently etched exhibited breaks in the oxidation curves. The presence of a singular break in the data reported by Giggins and Pettit (Ref. 73) for the oxidation behavior of a Ni-20 Cr alloys electropolished and not subsequently etched may have involved the similar entrapment of halogen in the anodic oxide scale.

The experimental observation that not every sample exposed to NaCl(g) produced a break in the thermogravimetric data suggests that the Ni-Cr alloys examined herein may be less susceptible to such effects as compared with pure Cr and Fe-Cr alloys (Ref. 96).

e. Oxidation in Air (dry) with HCl(g)

i. Thermogravimetric results

The thermogravimetric data for Ni-25 Cr oxidized at 900 and 1050°C are presented in Figs. 90, 91 and 92.

ii. Metallographic results

The sample of Ni-25 Cr oxidized at 1050°C in the presence of 10 ppm HCl exhibits microstructures ranging from a presumably dense compact Cr_2O_3 layer with acicular precipitates to internally oxidized regions, Fig. 93 and 94. The extensive regions of internally oxidized material, Fig. 93, are perhaps related to the large break in the thermogravimetric data, cf. Fig. 92.

The effect of low levels of HCl(g) (128 ppm) on the microstructure of the outer oxide scale formed on Ni-25 Cr at 1050°C can be seen in Figs. 95 and 96. Note that below the Cr_2O_3 layer, the grain boundaries of the substrate alloy have been preferentially attacked, Fig. 96. The EDAX unit could detect no measurable differences in Cr levels in areas immediately adjacent to such grain boundaries as opposed to those areas found in the middle of such grains. This effect may be analogous to that already reported for Ni-25 Cr exposed at 1050°C to NaCl.

The cross-sectional microstructure of Ni-25 Cr oxidized at 1050°C in the presence of 1260 ppm HCl indicates the occasional presence of numerous voids clustered at the metal-oxide interface, Fig. 97. The absence of such pores from the interior of samples suggests that these pores are not casting voids. Therefore these voids are possibly Kirkendall effects resulting from Cr depletion in the alloy by the HCl(g) in the oxidizing atmosphere.

f. Oxidation in Air (dry) with NaOH(g)

i. Thermogravimetric results

The thermogravimetric behavior of Ni-25 Cr oxidized in the presence of NaOH(g) suggests that at the 4.36 and 58.9 ppm levels parabolic oxidation kinetics are being observed while at the 0.16 ppm level other effects may be occuring, Fig. 98.

2. Condensed Studies

a. Na_2SO_4 in Air (dry)

i. Thermogravimetric results

The thermogravimetric data for Na_2SO_4-coated Ni-25 Cr is presented in Fig. 99. The initially rapid weight changes (both gain and loss) at 1050°C followed by slow parabolic behavior has been observed by others. Wright, Wilcox and Jaffee (Ref. 99) reported such behavior for a variety of Ni-Cr alloys which had been coated with Na_2SO_4 and subsequently oxidized in 100 torr oxygen at 1000 and 1100°C. Bornstein and DeCrescente have reported the weight loss behavior in the case of Ni-13 Cr and Ni-17 Cr coated with Na_2SO_4 and oxidized in oxygen at 1000°C (Ref. 15). However, Gobel, Pettit, and Goward did not observe this effect in the case of a Na_2SO_4-coated Ni-30 Cr sample oxidized in oxygen at

1000°C (Ref. 42).

ii. Metallographic results

The general surface of the sample coated with Na_2SO_4 and then oxidized at 1050°C is shown in Fig. 100. The bright regions seen in Fig. 100 are large crystals of Cr_2O_3 as determined by transmission election microscopy. Between these areas of well-formed Cr_2O_3 crystals and the nickel-rich chromium-containing surface oxide layer are slightly greyer regions, Fig. 101. These regions contained crystals which, when the sample was examined under a laboratory microscope, appeared to decompose from the heat of the microscope lamp. A magnified view of this debris lying above the compact Ni-rich chromium oxide layer is seen in Fig. 102. The EDAX indicates these particles contain Si. Examination of this material by transmission electron microscopy indicates it is composed of very small crystals of β-SiO_2. The source of this silica could be either the quartz tube containing the experimental gases or the metal sample itself which was cast in a crucible which had a silica binder. Such Si-containing deposits have not been seen before in either the Ni-25 Cr or the NiAl samples examined here.

Similar Cr_2O_3 crystals are also detected but in much smaller numbers in a Na_2SO_4-coated sample exposed to air at 900°C, Fig. 103. The matrix alloy in this micrograph is intentionally out of focus in order to accentuate the surface crystals. No such crystals were observed in samples of Ni-25 Cr subjected to simple oxidation. These crystals suggest that effects occurring at 1050°C also take place at 900°C but at a slower rate. This is consistant with the thermogravimetric data, cf. Fig. 99. Similar results were also observed at 900°C for Na_2SO_4-coated samples oxidized in atmospheres containing NaCl vapors. The substrate below the oxide surface has developed internal sulfides. Although no microprobe or EDAX data has been obtained from these regions, on the basis of other work it is anticipated that these regions are likely composed of a chromium sulfide, Fig. 104.

To determine if the growth of such crystals was an intrinsic property of chromium or if the nickel in the Ni-Cr alloy was necessary for such crystal growth, experiments were also conducted with Na_2SO_4-coated Cr subsequently oxidized at 1050°C. The resulting surface topography is replete with Cr_2O_3 platelets, Fig. 105. In the case of the samples of Ni-25 Cr where similar crystals formed, fewer but much larger Cr_2O_3 platelets developed. In the case of the experiments dealing with Na_2SO_4 deposits on elemental chromium or Ni-25 Cr, neither sodium nor sulfur was detected via EDAX procedures on the surface of the oxide scale. However, Cr sulfides were visible in the substrate.

Wright et al. (Ref. 99) have proposed that such Cr_2O_3 platelets arise from the reversibility of the reaction:

$$Cr_2O_3(c) + 3/2\ O_2(g) + 2\bar{O}(d) = 2CrO_4^{=}(c). \qquad (26)$$

The solution process is suggested to occur where the oxide ion level is high, i.e., the oxide-molten salt interface. The precipitation reaction then reportedly takes place when the oxide ion level is reduced, i.e., near the molten salt-ambient atmosphere interface (Ref. 99).

b. Na_2SO_4 in Air (dry) with NaCl(g)

i. Thermogravimetric results

The data for Ni-25 Cr coated with Na_2SO_4 and subsequently exposed to NaCl vapors in the range of 0.27 to 47 ppm at 900 and 1050°C are presented in Figs. 106 and 107, respectively. These results are analogous to the behavior observed for Na_2SO_4-coated Ni-25 Cr in the absence of NaCl(g). Accordingly based on the thermogravimetric data alone, the effect of NaCl vapor here is not known. However, the tendency to lose weight appears related to the level of NaCl(g) in the atmosphere.

A striking characteristic of the data for Na_2SO_4-coated samples oxidized at 1050°C in the presence of NaCl vapors is the initially large weight loss behavior lasting for several hours followed by very low oxidation (corrosion) kinetics. [The noted exceptions are the samples exposed to 124 and 136 ppm NaCl vapors.] The initial weight losses here correspond approximately to the amount of Na_2SO_4 deposited on the samples.

ii. Metallographic results

Examination of the sample exposed at 1050°C to 124 ppm NaCl shows surface topography almost analogous to that seen for the similarly exposed sample in the absence of NaCl. Again, very slight traces of Si and even finer traces of Ca were detected but could not be definitely assigned to any particular surface feature. Neither sodium nor chlorine were detected in any of the surface structures examined.

In the case of Ni-25 Cr samples coated with Na_2SO_4 and oxidized at 1050°C with and without NaCl vapors present in the atmospheres, the expected dense Cr_2O_3 oxide layer has been modified by the Na_2SO_4. The form of the Cr_2O_3 crystals observed here suggests that they grew by processes similar to those occurring in the case of Na_2SO_4-coated Ni-25 Cr oxidizing in air with no intentional additions of NaCl(g) present, cf. Fig. 100 and 101.

Thus, the molten salt possibly responsible for this crystalline growth has totally vaporized (since neither Na nor S were found by EDAX procedures). This suggestion is not unreasonable in view of the large weight losses associated with the thermogravimetric data, cf. Fig. 99 and 107. The compact oxide layer at the surface of Na_2SO_4-coated samples oxidized at 1050°C according to the EDAX is not likely Cr_2O_3 but the Ni-Cr spinel.

Recalling the deleterious effect of NaCl(g) on the oxidation behavior of both Ni-25 Cr and elemental Cr, experiments involving elemental chromium were conducted with both Na_2SO_4 and NaCl vapors in the atmosphere. Figure 108 shows the effect of 283 ppm of NaCl in the atmosphere on the 1050°C oxidation of Na_2SO_4-coated Cr. Apparently, on the basis of the thermogravimetric data alone and for the times examined here, the Na_2SO_4 mitigates the NaCl(g) attack on chromium, cf. Fig. 81. Subsequent examination of the surface microstructure of this chromium sample showed a dense fine-grained compact chromia layer adjacent to the Cr metal substrate, Fig. 109. Above this layer, Cr_2O_3 platelets are found. No Na, S or Cl were detected by EDAX on the surface of the oxidized sample. However, chromium sulfides were subsequently detected metallographically in the substrate below the metal-oxide interface.

The cause for the apparently beneficial behavior of Na_2SO_4 deposits toward NaCl(g) attack of the chromia formers Ni-25 Cr and Cr is currently not understood. However, this observation is in agreement with comments that in marine and industrial atmospheres containing both NaCl and sulfur species the chromia forming alloys are preferred.

c. Na_2SO_4 in Air (dry) with HCl(g)

i. Thermogravimetric results

The thermogravimetric data for Ni-25 Cr samples coated with Na_2SO_4 and exposed to HCl atmospheres at 900 and 1050°C is presented in Fig. 110 and 111, respectively. The oxidation behavior of the Na_2SO_4-coated samples exposed to 128 ppm HCl at both 900 and 1050°C in the gas atmosphere is, as seen before, commensurate with initially very transitory oxidation kinetics followed by apparently almost simple oxidation kinetics. Apparently at 900°C, 10 ppm HCl in the gas phase is insufficient to cause this type of behavior. The sample exposed to 10 ppm HCl at 900°C exhibited a few segregate yellowish deposits (Na_2SO_4 + some chromium bearing moiety, perhaps Na_2CrO_4) after corrosion while the samples exposed to 128 ppm HCl atmospheres exhibited no such visible deposits.

ii. Metallographic results

The sample exposed at 900°C to atmospheres containing 128 ppm HCl showed both Cr_2O_3 platelets growing from the surface and internal sulfide particles, Fig. 112. The crystals developing on the surface neither totally cover the entire surface nor are they an uncommon surface feature. After 20 hours exposure at 1050°C in air containing 10 ppm HCl, the external growth of Cr_2O_3 crystals is accentuated, Fig. 113. The compact oxide layer at the surface of the metal where a large growth of Cr_2O_3 crystals occurs is thinner and not apparently as dense and compact as where such crystals are absent, Fig. 114.

d. Carbon in Air (dry)

i. Thermogravimetric results

The thermogravimetric data for the oxidation of carbon-coated Ni-25 Cr at 1050°C in air is shown in Fig. 115. This curve is very similar to that shown by Ni-25 Cr in simple oxidation at this temperature, cf. Fig. 60.

e. Carbon in Air (dry) with NaCl(g)

i. Thermogravimetric results

The thermogravimetric results for carbon-coated Ni-25 Cr presented in Fig. 116 are similar to those found for simple oxidation in the presence of NaCl or HCl, e.g. Fig. 64 and 65.

f. Carbon in Air (dry) with HCl(g)

i. Thermogravimetric results

A carbon coating on the Ni-25 Cr sample resulted in almost continuous isothermal scale cracking and slight spallation at 900°C in air with HCl(g), Fig. 117.

g. Carbon in Air (dry) with NaOH(g)

i. Thermogravimetric results

The 1050°C oxidation behavior of carbon-coated Ni-25 Cr in atmospheres containing NaOH(g) indicates isothermal scale breakage and, perhaps, slight spallation effects, Fig. 118. These results are similar to those observed for carbon-coated Ni-25 Cr oxidized in atmospheres containing HCl(g), cf. Fig. 117. The data reported here do not indicate large differences in weight change behavior with variations in NaOH(g) concentrations in the range examined.

h. Carbon with Na_2SO_4 in Air (dry)

i. Thermogravimetric results

The 1050°C oxidation behavior of Ni-25 Cr coated with both Na_2SO_4 and graphite is shown in Fig. 119 and is similar to that observed for the Ni-25 Cr alloy coated with Na_2SO_4 alone, cf. Fig. 99. The amount of time required to remove the Na_2SO_4 deposit (1.72 mg/cm^2) here has increased by approximately a factor of 3 (i.e., 14 hours) compared with the 4 hours needed there to remove 0.56 mg/cm^2, Fig. 99. The carbon is not markedly affecting the behavior

of the Na_2SO_4 deposit with respect to its interaction with the substrates.

i. Carbon with Na_2SO_4 in Air (dry) with NaCl(g)

i. Thermogravimetric results

The Ni-25 Cr samples coated with carbon in addition to Na_2SO_4 and oxidized in air with NaCl(g) exhibit thermogravimetric data similar to that for the oxidized samples coated only with Na_2SO_4, Fig. 120, cf. Fig. 107.

j. Carbon with Na_2SO_4 in Air (dry) with HCl(g)

i. Thermogravimetric data

The thermogravimetric data for samples coated with both Na_2SO_4 and carbon and oxidized at 900 and 1050°C is presented in Fig. 121. These results indicate very erratic behavior quite unlike that followed by samples simply coated with Na_2SO_4 deposits and oxidized in HCl(g) atmospheres, cf. Fig. 111. Furthermore, the rate of loss of the Na_2SO_4 deposits is slower here than was the case when carbon was absent from the deposit. The reason for this behavior is not presently understood.

k. Carbon with Na_2SO_4(g) in Air (dry) with NaOH(g)

i. Thermogravimetric results

The thermogravimetric data for Ni-25 Cr coated both with Na_2SO_4 and carbon are presented in Fig. 122. These results are in qualitative agreement with what has been observed for Ni-25 Cr coated with Na_2SO_4 and oxidized in air alone, cf. Fig. 99. At 900°C slight but erratic weight gains are observed. At 1050°C, on the other hand, uniformly rapid weight loss is observed.

C. B-1900: A Superalloy.

The major thrust of this work has dealt with the elementary though technologically important alumina and chromia formers. However, a few experiments were performed to briefly determine if NaCl(g) at a low activity exhibits any effect on the oxidation behavior of the superalloy B-1900. The composition of B-1900 is 8.0 Cr, 10.0 Co, 1.0 Ti, 6.0 Al, 6.0 Mo, 0.11 C, 4.0 Ta, 0.015 B with the balance nickel (Ref. 100).

The oxidized surface of B-1900 exposed to air at 1050°C for 64 hours is seen in Fig. 123. This surface oxide layer is irregular with many elements from

the substrate present there. This result is in agreement with the work of Fryburg, et al. (Ref. 60) in which B-1900 at 1000°C in oxidation was described as an alumina-former with a little Cr_2O_3 and NiO dissolved in the protective alumina layer.

A B-1900 sample similarly oxidized at 1050°C in air with 195 ppm NaCl, Fig. 124, produced a heterogeneous surface as compared with the sample oxidized in air alone, Fig. 123. In addition, aluminum-rich blades as determined by EDAX are also present, Fig. 124 and 125. These aluminum-rich blades were not seen in the sample oxidized in air alone. Moreover, metallographic cross-sections of this sample showed a typical substrate microstructure that could be associated with the hot corrosion of this alloy, Fig. 126. It is emphasized that no Na_2SO_4 was present nor applied. Based on the previous work and the observation of alumina whiskers on the surface of the B-1900 sample oxidized in air with NaCl(g) present, it is expected that the substrate should exhibit areas highly depleted in γ' (Ni_3Al). Such areas are found in the regions in the substrate immediately below substrate regions affected by the anomolous oxidation process, Fig. 127. It is apparent that Al depletion is occurring faster than γ' coarsening occurs because areas of the substrate adjacent to normal oxide scales showed: 1) much thinner scales and no significant γ' depletion zones; and 2) slight γ' coarsening in the substrate at the base of such oxide scales, Fig. 128.

Therefore, this study has demonstrated that NaCl(g) at low activities affects the oxidation behavior of B-1900. The type of interaction here is similar to that seen in the case of NiAl. However, since B-1900 has much less aluminum than NiAl, i.e., 6.0 wt% compared with 31.06 wt%, respectively, the loss of aluminum in the case of the former will more rapidly lead to internal oxidation and alloy depletion effects as shown here. Furthermore, this can lead to a non-uniform attack of the substrate. Also, as was discussed in the case of NiAl, the NaCl normally present in Na_2SO_4 at impurity levels (low ppm values) is sufficient to effect alloy depletion of aluminum and alumina scale breakdown. Therefore work is needed to characterize the minimum concentration necessary for various gaseous corrodents to effect protective scale breakdown in both oxidizing and Na_2SO_4-induced corrosion conditions.

If the NaCl here is also interacting with the chromium present in the B-1900 substrates, such an interaction was not obviously apparent. However, such interaction, based on the results presented herein for Ni-25 Cr and elemental chromium, would be expected.

Furthermore, it is unreasonable to assume that B-1900 is unique among the superalloys regarding its interaction with NaCl(g). However, the extent of this interaction for other alloys may be different both qualitatively and quantitatively depending on both the alloy chemistry and the exact distribution of the chemical elements among the various phases present for each alloy.

V. SUMMARY AND CONCLUSIONS

The results of this work, largely discussed in each appropriate section, are summarized below:

1. The gaseous compounds NaCl, HCl and NaOH, have been shown to interact at low activities (~ 1 to 1000 ppm) with the alumina former NiAl, the chromia formers Ni-25 wt.% Cr and elemental chromium and the superalloy B-1900.

2. These interactions occur at low concentrations of the gaseous corrodent in both oxidation and sodium sulfate-induced hot corrosion.

3. In oxidation, mixtures of air and the gaseous corrodents form α-Al_2O_3 whiskers on the dense alumina scale. The formation of these whiskers locally depletes the substrate of aluminum and progressively weakens the mechanical bond between the dense scale and the substrate leading to isothermal scale rupture.

4. The rate of alumina scale rupturing varies inversely with the level of NaCl(g) in the oxidizing atmosphere for the concentrations examined here, i.e., approximately 0.1 to 150 ppm (by weight).

5. With respect to oxidation of the superalloy B-1900 in the presence of NaCl(g), Al_2O_3 crystals grew on the surface of the dense oxide scale. The source of the aluminum is the gamma prime which underwent irregular and local depletion along the substrate-oxide interface. The microstructure of the alloy is therefore similar in many respect to that observed for Na_2SO_4-induced corrosion.

6. With respect to the chromia former Ni-25 wt.% Cr, chlorides produce the "S" shaped curves characteristic of breakaway oxidation. Moreover, the oxide scale formed on the surface of the Ni-25 Cr alloy is Cr_2O_3 and $NiCr_2O_4$.

7. In the oxidizing atmospheres containing gaseous chlorides, chromium has been identified in residues deposited downstream from the chromium and Ni-25 wt.% Cr specimens. The vapor species responsible for this transport have recently been reported by Stearns et al. (Ref. 65) and Fryburg et al (Ref. 66) to be principally $(NaCl)_x\ CrO_3$, x = 1, 2, 3, and $(NaOH)_x\ CrO_3$, x = 1, 2. As a result of preferential chromium depletion, an extended Cr depletion zone is formed in the Ni-25 wt.% Cr alloy. Moreover the rate of chromium removal from the oxidizing surface and the type of surface oxide structure formed on Ni-25 wt.% Cr is dependent on the velocity of the NaCl(g)-containing atmosphere flowing across the surface.

8. The structure of the oxide scale formed on elemental chromium is dependent upon the concentration of NaCl(g) in the environment. The highly convoluted scale formed after electropolishing of chromium is reproduced when the metal is exposed to atmospheres containing gaseous NaCl.

9. NaCl found at impurity levels (i.e., low ppm values) in laboratory grade Na_2SO_4 is not preferentially lost by heating the salt at 900°C for 48 hours.

10. The sodium chloride present in Na_2SO_4 is responsible for the formation of Al_2O_3 whiskers that form on the Al_2O_3 surface. The formation of these whiskers infer that aluminum is removed from the metal-oxide interface thereby depleting the underlying area of aluminum and compromising the adherence of the oxide scale.

11. The results presented here suggest the use of aluminum compounds as sulfidation inhibitors. The success depends upon achieving suitable reducing conditions under which an "Al-NaCl" moiety can preferentially be formed with the aluminum supplied by the inhibitor.

12. The presence of carbon codeposited with Na_2SO_4 onto NiAl resulted in lower rates of oxidation at 900°C and virtually no effect at 1050°C. With respect to the alloy Ni-25 wt.% Cr, the thermogravimetric data suggested isothermal scale breakage occurring; the cause is not known.

13. With respect to the hot corrosion of Ni-25 wt.% Cr in the absence of the sodium sulfate, the gaseous NaCl depletes the surface of chromium. In the presence of Na_2SO_4, the role of NaCl(g) is unclear.

14. The precise mechanism involving aluminum transport in both oxidation and Na_2SO_4-induced hot corrosion processes has been described in qualitative terms. Virtually nothing is known of either the precise composition of the gaseous species involved in this transport cycle or the mechanistic pathways for diffusion of the pertinent species through otherwise dense scales. Similar comments also apply to the chromia formers in oxidation except that the vapor species resulting from the interaction of NaCl with chromia have been identified (Refs. 65 and 66).

VI. ACKNOWLEDGEMENTS

The authors gratefully acknowledge helpful discussions with Mr. C. A. Stearns, Dr. F. J. Kohl and Dr. G. C. Fryburg of NASA-Lewis Research Center, Cleveland, Ohio and with Dr. M. A. DeCrescente and Dr. R. A. Pike of the United Technologies Research Center, East Hartford, Connecticut. The efforts of Ms. J. Whitehead, Messrs. R. Brown, L. Jackman, J. Knecht and G. McCarthy for assistance in conducting the experiments presented here are also acknowledged.

VII. REFERENCES

1. Wasielewski, G. E. and R. A. Rapp: High Temperature Oxidation. The Superalloys, p. 287, ed. by C. T. Sims and W. C. Hagel, John Wiley and Sons, New York, New, 1972.

2. Simons, E., G. Browning, and H. Liebhafsky: Corrosion 11, 505 (1955).

3. Dean, A. V.: Investigation into Resistance of Various Nickel and Cobalt Base Alloys to Sea Salt Corrosion at Elevated Temperature, N.G.T.E. Report, January 1964.

4. Gambino, R.: Hot Corrosion Mechanism Studies, U.S. Naval Marine Engineering Laboratory Final Report, N-(600) (61533)-63219, February 1966.

5. Seybolt, A. U. and A. Beltran: ASTM STP-421, Philadelphia, Pennsylvania p. 21 (1967).

6. Seybolt, A. U.: TMS-AIME 242, 1955 (1968).

7. Rosenquist, T.: J. Iron and Steel Institute, 176, 37 (1954).

8. Erdos, E.: Sulfide Formation in Nickel-Base Superalloys. Deposition and Corrosion in Gas Turbines, p. 115, ed. by A. B. Hart and A. J. B. Cutler, John Wiley and Sons, New York, New York, 1973.

9. Strafford, K. N.: Metallurgical Reviews, 14, 153 (1969).

10. Czerski, L., S. Mrowec, and T. Werber: J. Electrochem. Soc., 109, 273 (1962).

11. Bergman, P. A.: Corrosion, 24, 72 (1967).

12. Spengler, C. and R. Viswanathan: Corrosion 26, 29 (1970); Met. Trans. 3, 161 (1972).

13. DeCrescente, M. A. and N. S. Bornstein: Corrosion, 24, 127 (1968).

14. Bornstein, N. A. and M. A. DeCrescente: TMS-AIME 245, 1947 (1969).

15. Bornstein, N. S. and M. A. DeCrescente: Investigation of Sulfidation Mechanism in Nickel-Base Superalloys. Final Report conducted for U.S. Naval Ship Research and Development Laboratory, Contract N00600-68-C-0639, April 1969, Annapolis Maryland.

REFERENCES (Cont'd)

16. Bornstein, N. S., M. A. DeCrescente, and H. A. Roth: Annual Report on the Effect of Vanadium and Sodium Compounds on Accelerated Oxidation of Nickel-Base Alloys. Contract N00014-70-C-0234, NR 036-089/1-12-70 (471), March 1971, June 1972, and June 1974.

17. Bornstein, N. S. and M. A. DeCrescente: TMS-AIME 2, 2875 (1971).

18. Goebel, J. A. and F. S. Pettit: Met. Trans. 1, 1943 (1970).

19. Brown, C. T., N. S. Bornstein and M. A. DeCrescente, "High Temperature Metallic Corrosion of Sulfur and Its Compounds," p. 170, ed. by Z. A. Foroulis, The Electrochemical Society, Inc., 1970.

20. Small, N. G. H., H. Strawson and A. Lewis: Recent Advances in the Chemistry of Fuel Oil Ash. The Mechanism of Corrosion by Fuel Impurities, p. 238, ed. by H. R. Johnson and D. J. Littler, London, 1963.

21. Condé, J. F. G.: The Mechanism of Hot Corrosion in Marine Gas Turbines, p. 17, Gas Turbine Materials Conference Proceedings, Washington, D.C., 1972.

22. McGrath, C. G.: Trans. Inst. Mar. Eng. 88, 145 (1976).

23. Bessen, I. I. and R. E. Fryxell: Proceedings of the 1974 Gas Turbine Materials in the Marine Environment Conference, p. 259, ed. by J. W. Fairbanks and I. Machlin, MCIC Report 75-27, Castine, Maine, 1974.

24. Ewing, C. T. and K. H. Stern: J. Phys. Chem. 78, 1998 (1974).

25. Stearns, C. A., R. A. Miller, F. J. Kohl and G. C. Fryburg: Gaseous Sodium Sulfate Formation in Flames and Flowing Gas Environments. Presented at Symposium on Corrosion Problems Involving Volatile Corrosion Products. Electrochemical Society Meeting, Philadelphia, Pennsylvania, May 1977; also NASA TM X-73600 (1977); also J. Electrochemical Soc. 124, 1145 (1977).

26. Kohl, F. G., G. J. Santoro, C. A. Stearns, G. C. Fryburg and D. E. Rosner: Theoretical and Experimental Studies of the Deposition of Na_2SO_4 from Seeded Combustion Gases. Presented at Symposium on Corrosion Problems Involving Volatile Corrosion Products. Electrochemical Society Meeting, Philadelphia, Pennsylvania, May 1977; also NASA TM X-73683 (1977).

REFERENCES (Cont'd)

27. Hanby, V. I.: Journal of Engineering for Power, 96, 129 (1974).

28. Hancock, P.: Corrosion of Alloys in High Temperatures in Atmospheres Consisting of Fuel Combustion Products and Associated Impurities - A Critical Review, Her Majesty's Stationary Office, London (1968).

29. Liander, H. and G. Olsson: IVA, Tidskrift for Tekniskvetenskaplig Forskring, 145 (1937).

30. Kröger, C. and J. Stratmann: Glastechnische Berichte, 34, 311 (1961).

31. Tschinkel, J. G.: Corrosion, 28, 161 (1972).

32. Kohl, F. J., C. A. Stearns, and G. C. Fryburg: Metal-Slag-Gas Reactions and Processes, p. 649, ed. by Z. A. Foroulis and W. W. Smeltzer, Electrochemical Society, (1975); also NASA TM X-71641 (1975).

33. a) Pilling, N. E. and R. E. Bedworth, J. Inst. Metals 29, 529 (1923).
b) Hauffe, K.: Oxidation of Metals, Plenum Press, New York, 1965.

34. Ward, G., B. S. Hockenhull, and P. Hancock: Met Trans. 5, 1451 (1974).

35. Unpublished data, N. S. Bornstein.

36. McKee, D. W. and G. Romeo: Trans. AIME 6A, 101 (1975).

37. Romeo, G. and D. McKee: J. Electrochem. Soc. 122, 188 (1975).

38. El-Dahshan, M. E., J. Stringer, and P. F. Whittle: Cobalt 57, 182 (1972).

39. Rentz, W. A.: Sulfidation Corrosion of Nickel Base Superalloys. Theses submitted to Rennselaer Polytechnic Institute, Hartford Graduate Center, January 1966.

40. Morrow, H. III, and E. Kalns: Climax Molybdenum Company Report RP 57-68-01, May 1971.

41. Gambino, R.: Hot Corrosion Mechanism Studies. U. S. Naval Marine Engineering Laboratory Final Report N-(600) (61533)-63219, February 1966.

42. Goebel, J. A., F. S. Pettit, and G. W. Goward, Met. Trans. 4, 261 (1973).

43. Hurst, R. C., J. B. Johnson, M. Davies, and P. Hancock: Deposition and Corrosion in Gas Turbines, p. 143, ed. by A. B. Hart and A. J. B. Cutler, John Wiley and Sons, 1973.

44. Hancock, P., R. C. Hurst, and A. R. Sollars: Published in Chemical Metallurgy of Iron and Steel, Special Publication by Iron and Steel Institute, p. 413 (1973).

45. Condé, J. F. G. and B. A. Wareham: Proceedings of the 1974 Gas Turbine Materials in the Marine Environment Conference, p. 73, ed. by J. W. Fairbanks and I. Machlin, MCIC 75-27, Castine, Maine, July 1974.

46. Hancock, P.: Proceedings of the 1974 Gas Turbine Materials in the Marine Environment Conference, p. 225, ed. by J. W. Fairbanks and I. Machlin, MCIC 75-27, Castine, Maine, July 1974.

47. Shirley, H. T.: J. of Iron and Steel Inst. 182, 144 (1956).

48. Pickering, H. W., F. H. Beck, and M. G. Fontana: Trans. ASM 53, 792 (1961).

49. Seybolt, A. U.: Oxid. of Metals 2, 119 (1970).

50. Seybolt, A. U.: Oxid. of Metals 2, 161 (1970).

51. Alexander, P. A.: Laboratory Studies of the Effects of Sulphates and Chlorides on the Oxidation of Superheated Alloys, The Mechanism of Hot Corrosion by Fuel Impurities, p. 571, ed. by H. R. Johnson and D. J. Littler, Butterworths, London, (1971).

52. Mansfeld, F., N. E. Paton, and W. M. Robertson: Met. Trans. 4, 321 (1973).

53. Johnson, D. M., D. P. Whittle, and J. Stringer: Corr. Sci. 15, 721 (1975).

54. Lewis, H. and R. A. Smith: Corrosion of High-Temperature Nickel-Base Alloys by Sulphate-Chloride Mixtures. First Int. Congress on Met. Corr., p. 202, Butterworths, London, 1961.

55. Felten, E. J. and F. S. Pettit: Degradation of Coating Alloys in Simulated Marine Environments. Contract No. N00173-76-C-0146. First Quarterly Report, June 15, 1976.

56. Radzavich, T. J. and F. S. Pettit: Degradation of Coating Alloys in Simulated Marine Environments. Contract No. N00173-76-C-0146, Third Quarterly Report, December 15, 1976.

58. Jones, R. L.: The Sulfidation of CoCrAlY Turbine Blade Coatings by Na_2SO_4-NaCl. Naval Research Laboratory LTR Report 6170859, December 1, 1975.

59. Jones, R. L., K. H. Stern, and S. T. Gadowski: Interactions of Sodium Chloride and Sodium Sulfate. To be published in Proceedings of the 1976 Gas Turbine Material in the Marine Environment Conference, Bath, England, July 1976.

60. Fryburg, G. C., F. J. Kohl, and C. A. Stearns: Oxidation in Oxygen at 900° and 1000°C of Four Nickel-Base Cast Superalloys: NASA-TRW VIA, B-1900, Alloy 713C and IN-738, NASA TN D-8388 (1977).

61. JANAF Tables, Dow Chemical Company, Midland, Michigan.

62. Pettit, F. S.: TMS-AIME 239, 1296 (1967).

63. Campbell, W. R.: Growth of Whiskers by Vapor-Phase Reactions. Whisker Technology, p. 15, ed. by A. Levitt, Wiley-Interscience New York, New York (1970).

64. Kuenzly, J. D. and D. L. Douglass: Oxid. of Met. 8, 139 (1974).

65. Stearns, C. A., F. J. Kohl, and G. C. Fryburg: Reactions of Chromium with Gaseous NaCl in an Oxygen Environments. Properties of High Temperature Alloys, ed. by Z. A. Foroulis and F. S. Pettit, Electrochemical Society/AIME, p. 655, (1976); also NASA TM X-73476 (1977).

66. Fryburg, G. C., R. A. Miller, F. J. Kohl, and C. A. Stearns: Volatile Products in the Corrosion of Cr, Mo, Ti and Four Superalloys Exposed to O_2 containing H_2O and Gaseous NaCl. Presented at Symposium on Corrosion Problems involving Volatile Corrosion Products. Electrochemical Society Meeting, Philadelphia, Pennsylvania, May 1977; also NASA TM X-73599 (1977).

67. Fryxell, R. E., C. A. Trythall, and R. J. Perkins: Corrosion 29, 423 (1968).

REFERENCES (Cont'd)

68. Wolters, A: a) Neues Jahrb. Mineral Geol. Beilage 30, 55 (1910); cf. Flood, H., T. Forland and A. Nesland, Acta Chem. Scand. 5, 1193 (1951); b) Neues Jb. Miner. Geol. Paläont. BeilBd. 30, 55 (1910), ~~cf. Thermodynamics of Molten Salt Mixtures, J. Lumsden, p. 280, Academic Press, London, 1966~~.

69. Flood, H., T. Forland and A. Nesland: Acta Chem. Scand. 5, 1193 (1951).

70. Goebel, J. A. and F. S. Pettit, Met. Trans. 1, 3421 (1970).

71. Bornstein, N. S. and M. A. DeCrescente, TMS-AIME 245, 1947 (1969).

72. Wood, G. C. and T. Hodgkiess: J. Electrochem. Soc. 113, 319 (1966).

73. Giggins. C. S. and F. S. Pettit: TMS-AIME 245, 2495 (1969).

74. Lowell, C. E.: Oxid. of Met. 7, 95 (1973).

75. Lowell, C. E. and D. L. Deadmore, Oxid. of Met. 7, 55 (1973).

76. Gulbransen, E. A. and T. P. Copan: Physical Metallurgy of Stress Corrosion Fracture, ed. by T. N. Rhodin, Pittsburgh, Pennsylvania, p. 155, (1959).

77. Birks, N. J., J. Inst. of Met. 91, 308, (1962-3).

78. Gulbransen, E. A. and K. F. Andrew, J. Electrochem. Soc. 106, 941 (1959).

79. Hickman, J. W.: An Electron Diffraction Study of Oxide Films Formed on Nickel-Chromium Alloys, AIME Technical Publication No. 2373, June 1948.

80. Gulbransen, E. A. and W. R. McMillan, Ind. and Eng. Chem. 45, 1734 (1953).

81. Lustman, B.: Trans. AIME, 188 , 995 (1950).

82. Capson, H. R. and F. S. Long: Corrosion-NACA 15, 44 (1955).

83. Spooner, N. J., M. Thomas, and L. Thomassen: J. of Metals, 5, 844 (1953).

84. Douglass, D. L.: Corr. Sci. 8, 664 (1968).

85. Douglass, D. L. and J. S. Armigo: Oxid. of Metals 2, 207 (1970).

86. Zima, G. E.: Trans. ASM 49, 924 (1957).

87. Giggins, C. S. and F. S. Pettit: TMS-AIME 345, 2509 (1969).

88. Wood, G. C.: Oxid. of Met. 2, 11 (1970).

89. Wood, G. C., T. Hodgkiess, and D. P. Whittle: Corr. Sci. 6, 129 (1966).

90. Wood, G. C. and D. P. Whittle: J. Iron and Steel Institute, 202, 979 (1964).

91. Wood, G. C. and D. P. Whittle: Corrosion Science 4, 263 (1964).

92. Wood, G. C. and D. P. Whittle: Corrosion Science 4, 293 (1964).

93. Davis, H. H., H. C. Graham, and I. A. Kvernes: Oxid. of Met. 3, 431 (1971).

94. Gulbransen, E. A. and K. F. Andrew: J. Electrochem. Soc. 106, 294 (1959).

95. Michels, H. H.: Met. Trans. 7A, 379 (1976).

96. Caplan, D. and M. Cohen: J. Electrochem. Soc. 112, 471 (1961).

97. Caplan, D., A. Harvey, and M. Cohen: J. Electrochem. Soc. 108, 134 (1961).

98. Caplan, D., A. Harvey, and M. Cohen: Corr. Sci. 3, 161 (1963).

99. Wright, I. G., B. A. Wilcox, and R. I. Jaffee: Oxidation and Hot Corrosion of Ni-Cr and Co-Cr Base Alloys Containing Rare Earth Oxide Dispersions. Contract No. N00019-72-C-0190, Final Report, January 30, 1973, Battelle Laboratories, Columbus, Ohio.

100. The Superalloys, Appendix B, Superalloy Data, p. 596, ed. by C. T. Sims and W. C. Hagel, John Wiley and Sons, New York, New York, 1972.

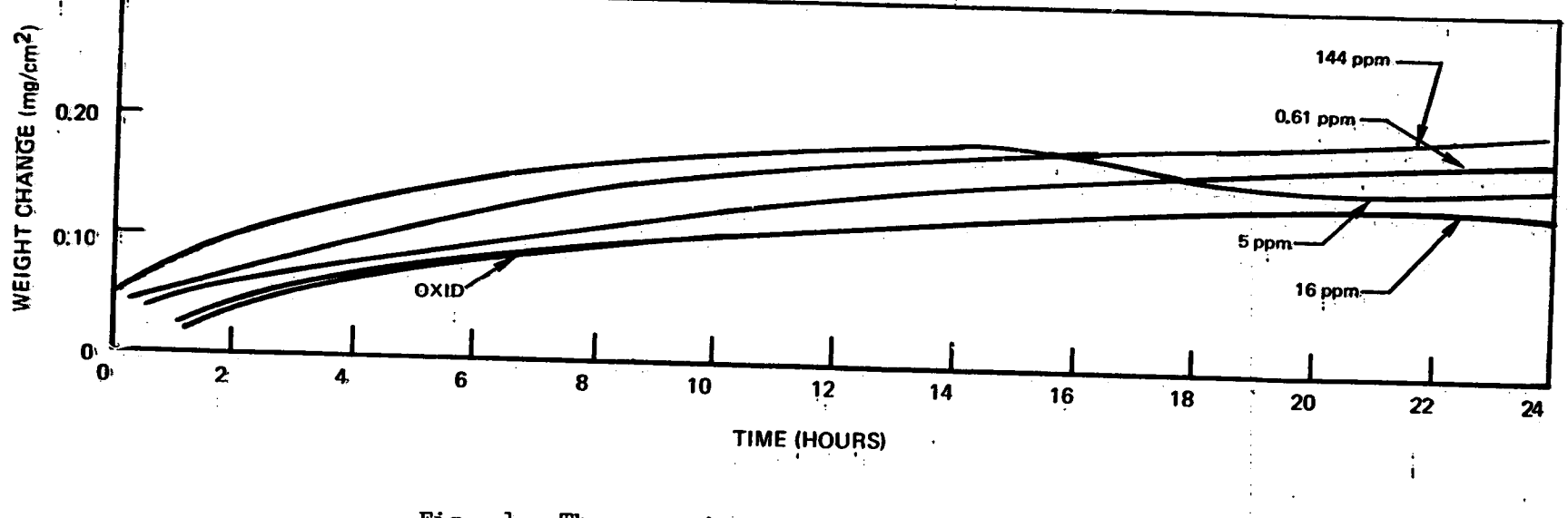

Fig. 1. Thermogravimetric data for NiAl oxidized in air with and without NaCl vapors present at 900°C.

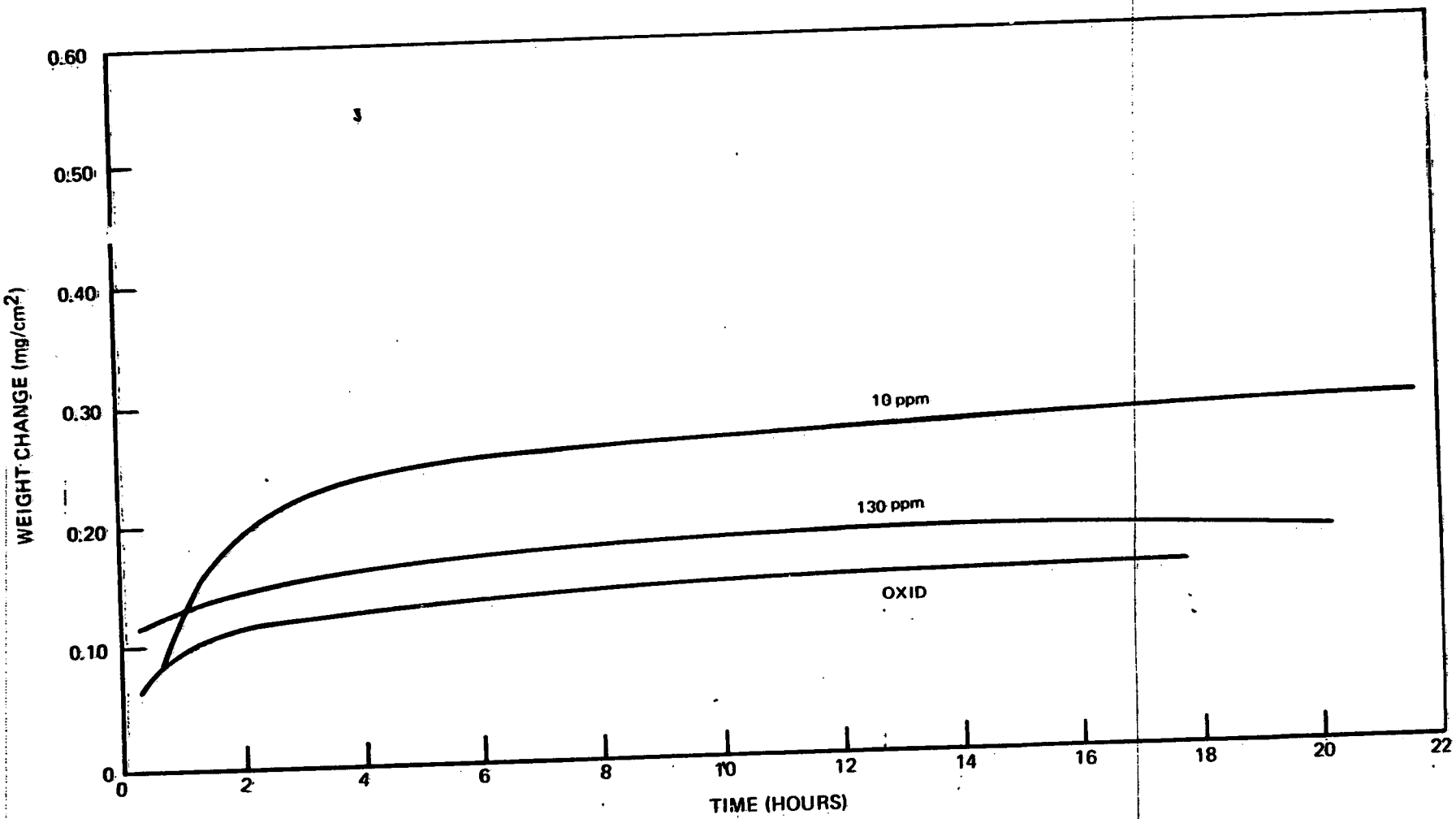

Fig. 2. Thermogravimetric data for NiAl oxidized in air with and without NaCl vapors present at 1050°C.

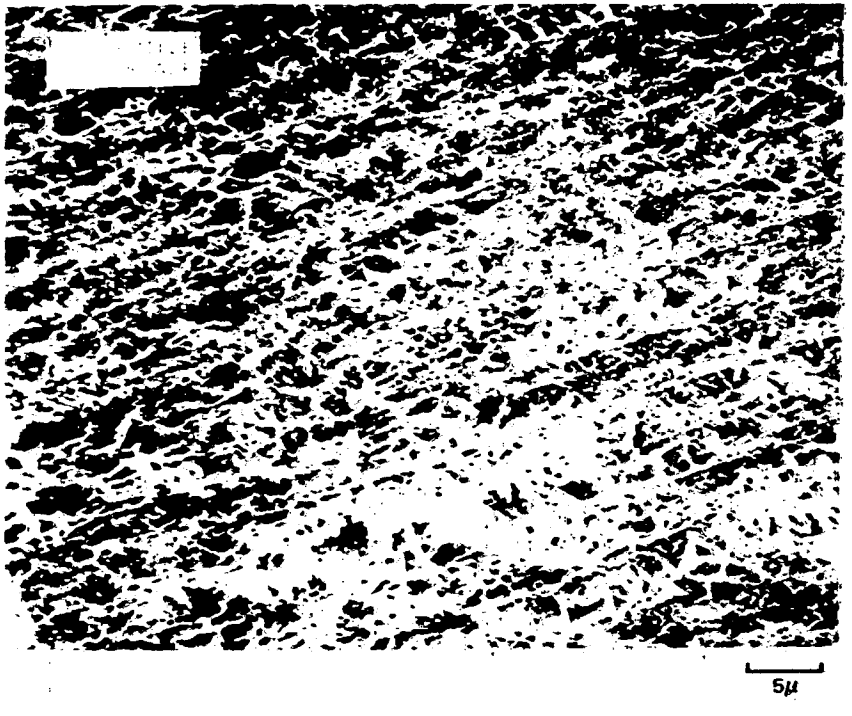

Fig. 3 NiAl oxidized in air at 1050°C for 24 hours.

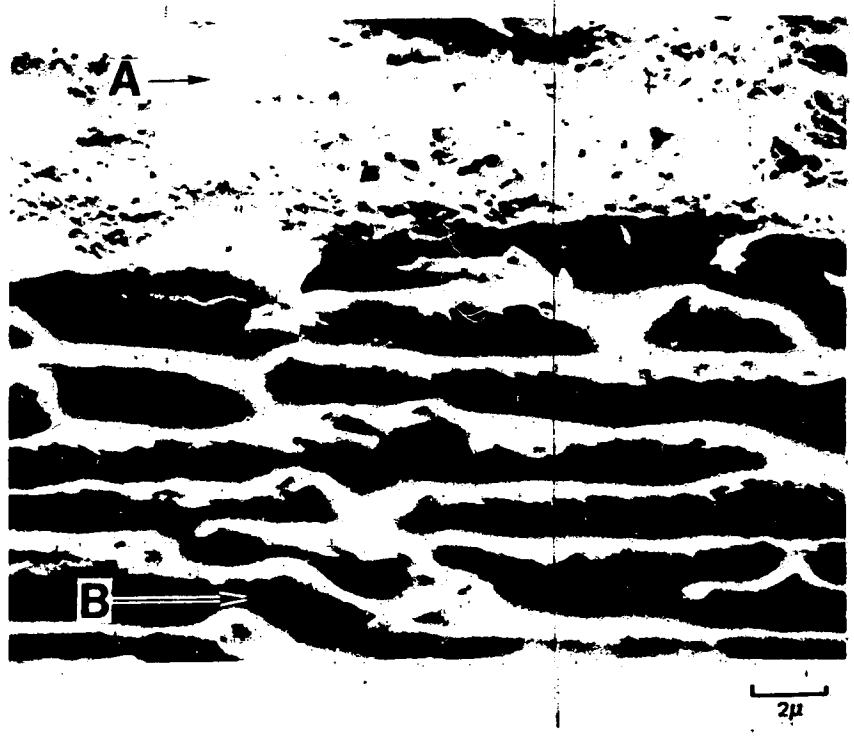

Fig. 4 NiAl oxidized in air at 1050°C for 24 hours showing a break in the compact oxide layer.
A. Protective Al_2O_3 scale
B. NiAl substrate

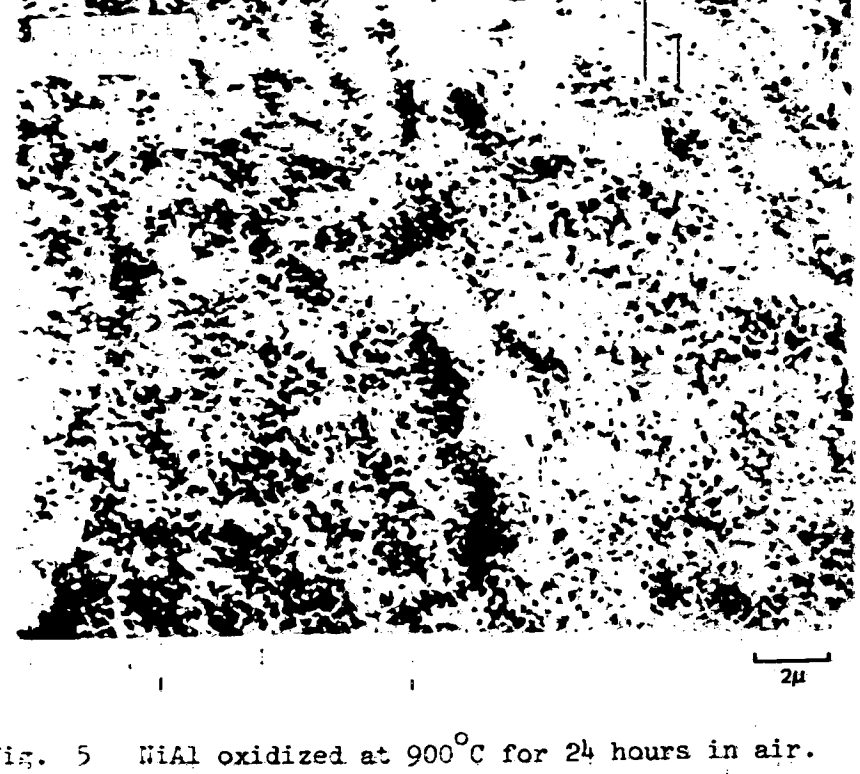

Fig. 5 NiAl oxidized at 900°C for 24 hours in air.

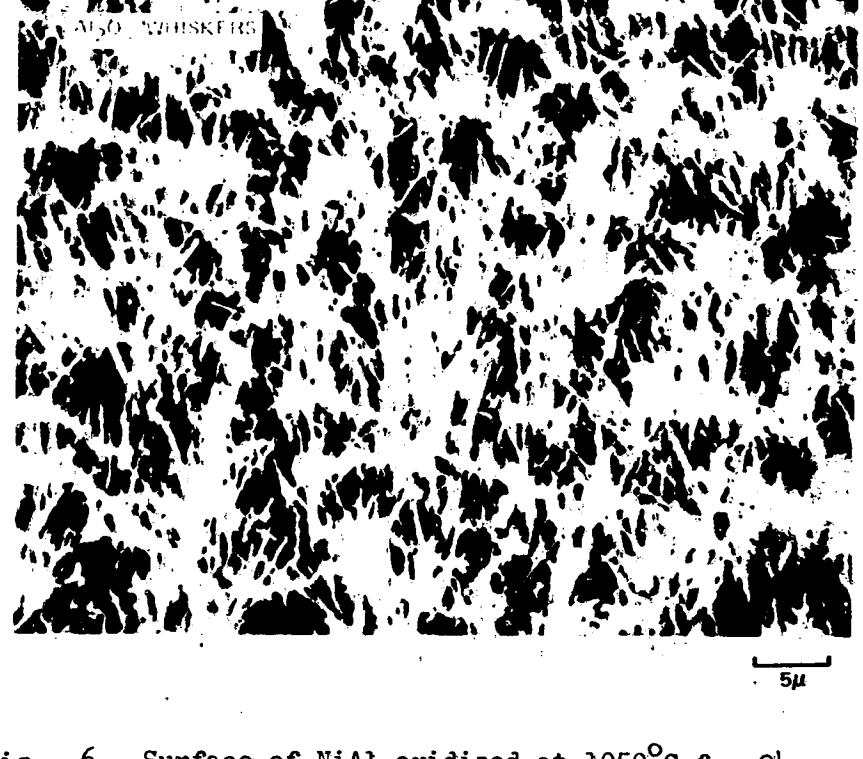

Fig. 6 Surface of NiAl oxidized at 1050°C for 24 hours with 10 ppm NaCl vapor present.

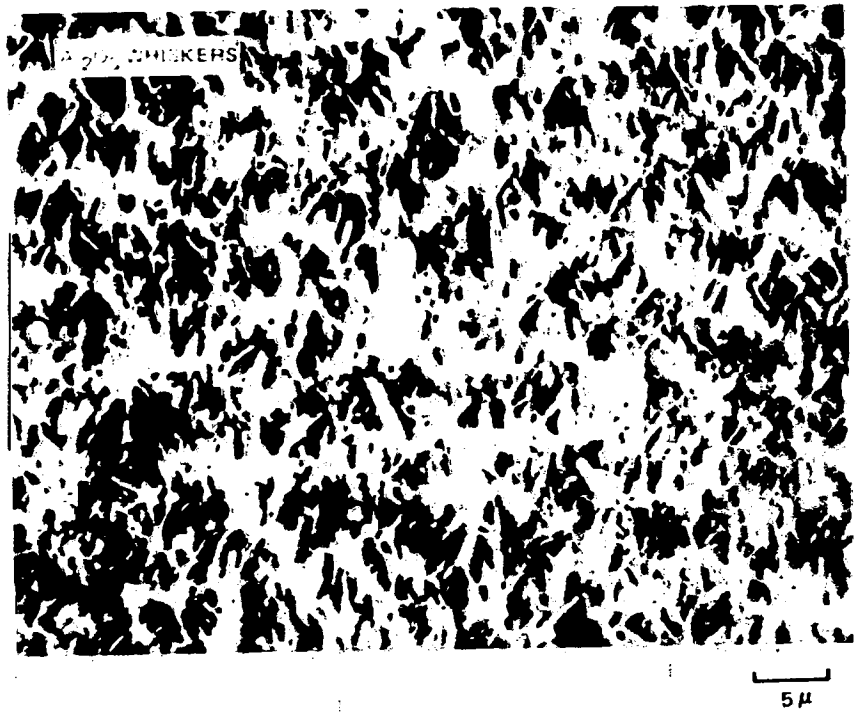

Fig. 7 Surface of NiAl oxidized at 1050°C for 24 hours with 130 ppm NaCl vapor present.

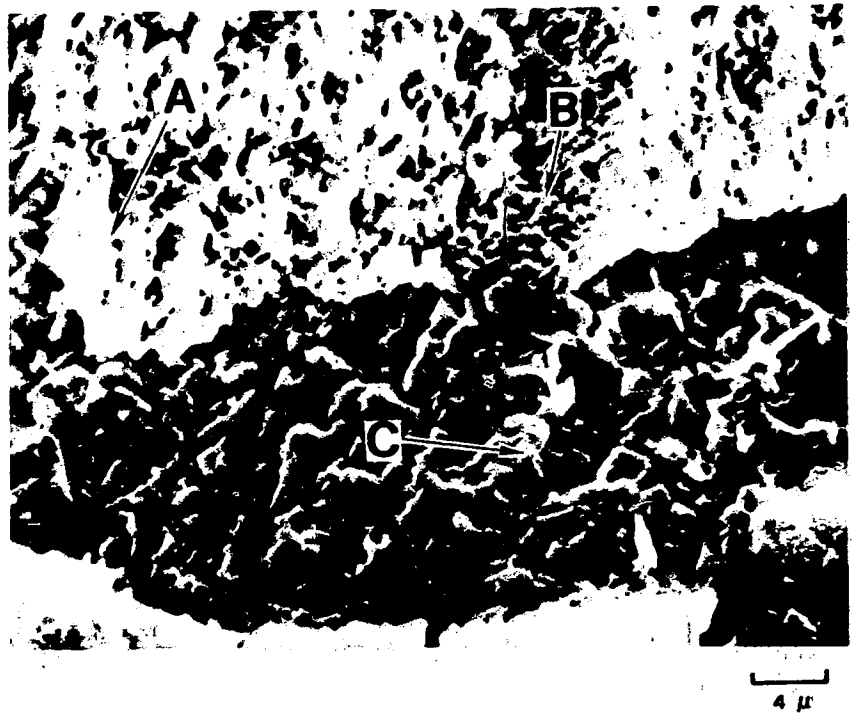

Fig. 8 α-Al_2O_3 fibers growing from dense Al_2O_3 found on NiAl oxidized at 1050°C for 24 hours.
A. Al_2O_3 whiskers
B. Protective Al_2O_3 scale
C. NiAl

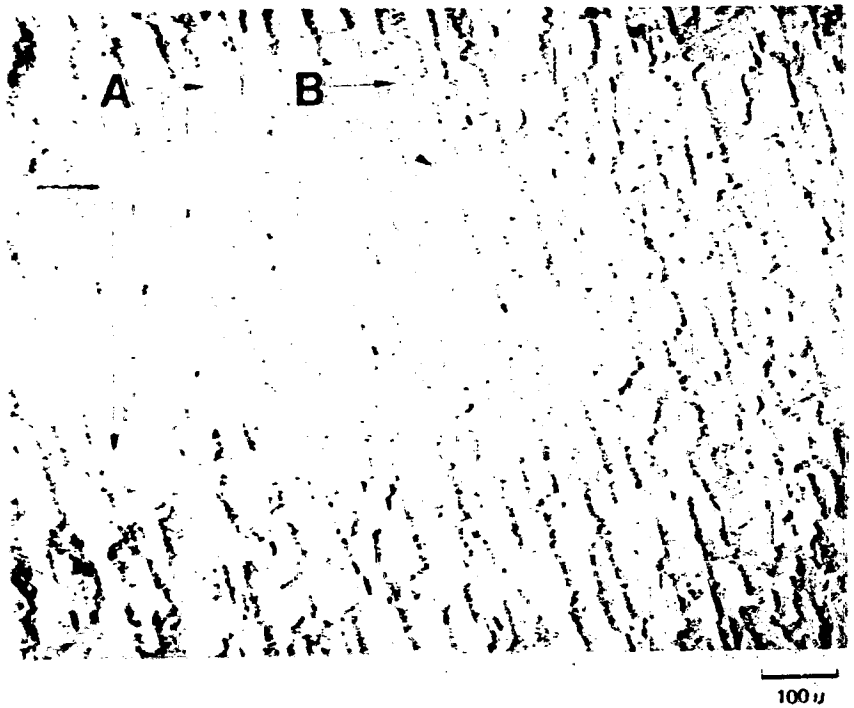

Fig. 9 NiAl oxidized for 24 hours at 900°C in air containing 16 ppm NaCl(g)
A. NiAl
B. Protective Al_2O_3 scale

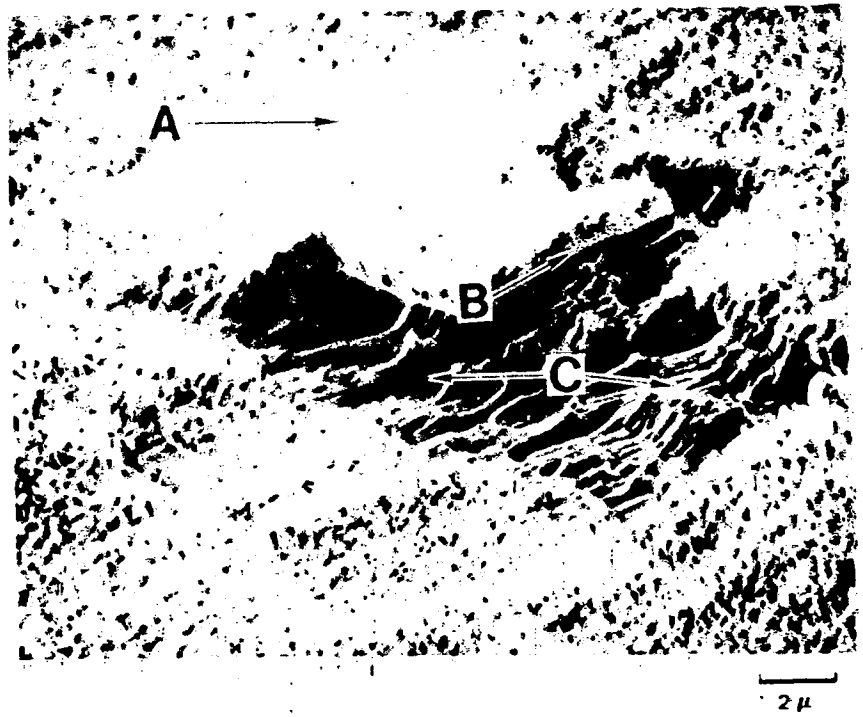

Fig. 10 NiAl oxidized for 24 hours at 900°C in air containing 16 ppm NaCl(g)
A. Al_2O_3 whiskers
B. Protective oxide layer
C. NiAl

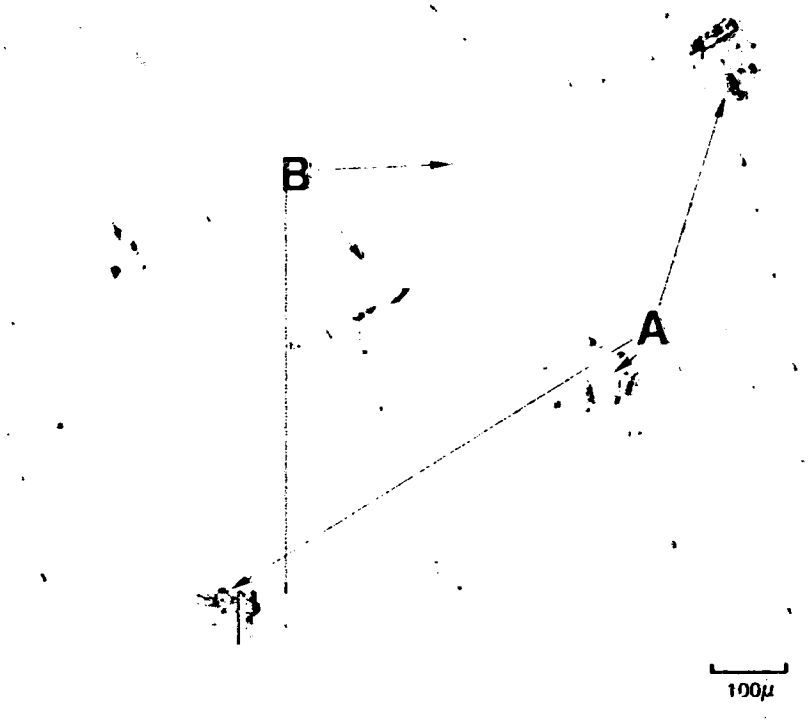

Fig. 11 NiAl oxidized at 900°C for 24 hours in air with 0.61 ppm NaCl vapor present.
A. Overturned dense oxide layer
B. Spalling protective oxide scale

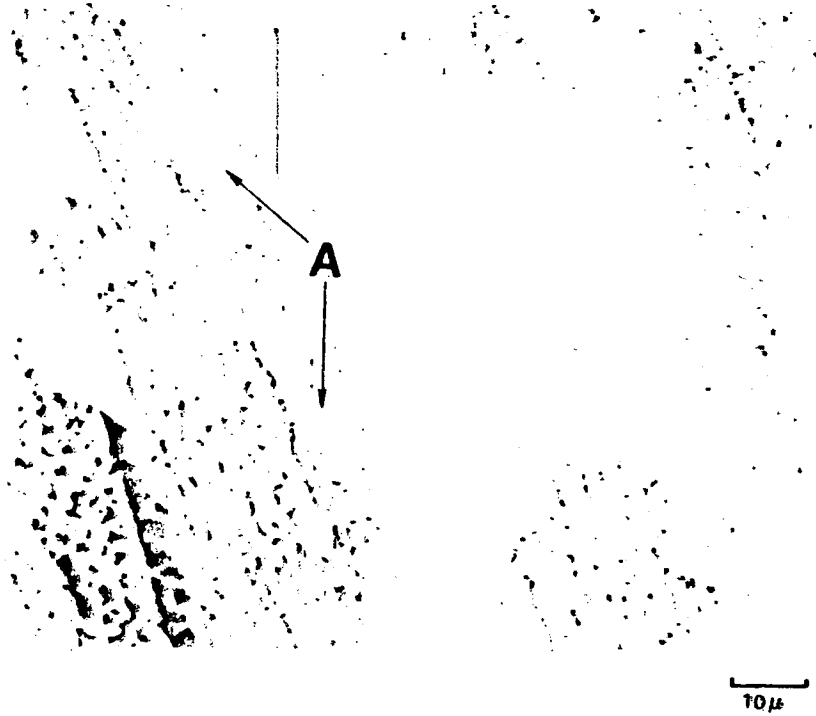

Fig. 12 NiAl oxidized at 900°C for 24 hours in air with 0.61 ppm NaCl vapor present.
A. Cracks in the protective Al_2O_3 scale

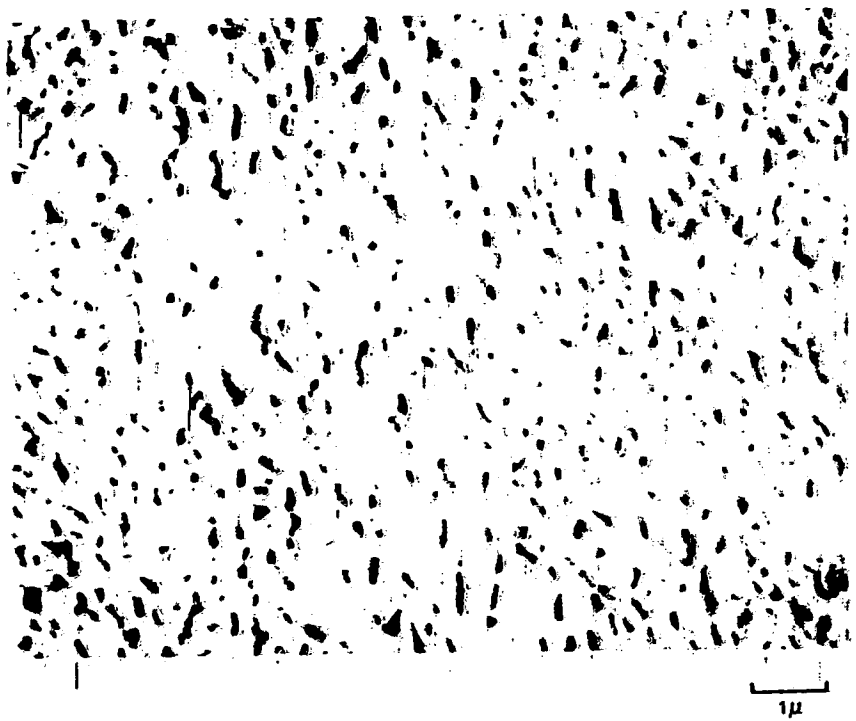

Fig. 13 α-Al_2O_3 whiskers growing on NiAl oxidized at 900°C for 24 hours with 0.61 ppm NaCl present.

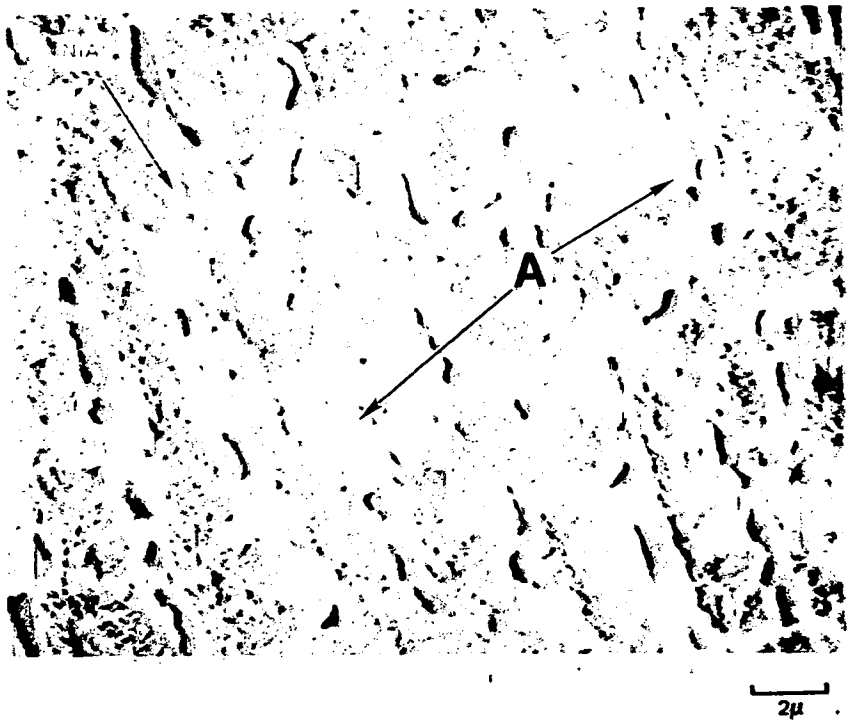

Fig. 14 NiAl oxidized at 900°C for 24 hours in air with 0.61 ppm NaCl vapor showing a region where the compact Al_2O_3 oxide spalled.
A. Remains of spalled dense Al_2O_3 layer

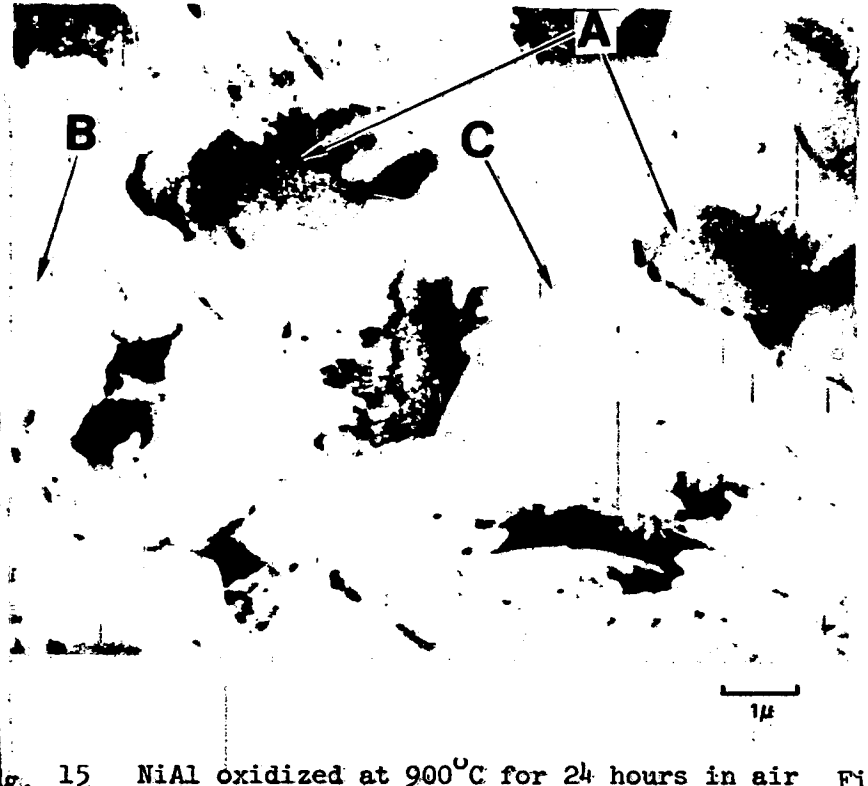

g. 15 NiAl oxidized at 900°C for 24 hours in air with 0.61 ppm NaCl(g) showing Al_2O_3 scale reforming over spalled oxide region.
A. NiAl
B. Original protective Al_2O_3 scale
C. Reforming protective Al_2O_3 scale

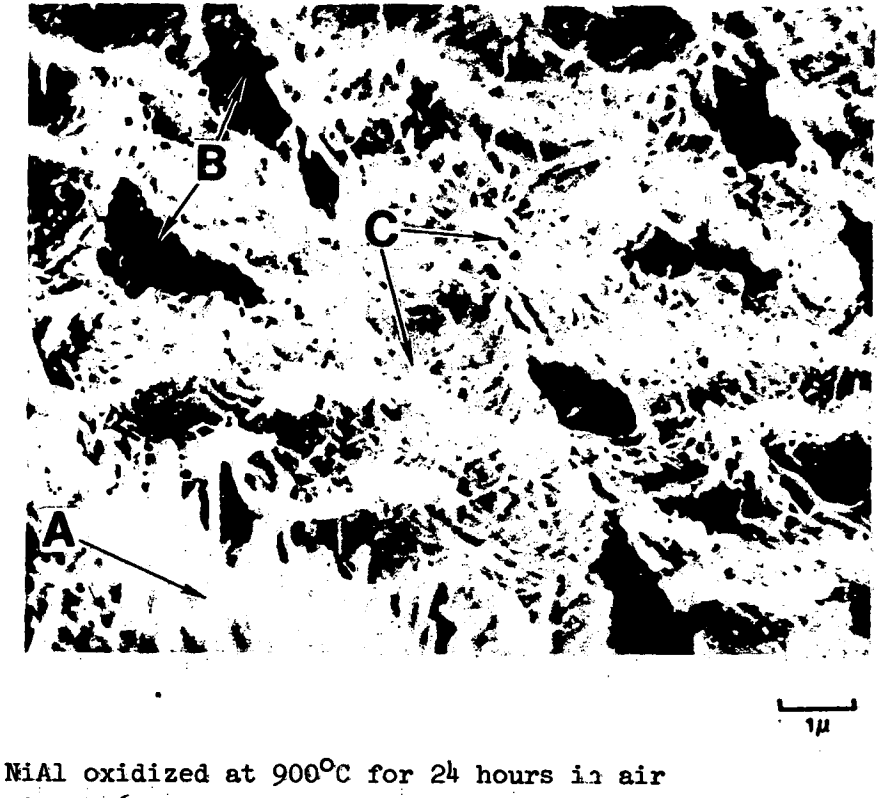

Fig. 16 NiAl oxidized at 900°C for 24 hours in air with 0.61 ppm NaCl showing Al_2O_3 scale reforming over spalled oxide region.
A. Original Al_2O_3 scale
B. Pegs from spalled oxide
C. Protective Al_2O_3 scale reformed over spalled oxide region

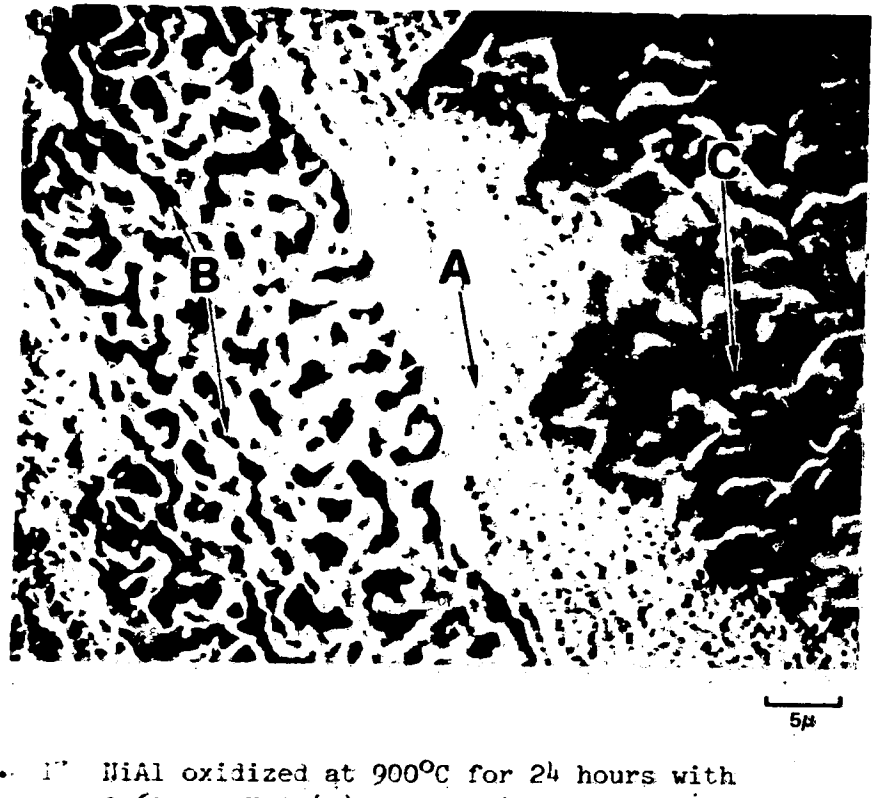

Fig. 17 NiAl oxidized at 900°C for 24 hours with 0.61 ppm NaCl(g) showing regions with
A. adherent scale and Al_2O_3 fibers growing on it
B. NiAl substrate on which a protective oxide scale is reforming
C. overturned spalled oxide

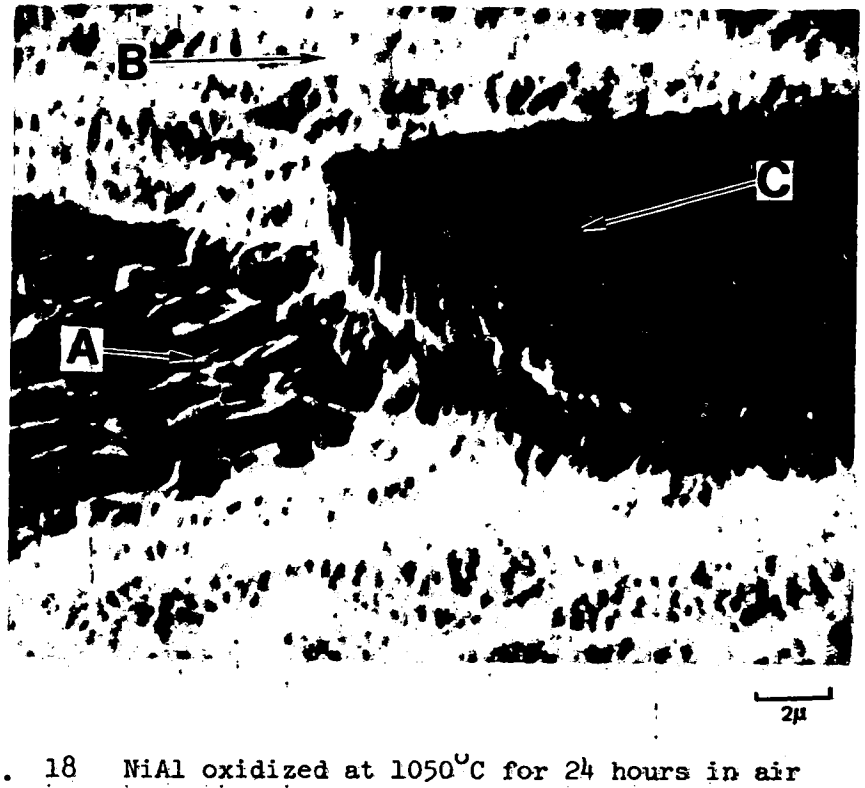

Fig. 18 NiAl oxidized at 1050°C for 24 hours in air with 128 ppm HCl showing a region of the spalled overturned oxide.
Note the Al_2O_3 fibers growing from the original surface of the spalled oxide segment.
A. NiAl
B. Al_2O_3 whiskers
C. Spalled protective oxide surface originally attached to the NiAl Substrate

Fig. 19 Al_2O_3 fibers growing from the upturned side of the spalled Al_2O_3 segment.

A. Base of overturned oxide
B. Al_2O_3 whiskers growing on surface of overturned oxide
C. Hole in overturned oxide showing Al_2O_3 whiskers from the surface of the scale below

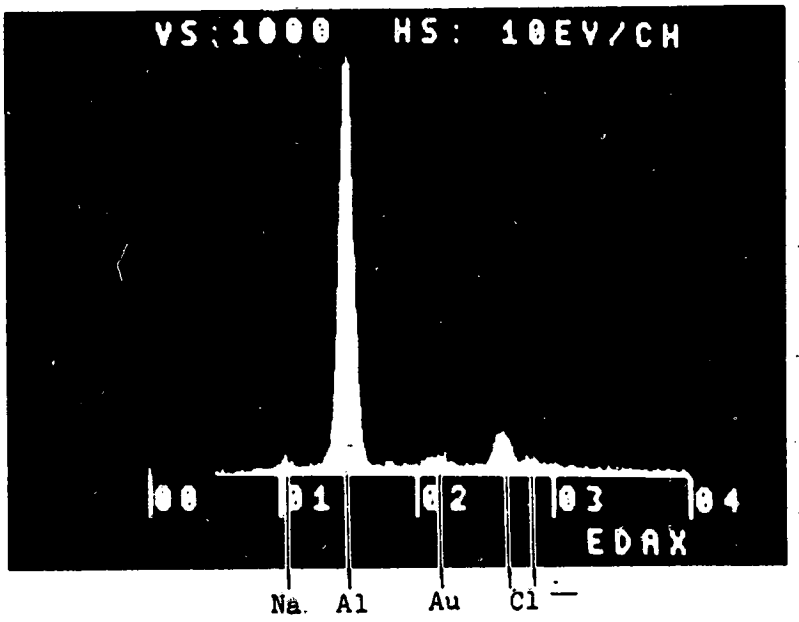

(a) EDAX of white crystals showing high Al (Al_2O_3) and low Na and Cl peaks.

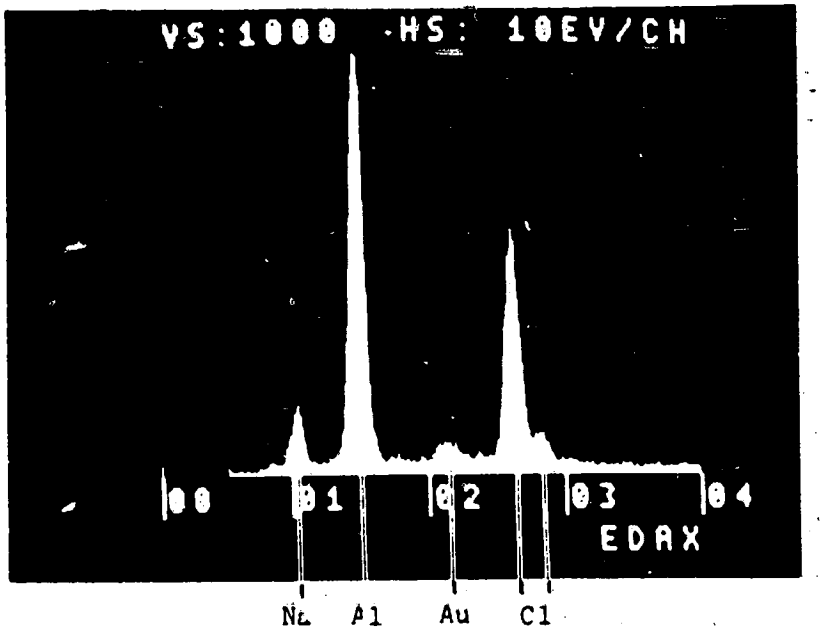

(b) EDAX of the dense black scale showing high Na and Cl levels (samples Au coated to prevent surface charging).

Fig. 20 Investigation of the oxide surface adjacent ~~to the~~ substrate.

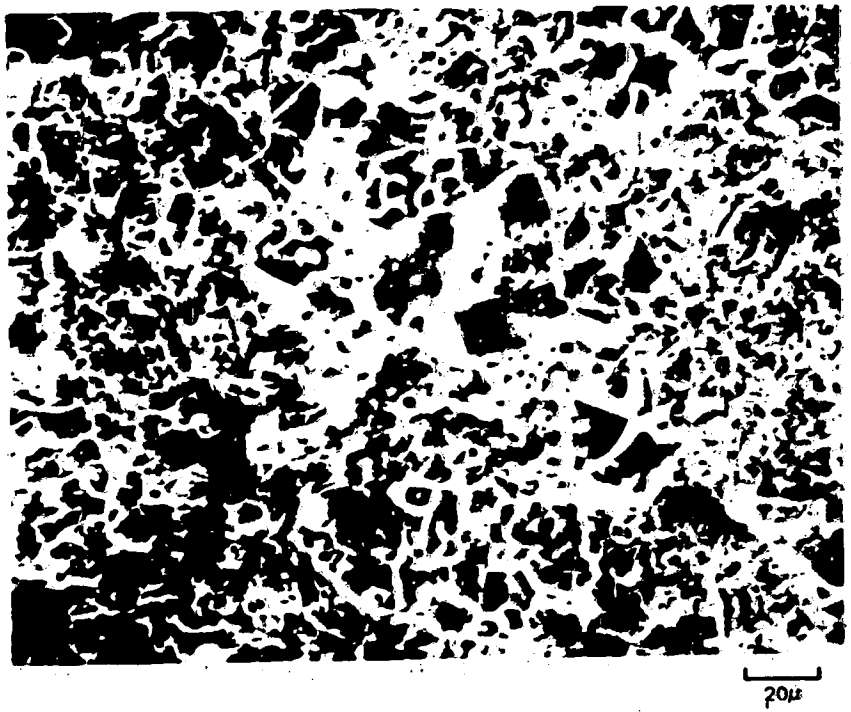

Fig. 21 Dense Al_2O_3 exposed to NaCl vapors at 1050°C showing absence of Al_2O_3 whiskers.

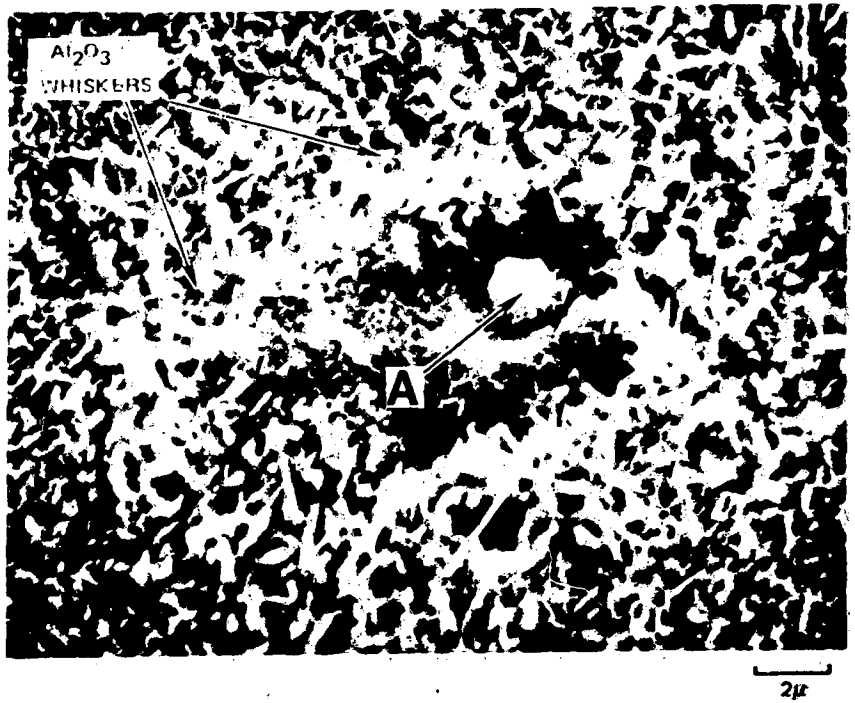

Fig. 22 NiAl oxidized at 900°C for 24 hours in air showing Al_2O_3 whiskers distributed around a Ni-rich imperfection (A) in the protective Al_2O_3 scale.

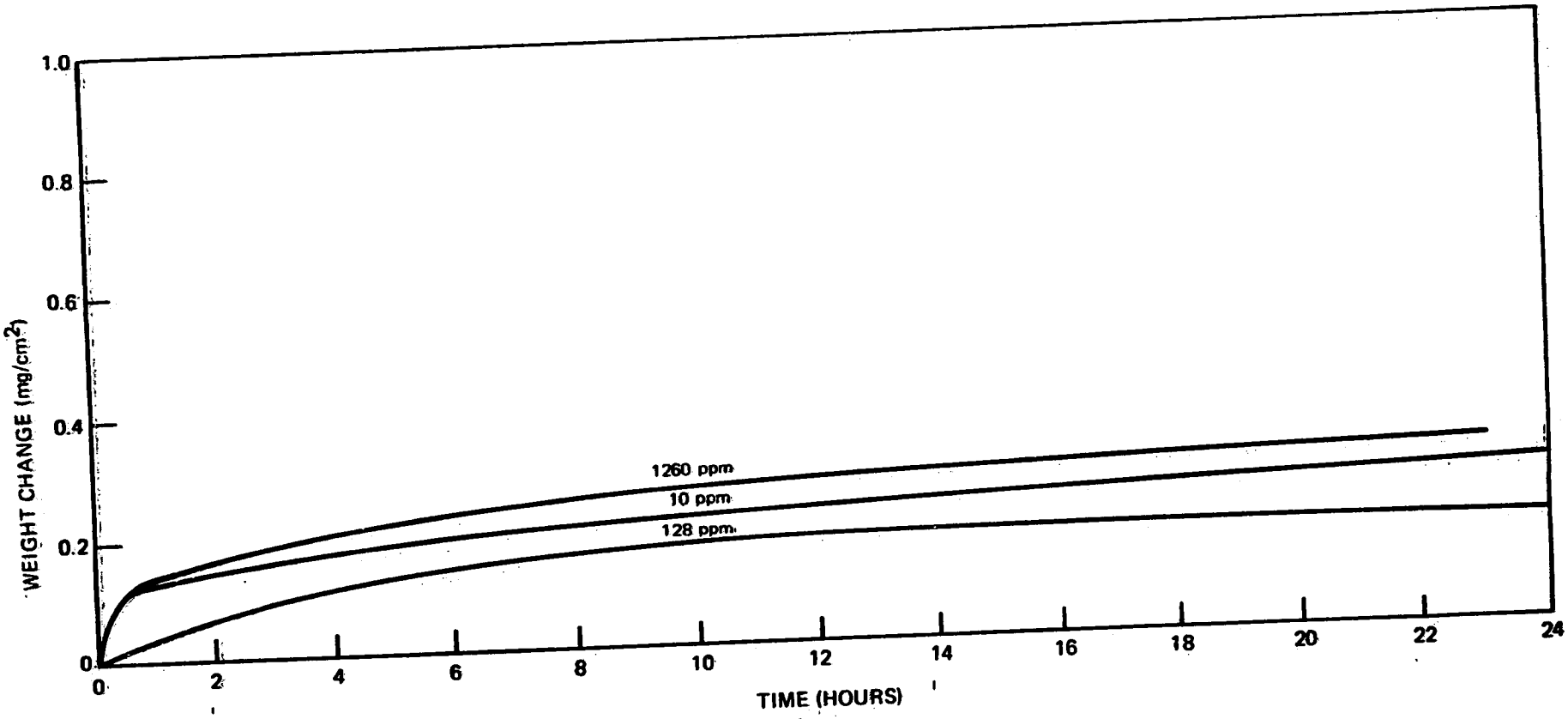

Fig. 23 NiAl oxidized at 900°C in air with HCl gas.

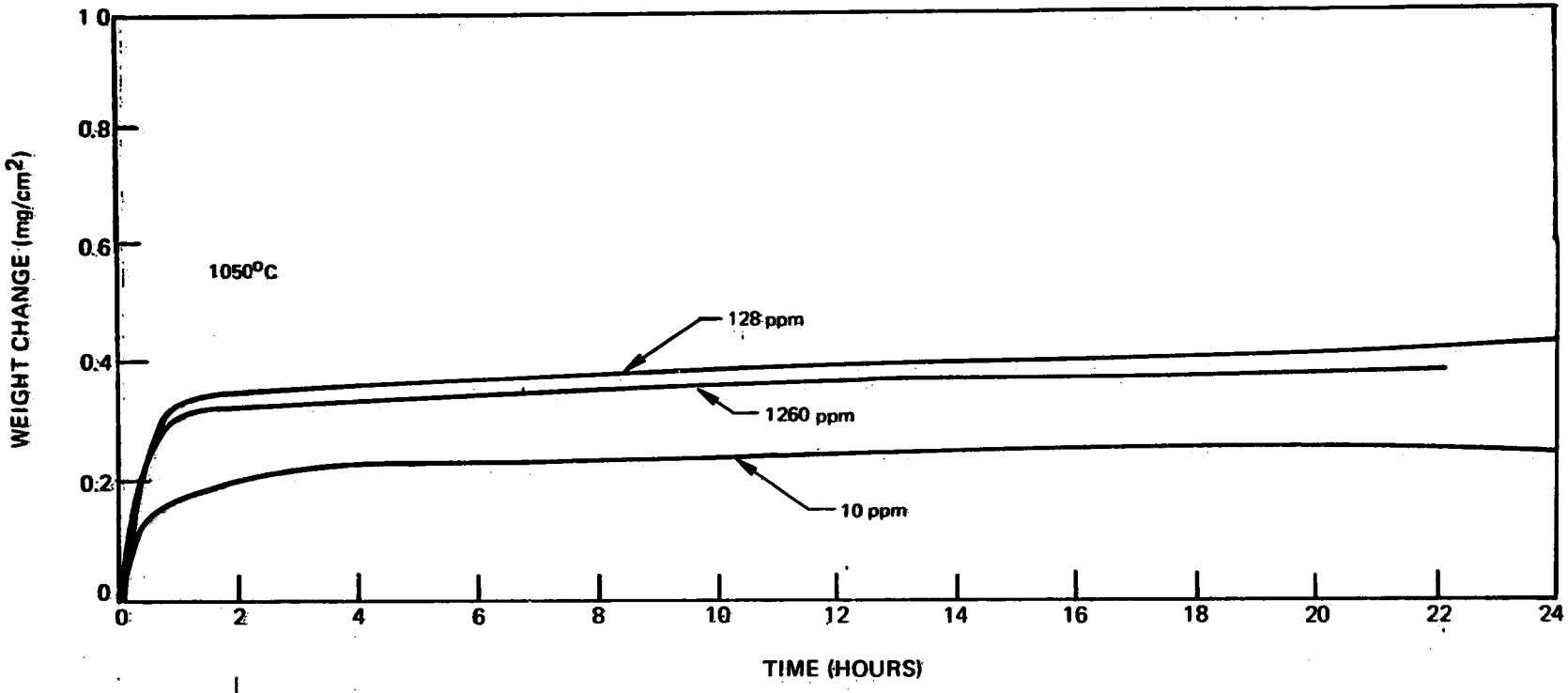

Fig. 24 1050°C oxidation of NiAl with HCl gas.

Fig. 25. NiAl oxidized at 900°C for 24 hours in air with 1260 ppm HCl.

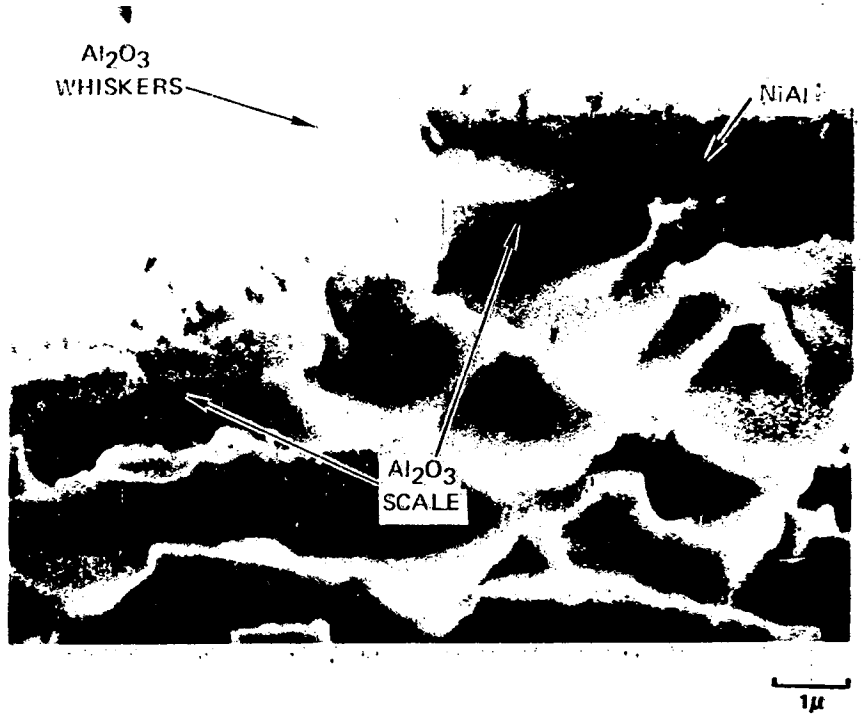

Fig. 26. NiAl oxidized at 900° for 24 hours in air with 1260 ppm HCl.

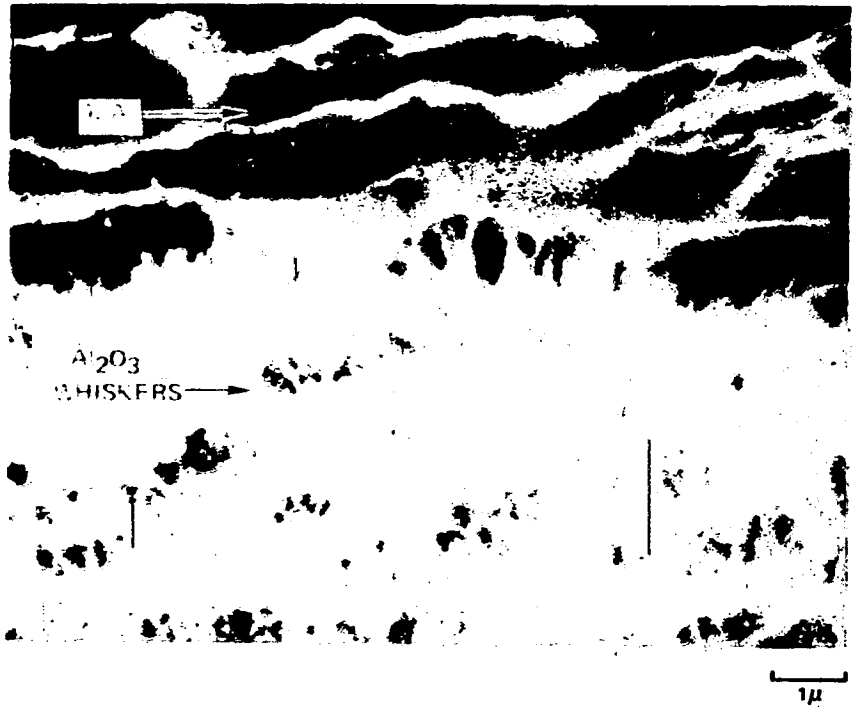

Fig. 27. NiAl oxidized at 1050°C for 24 hours in air with 128 ppm HCl.

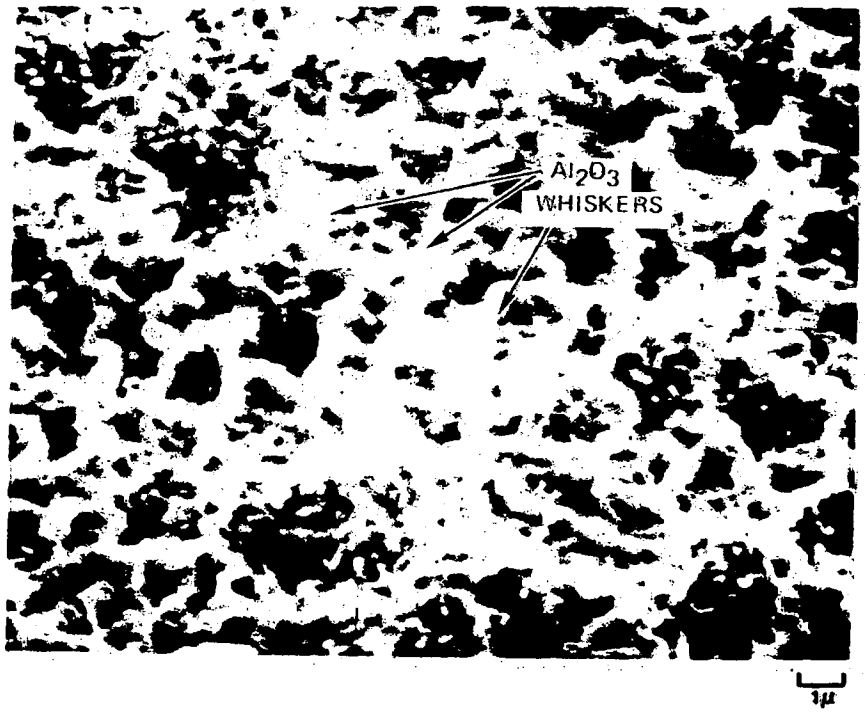

Fig. 28 Al_2O_3 whiskers on NiAl exposed to 10 ppm HCl at 1050°C for 24 hours.

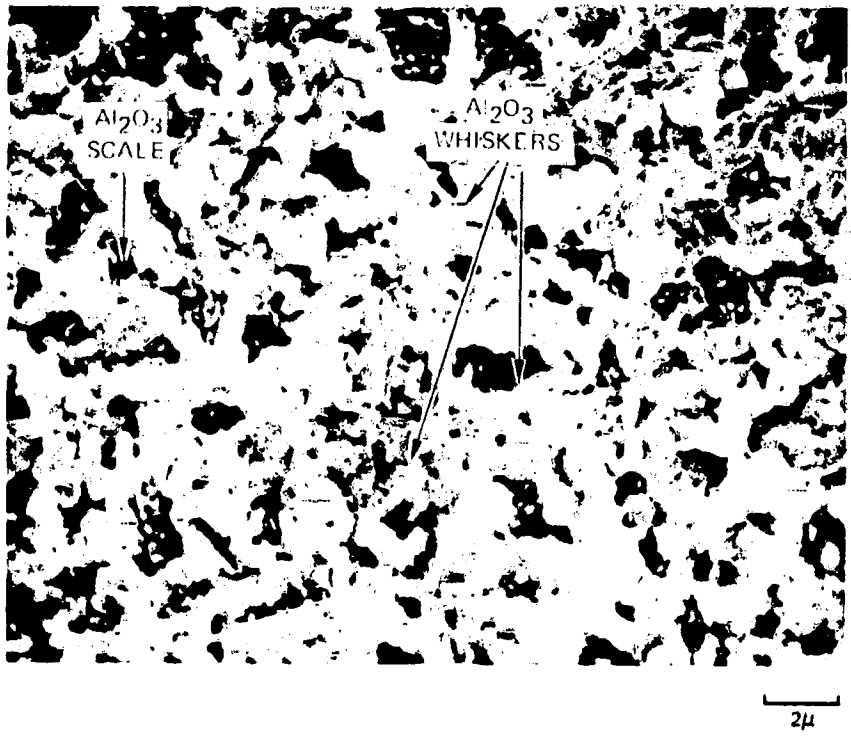

Fig. 29 NiAl oxidized at 1050°C in air for 64 hours and then in air with 129 ppm HCl(g) for 25 hours showing Al_2O_3 fibers formed by diffusion through Al_2O_3 layer.

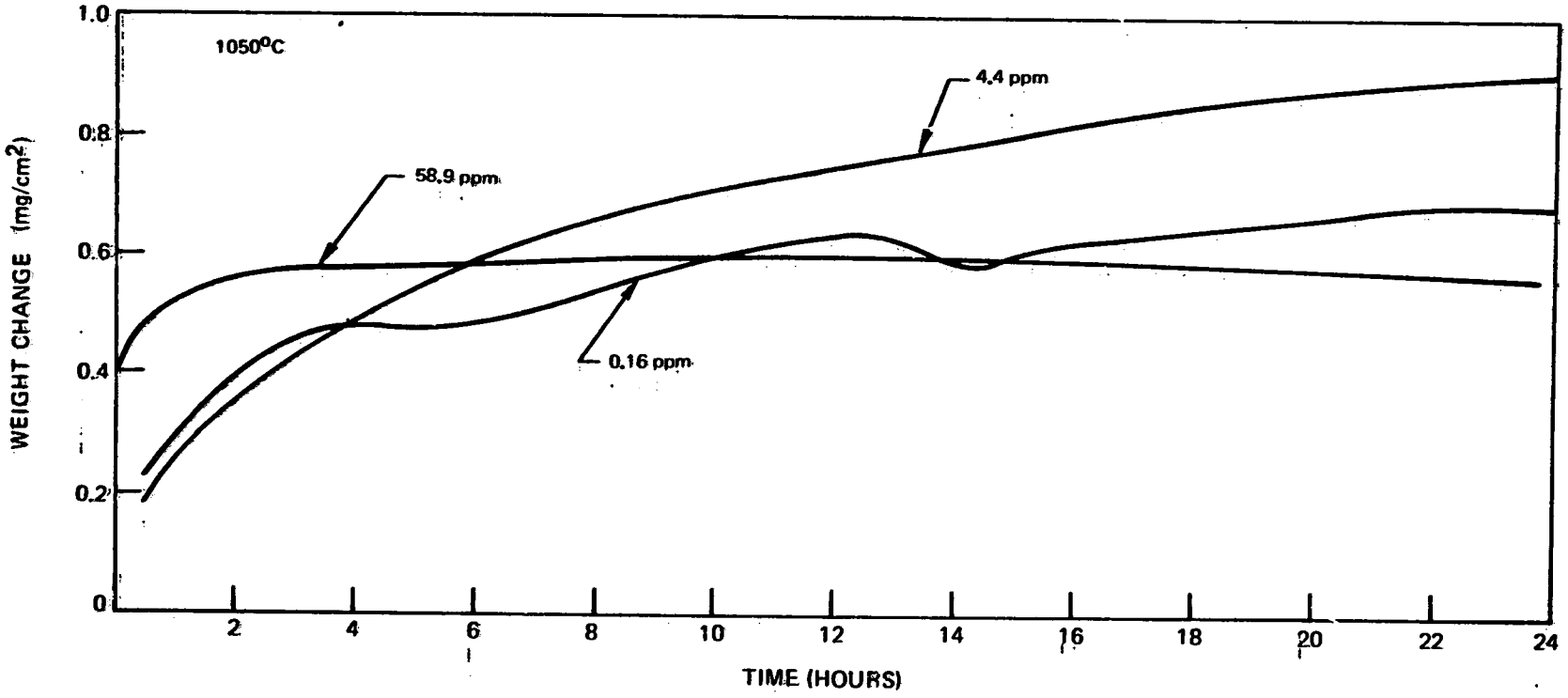

Fig. 30 1050°C oxidation data for NiAl in air with NaOH vapors.

Fig. 32 NiAl oxidized for 24 hours at 1050°C in air containing 58.9 ppm NaOH(g) showing Al_2O_3 crystals growing on the surface oxide.

Fig. 31 NiAl oxidized for 24 hours in air containing 58.9 ppm NaOH(g).

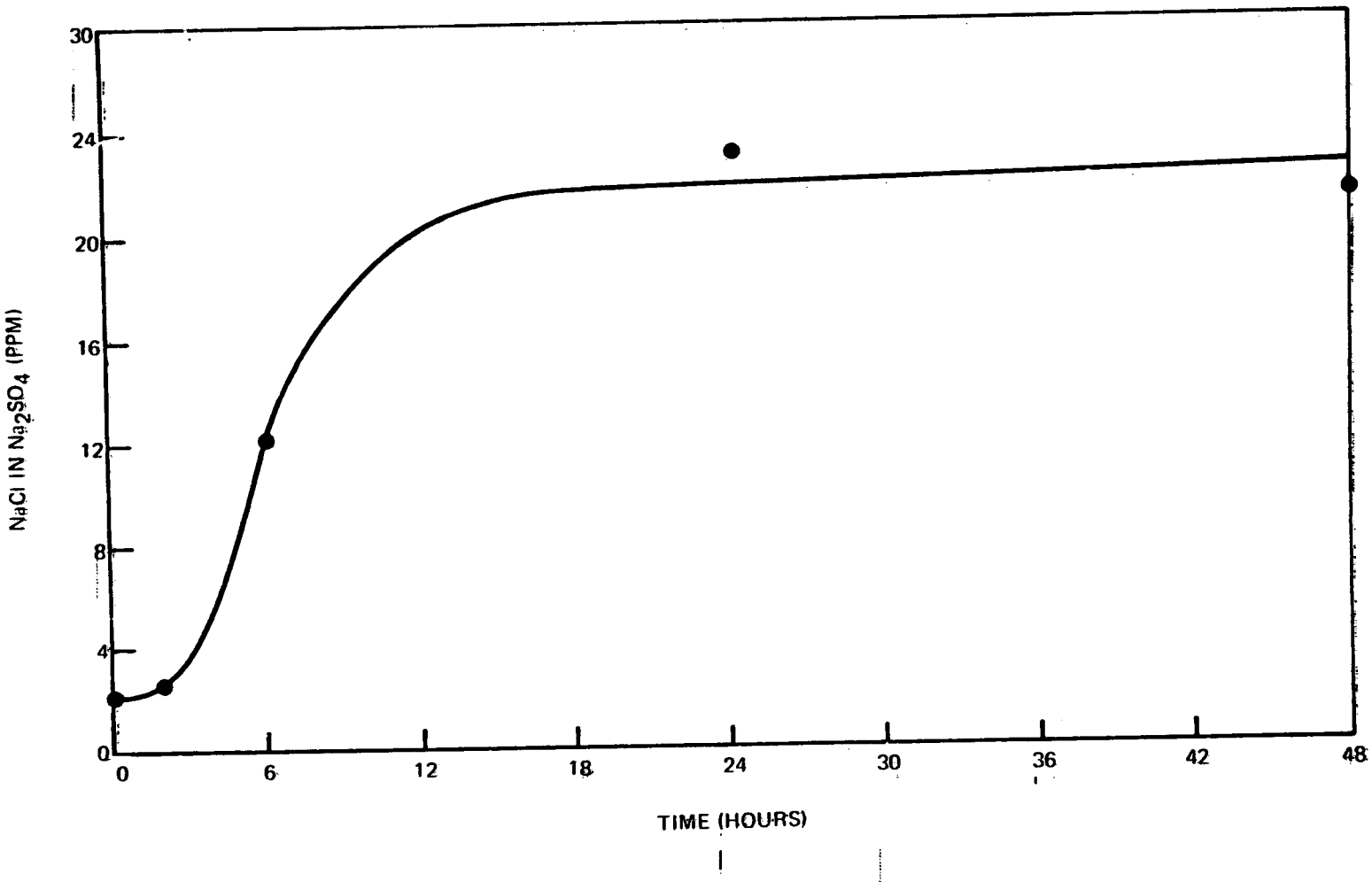

Fig. 33 Level of NaCl in Na_2SO_4 heated at 900°C.

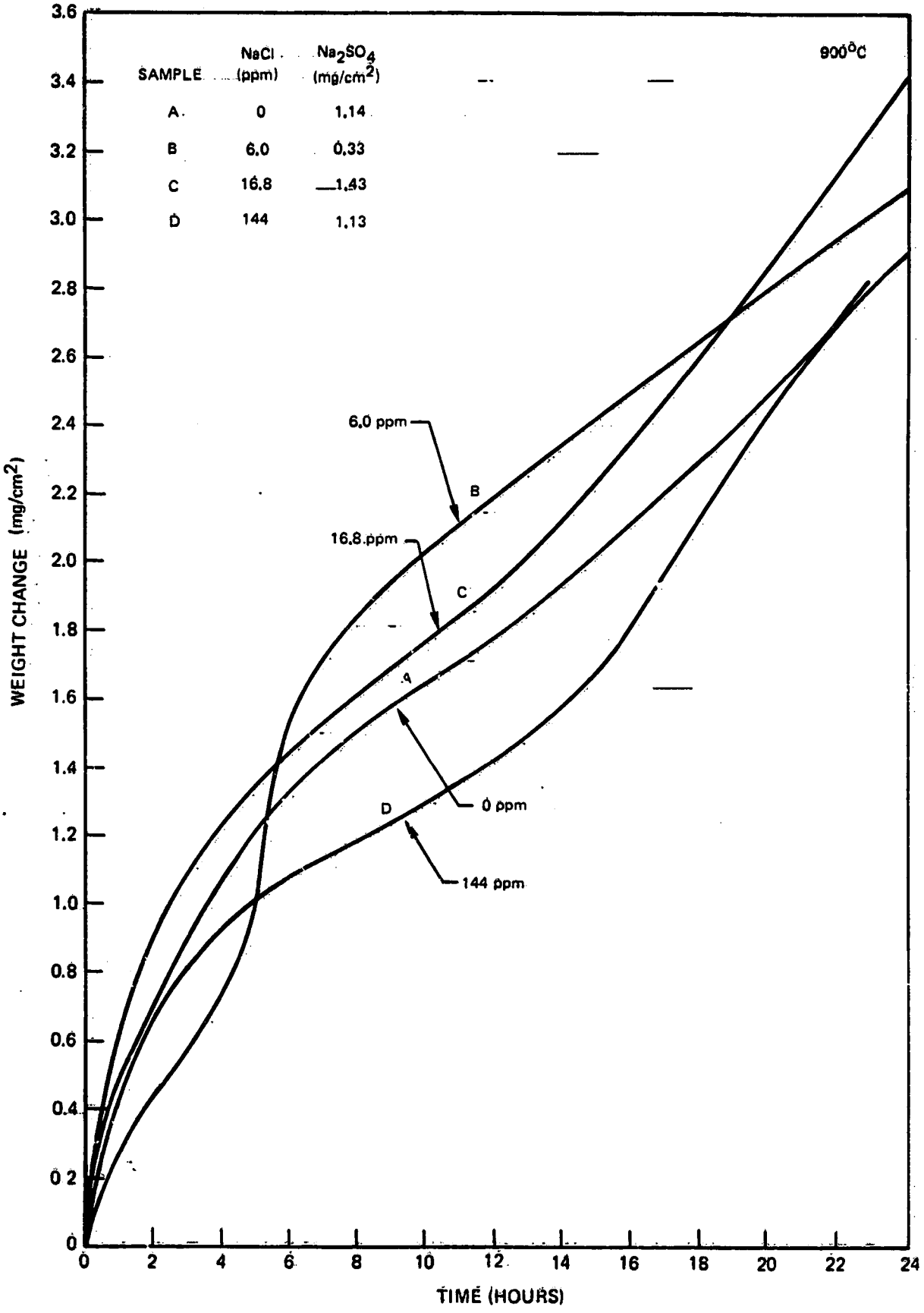

Fig. 34 Na_2SO_4-coated NiAl oxidized at 900°C in air with NaCl vapors.

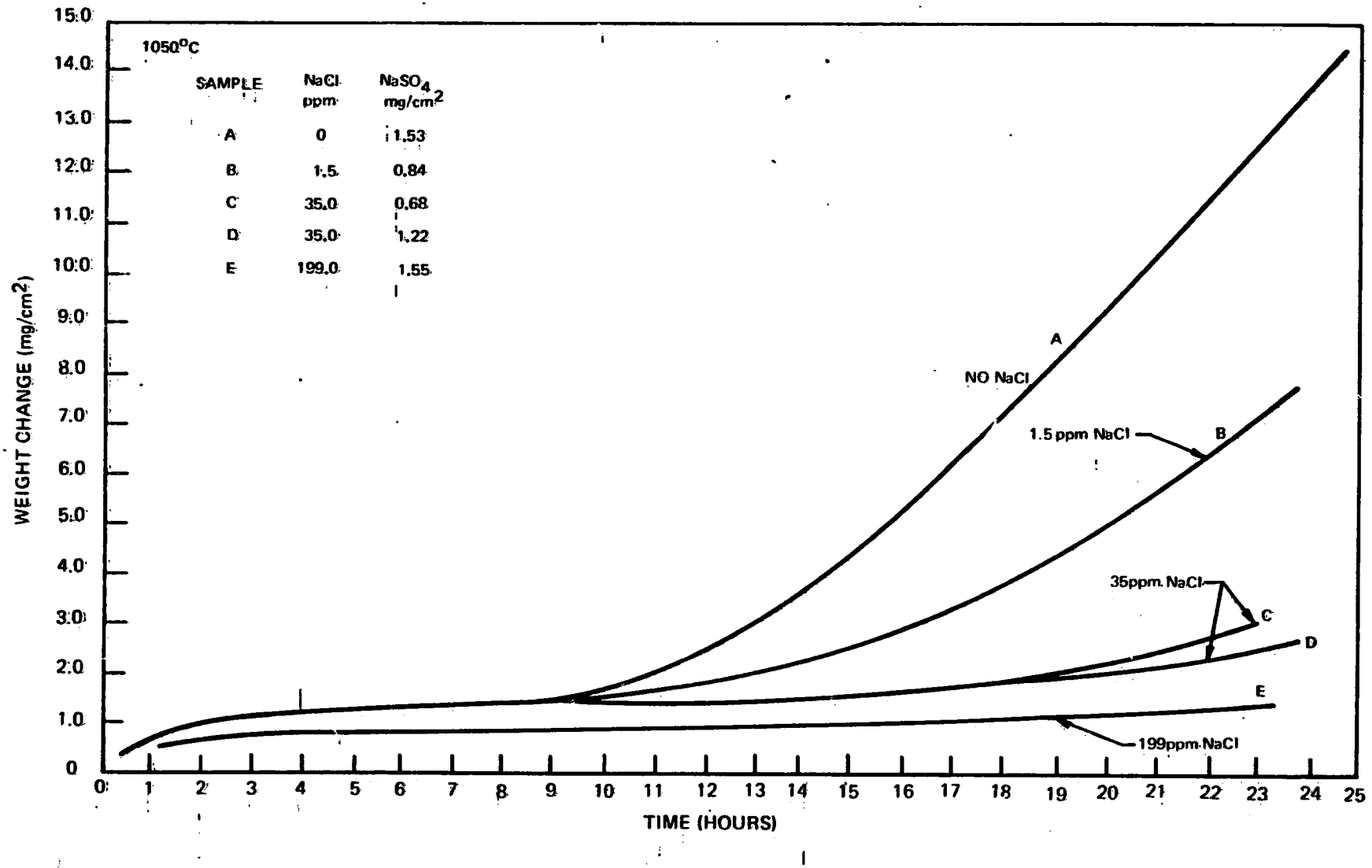

Fig. 35 Na_2SO_4-coated NiAl oxidized at 1050°C in air with NaCl vapors.

Fig. 36 NiAl coated with Na_2SO_4 (1.14 mg/cm^2) and oxidized in air at 900°C for 24 hours.

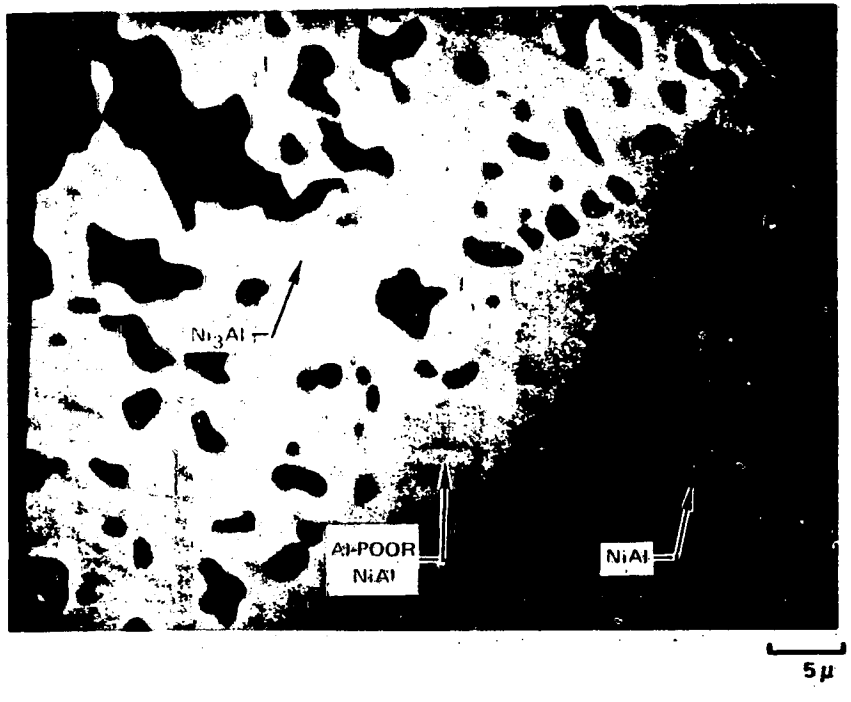

Fig. 37 NiAl coated with Na_2SO_4 (1.14 mg/cm^2) and oxidized in air at 900°C for 24 hours showing particles largely contained in a Ni_3Al layer.

ORIGINAL PAGE IS
OF POOR QUALITY

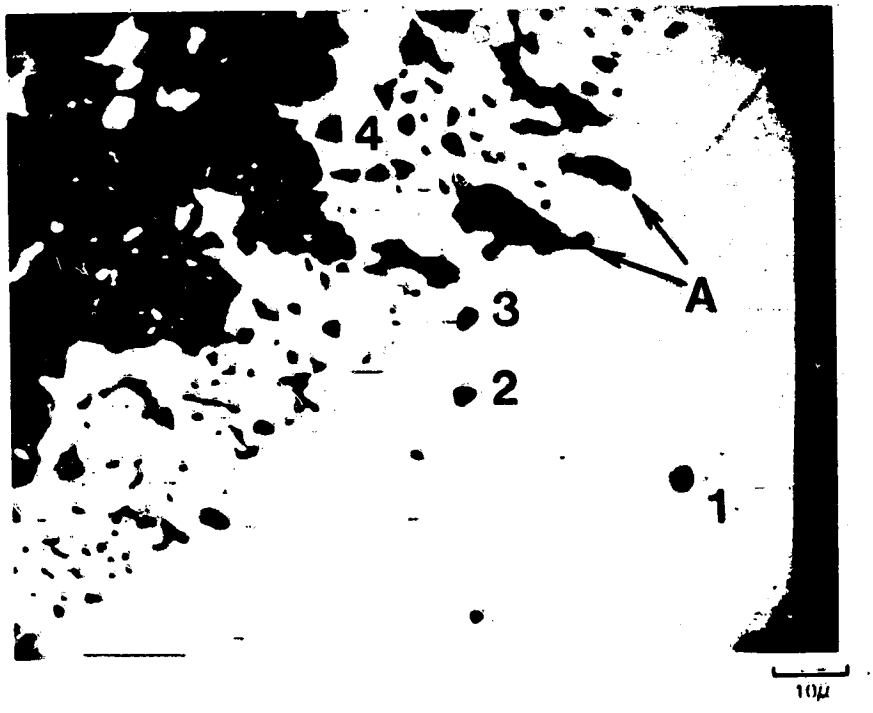

Fig. 38 NiAl coated with Na_2SO_4 (1.14 mg/cm^2) and oxidized at 900°C for 24 hours in air.

1. NiAl (29.76 ± 0.04 wt. % Al)
2. NiAl (29.54 ± 0.05 wt. % Al)
3. Al-depleted NiAl (21.38 ± 0.03 wt. % Al)
4. Ni_3Al (11.38 ± 0.19 wt. % Al)

Particles (A) extending into Al depleted NiAl layer

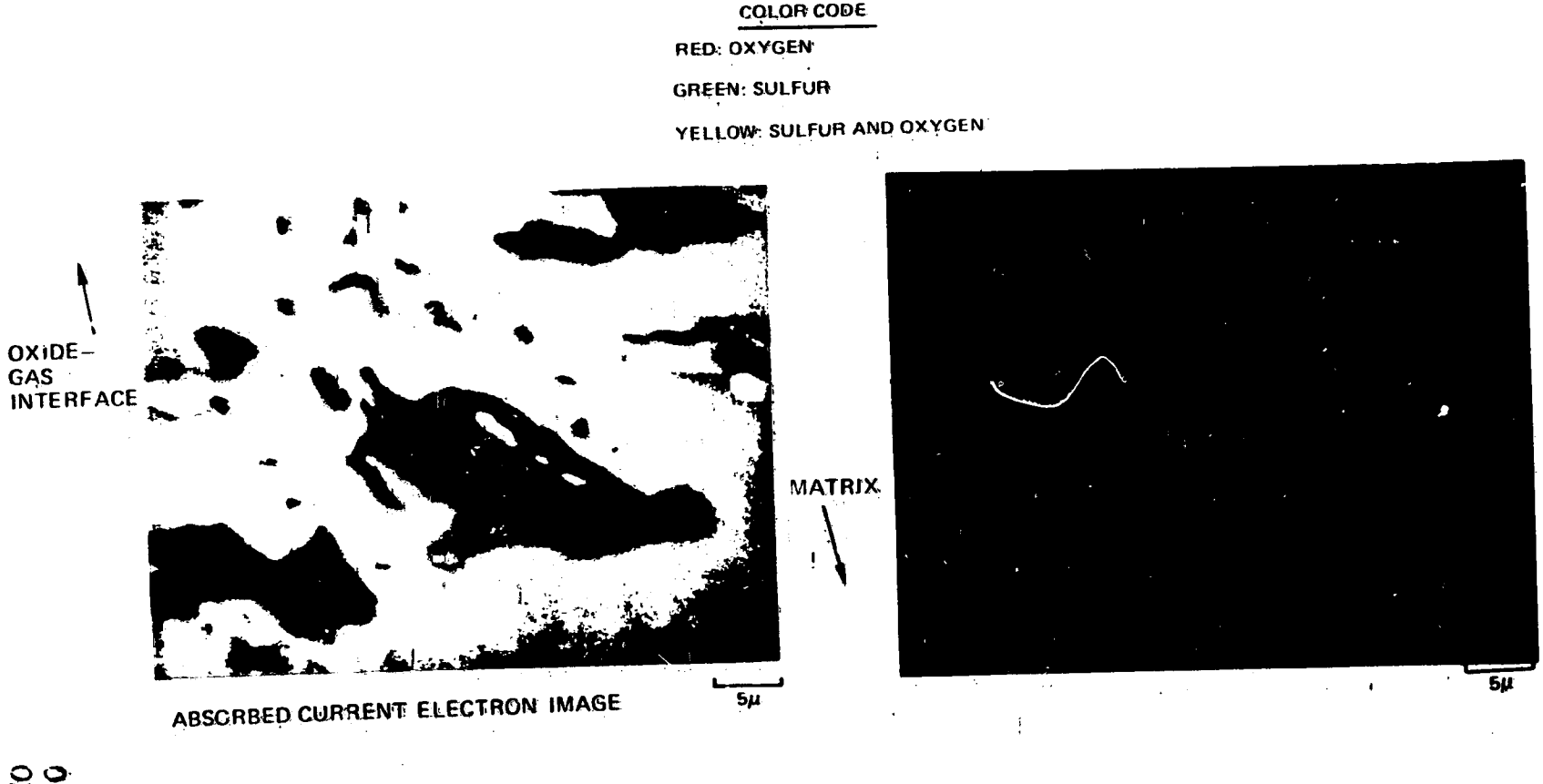

Fig. 39 Oxygen-Sulfur Distribution in Particles Extending into the Al-deficient NiAl layer.

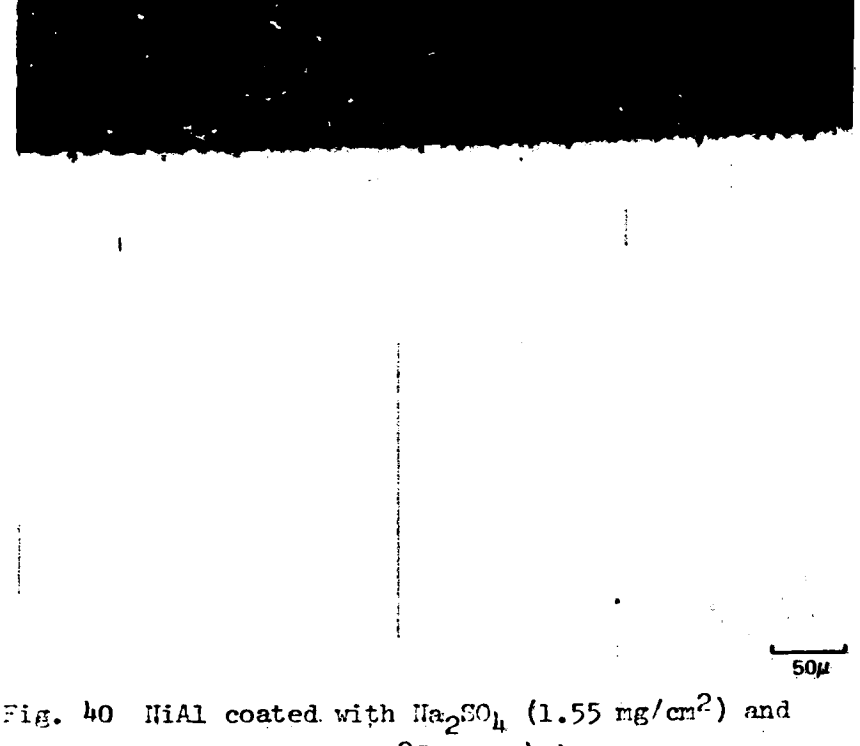

Fig. 40 NiAl coated with Na_2SO_4 (1.55 mg/cm^2) and oxidized at 1050°C for 24 hours in air with 199 ppm NaCl(g).

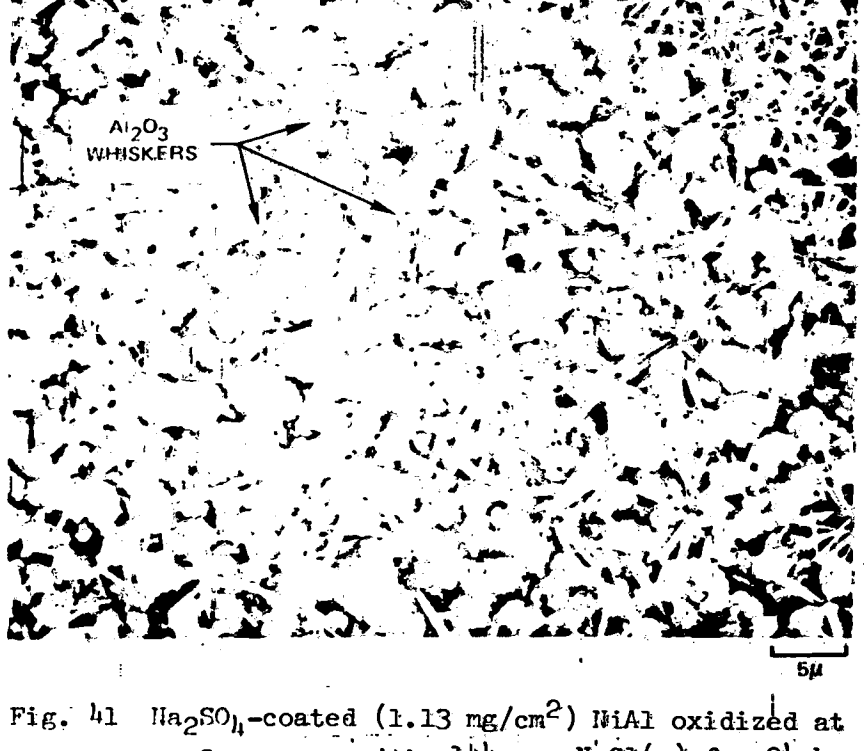

Fig. 41 Na_2SO_4-coated (1.13 mg/cm^2) NiAl oxidized at 900°C in air with 144 ppm NaCl(g) for 24 hours.

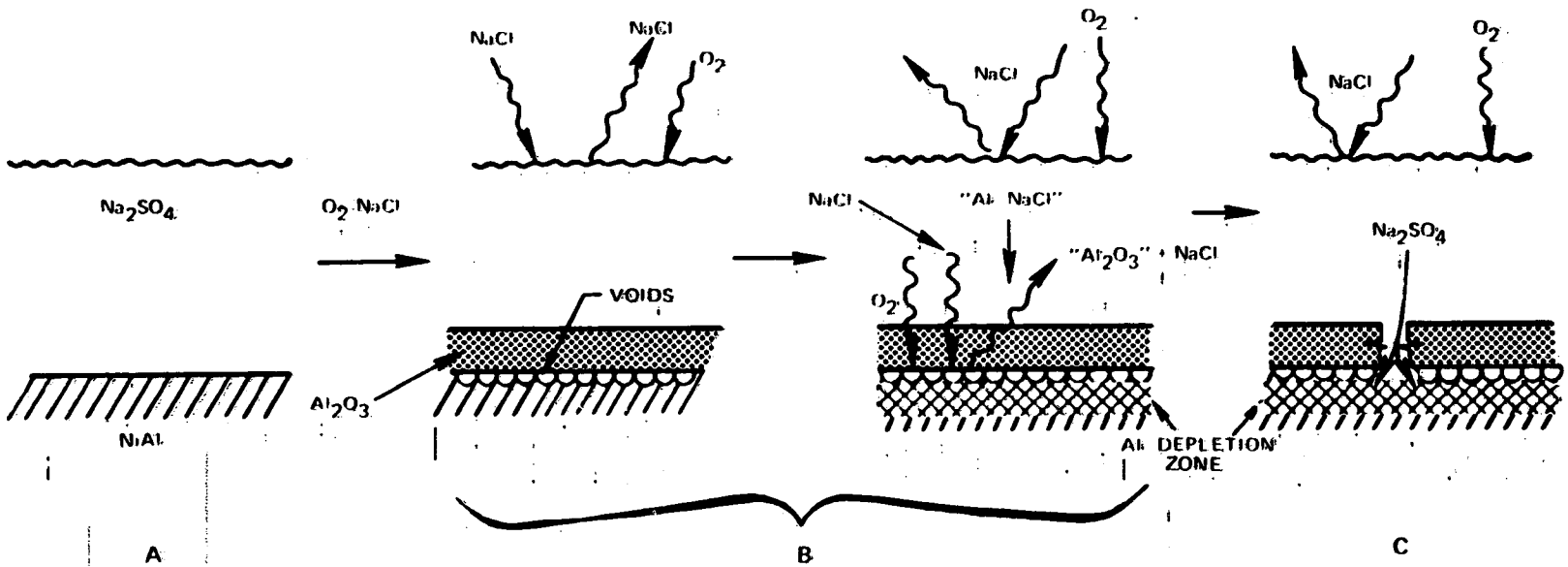

Fig. 42 Effect of NaCl(g) on the Na_2SO_4-Induced corrosion of NiAl.
A. Prior to oxidation.
B. Incubation phase.
C. Propogation phase.

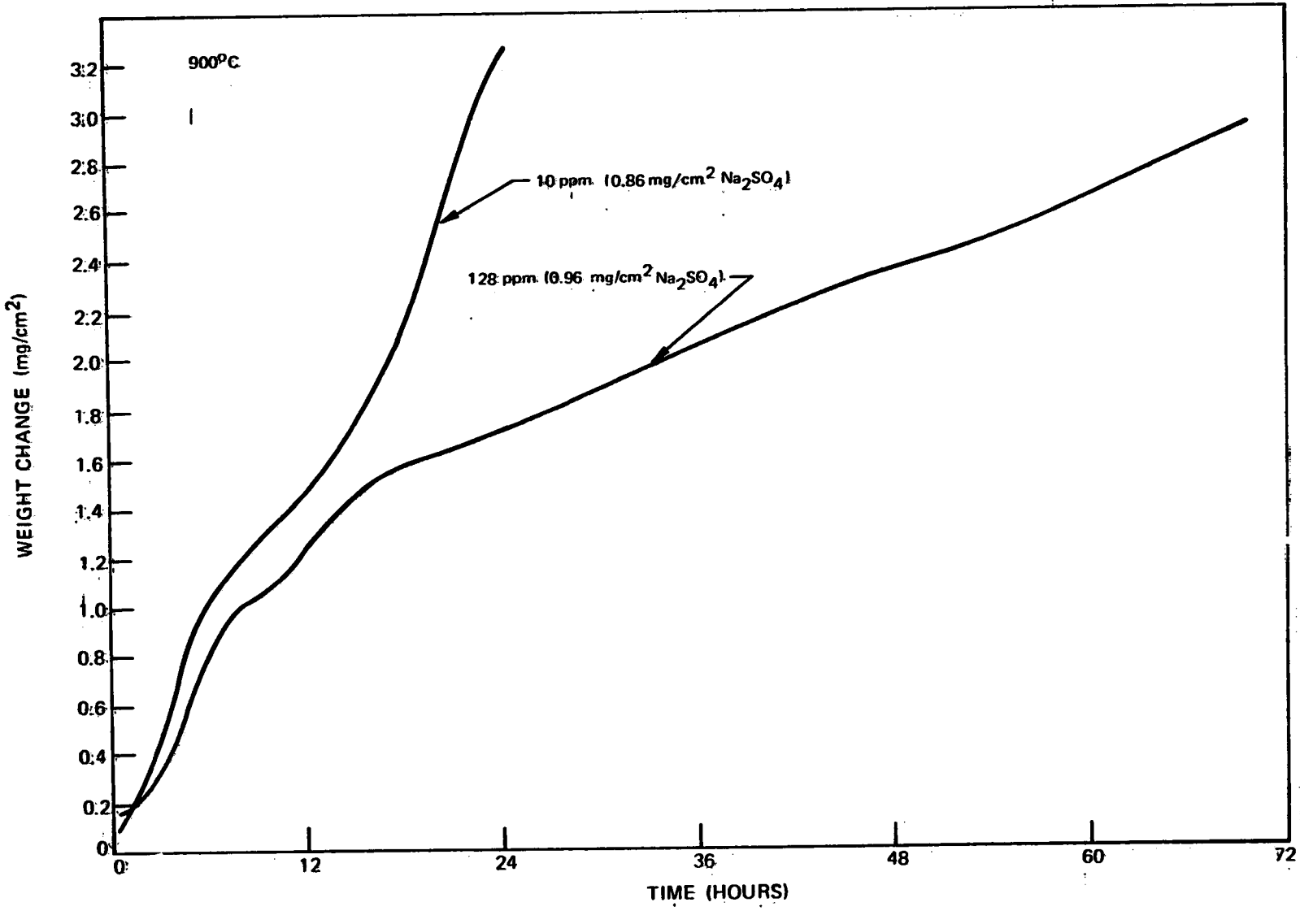

Fig. 43 NiAl oxidized for 24 hours in air containing 10 ppm and 128 ppm HCl(g) at 900°C.

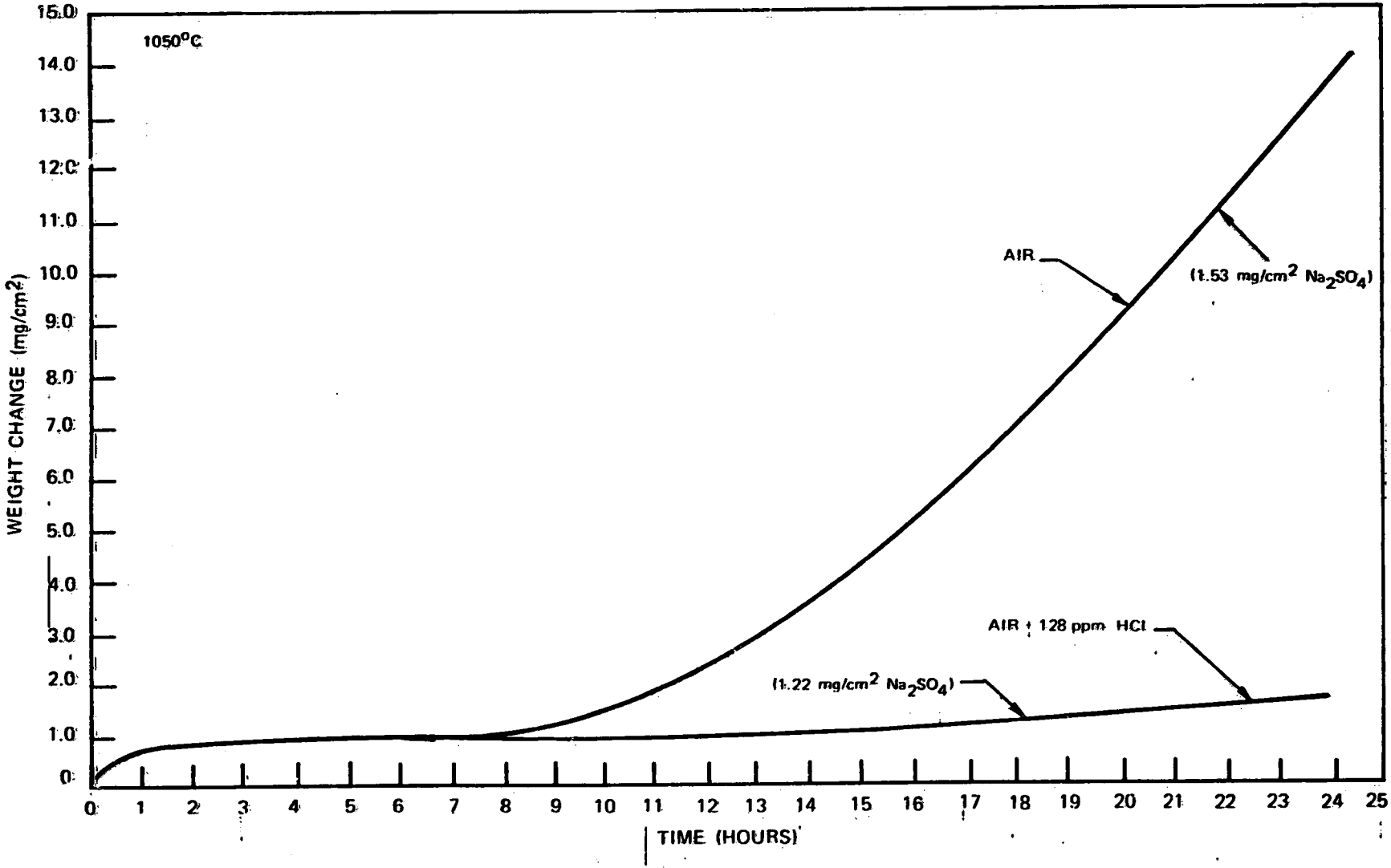

Fig. 44 The effect of 128 ppm HCl(g) on the 1050°C oxidation of Na_2SO_4-coated NiAl.

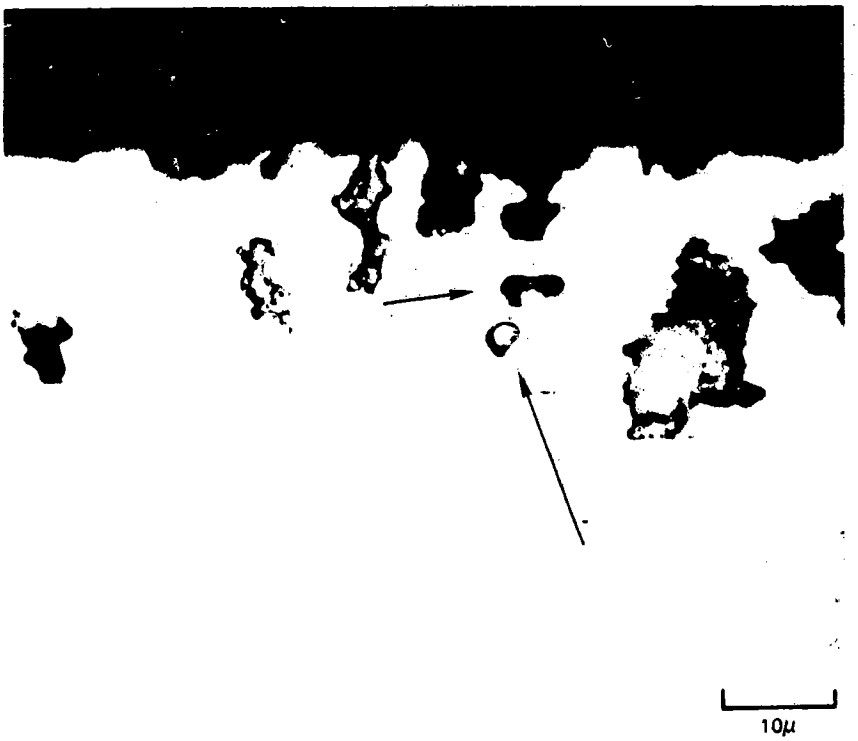

Fig. 45 Na_2SO_4-coated (1.22 mg/cm^2) NiAl oxidized at 1050°C for 24 hours in air containing 128 ppm HCl(g). Note the shiny surfaces on the voids (arrows).

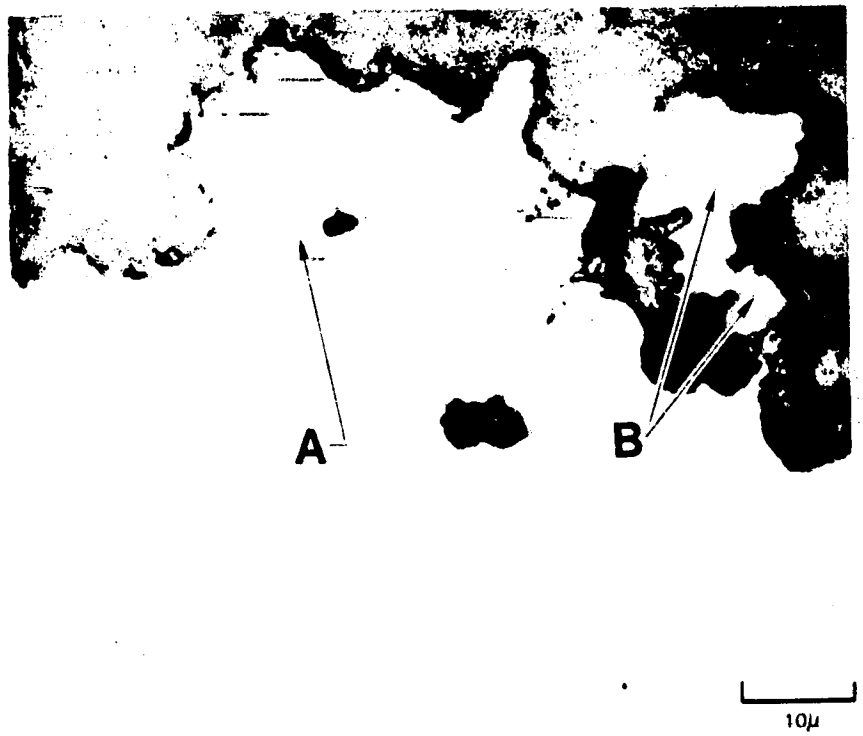

Fig. 46 Na_2SO_4-coated (1.22 mg/cm^2) NiAl oxidized at 1050°C for 24 hours in air containing 128 ppm HCl(g). Note the martensitic structure (A) and possible γ' (B).

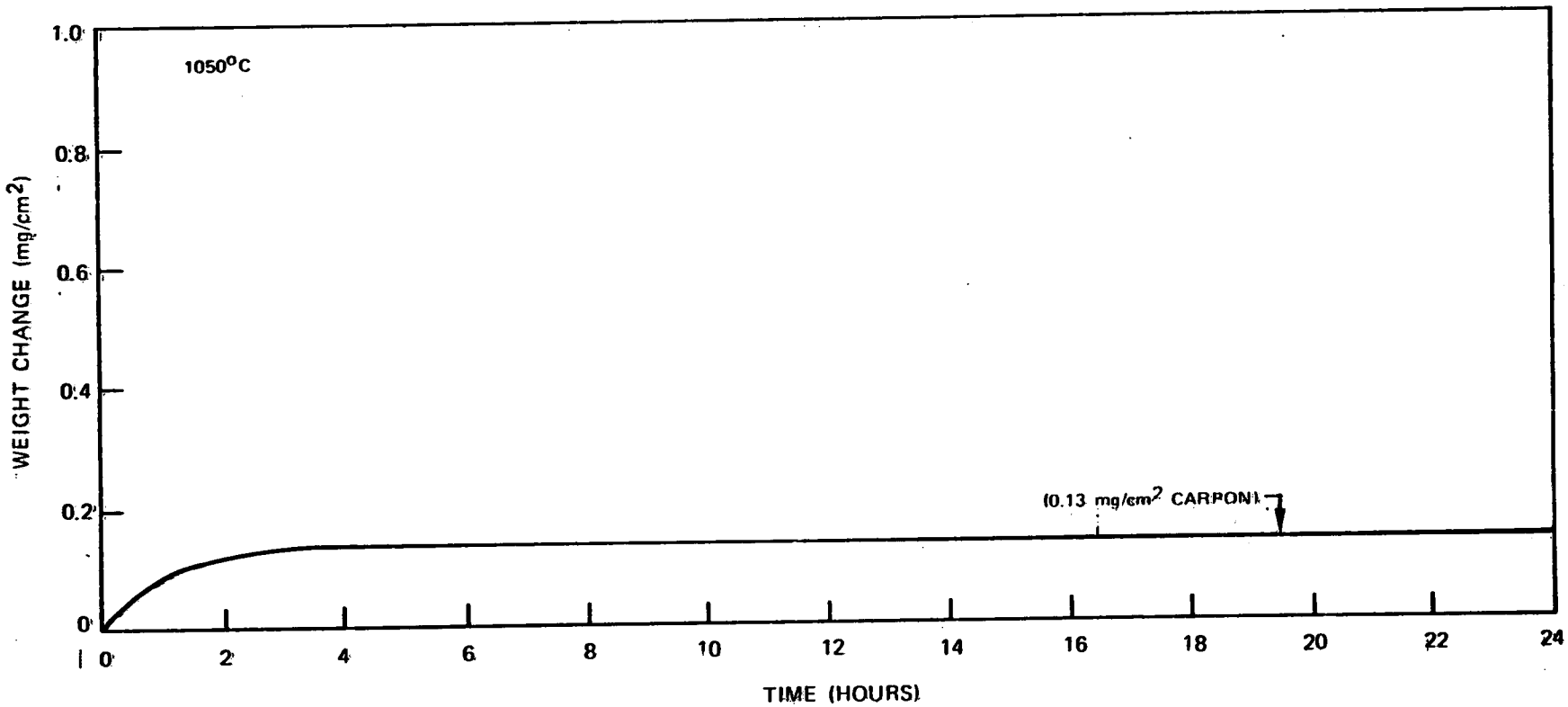

Fig. 47 NiAl coated with carbon (0.13 mg/cm^2) and oxidized in air at 1050°C.

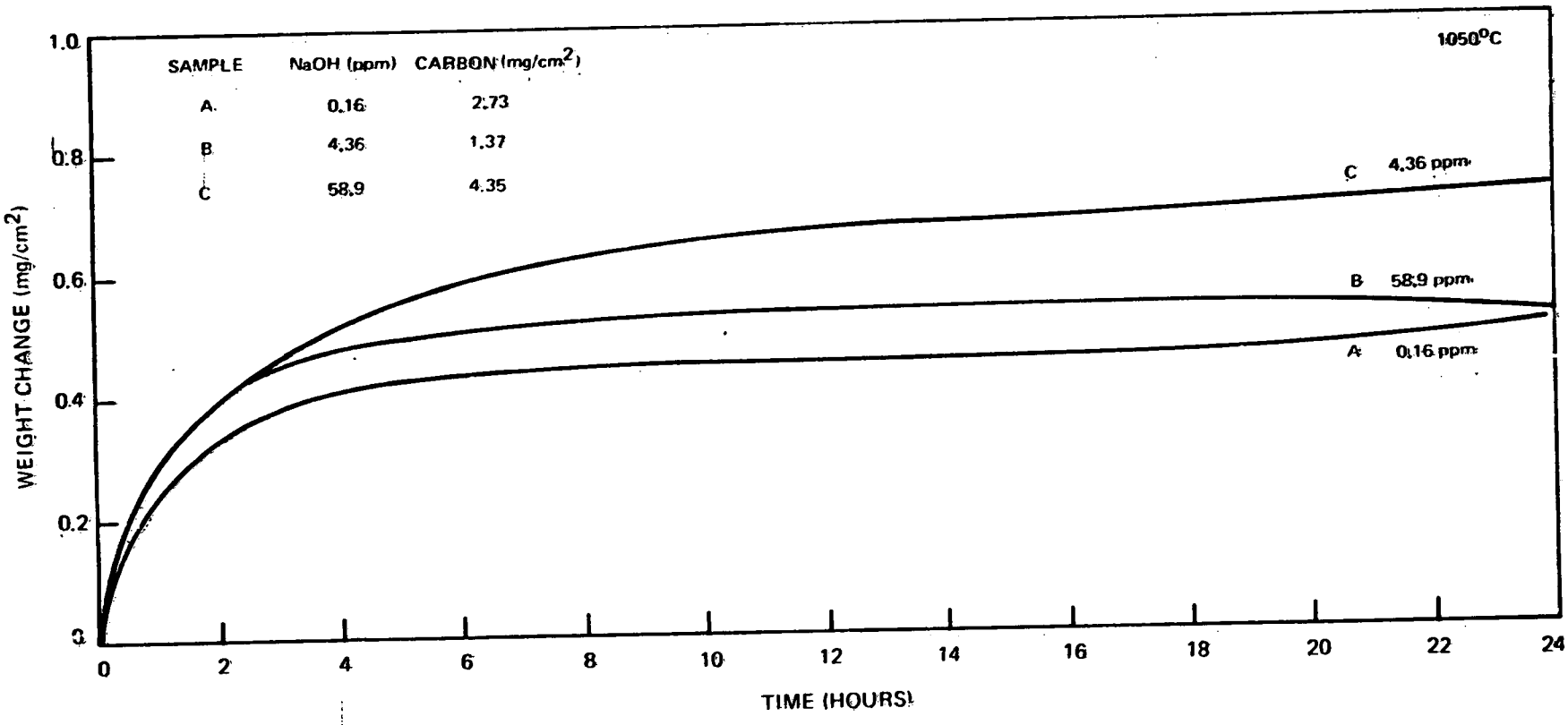

Fig. 4: Carbon-coated NiAl oxidized in air with NaOH(g) at 1050°C.

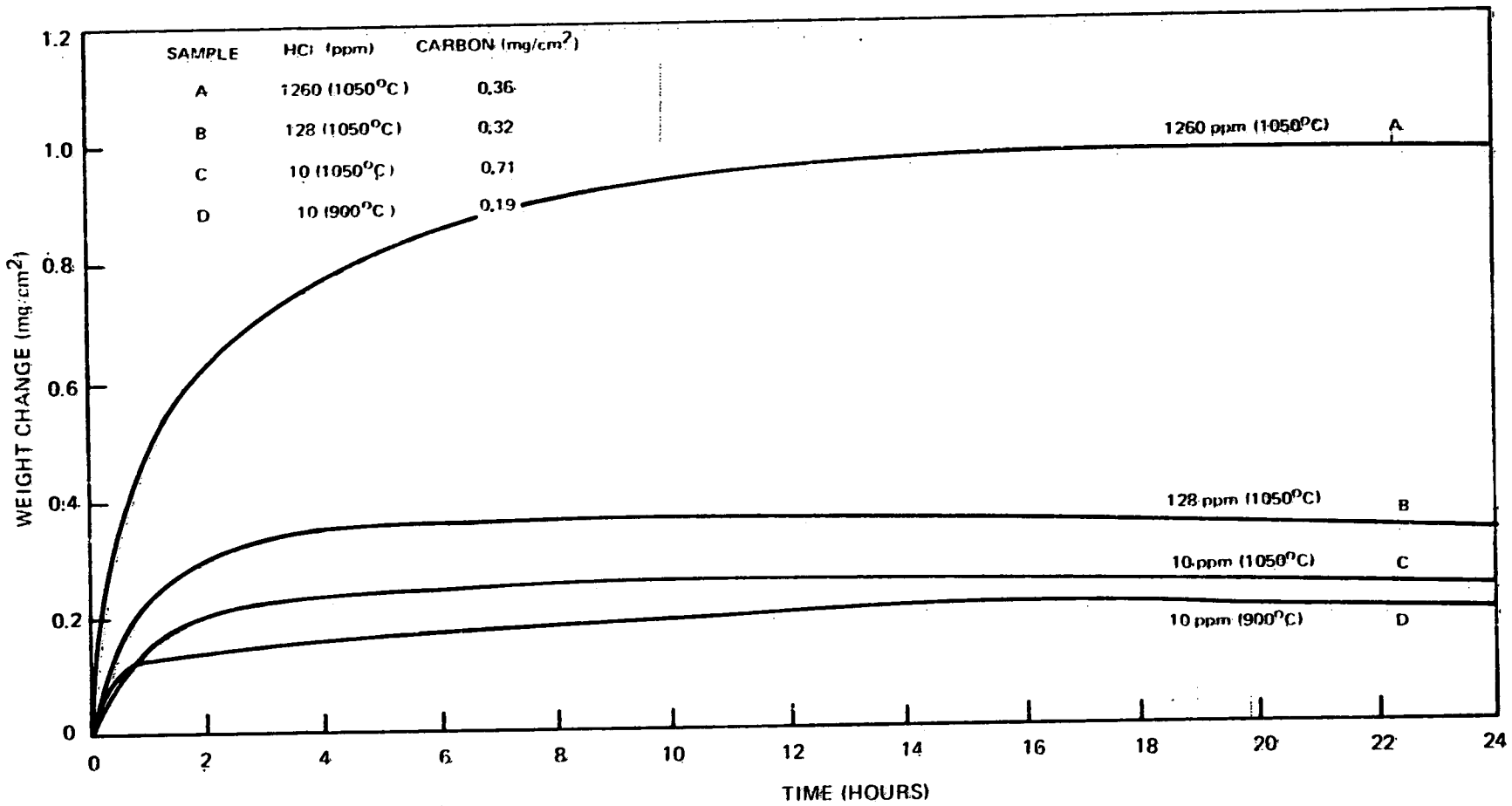

Fig. 49 Carbon-coated NiAl oxidized in air with HCl(g).

C-2

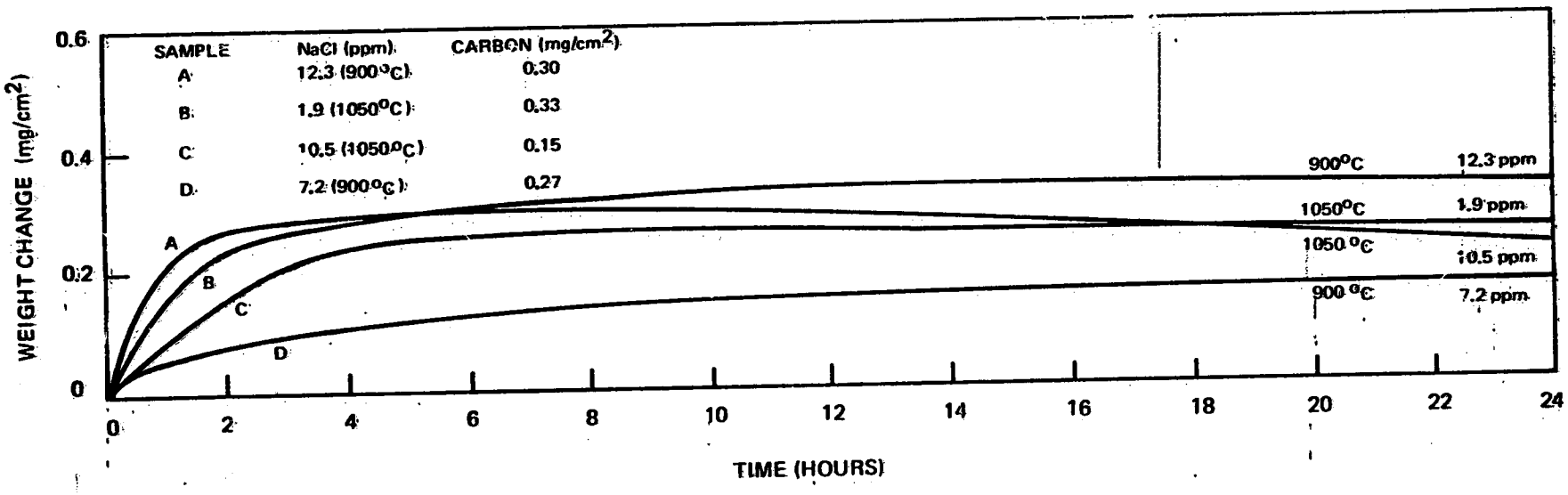

Fig. 50 Carbon-coated NiAl oxidized in air with NaCl(g).

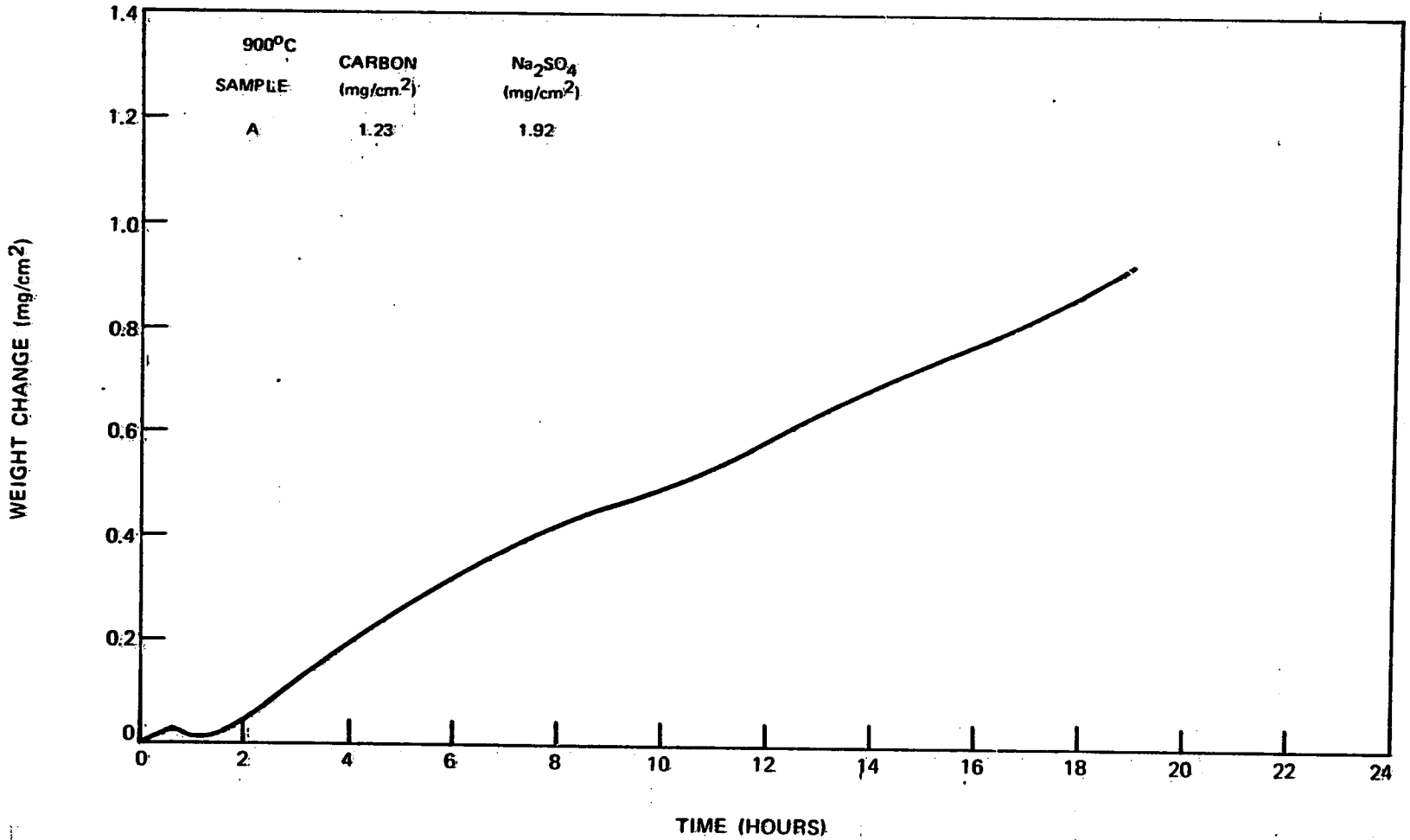

Fig. 51 Oxidation data for Na_2SO_4-carbon coated NiAl oxidized at 900°C.

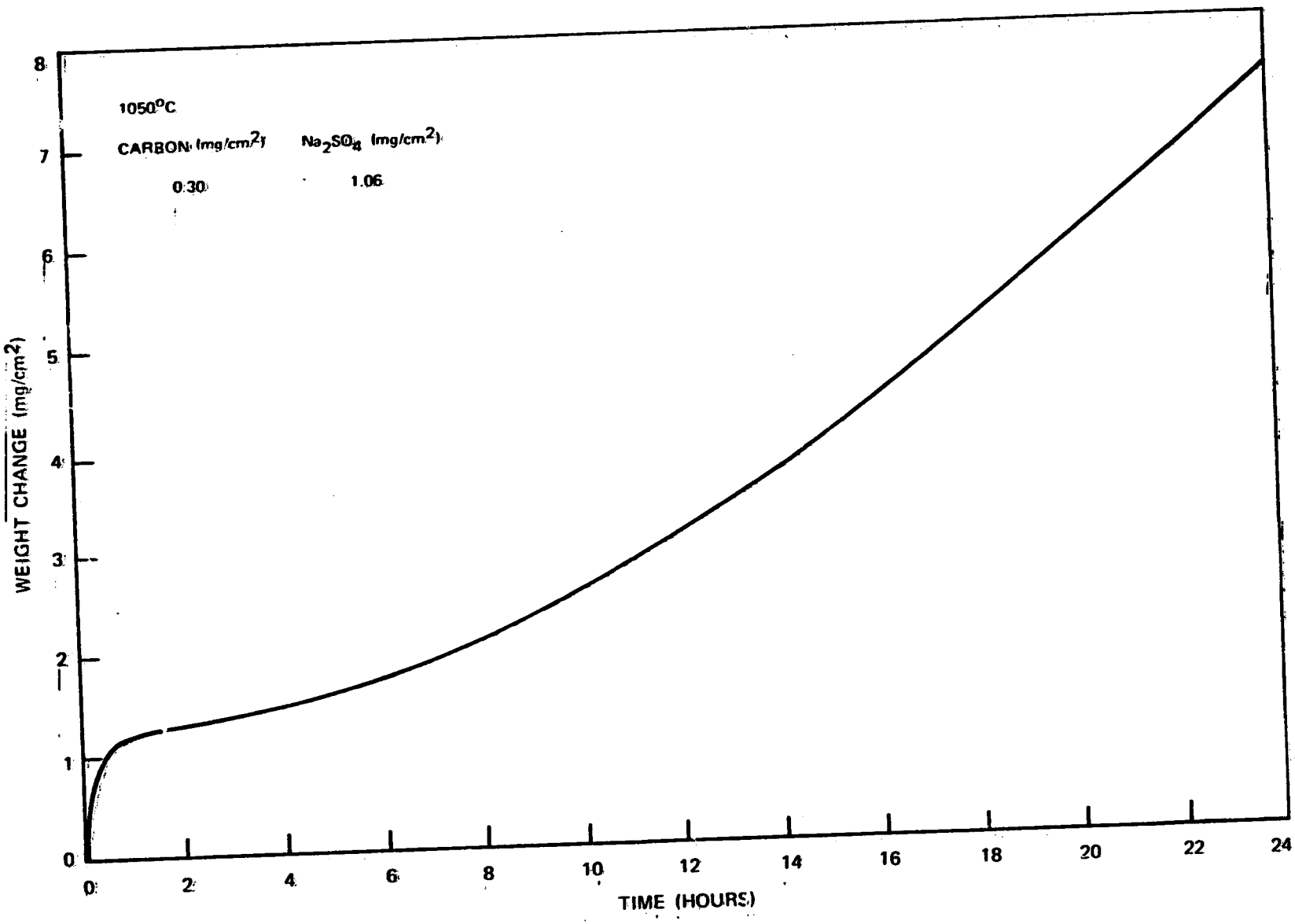

Fig. 52 IN-Al coated with carbon and Na_2SO_4 and oxidized at 1050°C in air.

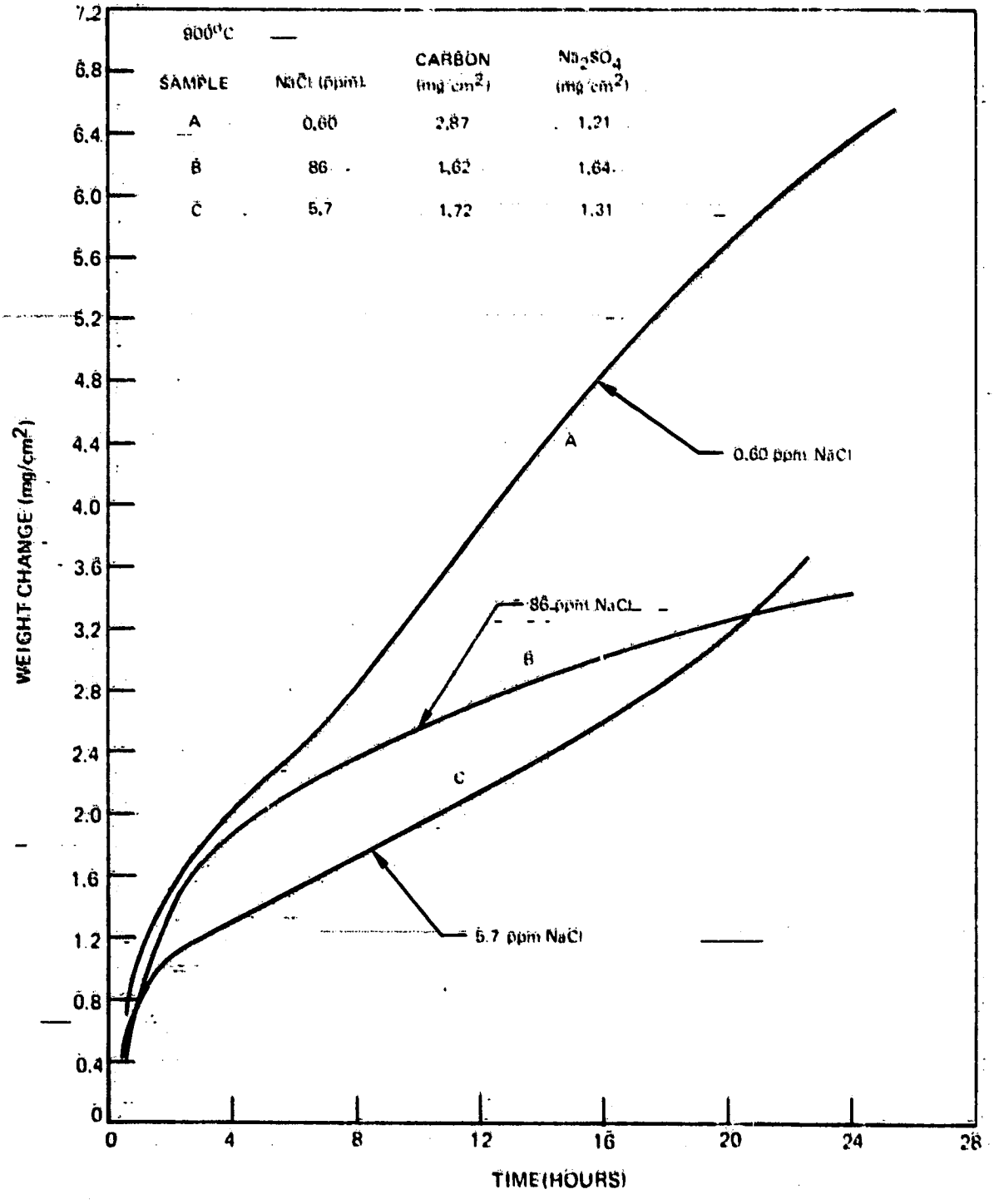

Fig. [illegible] Oxidation data for Na_2SO_4-carbon coated NiAl exposed at 900°C to [illegible] atmospheres containing NaCl vapors.

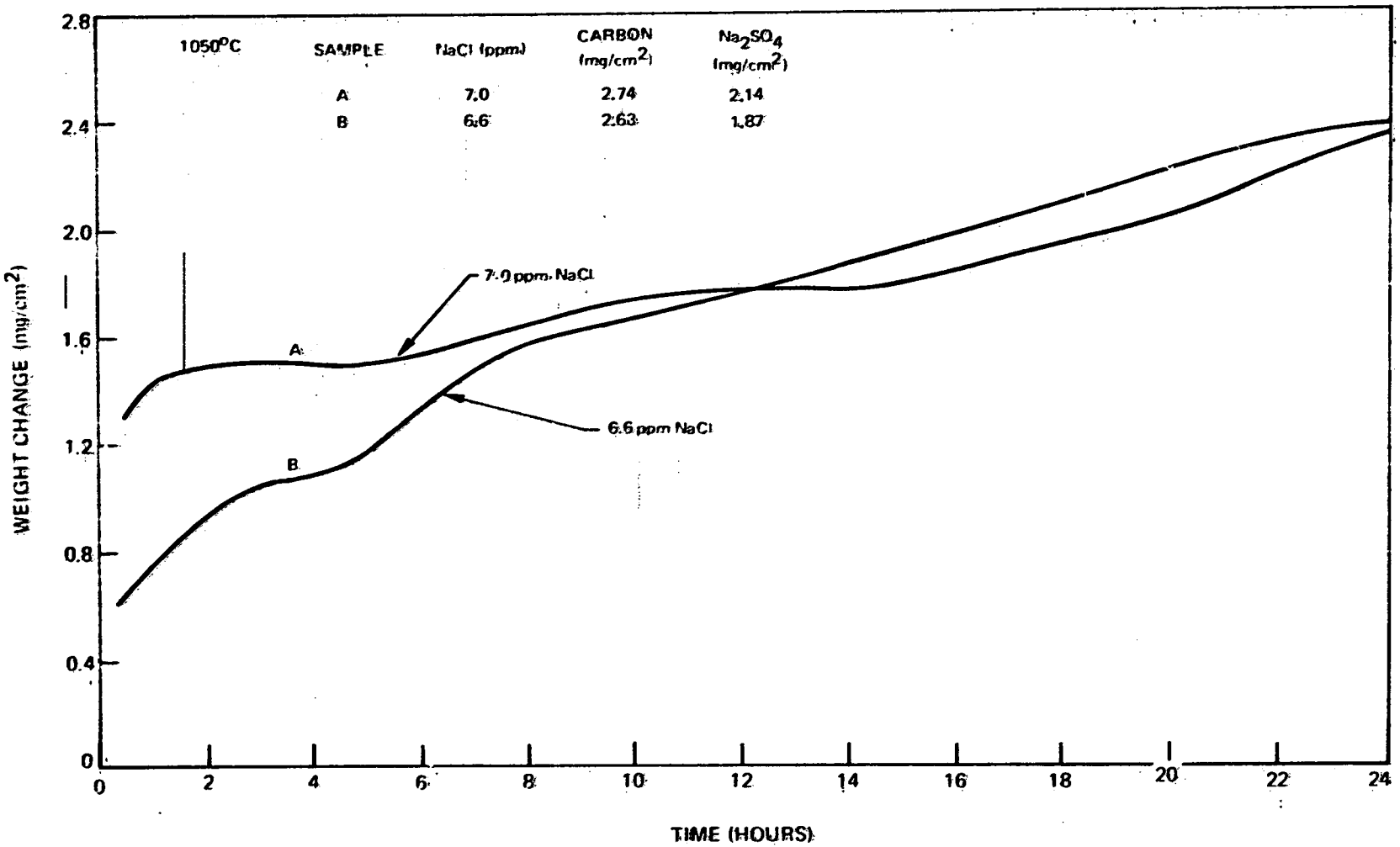

Fig. 54 Oxidation data for Na_2SO_4-carbon coated NiAl exposed at 1050°C to atmospheres containing NaCl vapors.

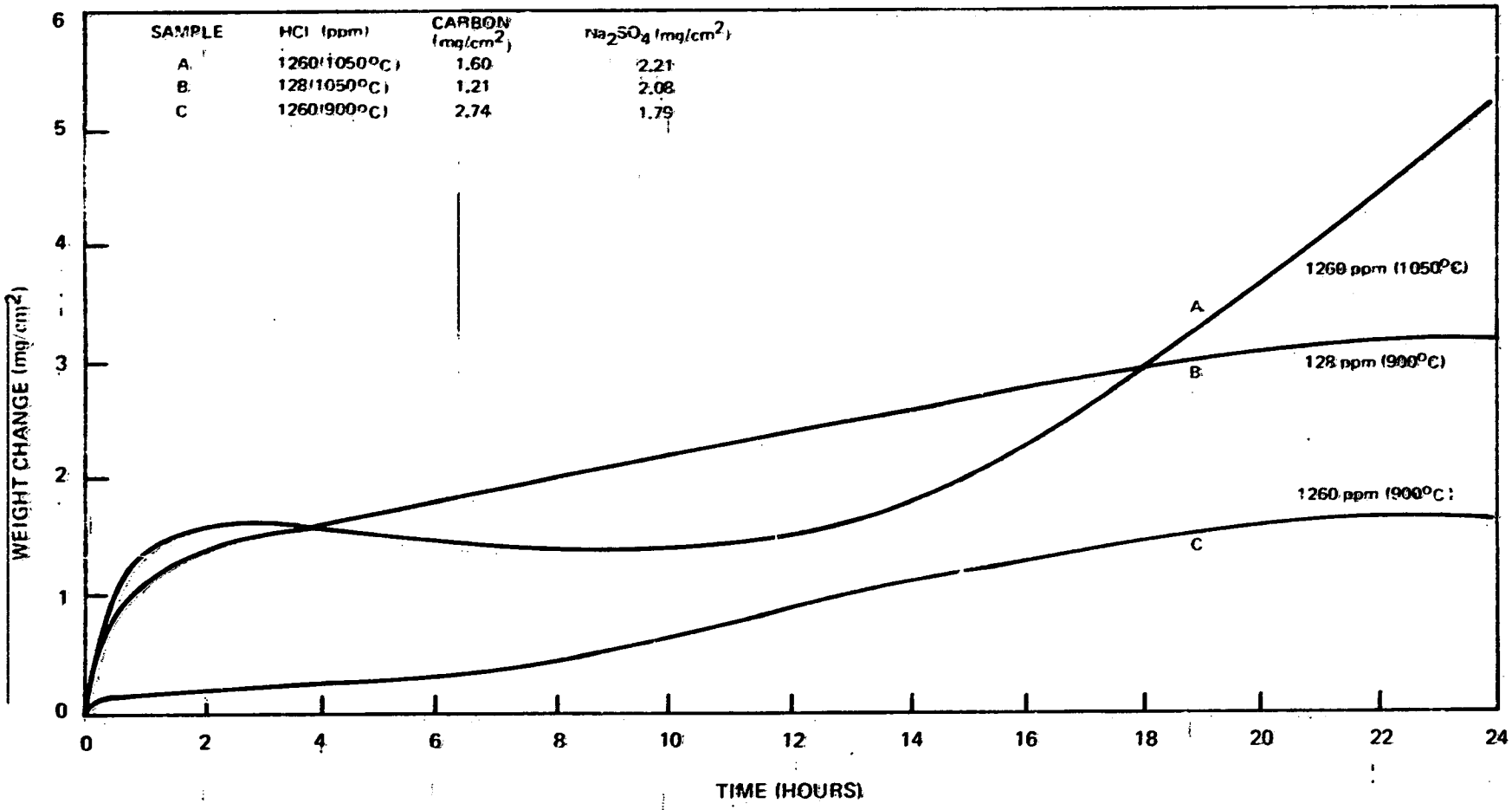

Fig. 55 NiAl coated with carbon and Na_2SO_4 and oxidized in air with $HCl(g)$.

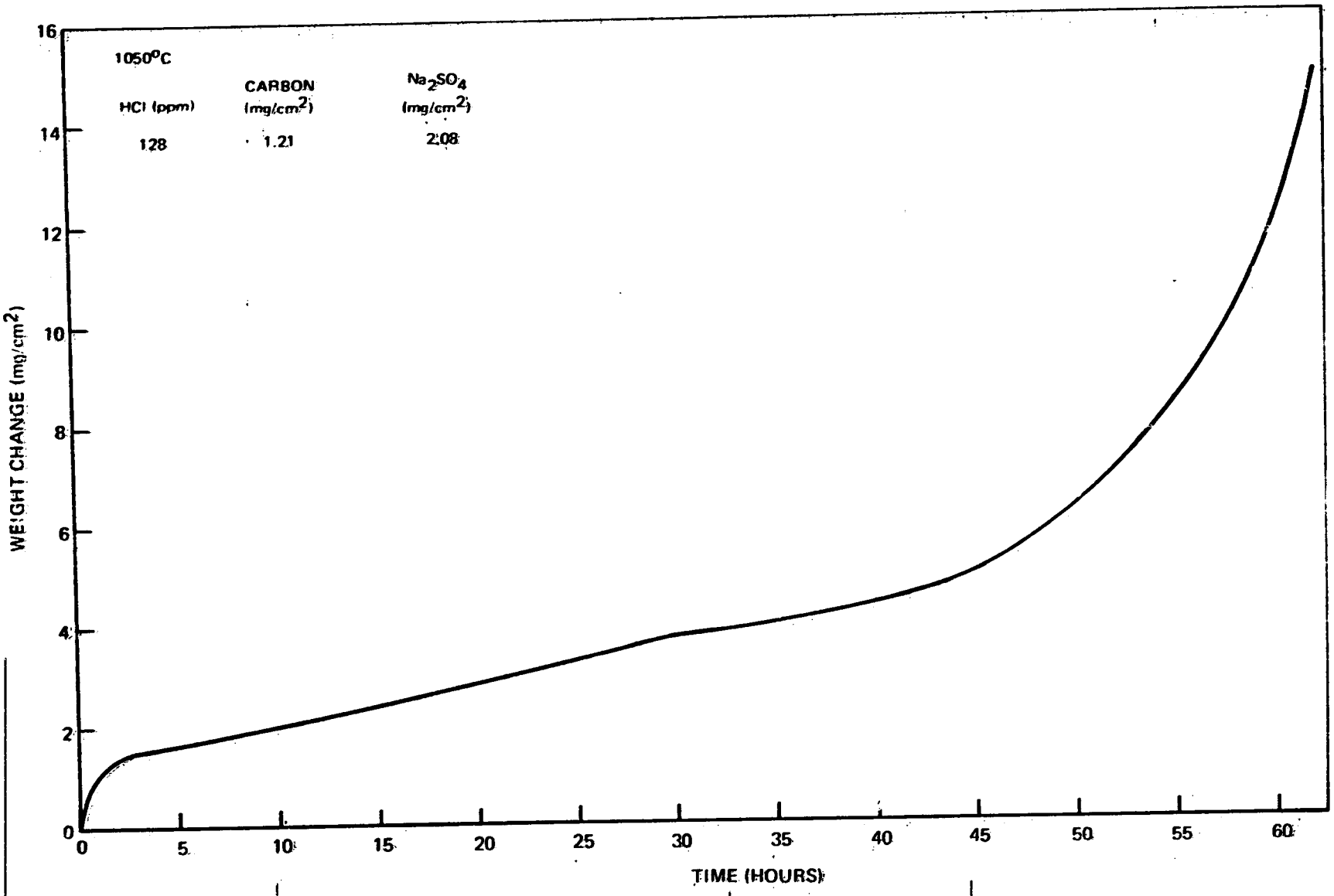

Fig. 56 NiAl coated with Na_2SO_4 and carbon and oxidized at 1050°C in air with 128 ppm HCl(g) showing accelerated attack after about 45 hours.

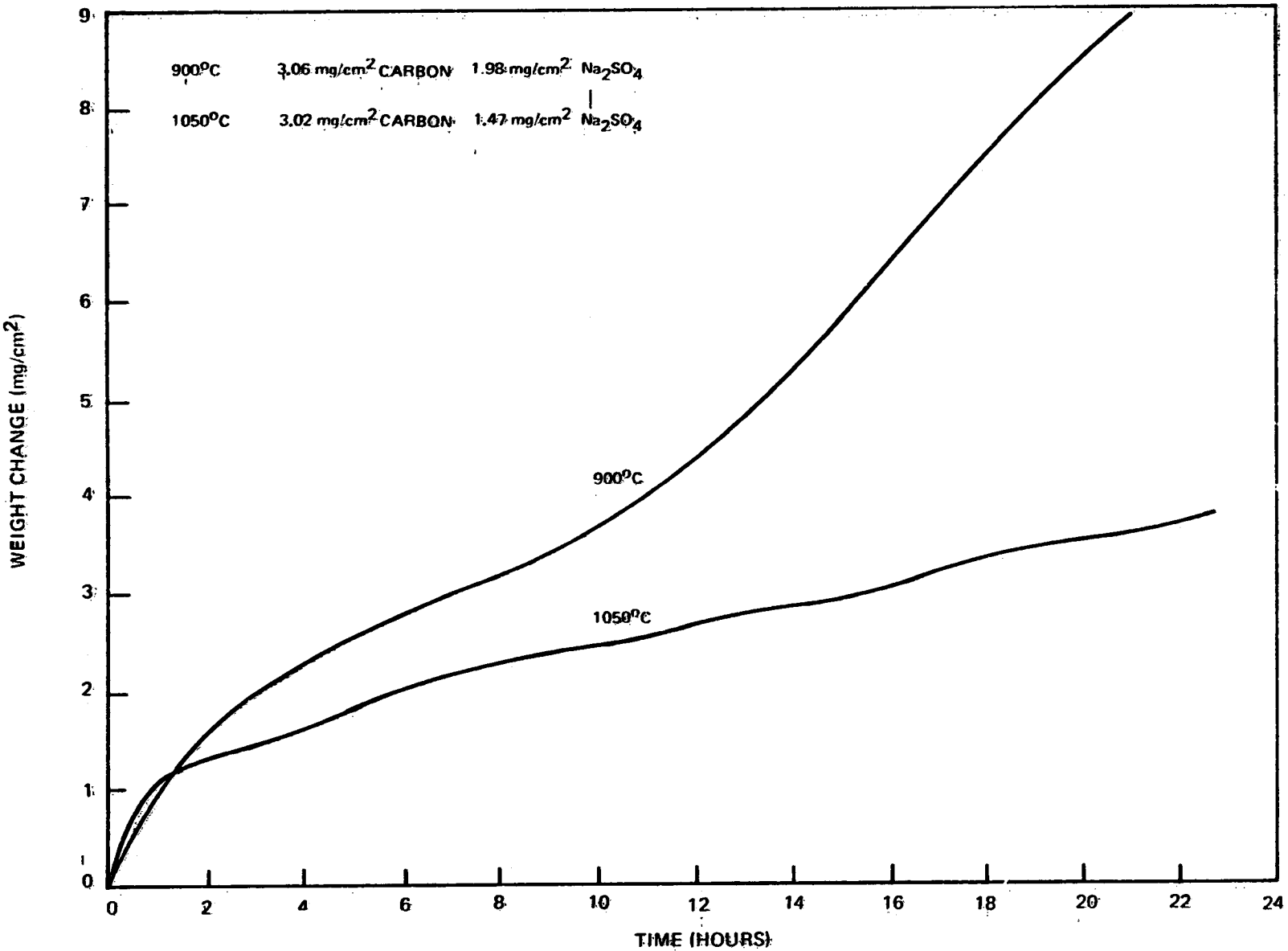

Fig. 57 NiAl coated with Na_2SO_4 and carbon oxidized in air with 58.9 ppm NaOH(g) at 900 and 1050°C.

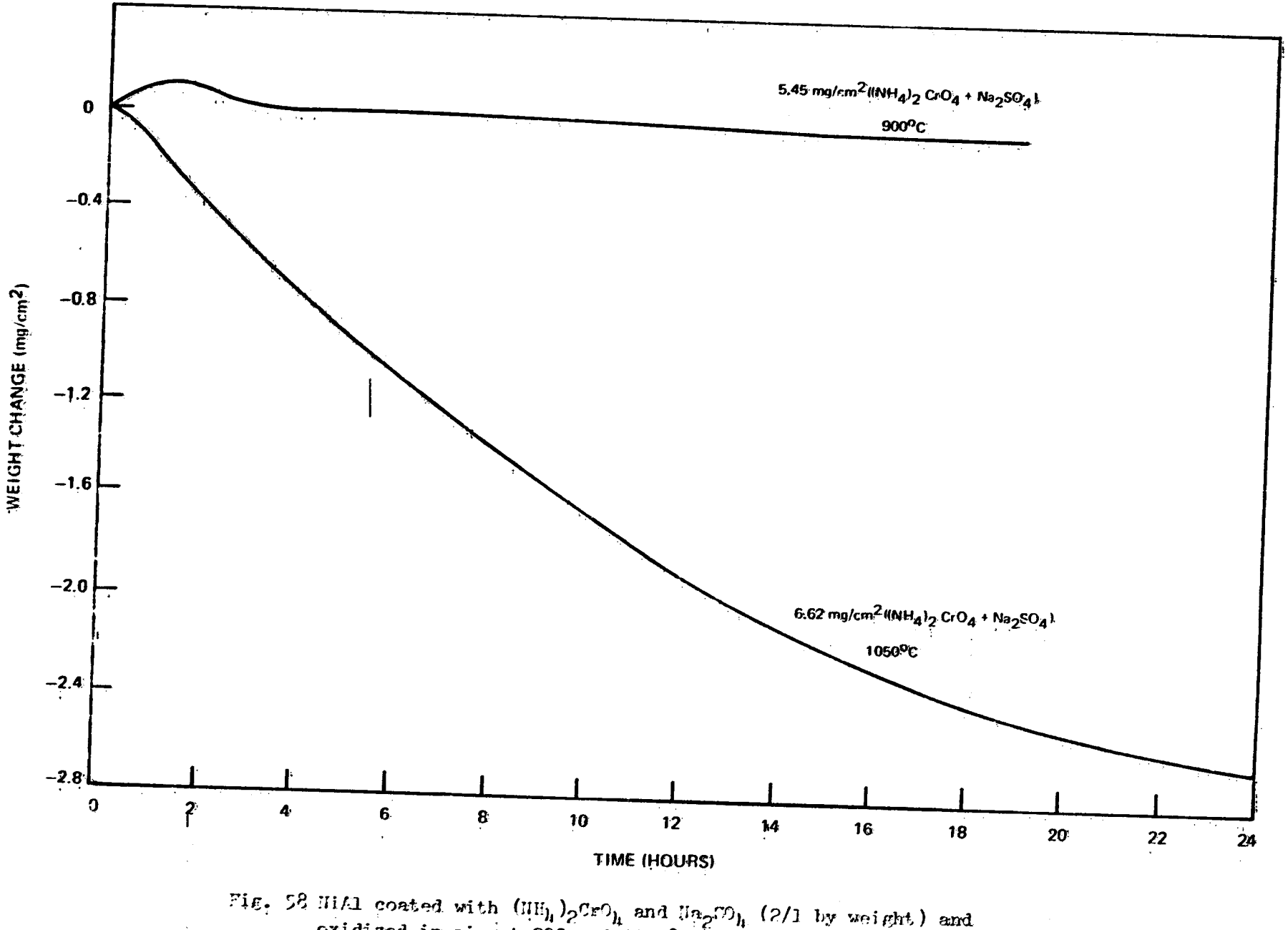

Fig. 58 NiAl coated with $(NH_4)_2CrO_4$ and Na_2SO_4 (2/1 by weight) and oxidized in air at 900 and 1050°C.

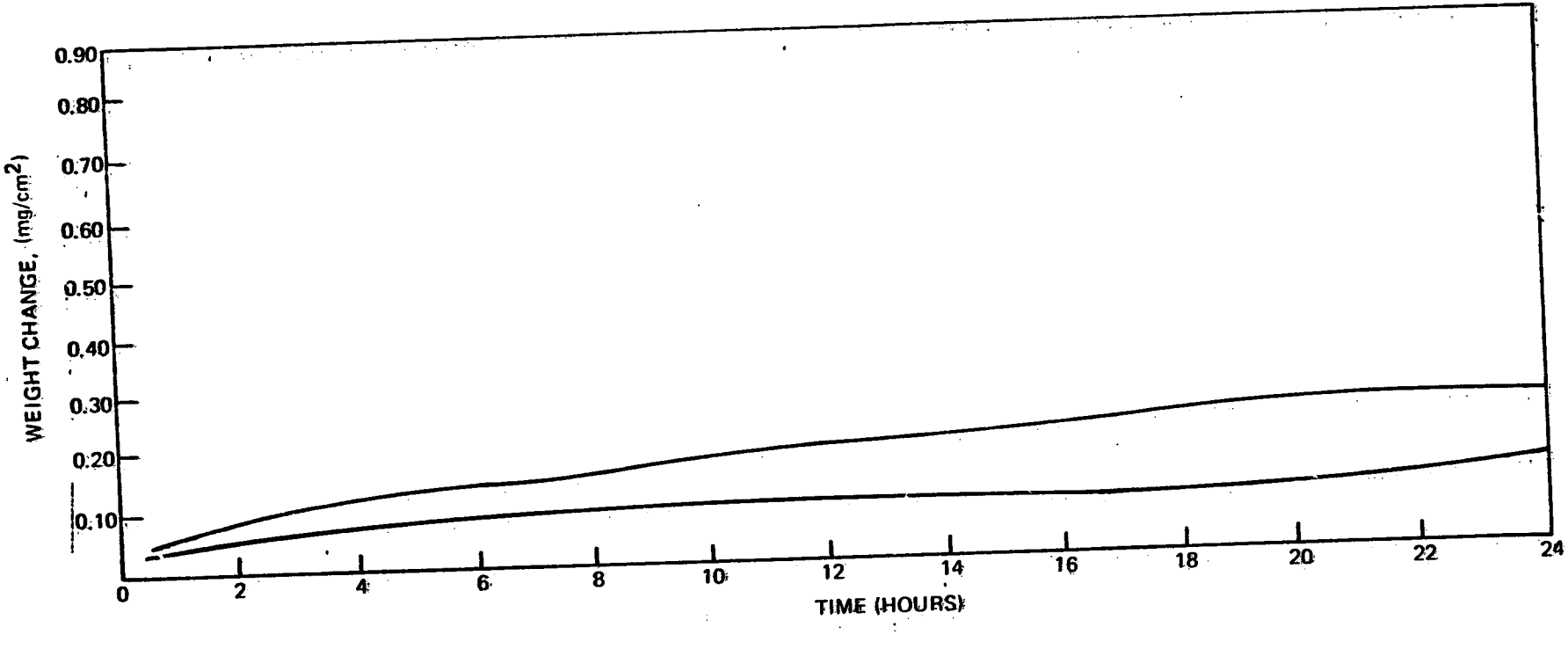

Fig. 59 Ni-25 Cr oxidized in air at 900°C.

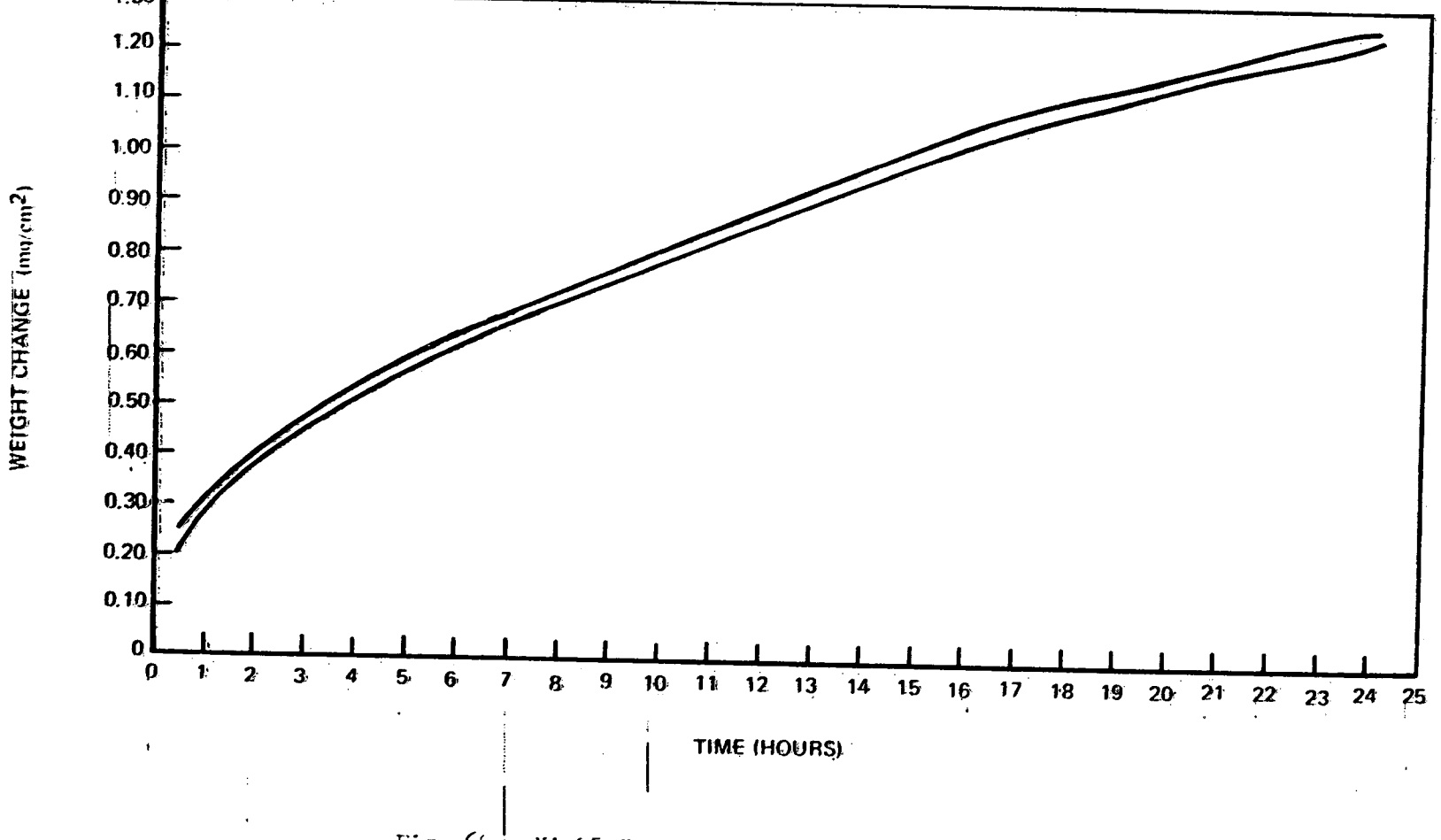

Fig. 6[illegible] Ni-25 Cr oxidized in air at 1050°C.

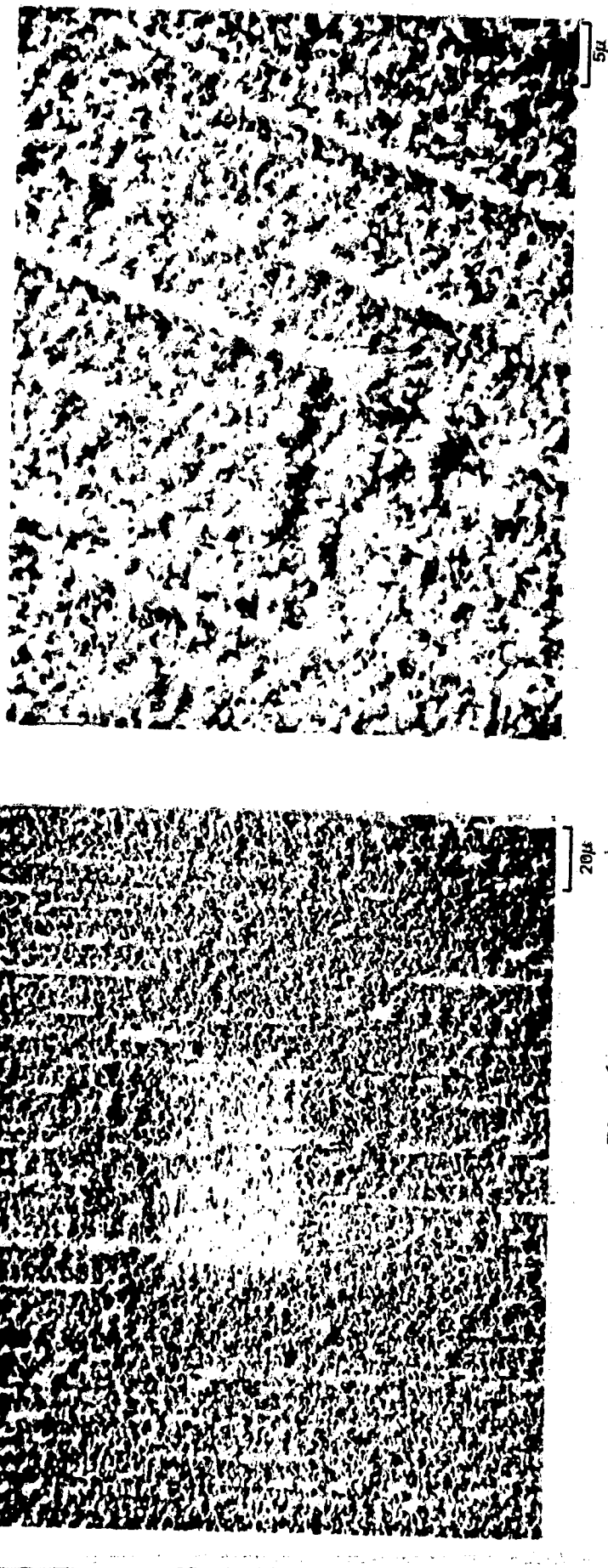

Fig. 61 Ni-25 Cr oxidized for 24 hours at 900°C.

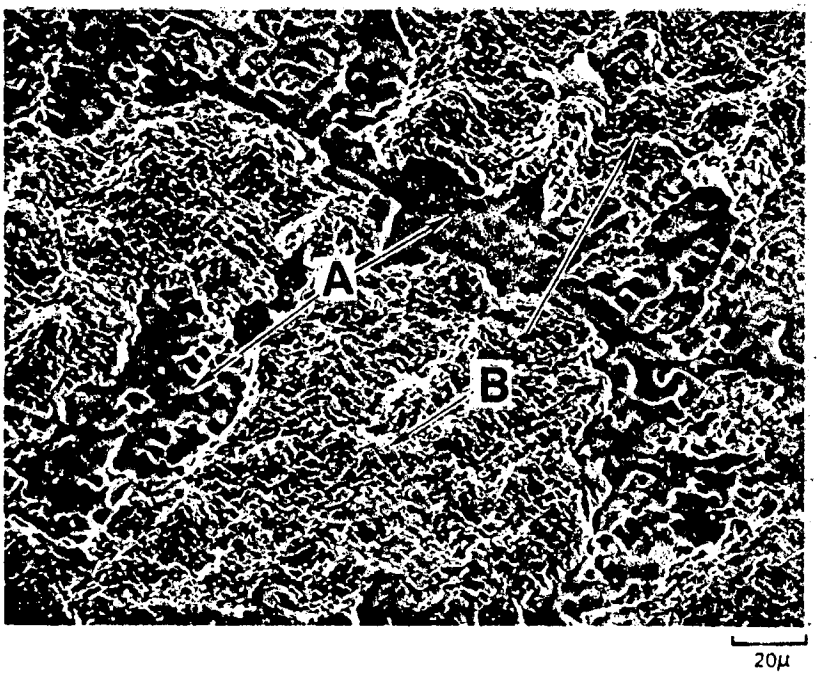

Fig. 62. Hi-25Cr oxidized at 1050°C for 24 hours.
A. Hi-25Cr substrate.
B. Cr_2O_3 scale.

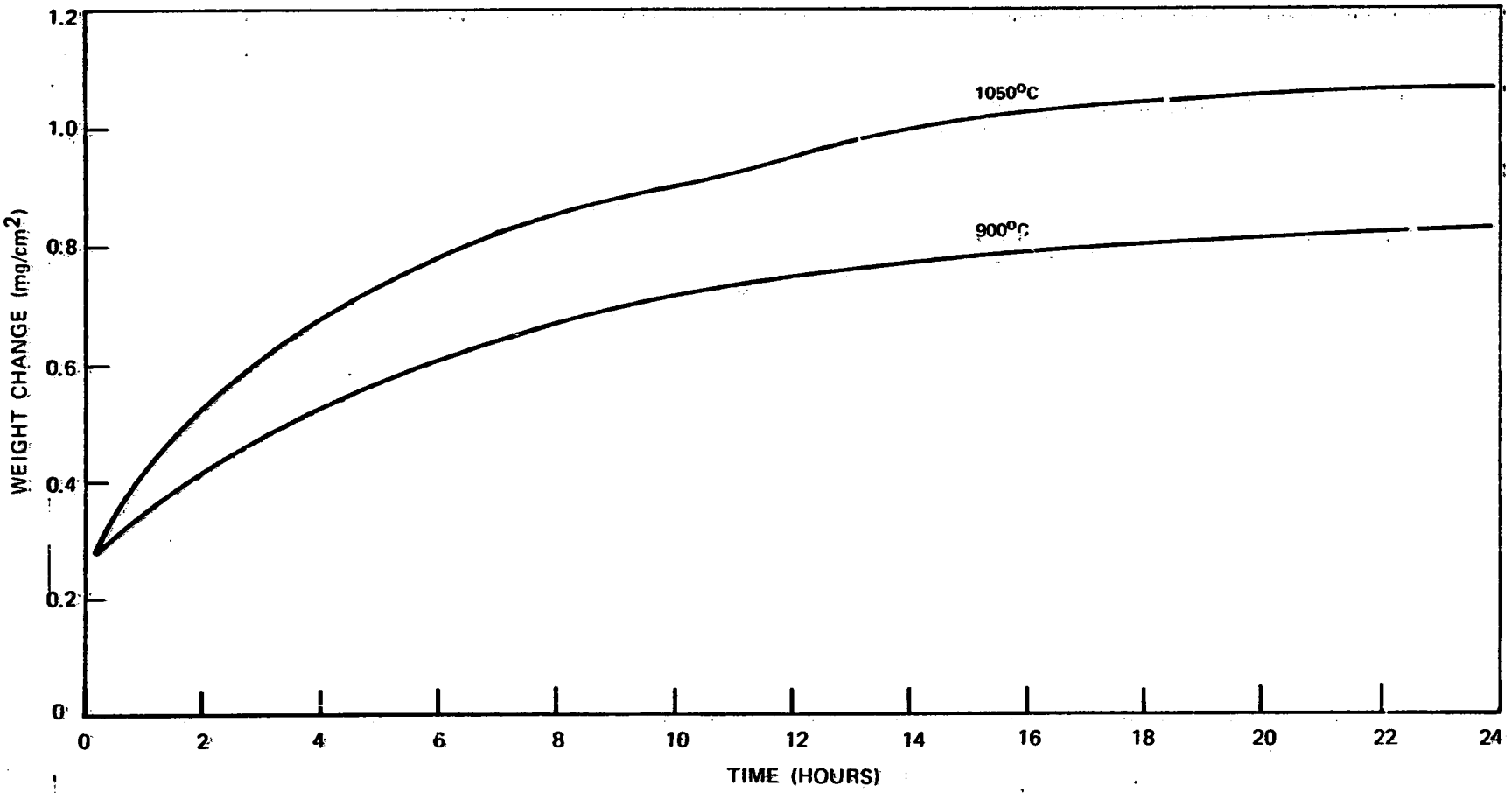

Fig. 63 Ni-25Cr oxidized in wet air at 900 and 1050°C.

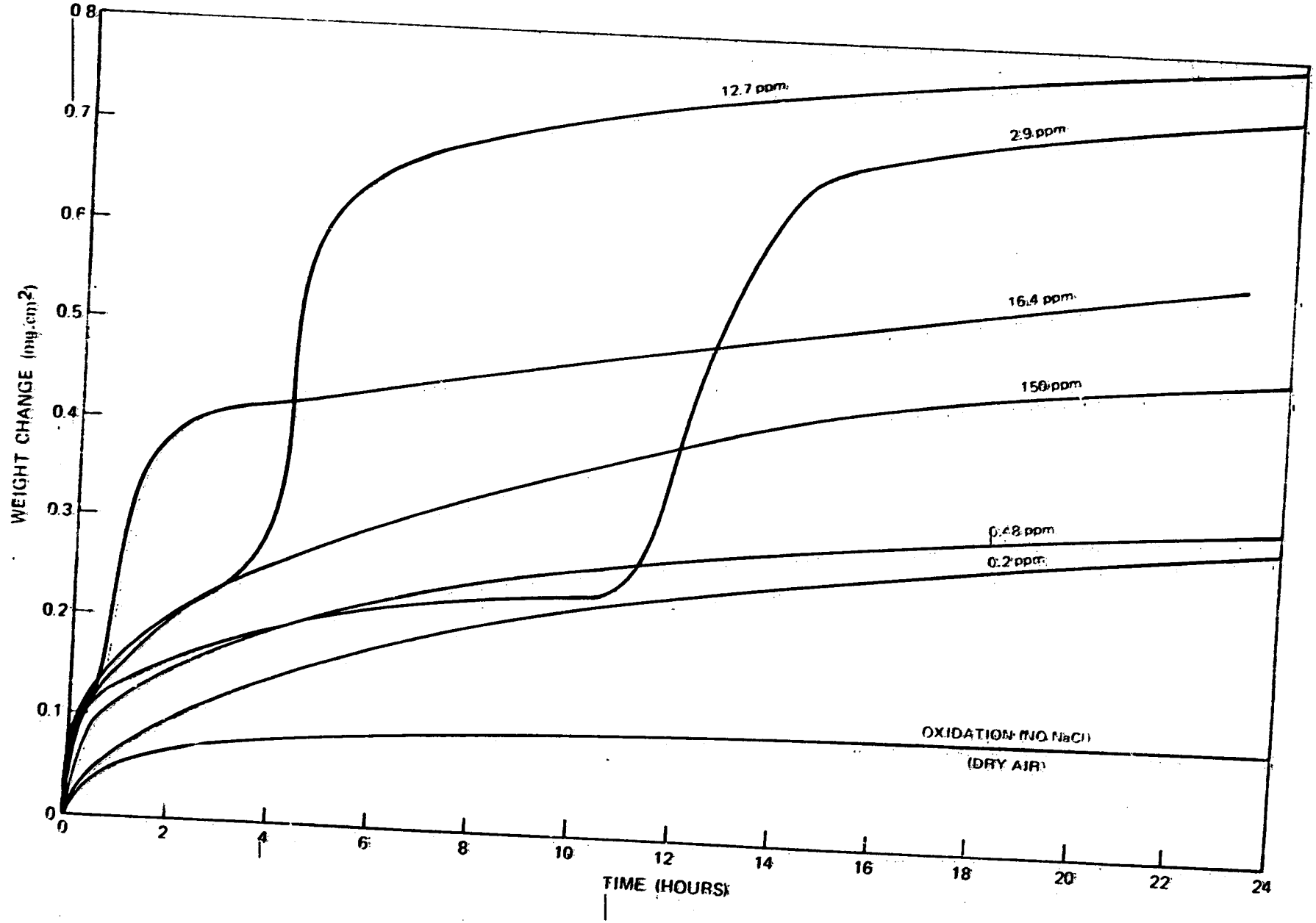

Fig. 34 900°C oxidation of Ni-25 Cr with NaCl vapor.

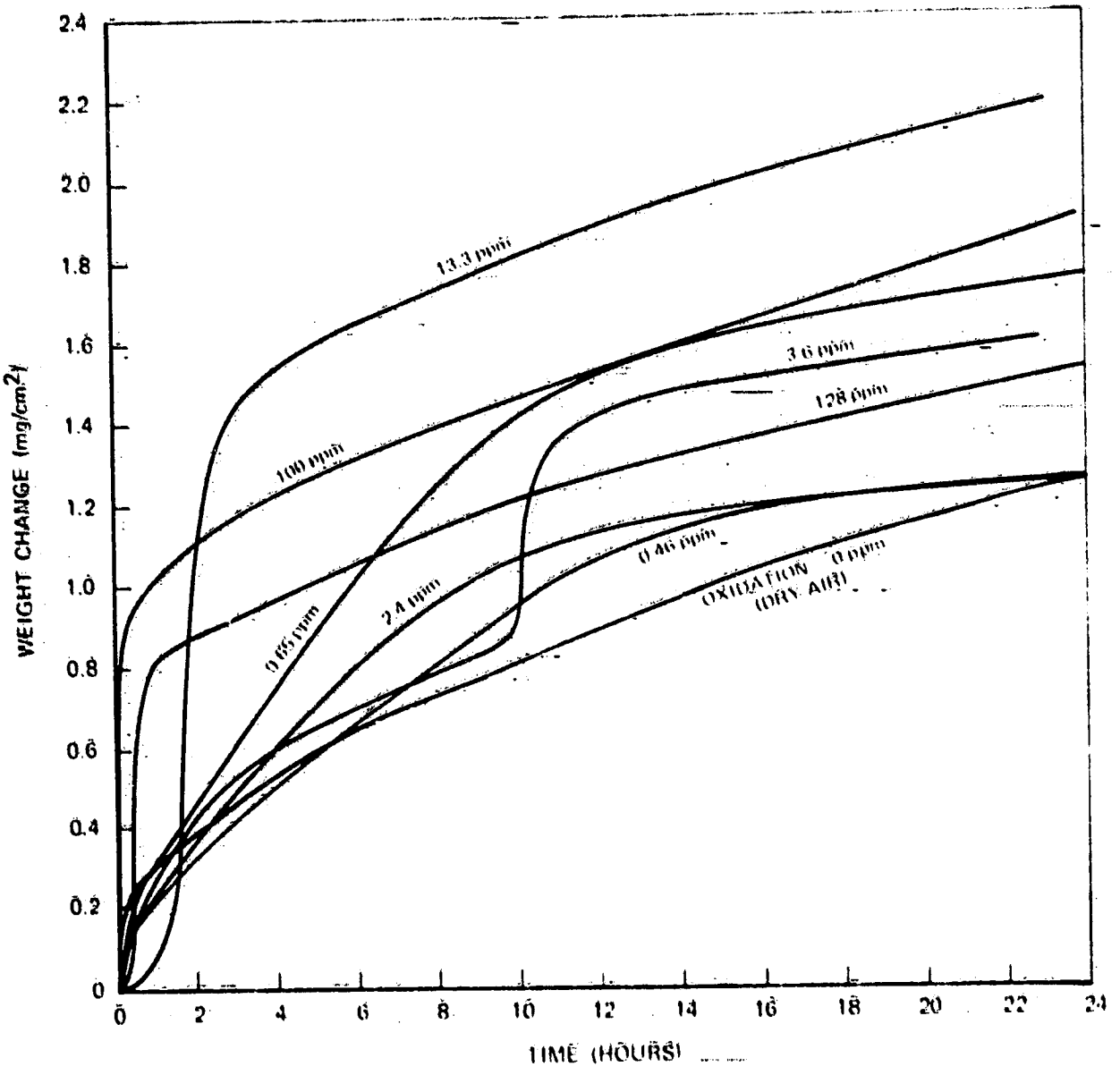

Fig. 65 1200°C oxidation of Ni-2% Cr with NaCl vapor.

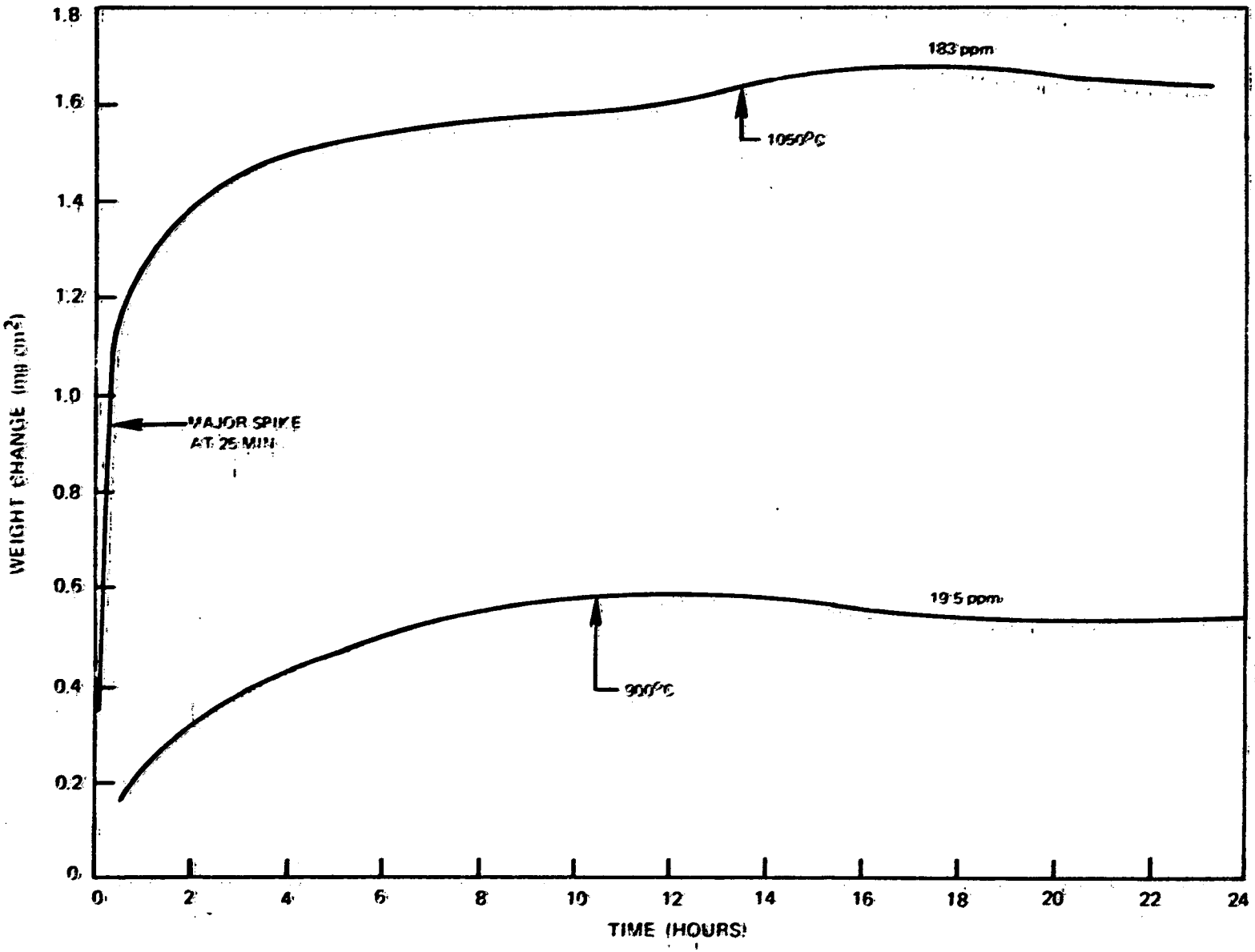

Fig. 66 Oxidation Behavior of Ni-25 Cr in the presence of both water vapor and NaCl(g) at 900 and 1050°C.

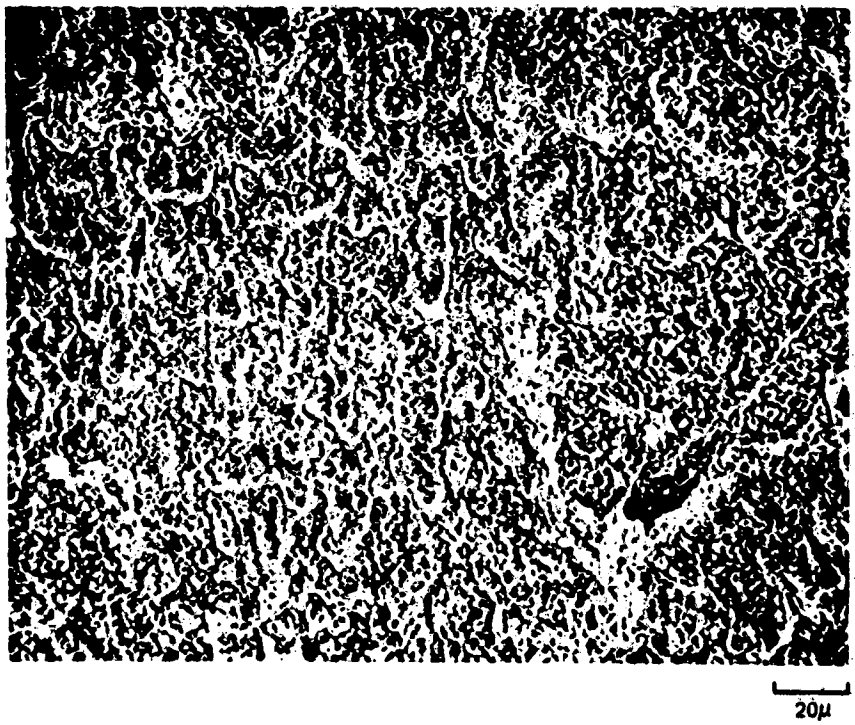

Fig. 67 Ni-25 Cr oxidized at 900°C in air with 2.9 ppm NaCl(g) showing an apparently open oxide structure.

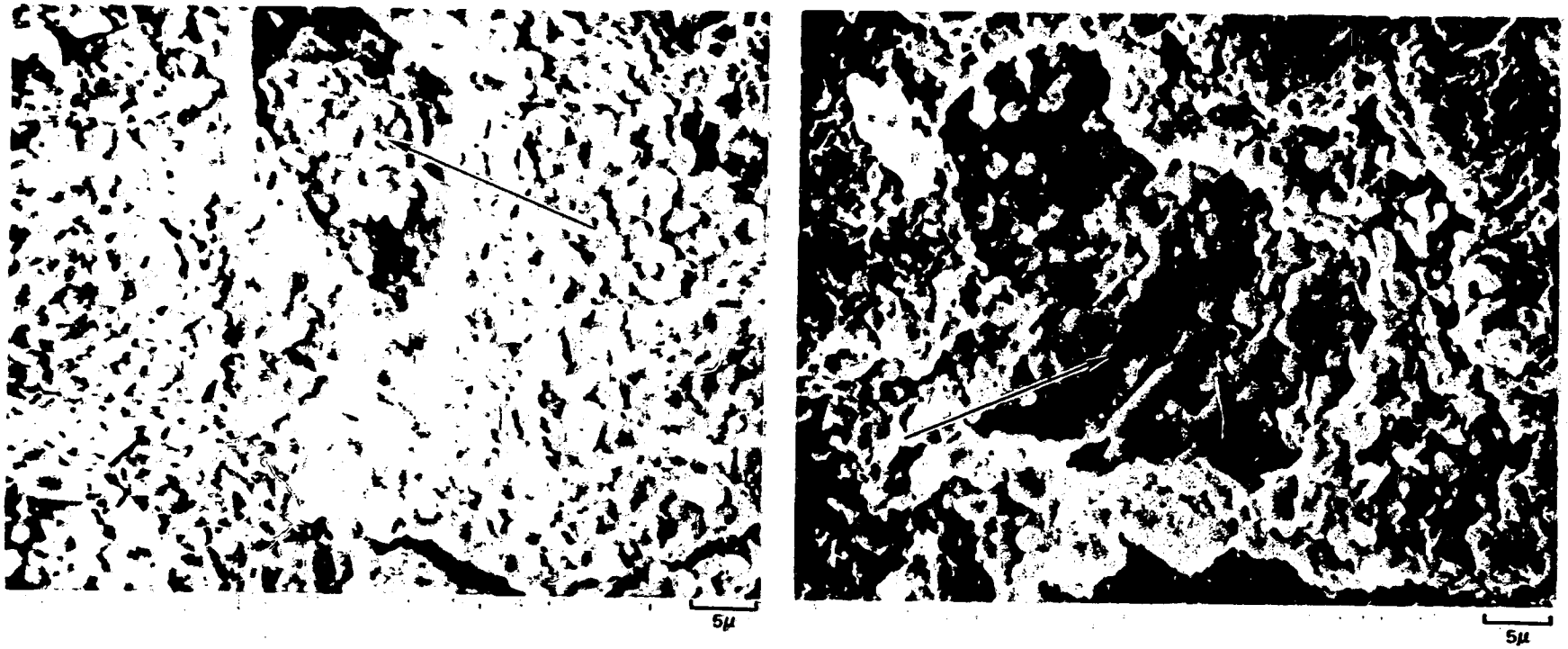

Fig. 68 Ni-25 Cr oxidized at 900°C in air with 2.9 ppm NaCl(g) showing open hills as surface of the oxide.

A. Broken oxide hill showing non-geometric Cr particles at base.

B. Broken oxide hill with Ni-enriched geometries oxide at the base.

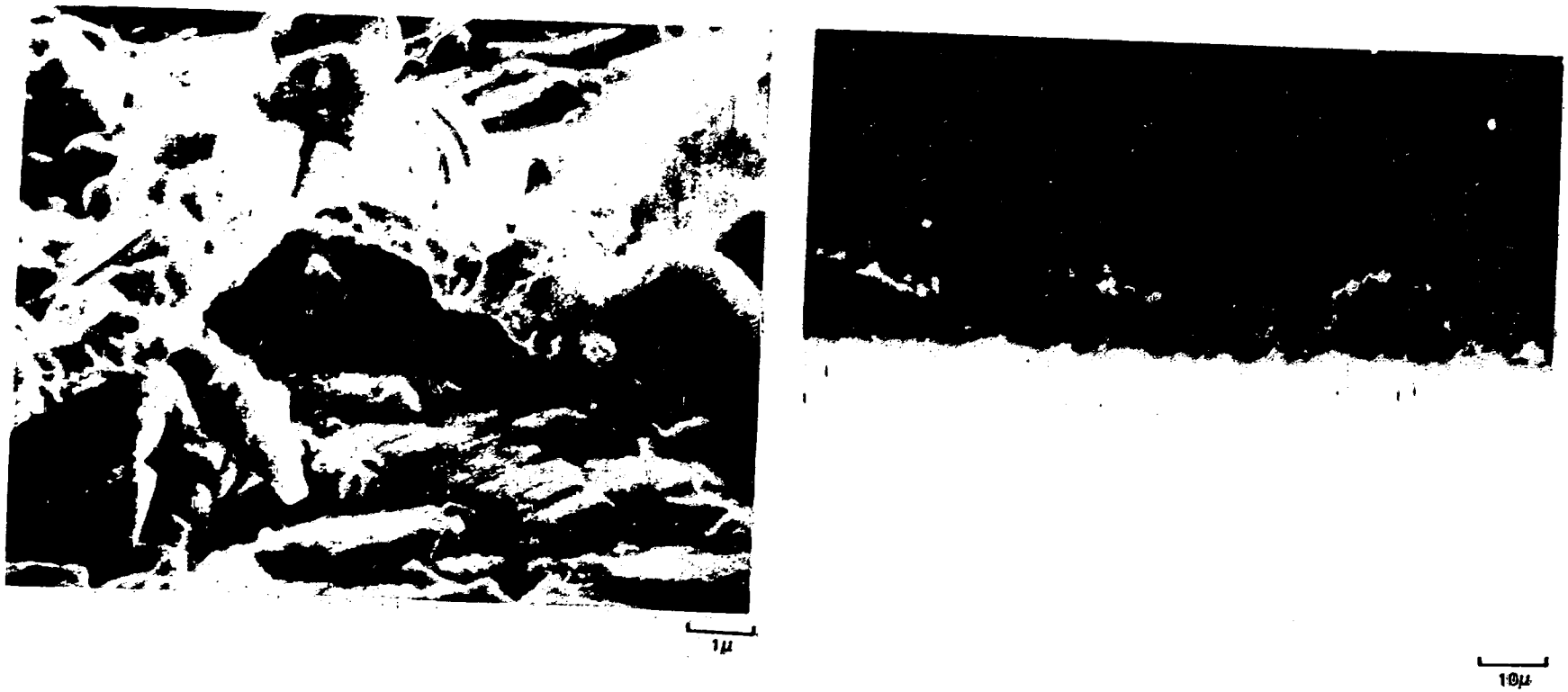

Fig. 69 Cross-sectional view of open hill on Ni-25 Cr oxidized in air with 2.9 ppm NaCl at 900°C.

Fig. 70 Scanning electron micrograph of Ni-25 Cr oxidized at 900°C for 24 hours in air with 1.9 ppm NaCl/g).

1. Base alloy: 75.2 wt.% Ni, 24.5 wt. % Cr
2. Metal surrounded by oxide: 81.9 wt. % Ni, 16.9 wt. % Cr
3. Cr-depleted substrate: 82.5 wt. % Ni, 15.8 wt. % Cr
4. Protective scale: 5.1 wt. % Ni, 58.3 wt. % Cr
5. Adjacent oxide scale: 64.2 wt. % Ni, 7.8 wt. % Cr.

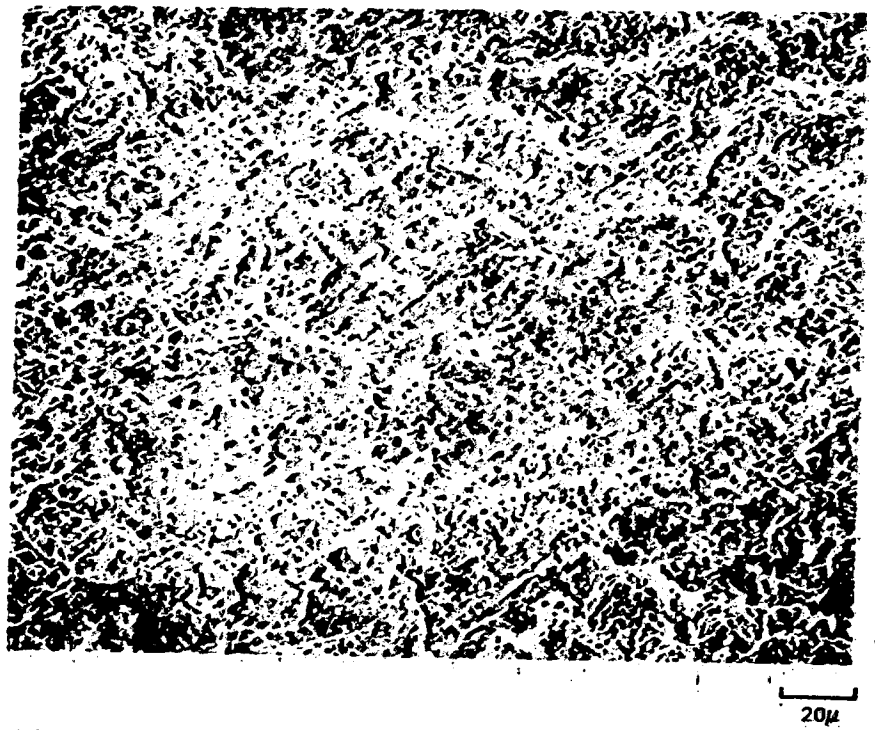

Fig. 71 Ni-25 Cr oxidized at 1050°C for 24 hours in air with 0.59 ppm NaCl.

Fig. 72 Ni-25 Cr oxidized at 1050°C for 24 hours in air with 0.59 ppm NaCl(g).

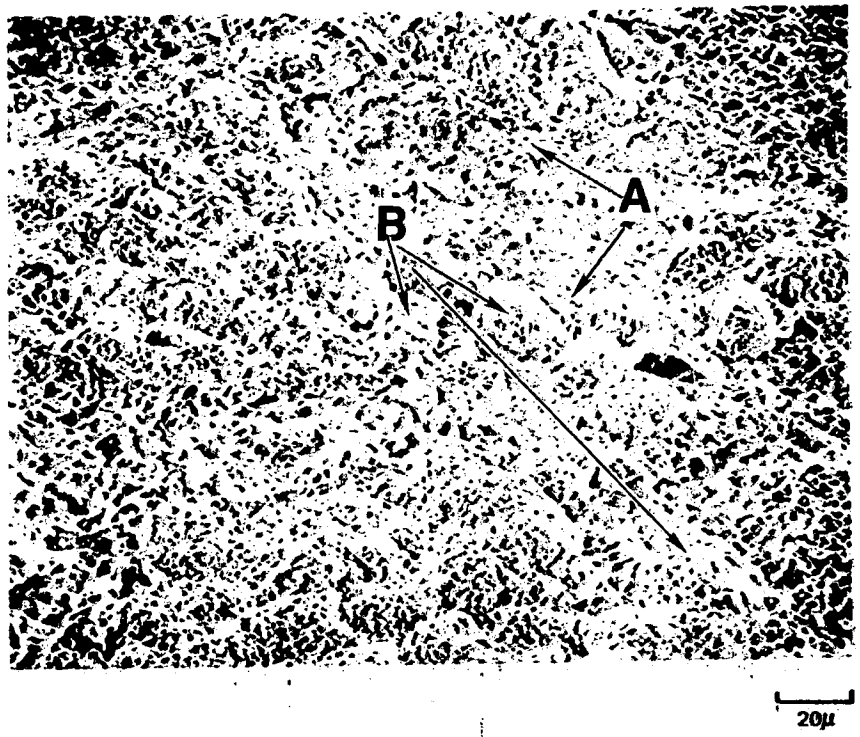

Fig. 73 Ni-25 Cr oxidized at 1050°C in air with 13.3 ppm NaCl(g).
A. Small Cr_2O_3 crystals
B. Eruptions enriched in $NiCr_2O_4$.

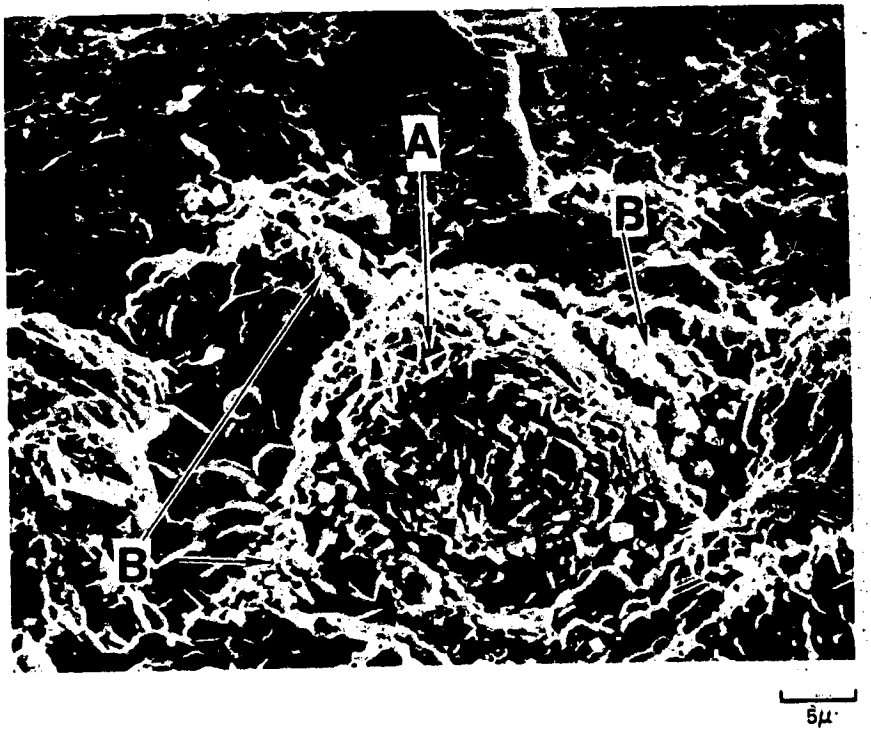

Fig. 74 Ni-25 Cr oxidized at 1050°C for 24 hours in air with 13.3 ppm - NaCl(g). An eruption of Ni-rich Cr-containing oxide (probably $NiCr_2O_4$) (A) is largely surrounded by small Cr_2O_3 crystals (B).

Fig. 75 Ni-25 Cr oxidized at 1050°C for 24 hours in air with 128 ppm NaCl(g).
A. Ni-enriched Cr oxide (probably $NiCr_2O_4$)
B. Essentially only Cr_2O_3.

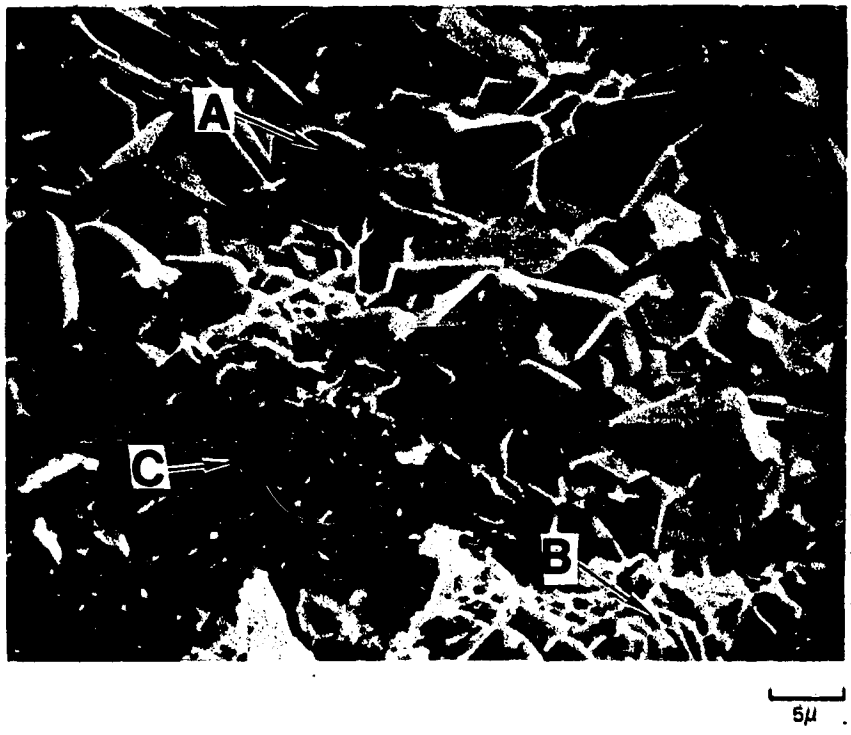

Fig. 76 Ni-25 Cr oxidized at 1050°C for 24 hours in air with 128 ppm NaCl(g).

A. Large grains (Ni-enriched Cr oxide)
B. Small grains (virtually pure Cr oxide)
C. Compact flat oxide (Cr oxide)

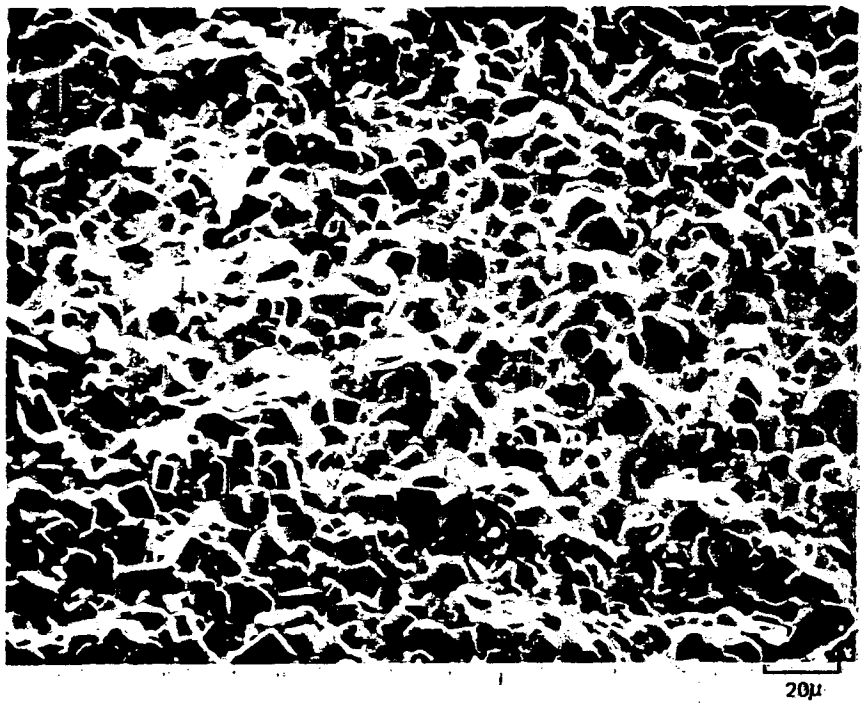

Fig. 77 Ni-25 Cr oxidized in air (wet) with 183 ppm NaCl(g) at 1050°C for 24 hours showing a dense compact oxide layer.

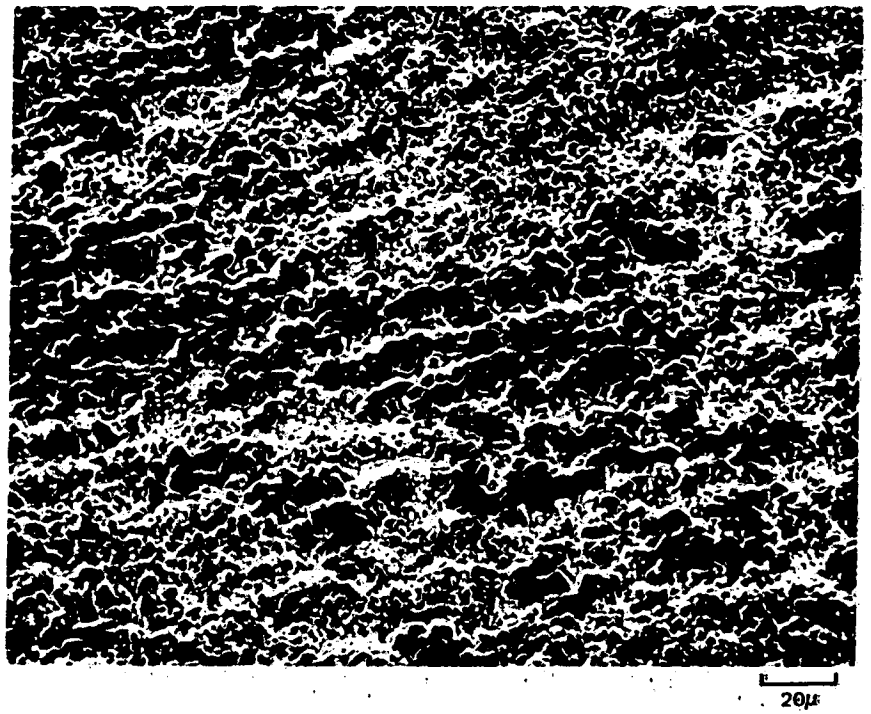

Fig. 78 Ni-25 Cr oxidized at 1050°C in oxygen with 25 ppm NaCl(g) flowing at 1.7 cm/sec.

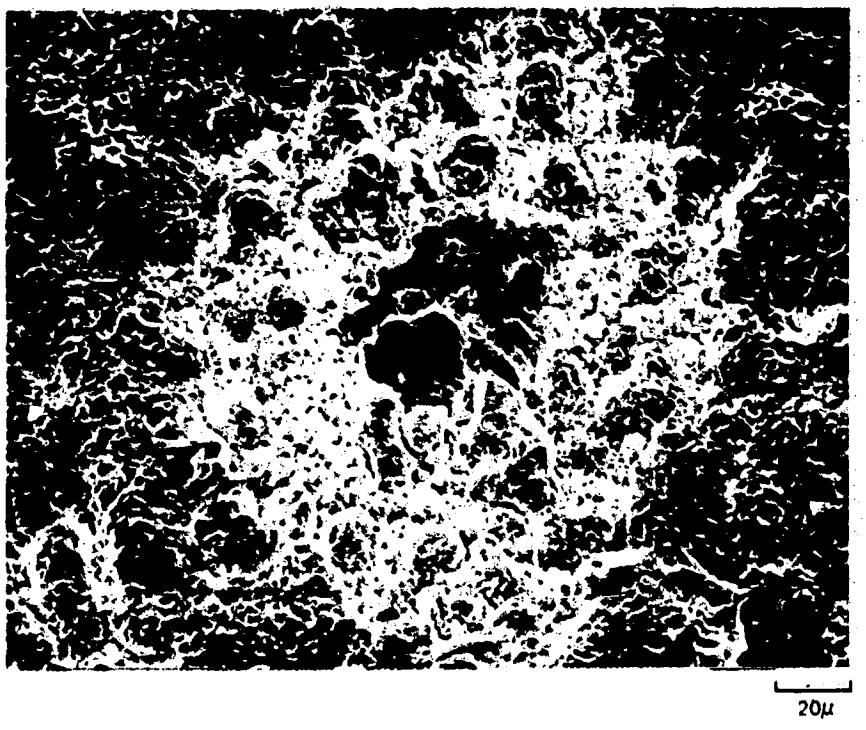

Fig. 79 Ni-25 Cr oxidized at 1050°C in an atmosphere of oxygen with 25 ppm NaCl(g) flowing at 0.17 cm/sec.

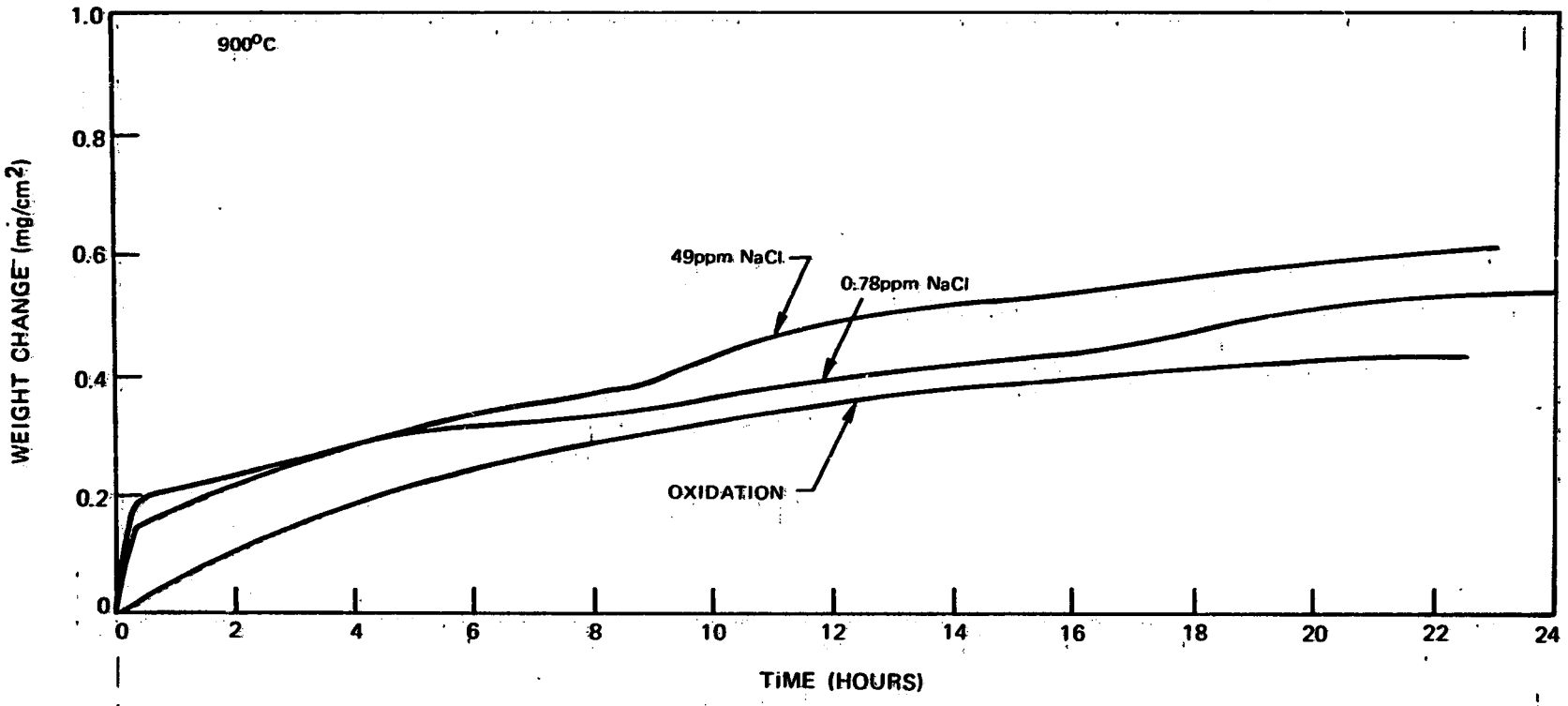

Fig. 80 Cr oxidized in air (dry) with NaCl vapors at 900°C.

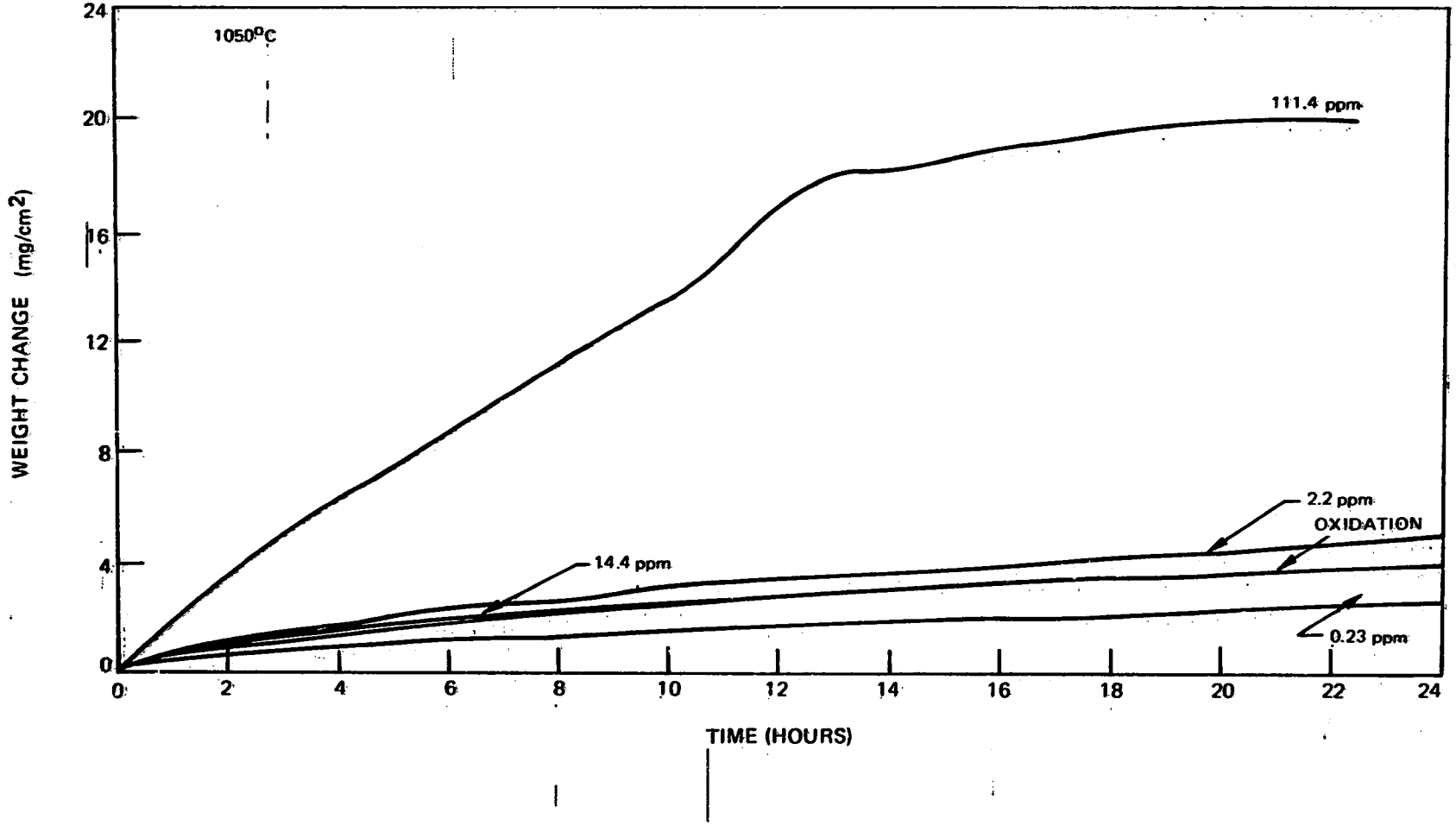

Fig. 81 Cr oxidized in air (dry) with NaCl vapors at 1050°C.

Fig. 82 Cr oxidized in air (dry) at 900°C for 24 hours.

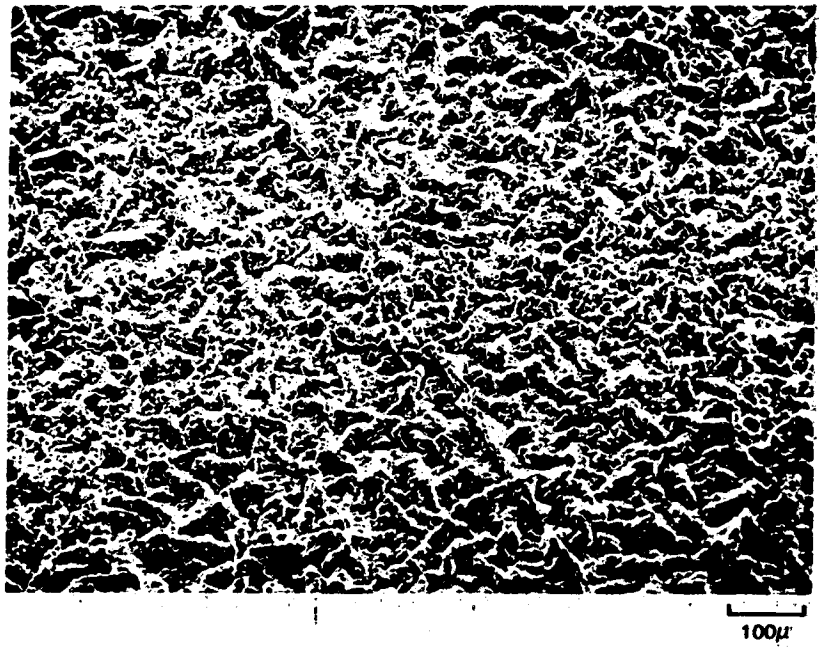

Fig. 83 Cr oxidized in air with 0.78 ppm NaCl(g) at 900°C for 24 hours.

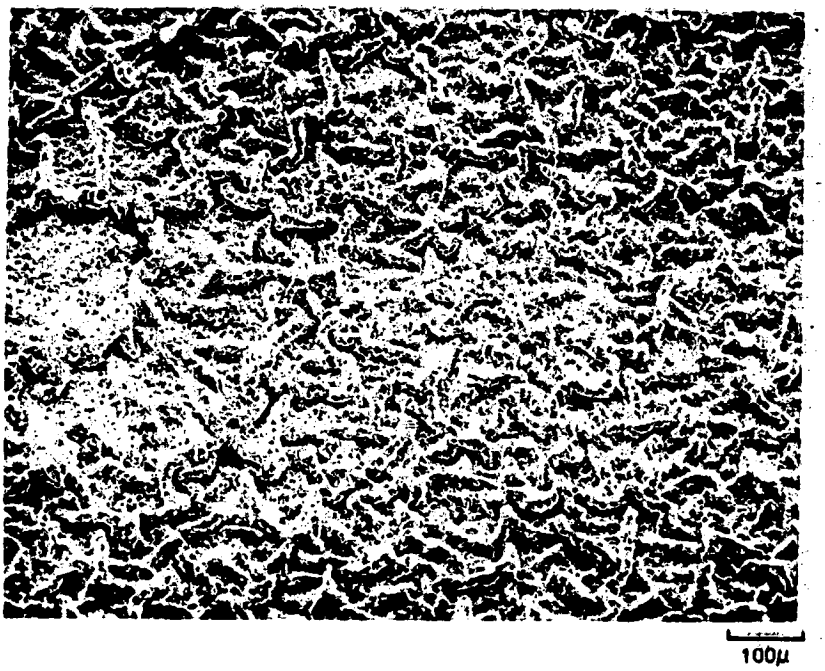

Fig. 84 Cr oxidized in air with 49 ppm NaCl(g) at 900°C for 24 hours.

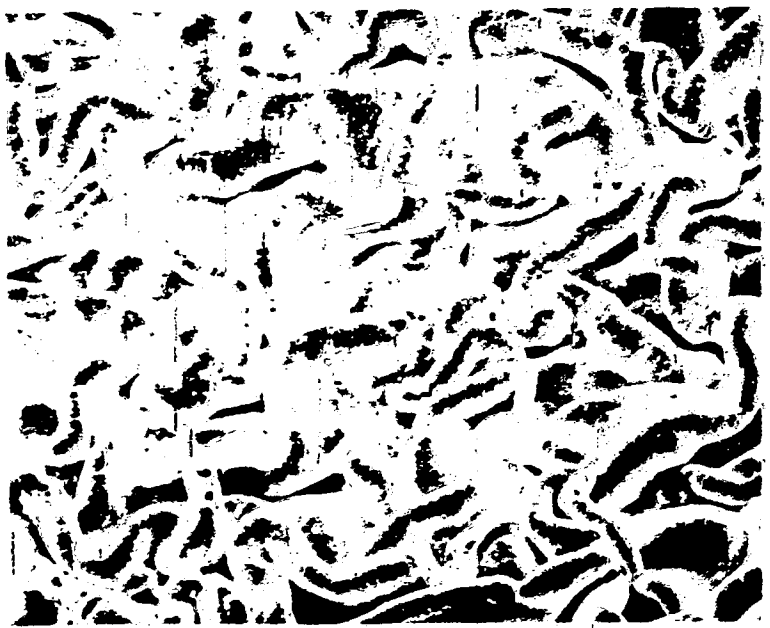

a. Oxide scale adjacent to the atmosphere 100μ

b. Oxide scale adjacent to the substrate 100μ
A. Points of attachment to the substrate.

Fig. 85 Cr oxidized in air at 1050°C for 24 hours.

a. Oxide scale adjacent to the atmosphere showing many fine crystals

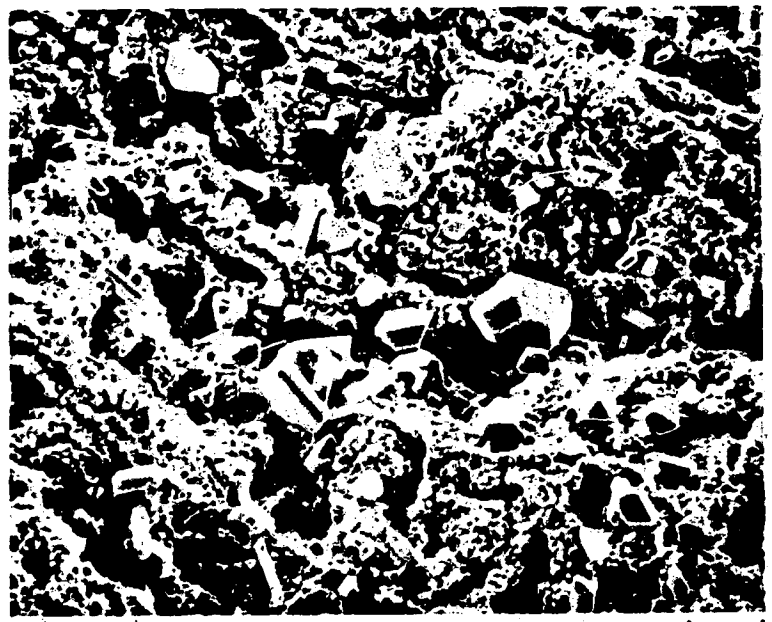

b. Not infrequent crystal growth found on the oxide surface

Fig. 86 Cr oxidized in air with 0.23 ppm NaCl(g) at 1050°C for 24 hours.

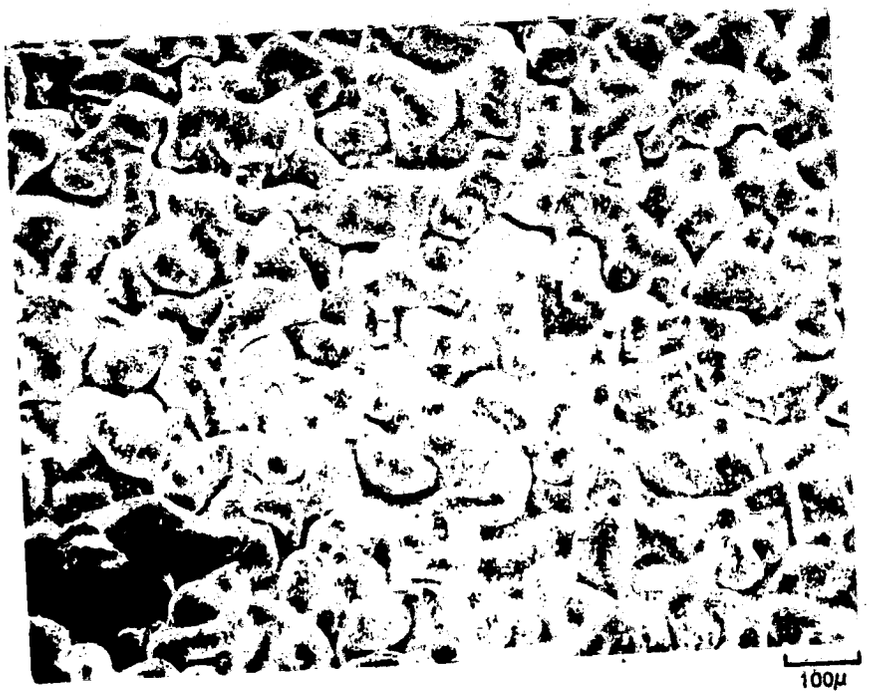

Fig. 87 Cr oxidized in air with 2.2 ppm NaCl(g) at 1050°C for 24 hours.

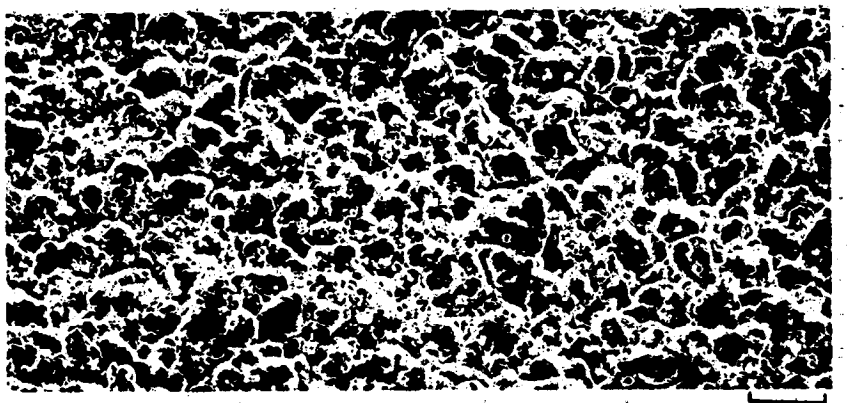

a. Oxide scale adjacent to the atmosphere

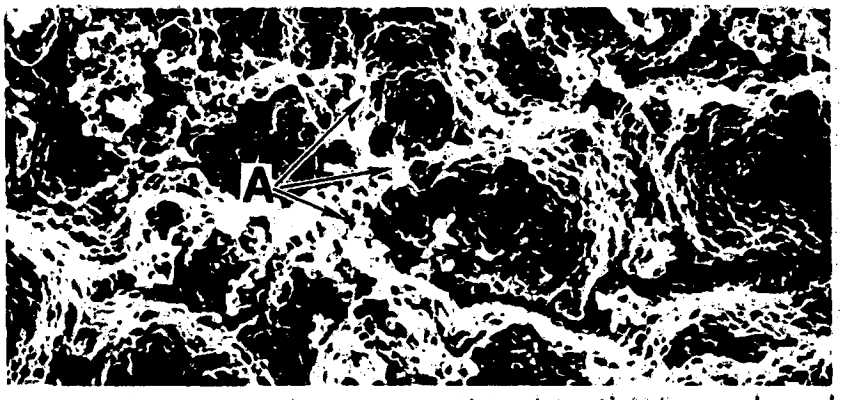

b. Oxide scale adjacent to the atmosphere showing fine Cr_2O_3 crystals on the undulating Cr_2O_3 scale(A)

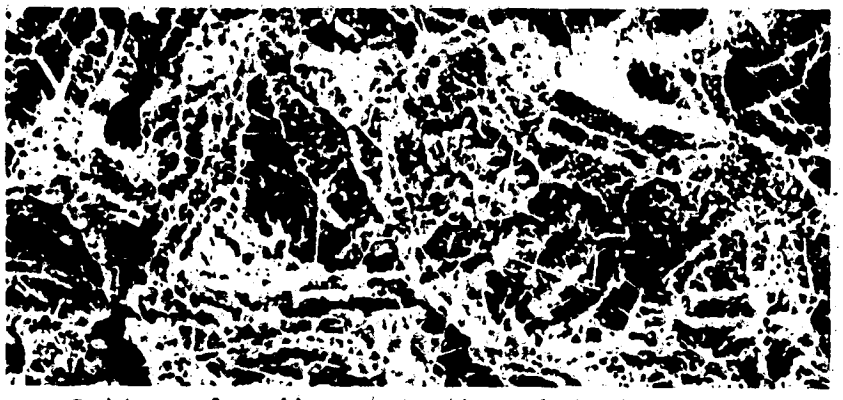

c. Oxide scale adjacent to the substrate showing fine Cr_2O_3 needles growing from the compact oxide surface

Fig. 88 Cr oxidized in air with 14.4 ppm NaCl(g) at 1050°C for 24 hours.

Fig. 89 Cr oxidized at 1050°C in air with 111 ppm NaCl(g) for 24 hours.
A. Cr_2O_3 scale
B. Chromium substrate

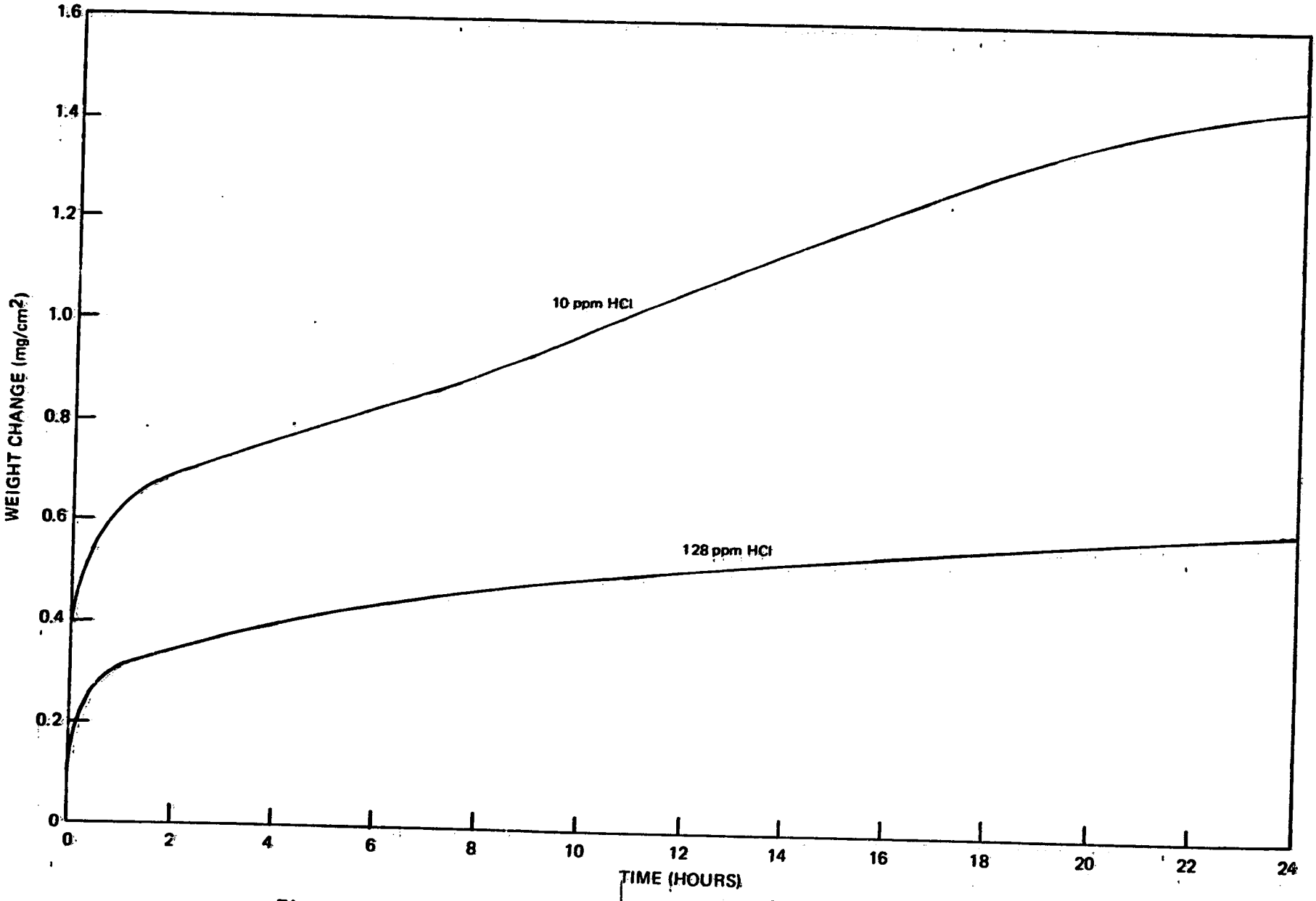

Fig. 90 Ni-25 Cr oxidized at 900°C in air with 10 ppm and 128 ppm HCl(g).

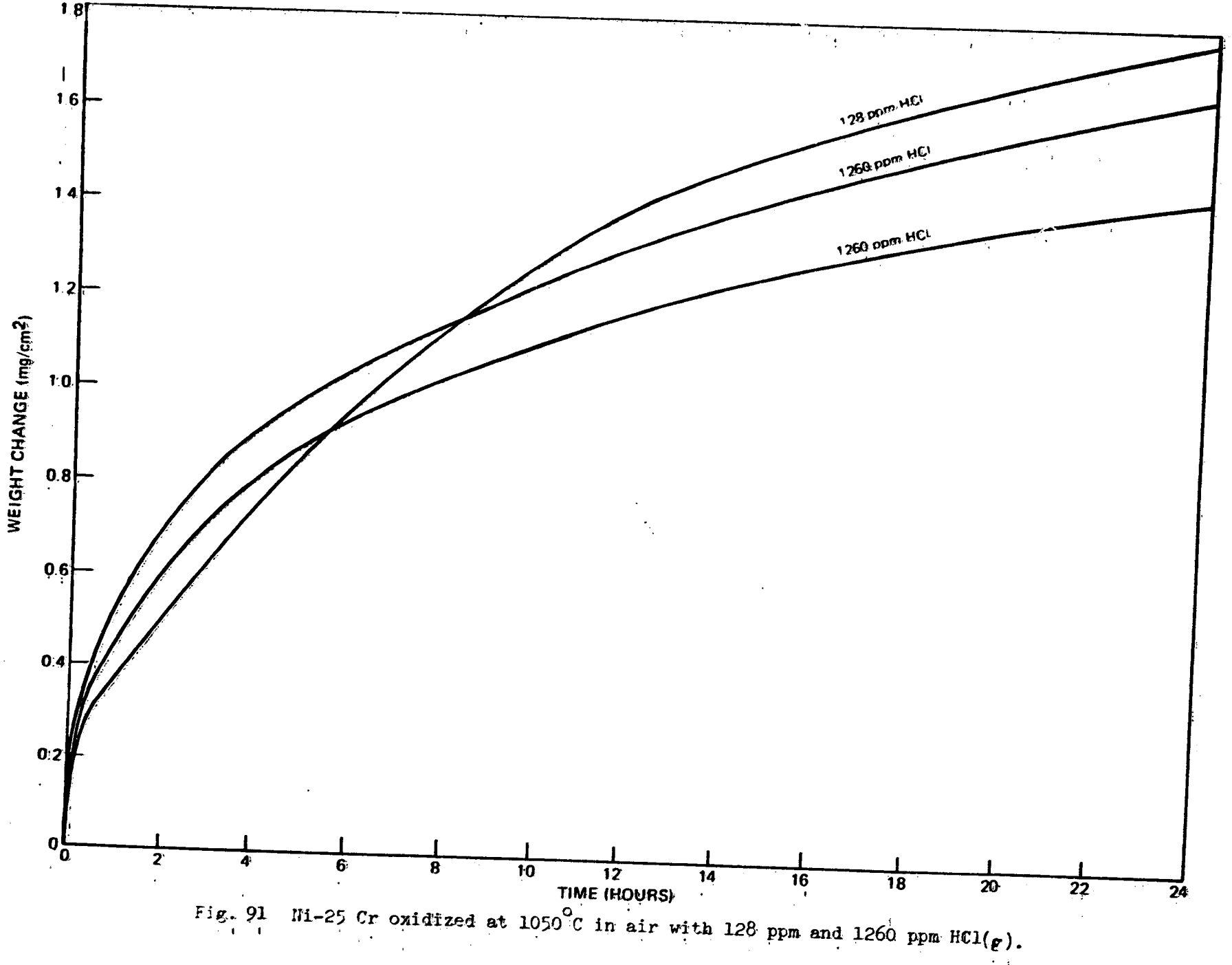

Fig. 91 Ni-25 Cr oxidized at 1050°C in air with 128 ppm and 1260 ppm HCl(g).

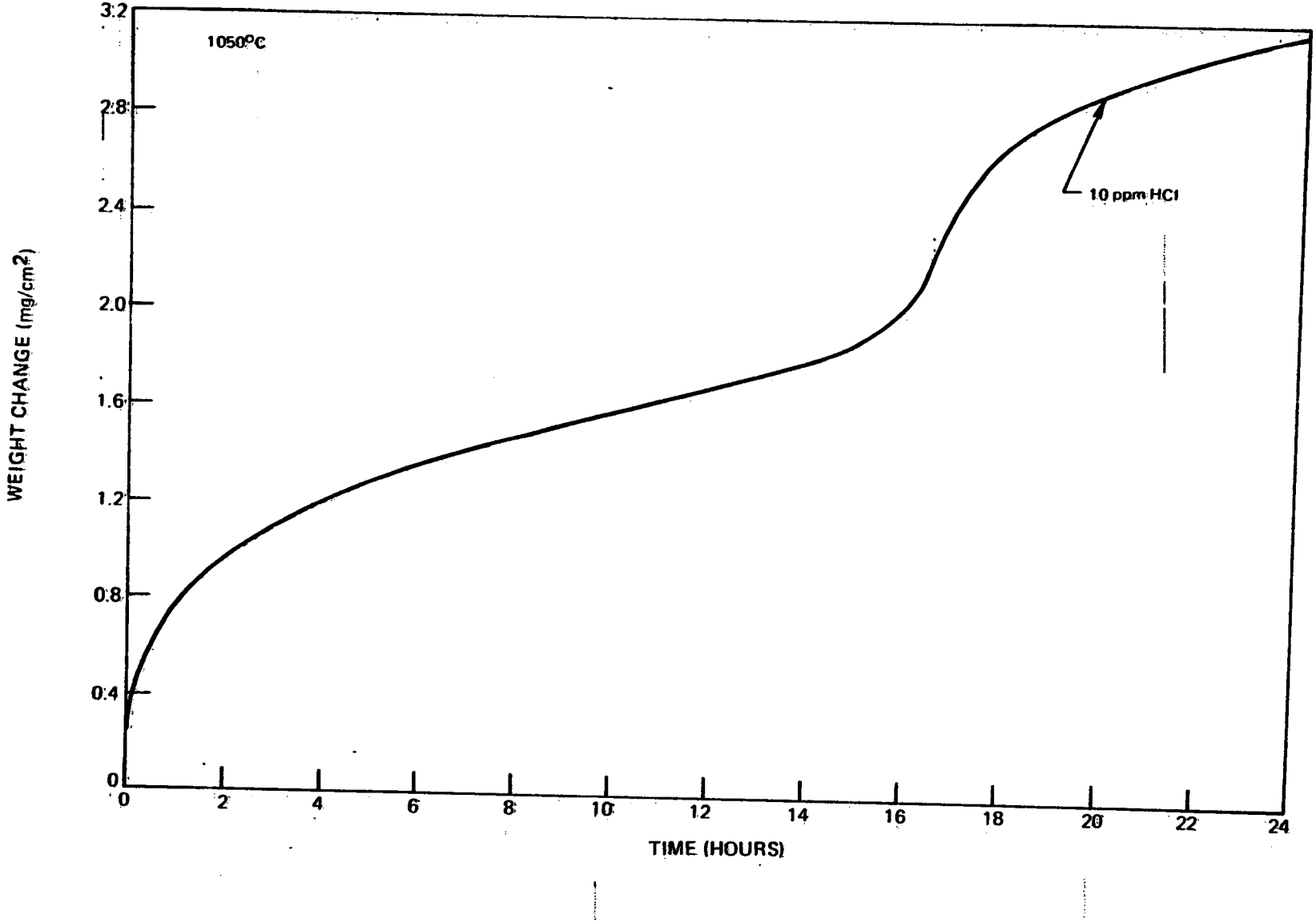

Fig. 92 1050°C oxidation of Ni-25 Cr with 10 ppm HCl(g).

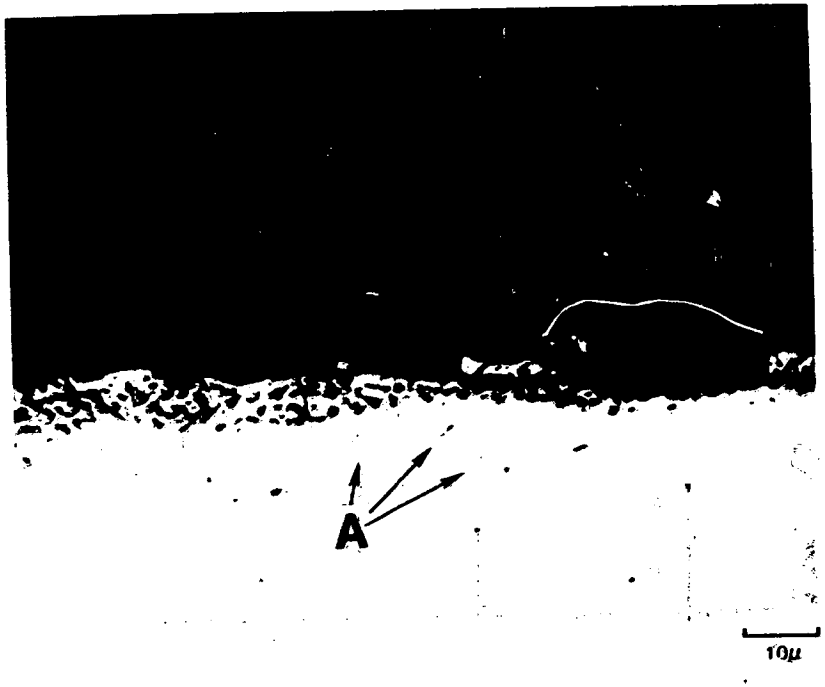

Fig. 93 Ni-25 Cr oxidized for 24 hours at 1050°C in air containing 10 ppm HCl(g).
A. Acicular precipitates.

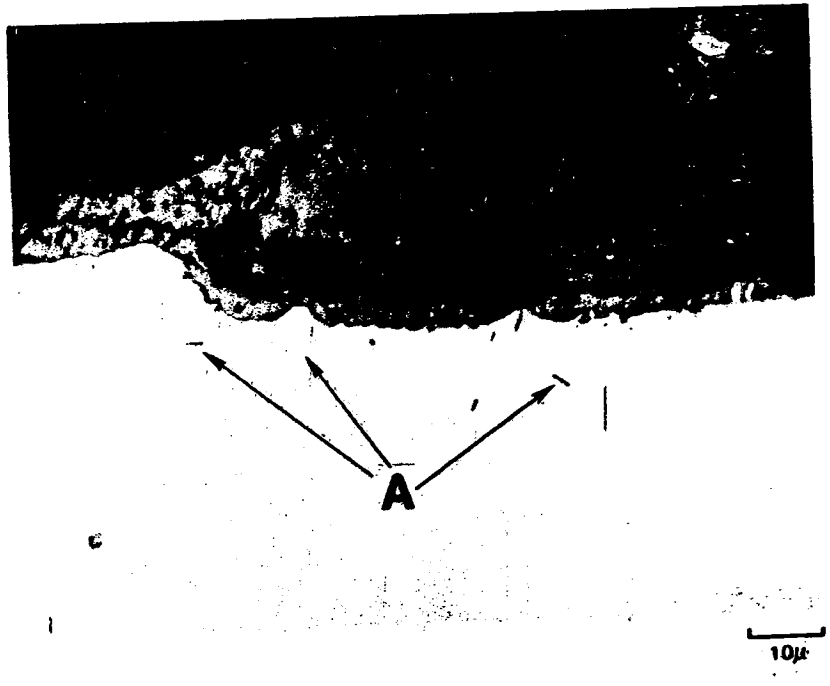

Fig. 94. Ni-25 Cr oxidized for 24 hours at 1050°C in air containing 10 ppm HCl(g).
A. Acicular precipitates.

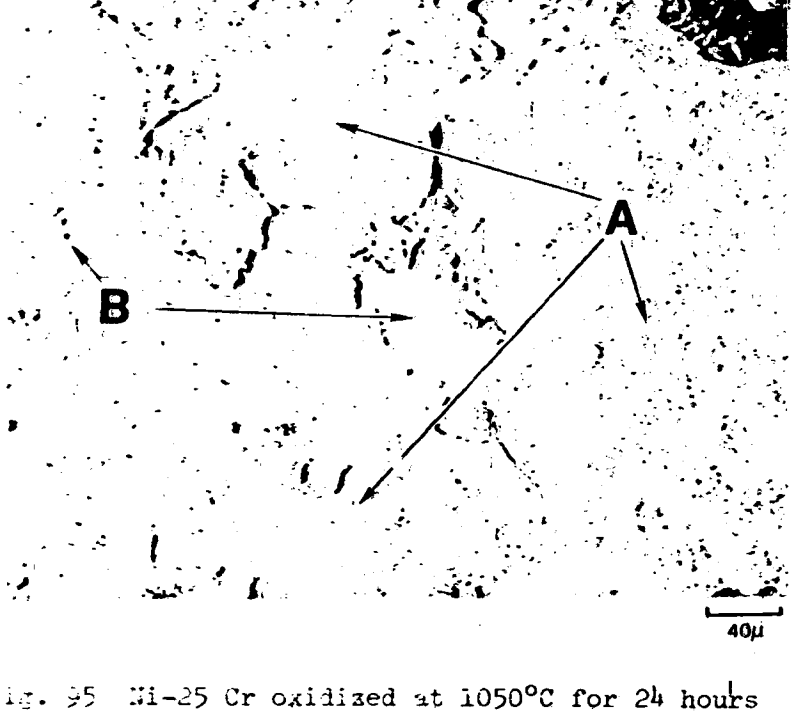

Fig. 95 Ni-25 Cr oxidized at 1050°C for 24 hours in air with 128 ppm HCl(g).
A. Cr_2O_3 scale
B. Ni-25 Cr substrate.

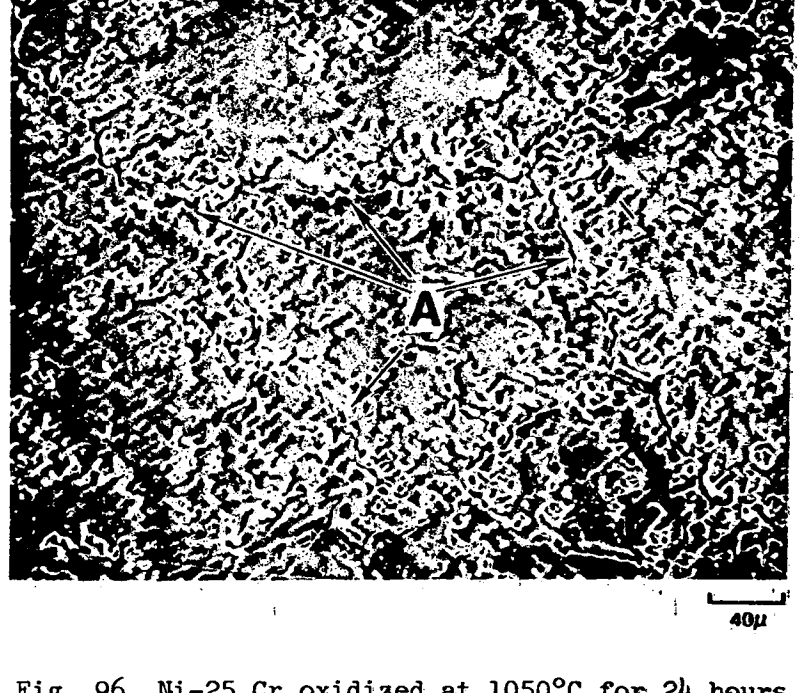

Fig. 96 Ni-25 Cr oxidized at 1050°C for 24 hours in air with 128 ppm HCl(g).
A. Grain boundary.

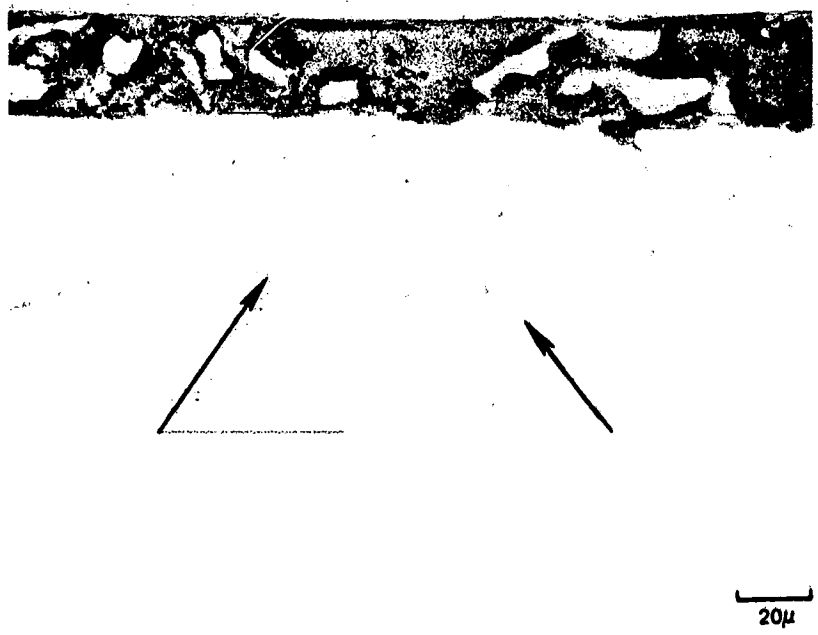

Fig. 97 Ni-25 Cr oxidized at 1050°C in the presence of 1260 ppm HCl(g) showing Kirkendall voids near the metal-oxide interface.

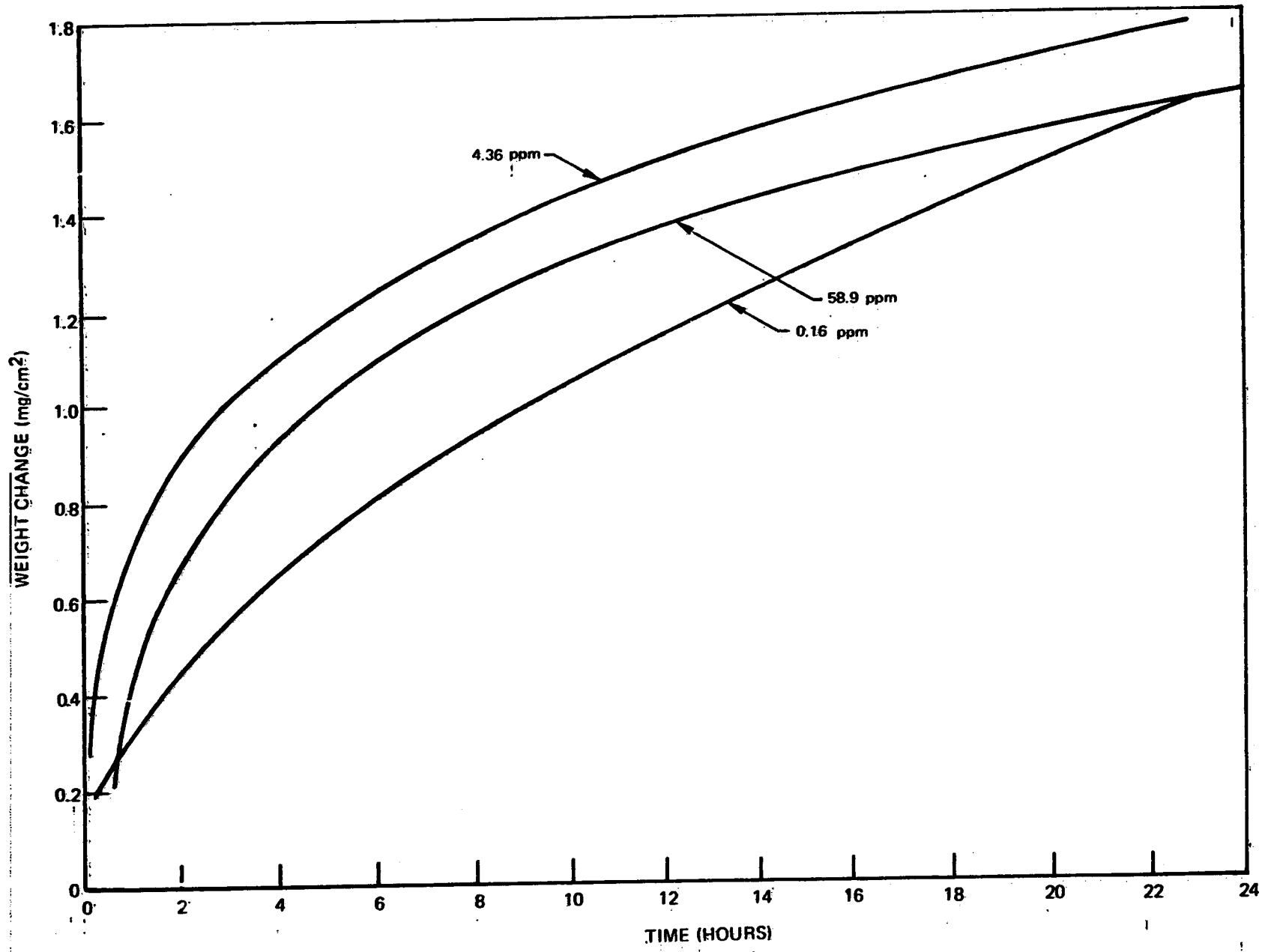

Fig. 98 Hi-25 Cr oxidized at 1050°C in air with NaOH(g).

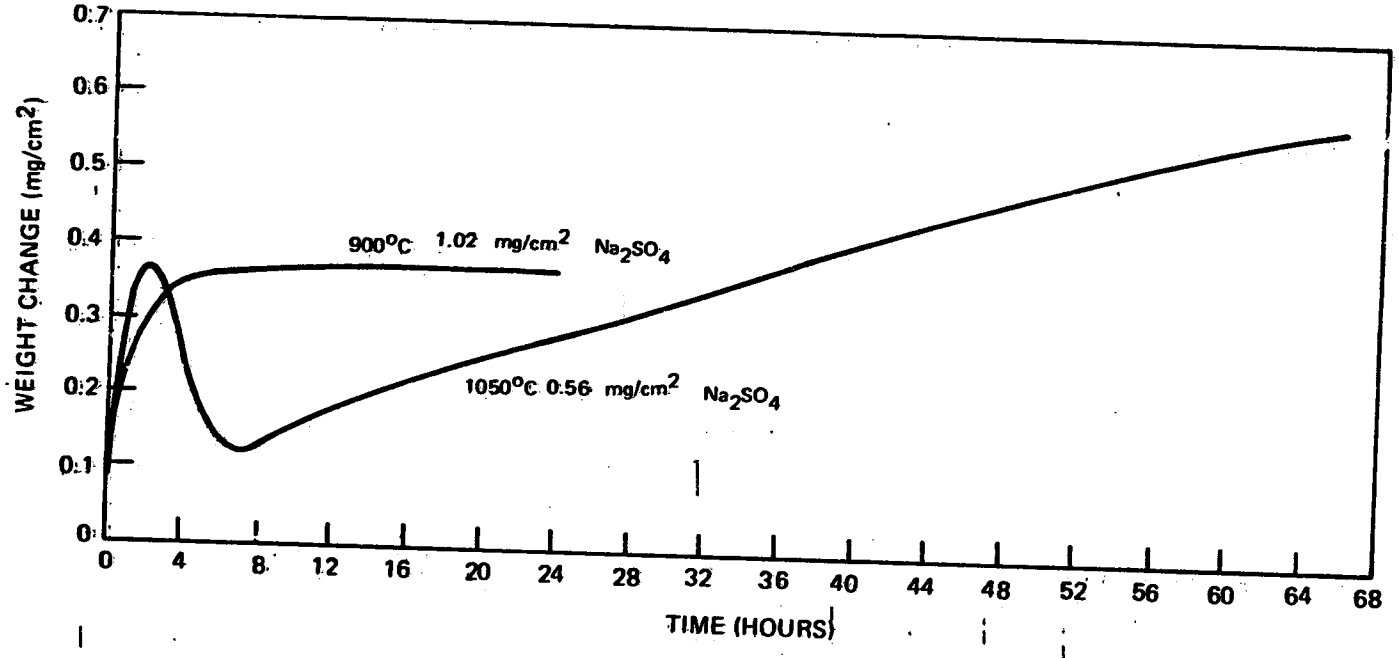

Fig. 99 Na_2SO_4-coated Ni-25 Cr oxidized at 900 and 1050°C.

Fig. 100 Na_2SO_4-coated (0.56 mg/cm^2) Ni-25 Cr oxidized at 1050°C for 24 hours.

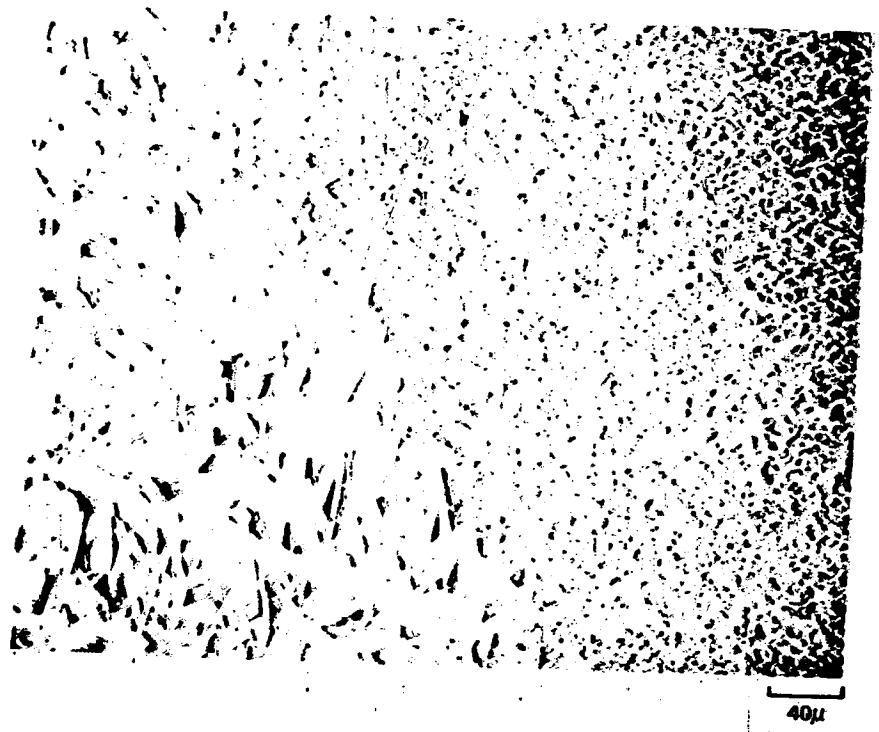

Fig. 101 Na_2SO_4-coated (0.56 mg/cm^2) Ni-25 Cr oxidized at 1050°C for 24 hours.

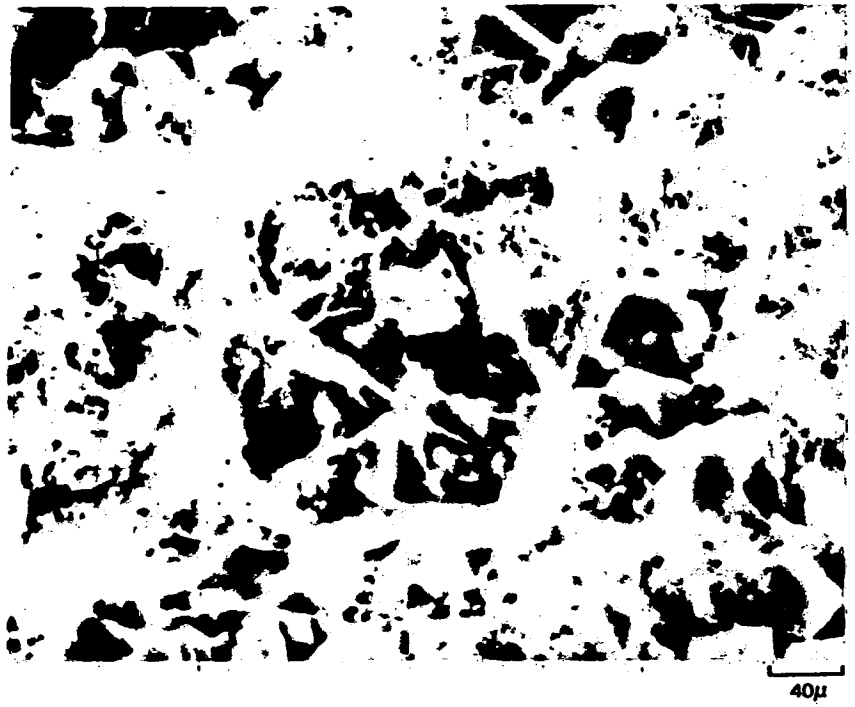

Fig. 102 Na_2SO_4-coated (0.56 mg/cm^2) Ni-25 Cr oxidized at 1050°C for 24 hours showing delicate β-SiO_2 crystals on the surface of the compact Ni-enriched Cr oxide layer.

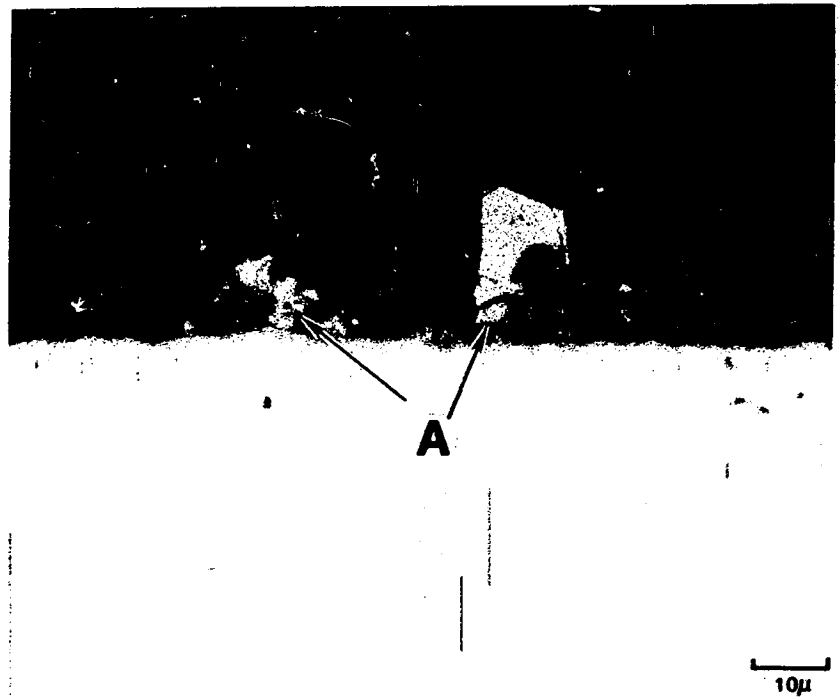

Fig. 103 Cr_2O_3 crystals growing on Na_2SO_4-coated (1.02 mg/cm^2) Ni-25 Cr oxidized at 900°C for 24 hours.
A. Cr_2O_3 crystals

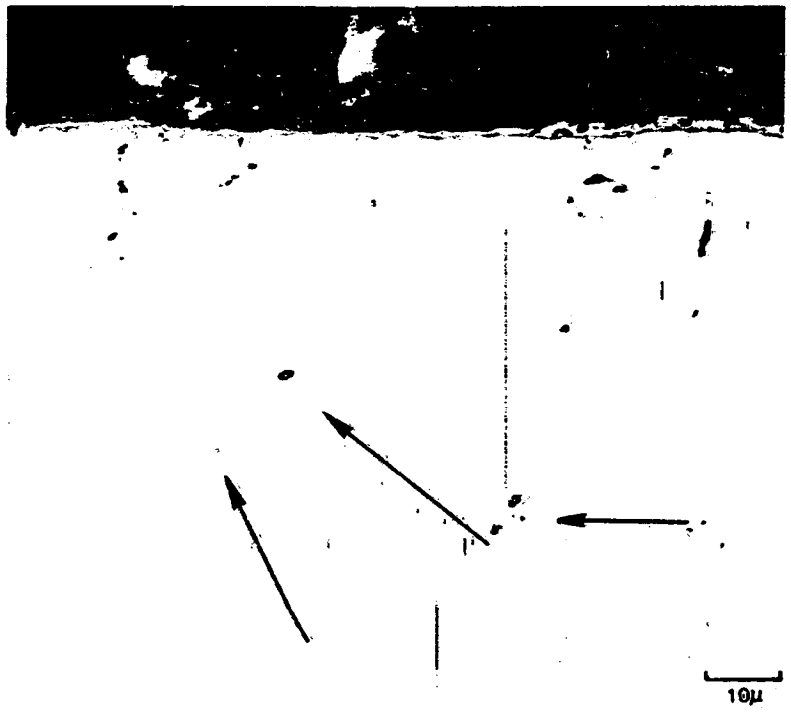

Fig. 104. Chromium sulfide particles below the metal-oxide scale of Ni-25 Cr (1.02 mg/cm^2) oxidized at 900°C for 24 hours.

Fig. 105. Na_2SO_4-coated (3.62 mg/cm^2) elemental chromium oxidized at 1050°C for 24 hours.

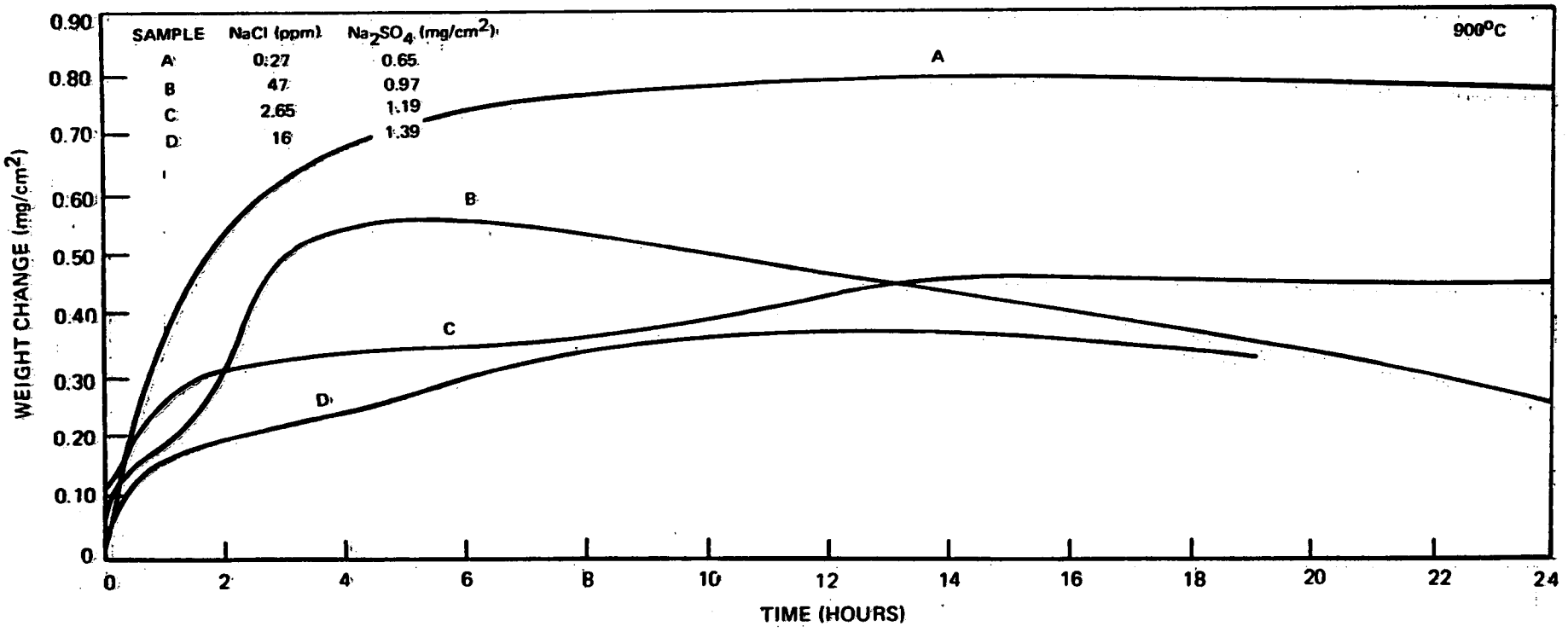

Fig. 106 The effect of NaCl vapors on the 900°C oxidation of Na_2SO_4-coated Ni-25 Cr.

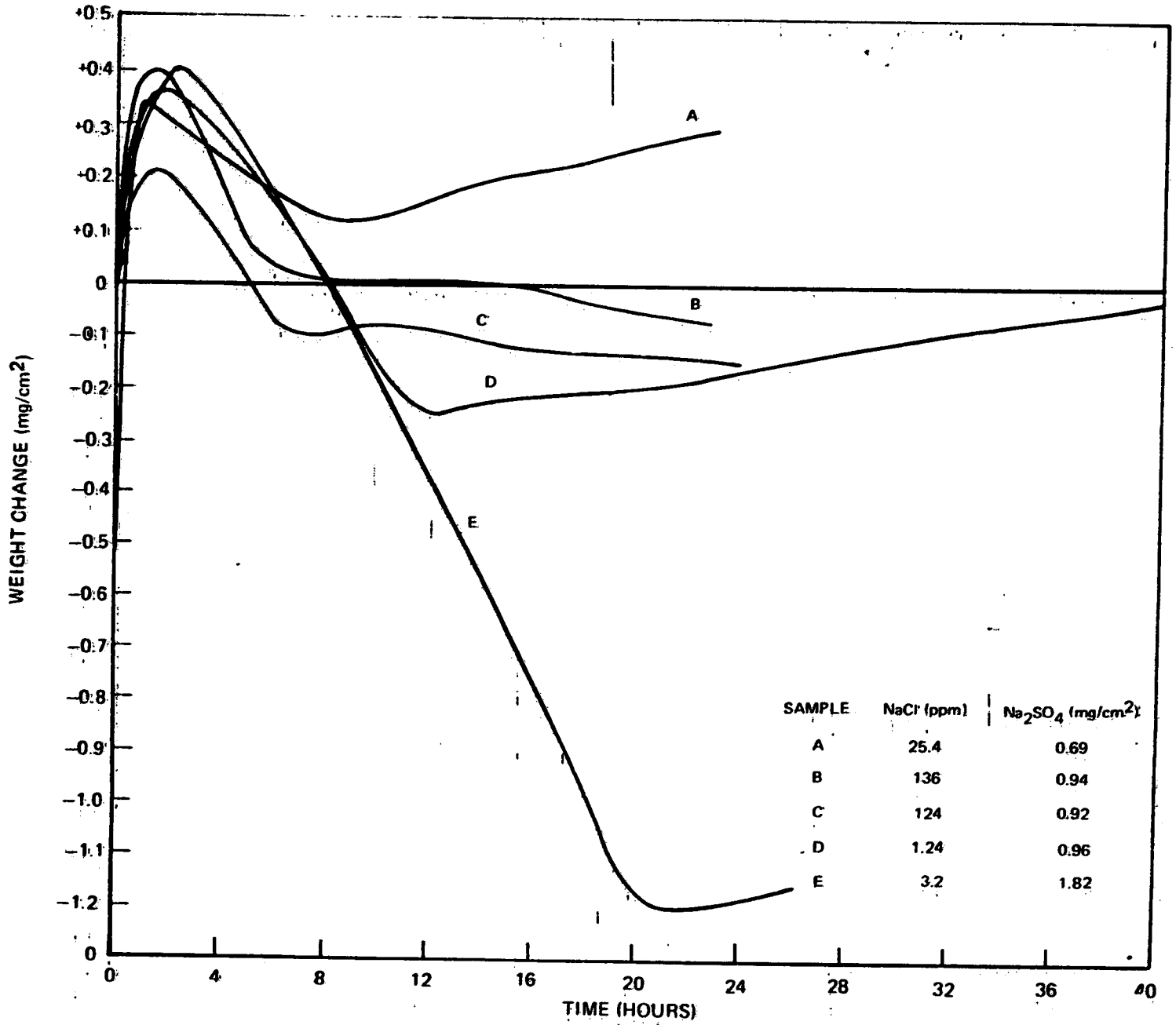

Fig. 107 The effect of NaCl vapors on the 1050°C oxidation of Na_2SO_4-coated Ni-25 Cr.

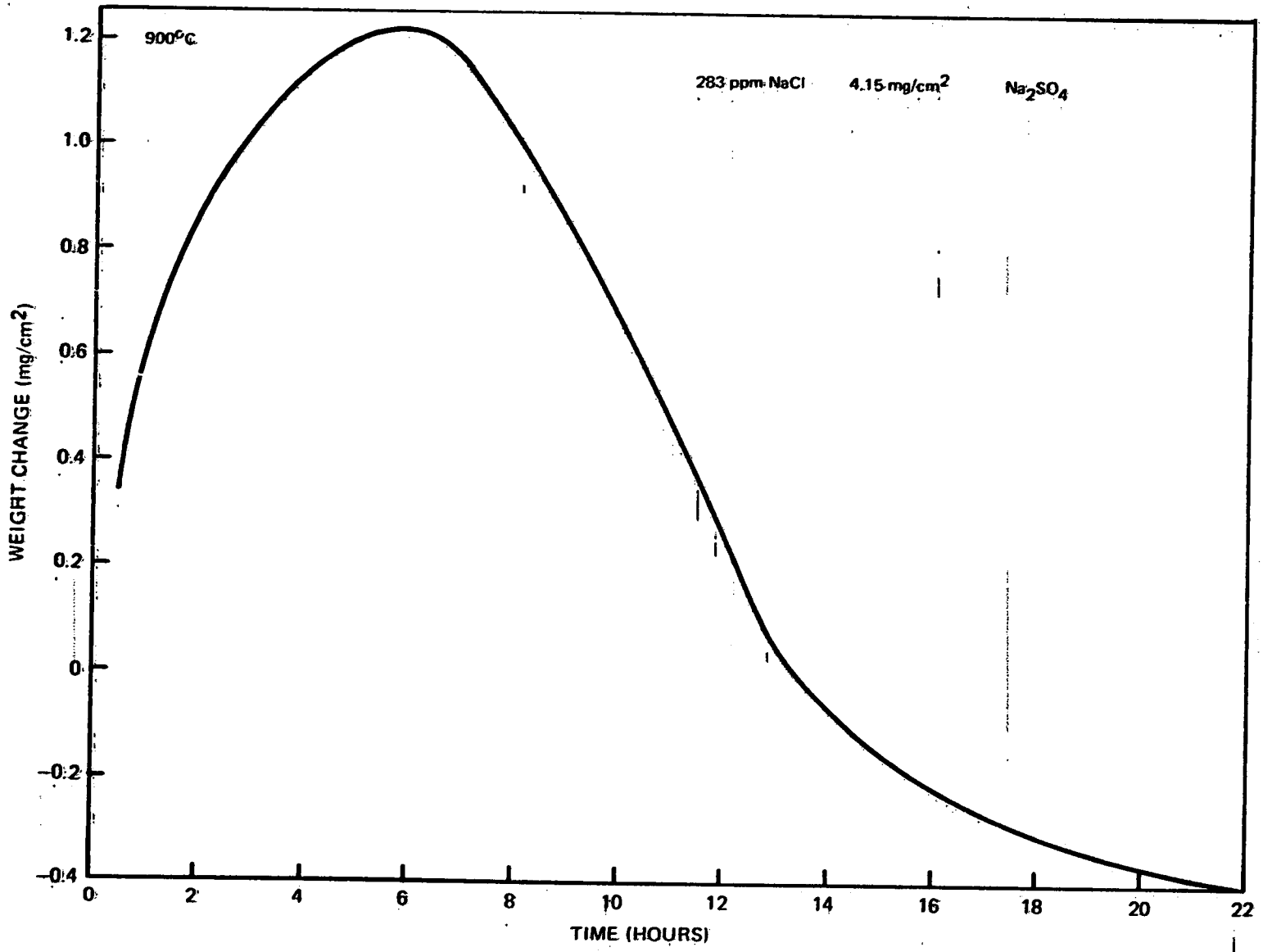

Fig. 108 Na_2SO_4-coated (4.15 mg/cm^2) elemental chromium oxidized in air with 283 ppm NaCl(g) at 1050°C for 24 hours.

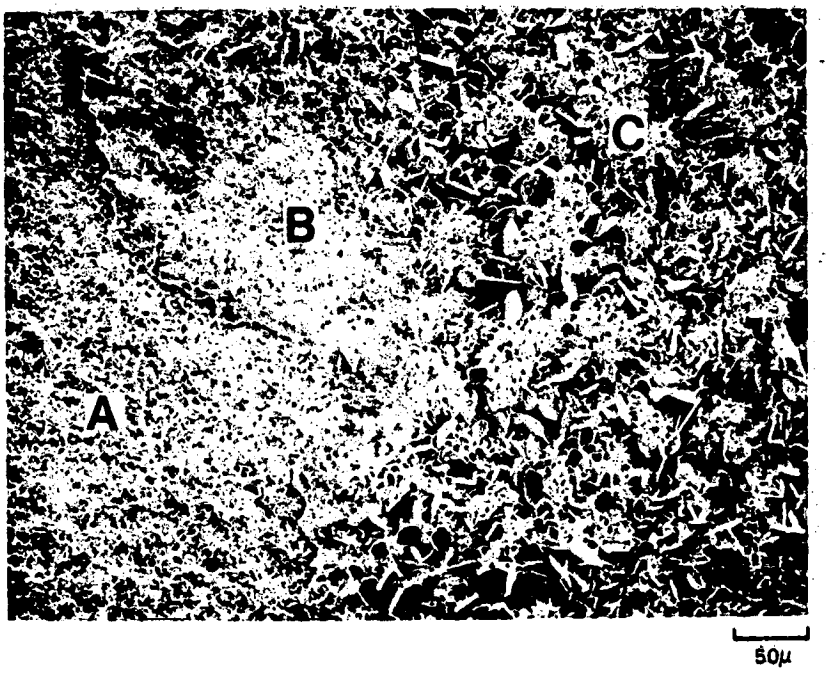

Fig. 109 Na_2SO_4-coated (4.15 mg/cm^2) elemental chromium oxidized for 22 hours at 1050°C in air with 283 ppm NaCl(g).
A. Elemental chromium substrate
B. Dense Cr_2O_3 scale.
C. Cr_2O_3 crystal platelets

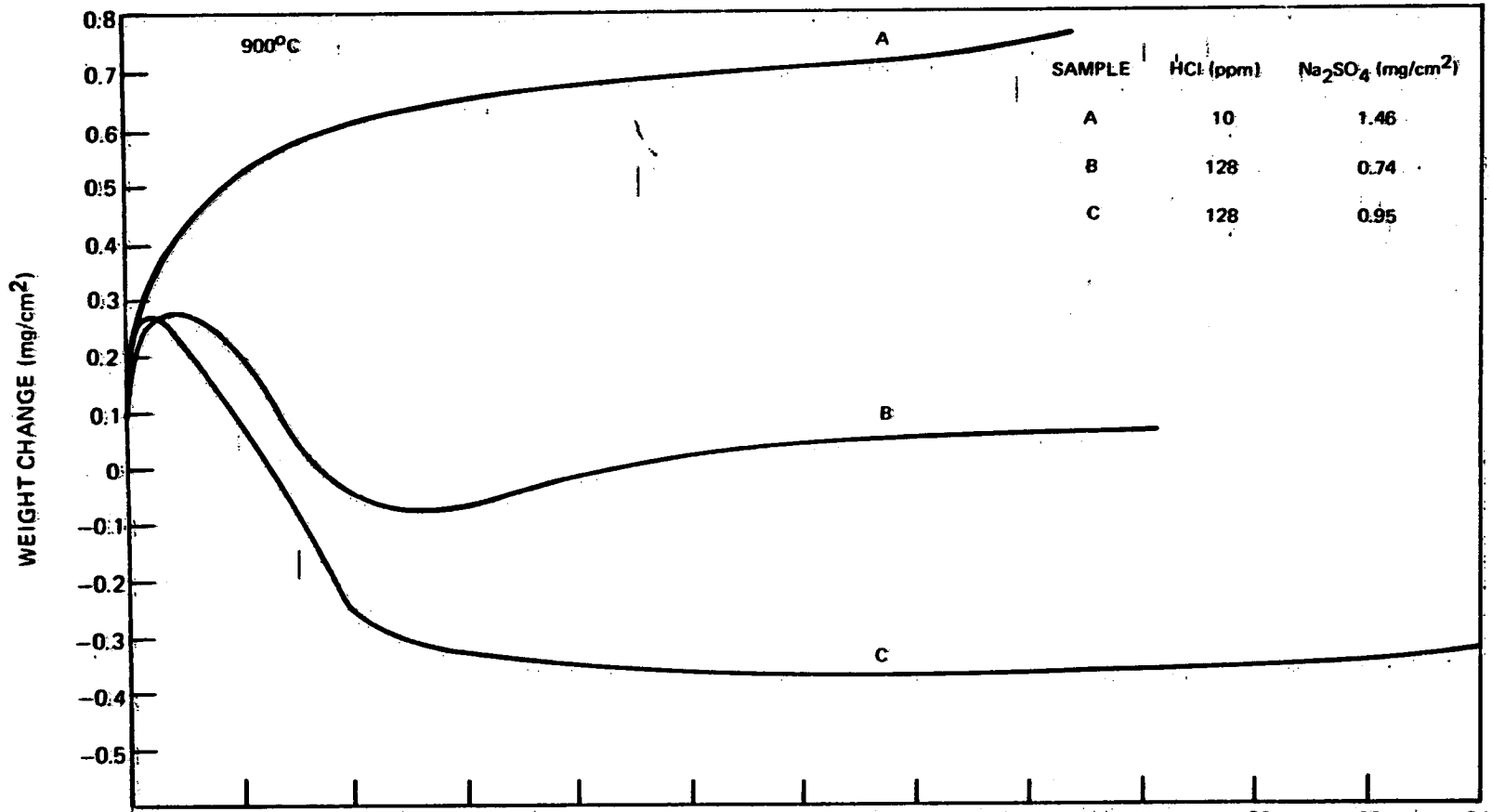

Fig. 110 Oxidation data for Na_2SO_4-coated Ni-25 Cr exposed to atmospheres containing HCl gas at 900°C.

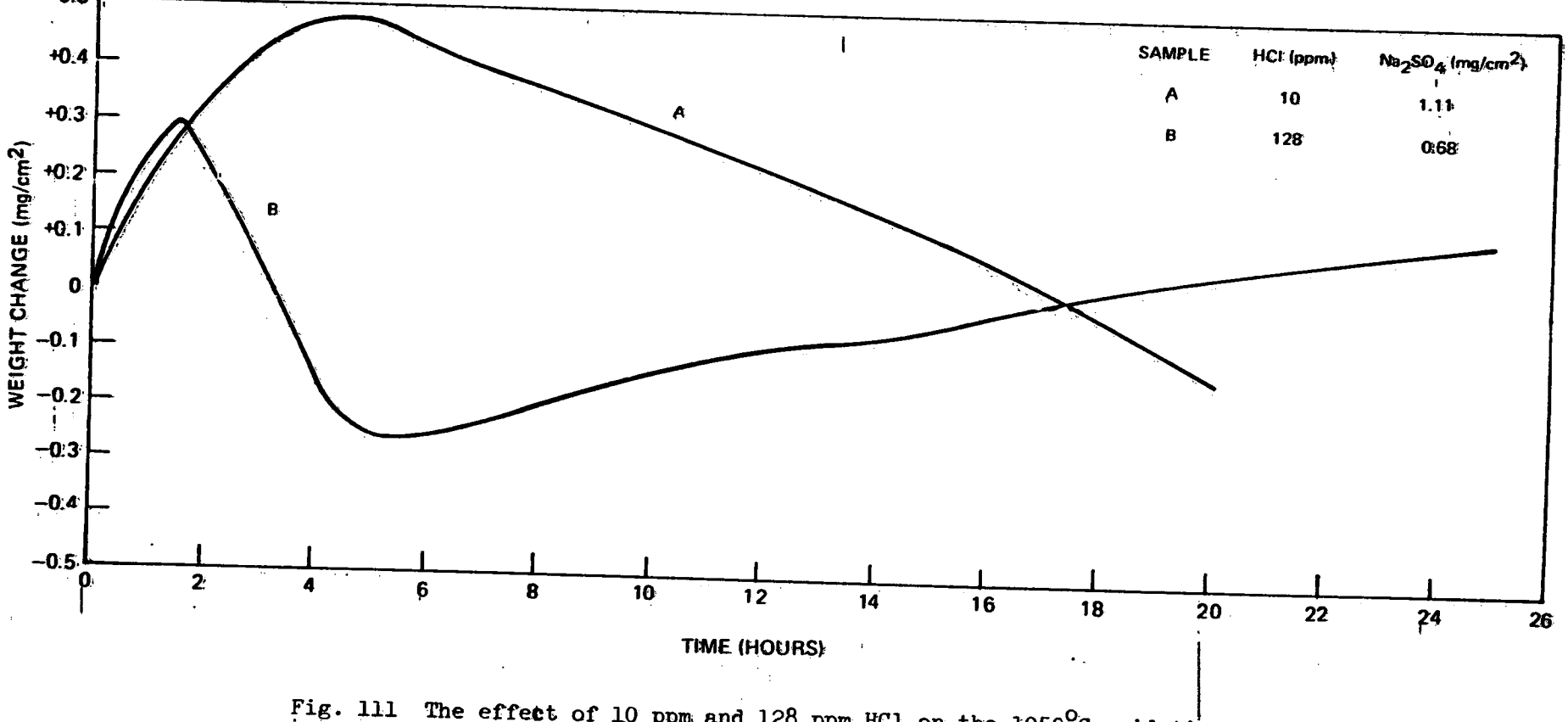

Fig. 111 The effect of 10 ppm and 128 ppm HCl on the 1050°C oxidation of Na_2SO_4-coated Ni-25 Cr.

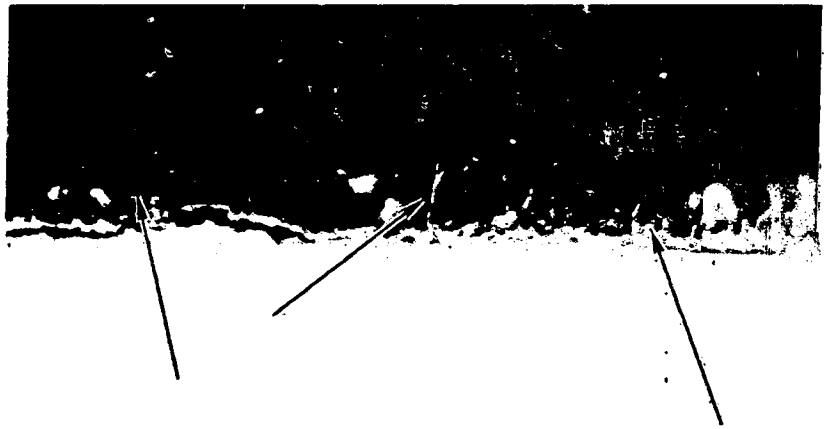

a. Crystallites growing on the surface

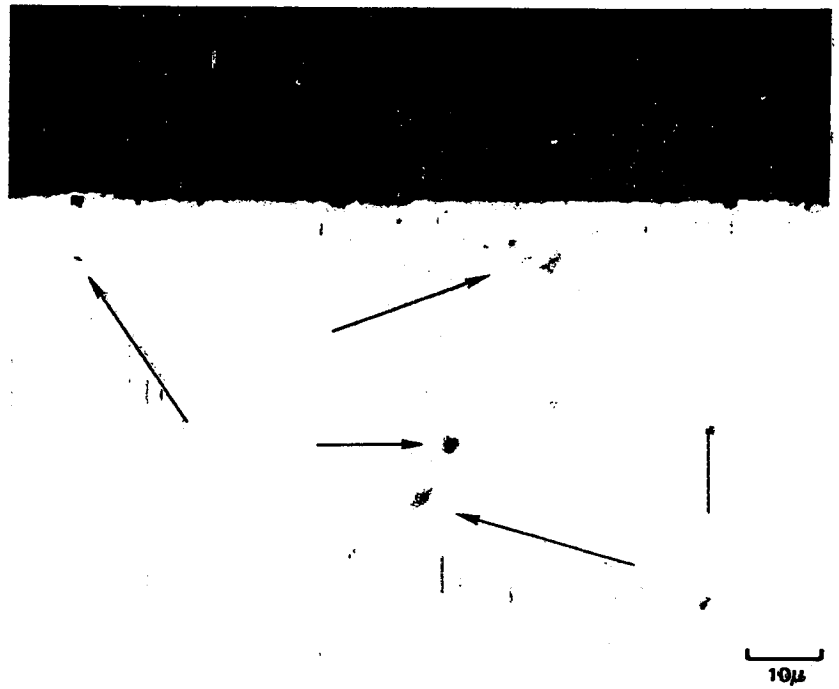

b. Area of the surface showing substrate

Fig. 112 Ni-25 Cr coated with Na_2SO_4 (0.95 mg/cm^2) and oxidized at 900°C for 24 hours in air containing 128 ppm HCl(g).

Fig. 113 Ni-25 Cr coated with Na_2SO_4 (1.11 mg/cm^2) and oxidized at 1050°C for 20 hours in air containing 10 ppm HCl(g).

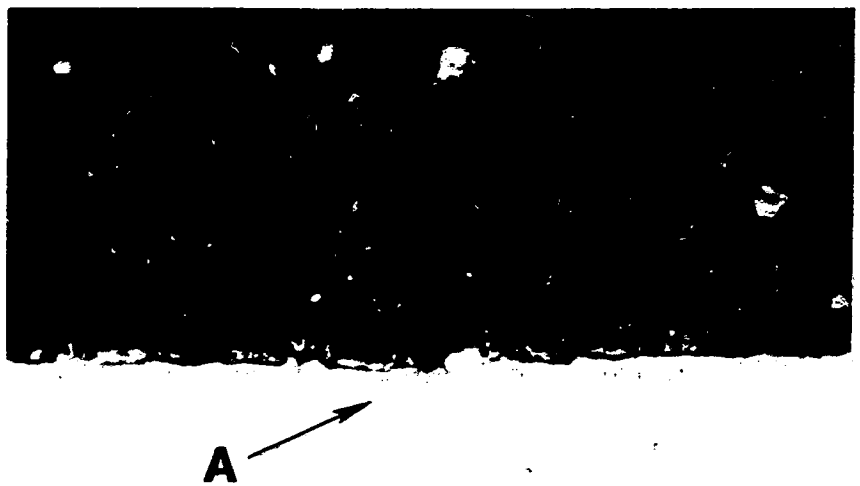

a. Dense oxide layer immediately below large Cr_2O_3 growth. 10μ

b. Dense oxide layer where no Cr_2O_3 crystals are seen 10μ

Fig. 114 Ni-25 Cr coated with Na_2SO_4 (1.11 mg/cm^2) and oxidized at 1050°C for 20 hours in air containing 10 ppm HCl(g). Note internal sulfides (A).

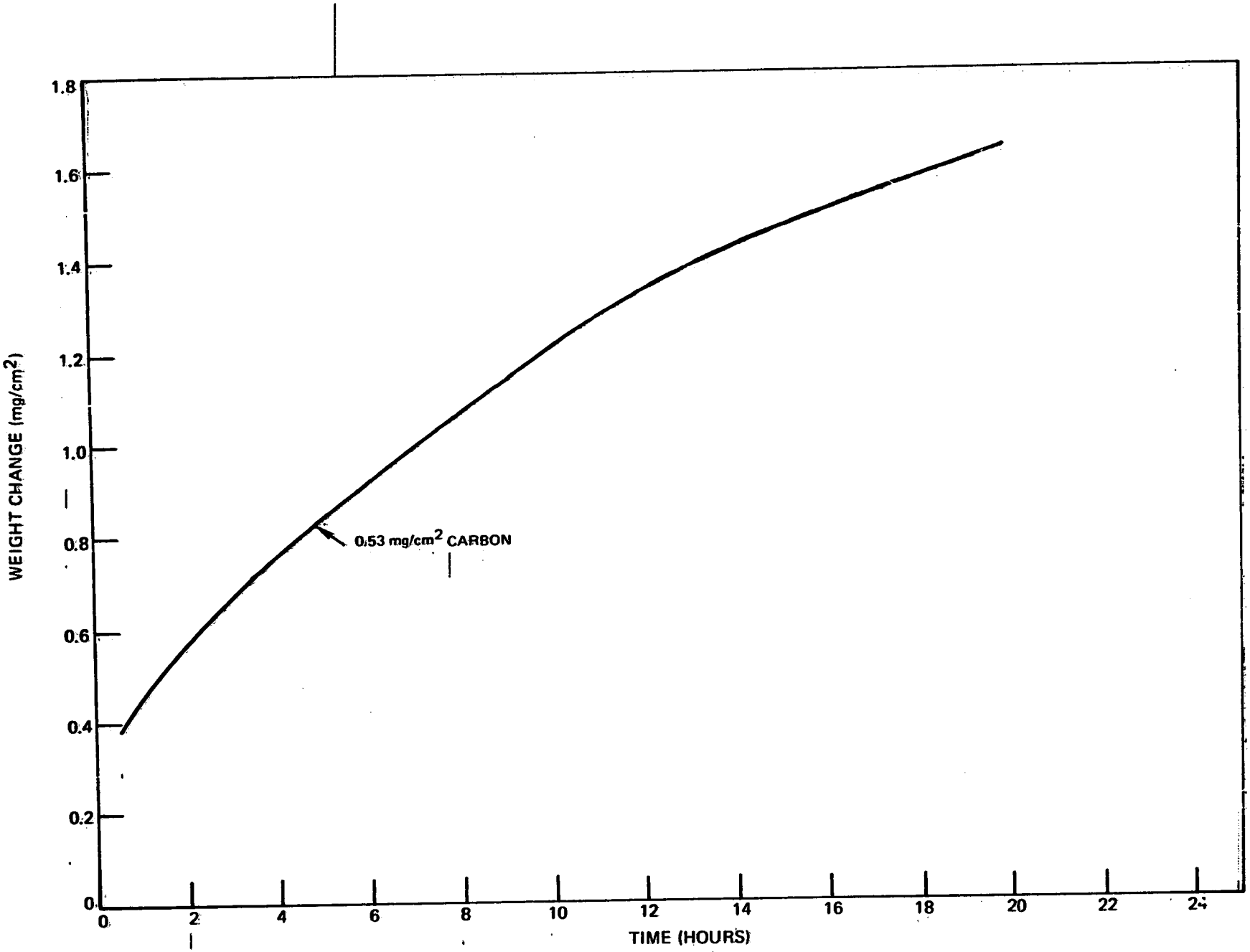

Fig. 115 Carbon-coated Ni-25 Cr oxidized at 1050°C.

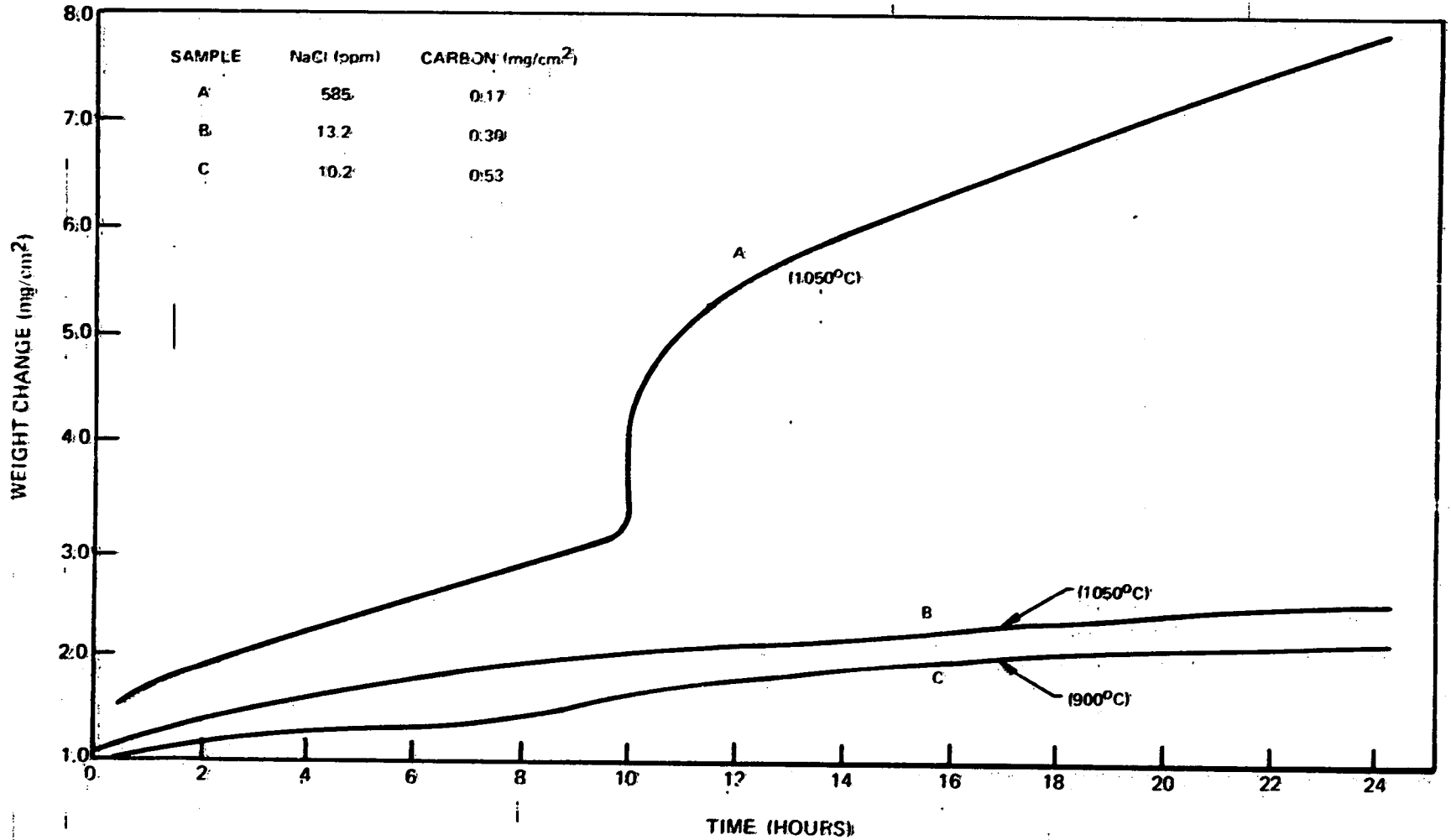

Fig. 116 Carbon-coated Ni-25 Cr oxidized in air with NaCl(g).

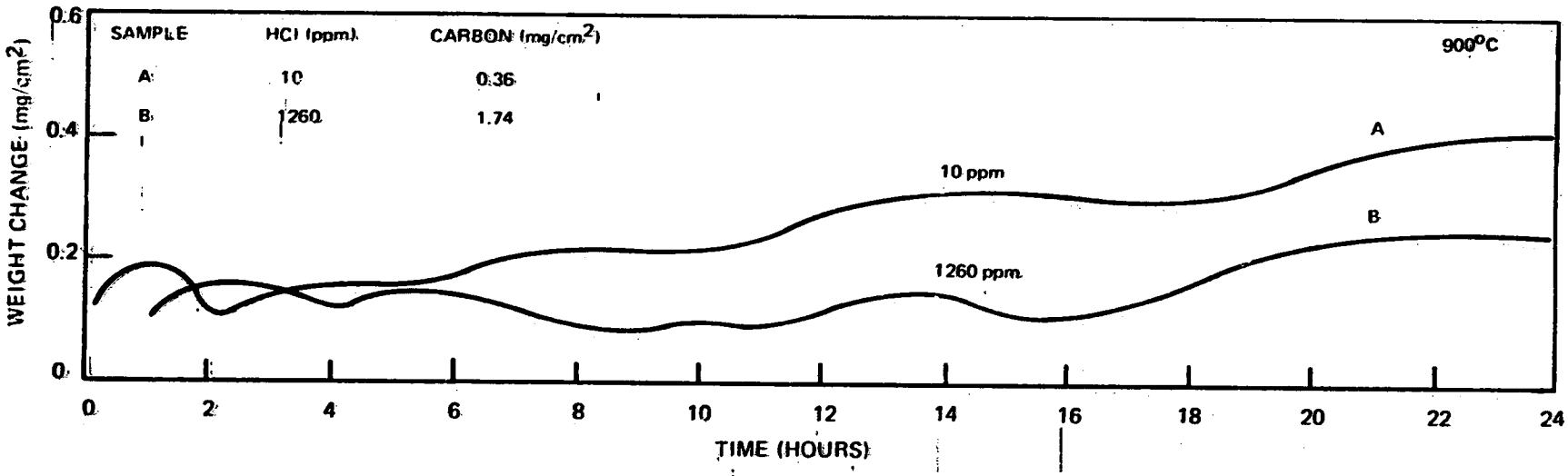

Fig. 117 Carbon-coated Ni-25 Cr oxidized at 900°C in air with HCl(g).

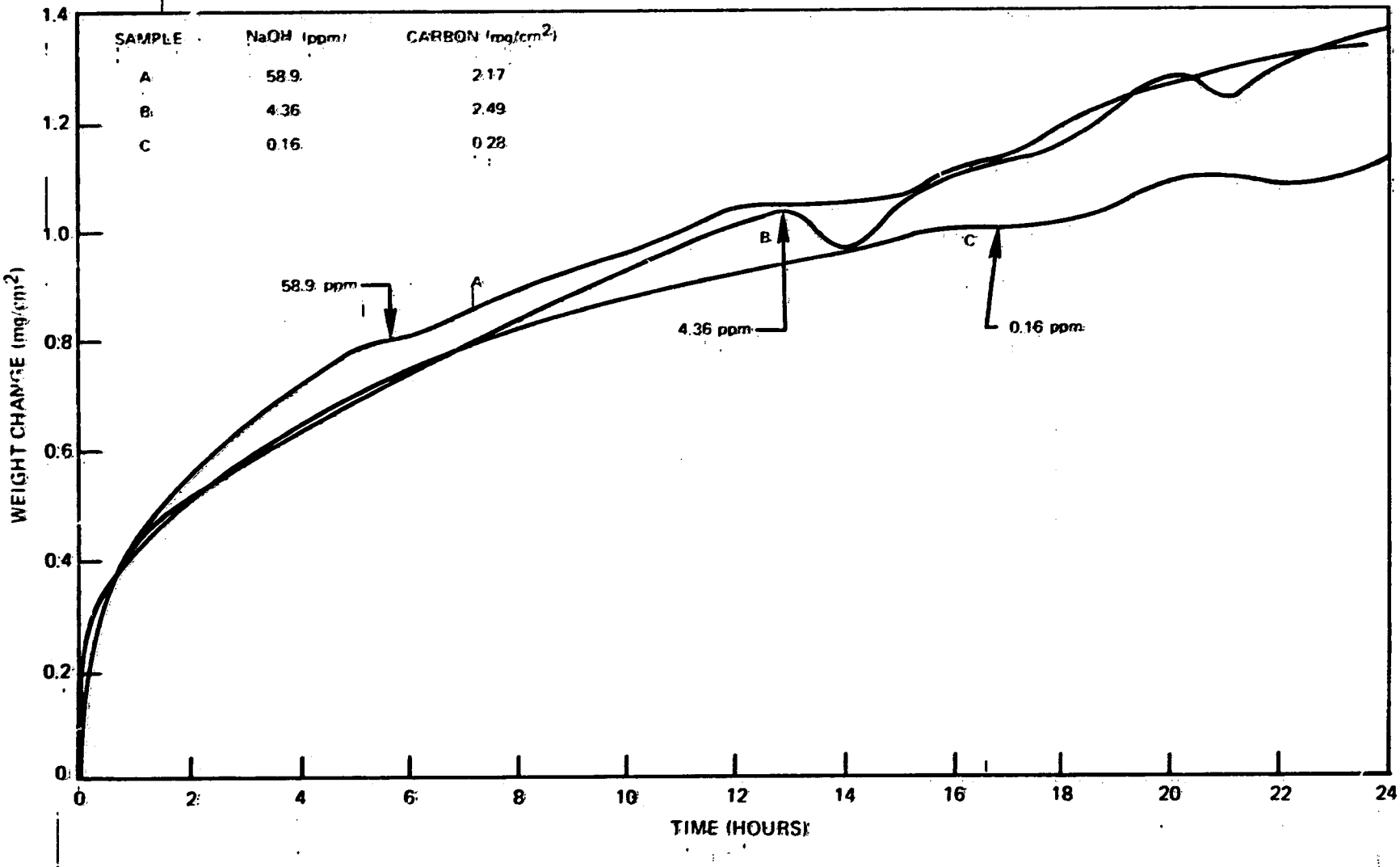

Fig. 118 Carbon-coated Ni-25 Cr oxidized at 1050°C in air with NaOH(g).

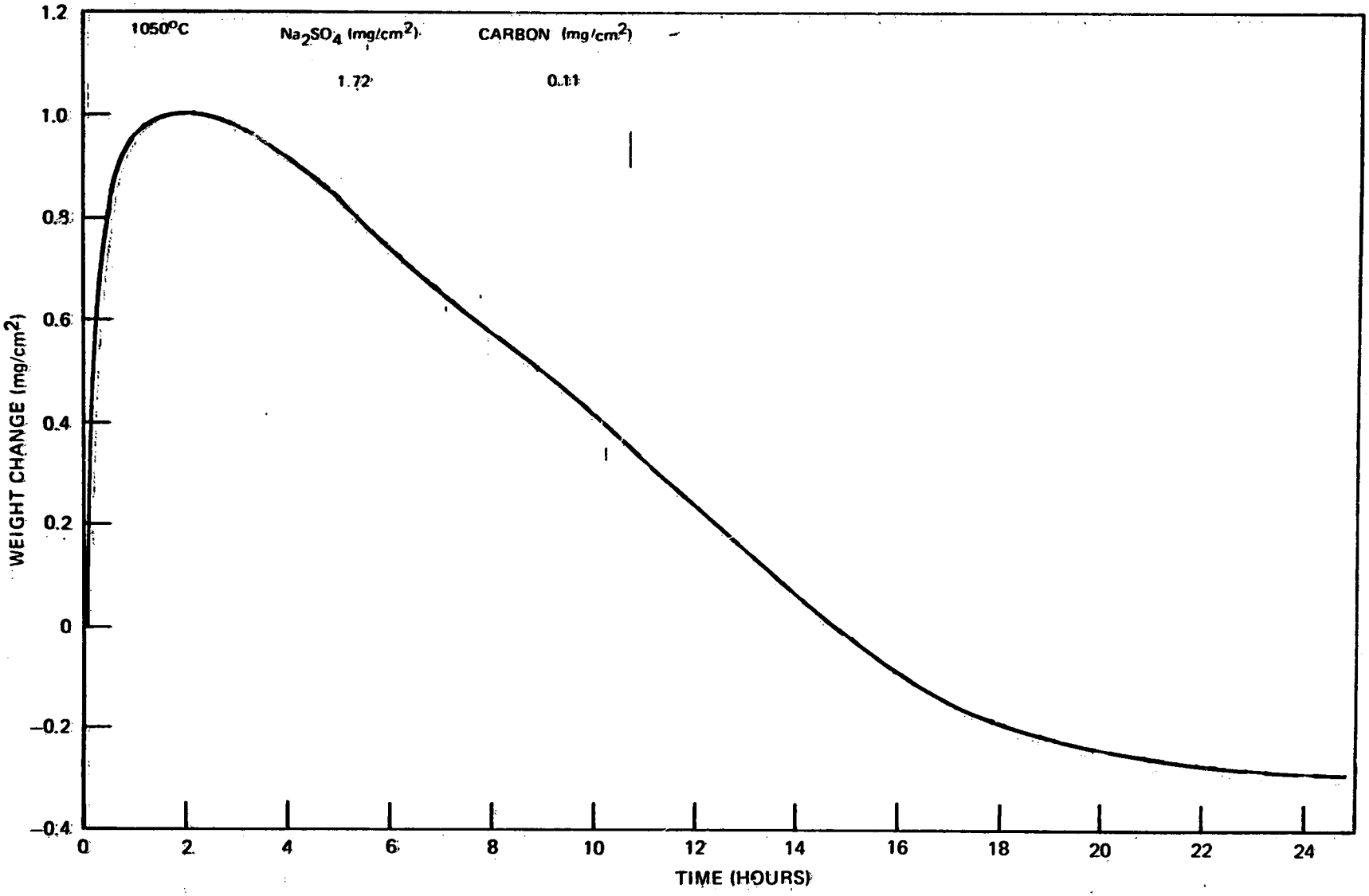

Fig. 119 Ni-25 Cr coated with both Na_2SO_4 and carbon and oxidized at 1050°C in air.

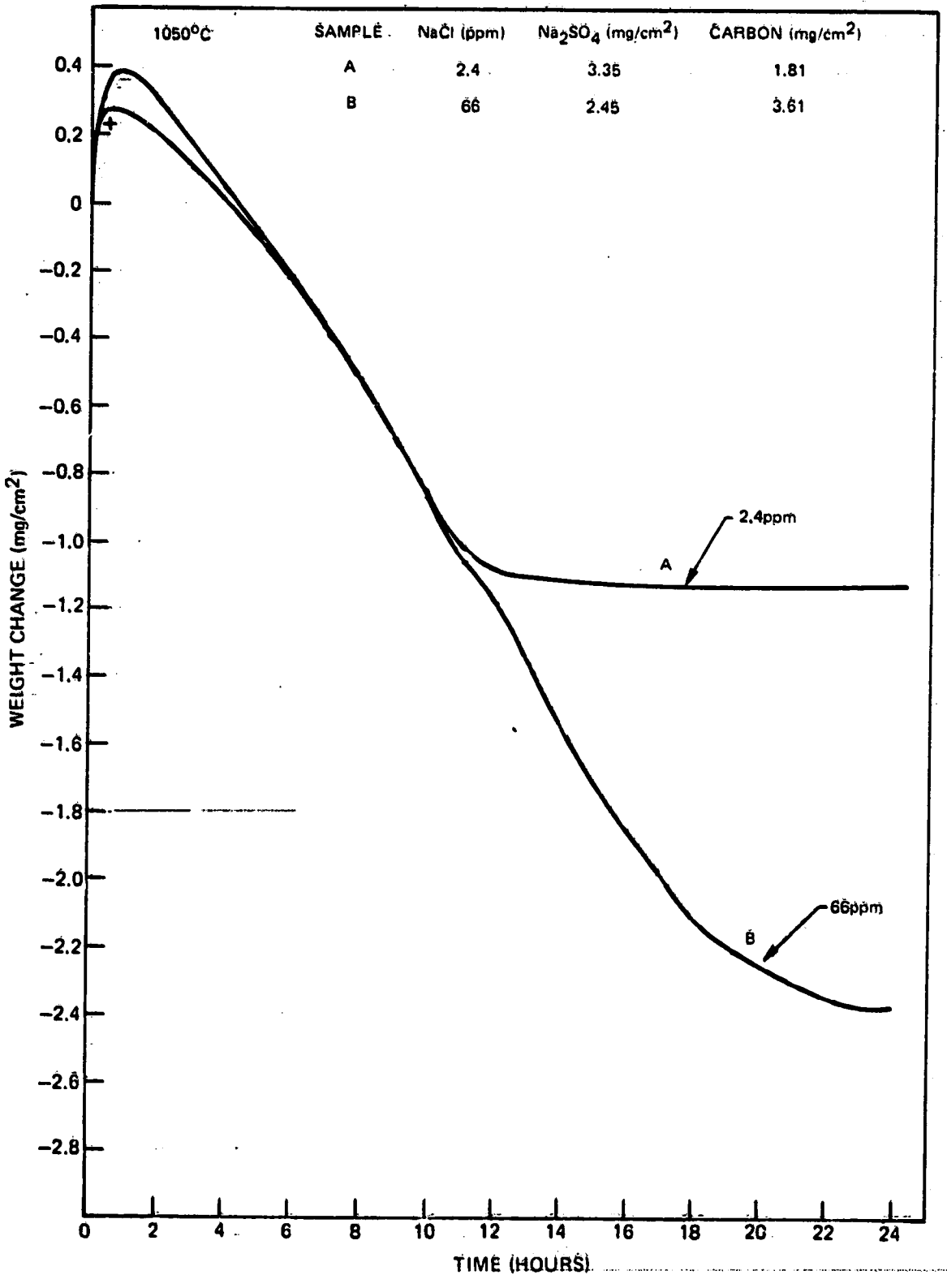

Fig. 120 Ni-25 Cr coated with carbon and Na_2SO_4 and oxidized at 1050°C in air with NaCl(g).

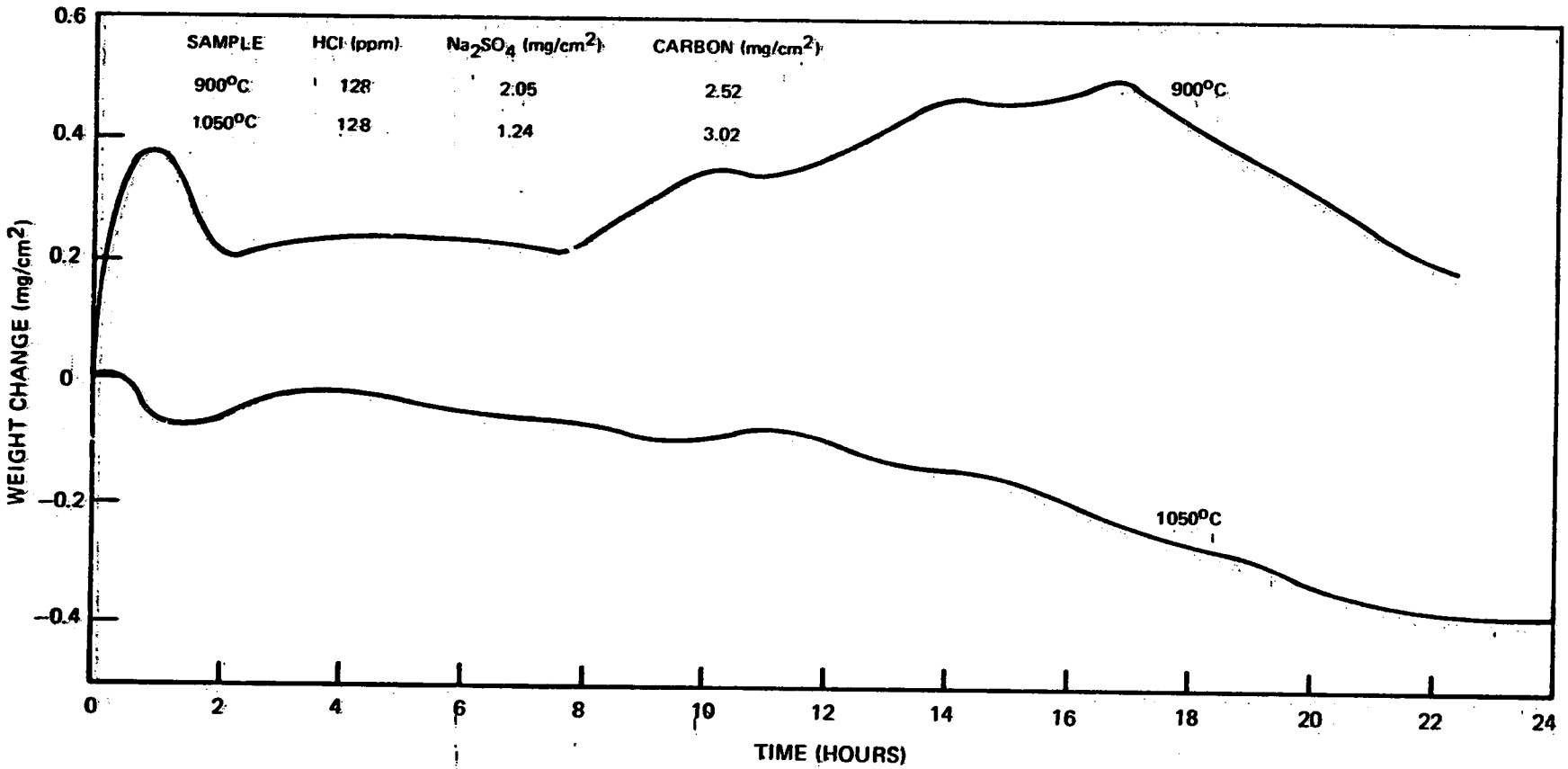

Fig. 121 Ni-25 Cr coated with Na_2SO_4 and carbon and oxidized in air with 128 ppm HCl(g).

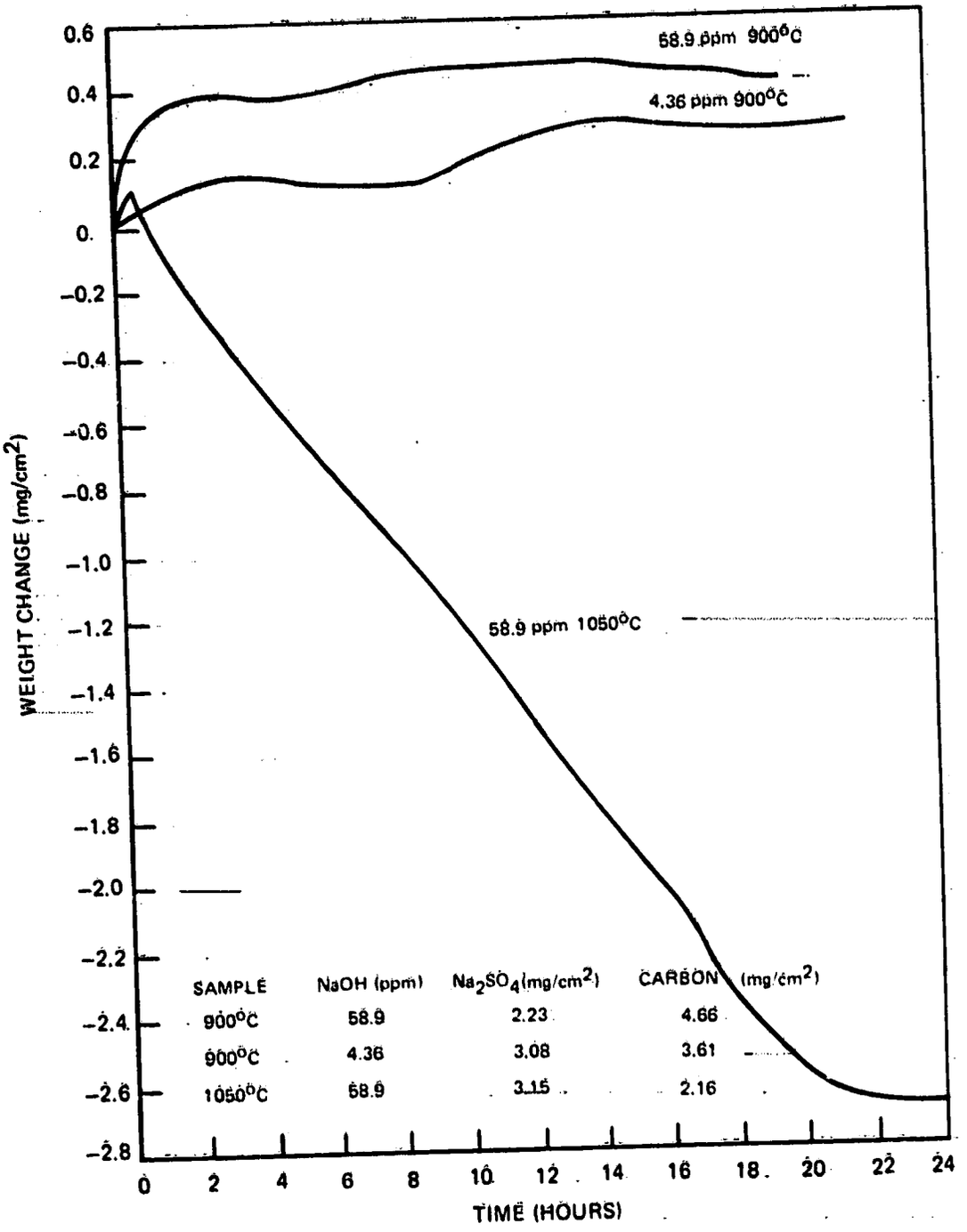

Fig. 122 Ni-25 Cr coated with Na_2SO_4 and carbon and oxidized in air with NaOH(g).

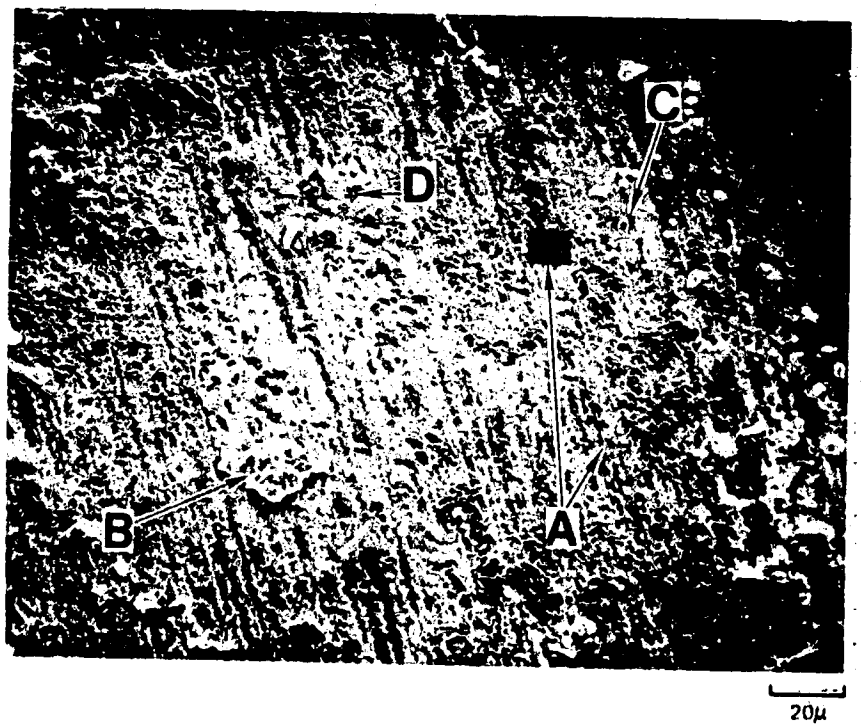

Fig. 123 B-1900 oxidized in air at 1050°C for 64-hours showing a highly irregular surface oxide

A. Al-enriched oxide
B. Ta-, Cr-and Ni-rich oxide flake resting on the surface
C. Ta-rich oxide particle
D. Oxide eruptions enriched in Ni and Cr

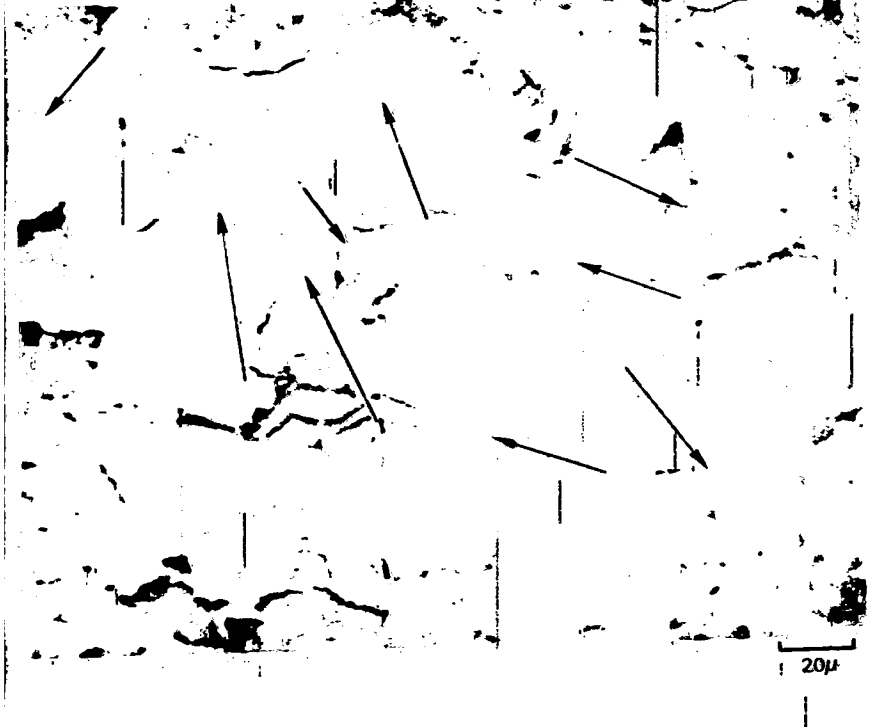

Fig. 124 B-1900 oxidized at 1050°C in air with 195 ppm NaCl for 64 hours showing broken oxide scale and alumina whiskers (arrows).

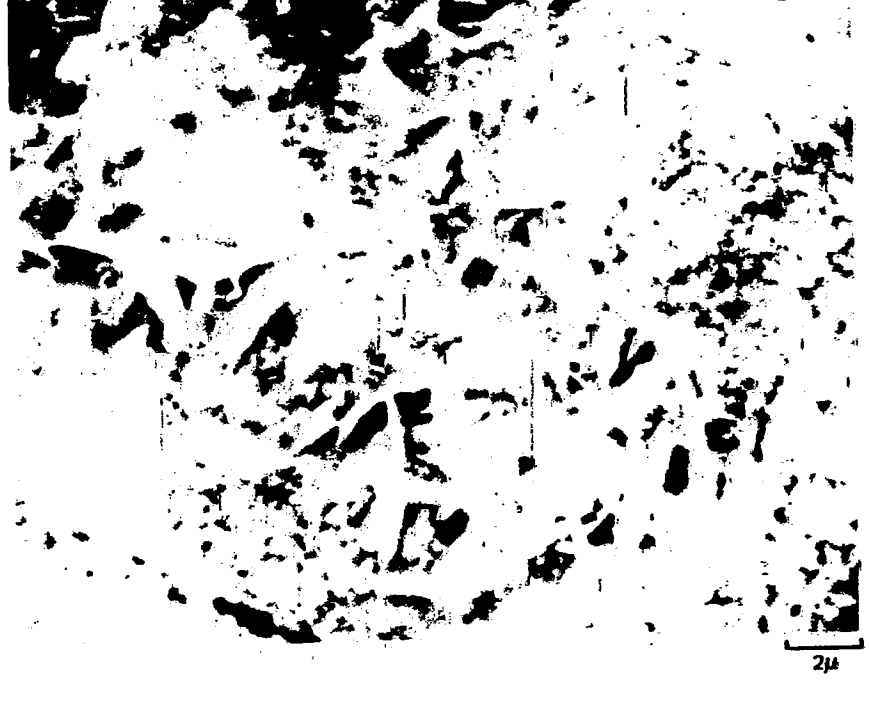

Fig. 125 Al_2O_3 blades on the surface of B-1900 oxidized in air at 1050°C with 195 ppm NaCl.

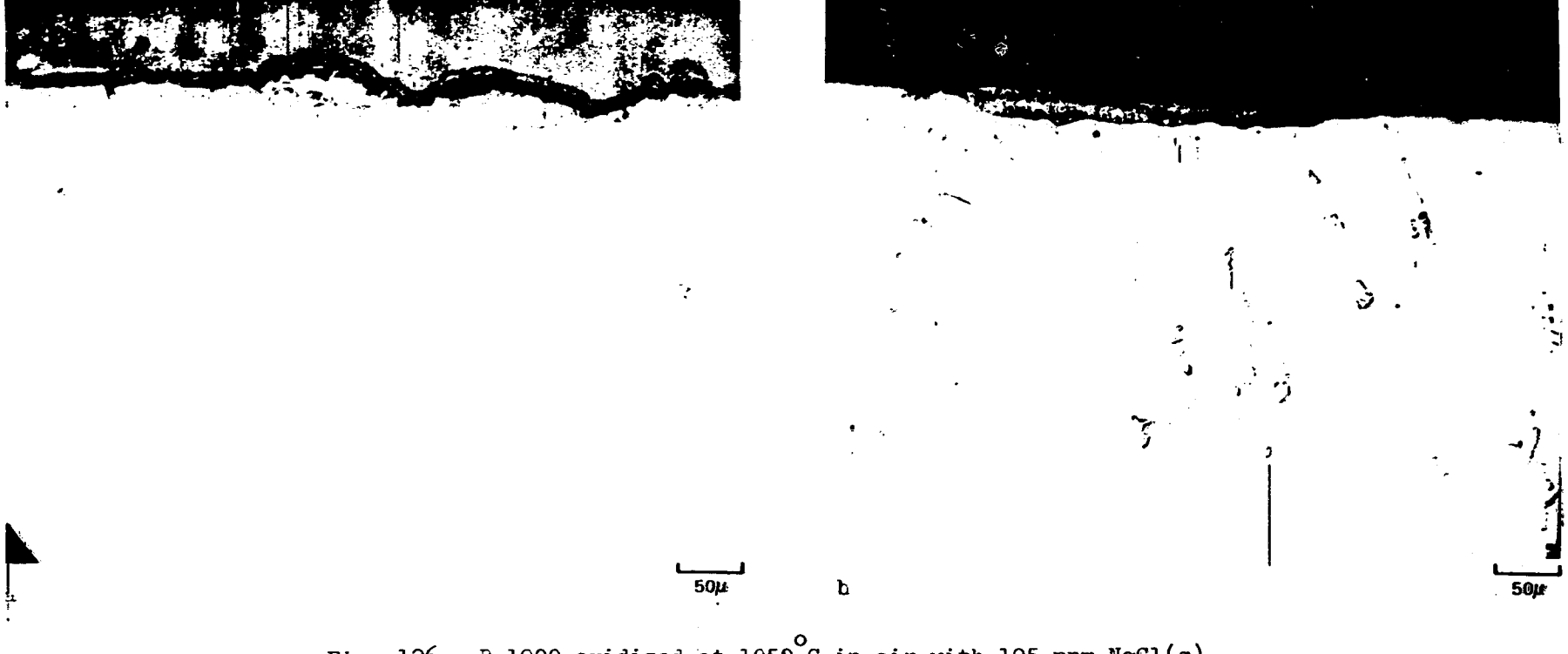

Fig. 126 B-1900 oxidized at 1050°C in air with 195 ppm NaCl(g) showing surface attack atypical of oxidation in air.

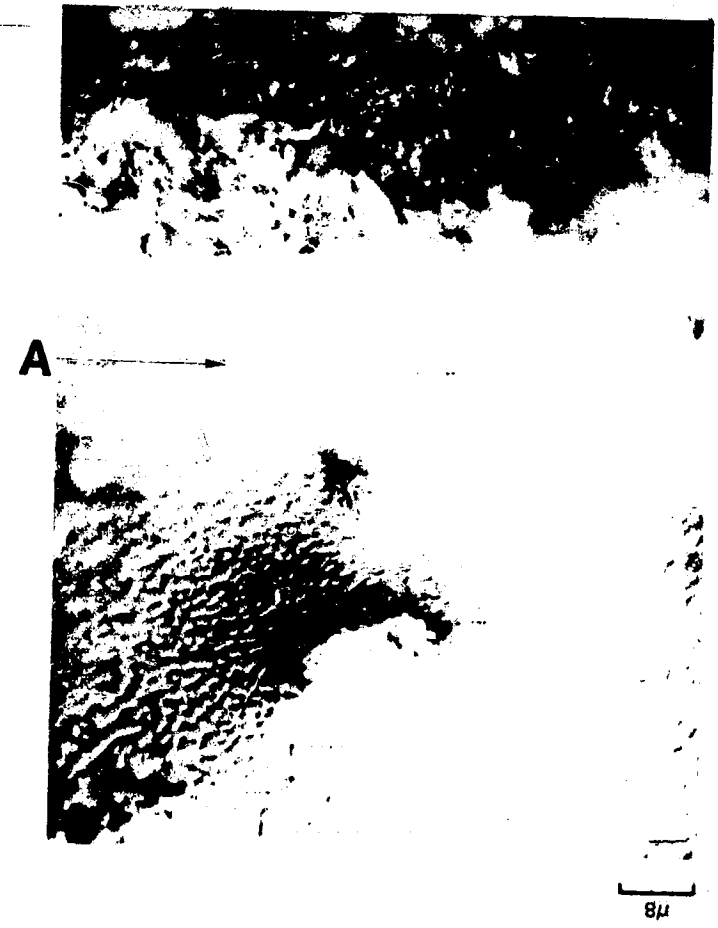

Fig. 127 An enlargement of the substrate immediately adjacent to the anomalous oxide found in Fig. 126b showing the γ' depletion area (A). (Normarski Interference Contrast Illumination).

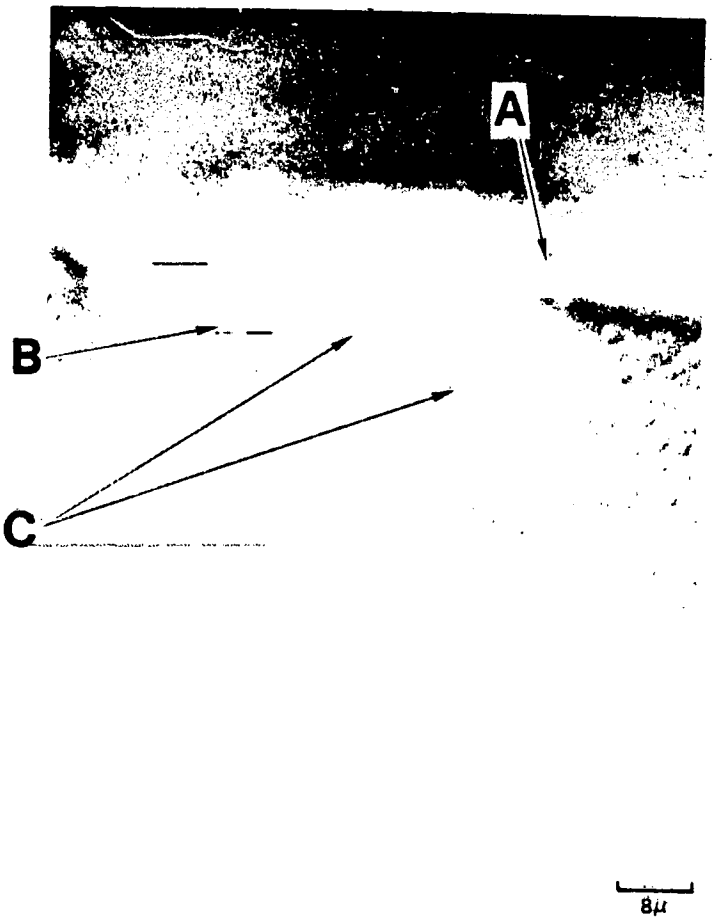

Fig. 128. B-1900 oxidized at 1050°C in air with 195 ppm NaCl(g) showing oxide scales (A), γ'-depleted zone(B), and γ' coarsening effects (C) related to normal oxidation (Normarski Interference Contrast Illumination).